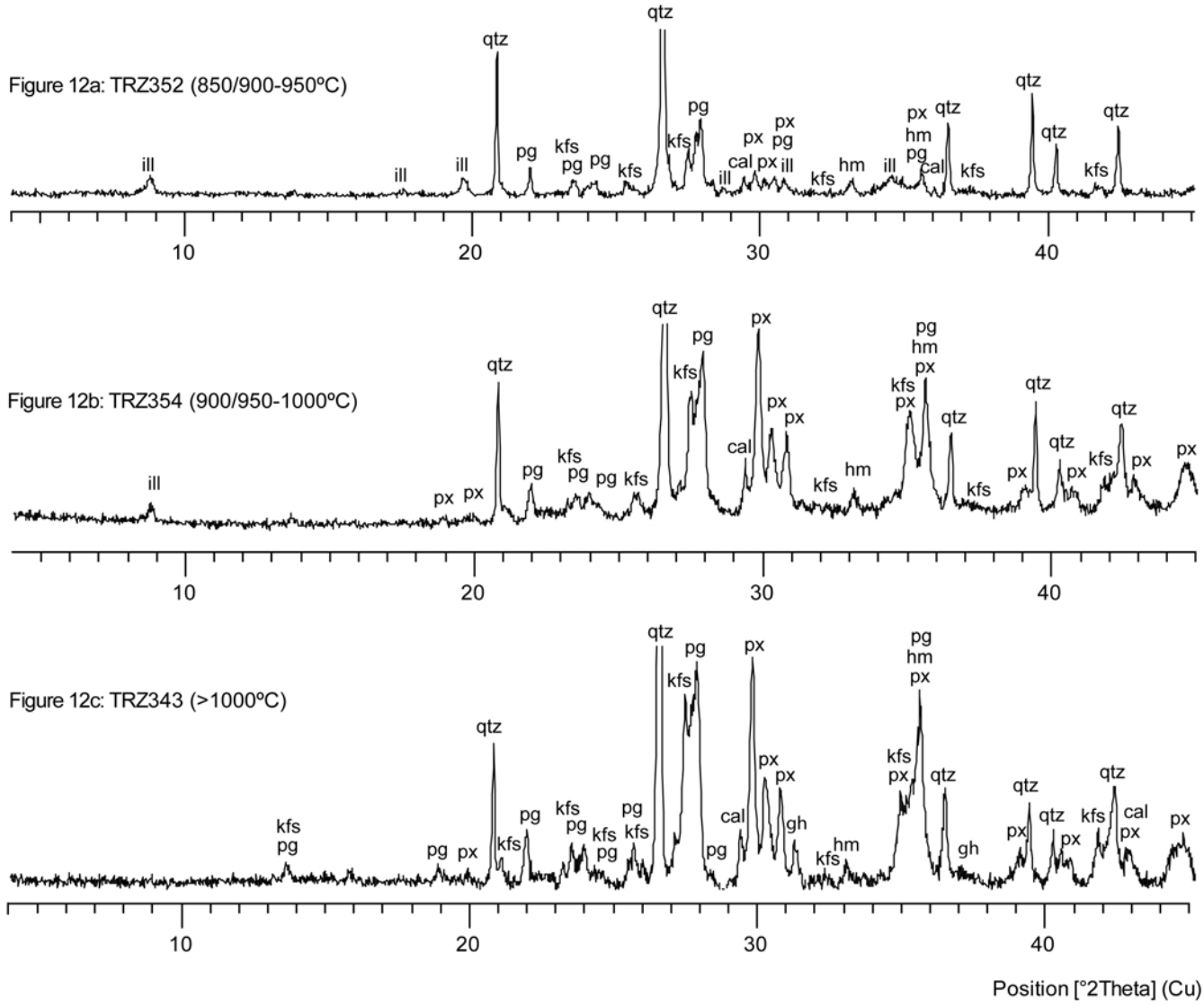

Figure 12: Diffractograms of the individuals TRZ352 representing the chemical group **AC2-A** and TRZ354 and TRZ343 representing the chemical group **AC2-C**; cal: calcite, gh: gehlenite, hm: hematite, ill: illite-muscovite, kfs: k-feldspar, pg: plagioclase, px: pyroxene, qtz: quartz

The eighteen ceramics from **AC2-B** (Figure 13a) can be divided in three different EFT and mineralogical categories. TRZ342 is the only ceramic from this group fired at low temperature. This shard presents only primary phases (quartz, calcite, illite-muscovite, k-feldspars, plagioclase and hematite) and EFT can be estimated around 850-900ºC. Thirteen shards (TRZ333, TRZ334, TRZ337, TRZ341, TRZ344, TRZ350, TRZ351, TRZ355, TRZ356, TRZ358, TRZ359, TRZ361 and TRZ364) are related to a second category of well fired vessels (900-950ºC) according to the presence of primary phases (quartz, calcite, illite-muscovite, k-feldspars, plagioclase and hematite) and fired phases (pyroxene and gehlenite) (Figure 13b). Finally, diffractograms of the last five ceramics shards (TRZ332, TRZ336, TRZ338, TRZ349 and TRZ361) show the total decomposition of illite-muscovite and calcite is much most reduced. Because of that, the EFT estimated must be higher than 1000ºC and these ceramics can be considered as over fired (Figure 13c). Moreover, TRZ338 and TRZ361 present analcime which is a result of postdepositional alteration and/or contamination processes.

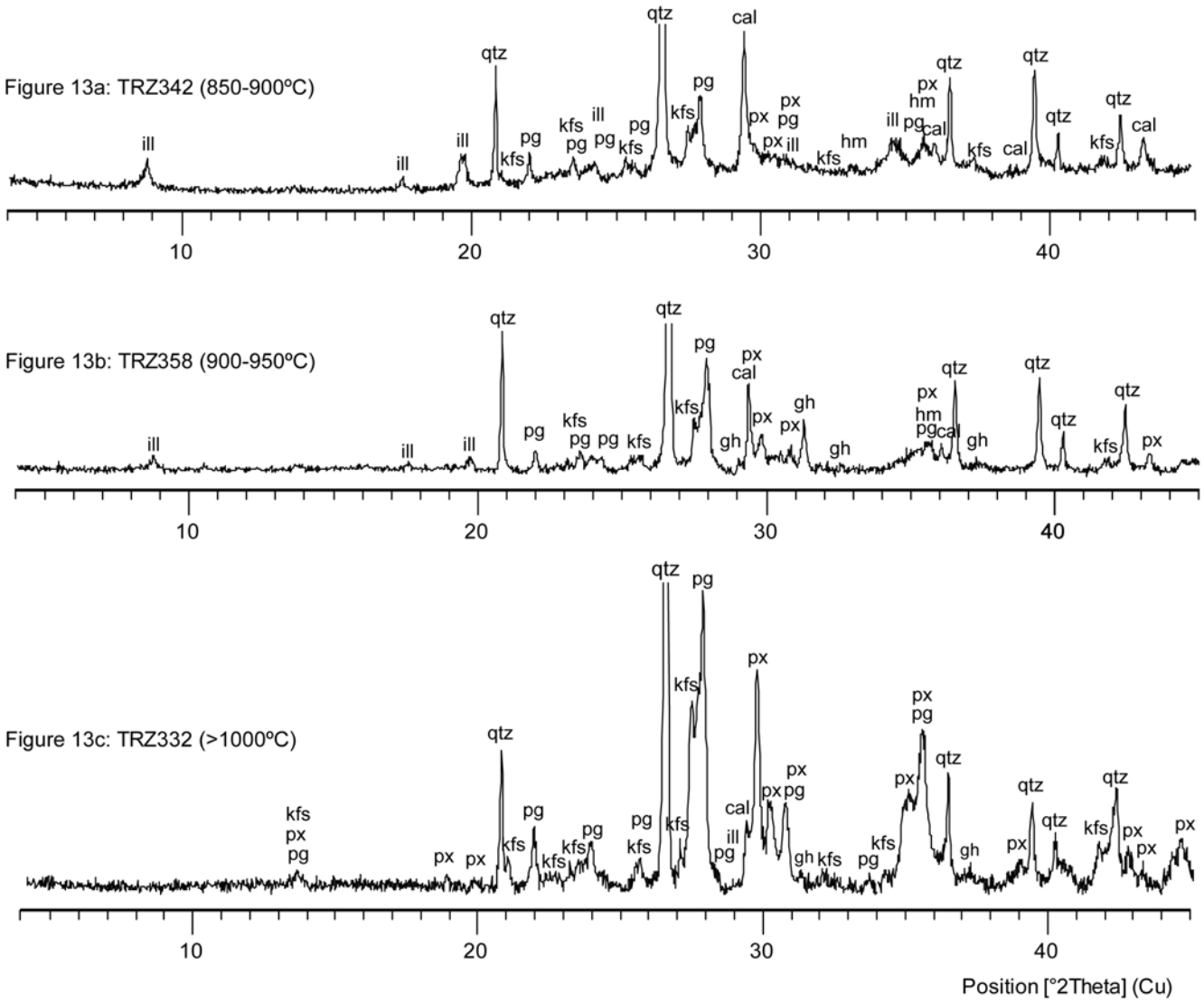

Figure 13: Diffractograms of the individuals TRZ342, TRZ358 and TRZ333 representing the chemical group **AC2-B**; cal: calcite, gh: gehlenite, hm: hematite, ill: illite-muscovite, kfs: k-feldspar, pg: plagioclase, px: pyroxene, qtz: quartz

5.1.4. Surface treatment (SEM analysis)

The study of the slip that covers some of the common wares was carried out by SEM-EDS over polished sections of five ceramics from the Ancient Military Quarters sector. The quantitative chemical microanalysis was carried out upon the normalised subcomposition O, Na, Mg, Al, Si, K, Ca, Ti, Mn and Fe in 5 to 10 different points of the slip and different areas of the body of the samples.

TRZ146 is a plate with a surface painted with a red-orange slip. **TRZ149** is a reduced plate of grey paste which surface seems to be covered with a greyish slip (Figure 14). The surface of the plate **TRZ333** is covered with a red slip whereas that of the ceramic **TRZ337** has a brownish tonality, darker over the rim than in the rest of the ceramic body. Finally, **TRZ358** is a reduced plate or bowl which surface seems to be covered with a greyish slip.

Figure 14: Photographs of the painted ceramics from sectors **AC1** and **AC2** analysed by SEM-EDS

The state of vitrification and other characteristics of the slip and the ceramic body of all ceramic cases can be evaluated by the microphotographs of the polished sections (Figure 15). In **TRZ146**, the state of vitrification of the ceramic body is higher than the slip and particles of the microstructure appear more sintered. The layer of slip is fine (50μm) and relatively homogeneous. Looking at the interface between the red-orange slip and the clay matrix, no clear separation line could be observed but only a fine insertion zone. That clearly indicates a biscuit, just fired at ones, and no glaze firing. However, in **TRZ333** and **TRZ337,** the interface between the red-orange slip and the clay matrix is clearly marked and that indicates that a well glassified slip was produced during firing. Both slips have been fired at high temperature as it can be seen by the relatively extended glassy face that indicates the high vitrification state of the slip. The reddish slip of **TRZ333** presents an irregular thickness of 20-40 μm. In **TRZ337** is possible to distinguish two different irregular layers of slip. Each one measures 10μm and can be related to the degraded of colours observed on the surface. The surface of the ceramic is brown clear but a second layer of dark brown covers the rim. The reduced plate **TRZ358** present a thick layer of low glazed slip (100μm). The interface between the layer and the clay matrix is relatively well defined because of the high degree of vitrification of the ceramic body. However, the greyish slip of **TRZ149** is less thick (10 μm), heterogeneous and more sintered. The quantitative chemical microanalysis performed over **TRZ146, TRZ333 and TRZ337** reveal slight differences in Si, Ca and Fe relative compositions between the orange-reddish-brownish slips and the pastes of these shards. The mean normalised chemical composition of the several microanalyses made at different points of the slip and clay of the same shard is given at Figure 16. In all cases, the clay is more calcareous and richer in silica, but the percentage in Fe in the clay matrix is lower than in the slip chemical composition. The similarity in the composition between the clay and slip in the case of the plate TRZ333 probably means that a finer fracture of the clay used to fabricate the pot was applied to produce the red slip. Reduced ceramic **TRZ149** shows important differences between the clay and slip chemical composition. In this case, the fine fraction used to produce the slip has higher Fe percentage and is more calcareous than the clay, although the clay is richer in silica. A similar case is the reduced ceramic **TRZ358.** However, the chemical composition of clay and slip in this individual is really similar and differences are related to the higher Ca content of the slip.

Figure 15: SEM photomicrographs of the polished sections of the slip and paste area observed in SEM-EDS upon the common wares TRZ146, TRZ149, TRZ333, TRZ337 and TRZ358 from sectors **AC1** and **AC2** (Termez)

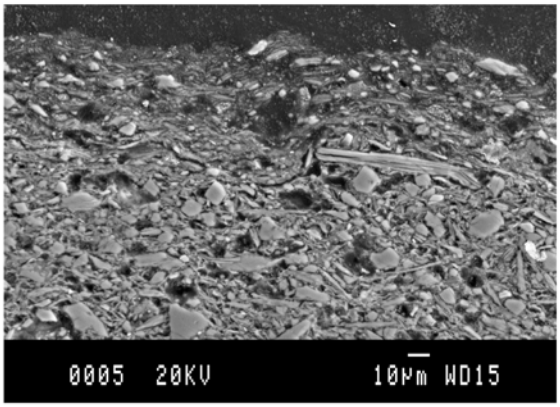

TRZ146 500x

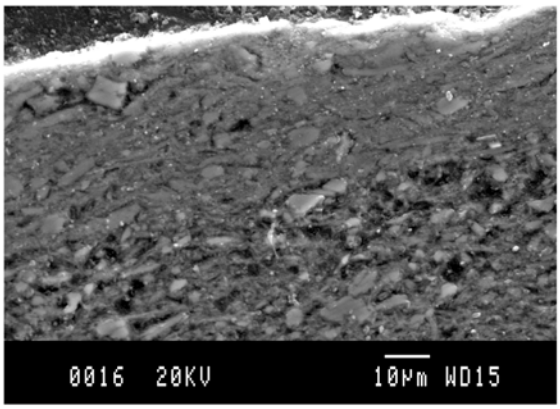

TRZ333 1000x

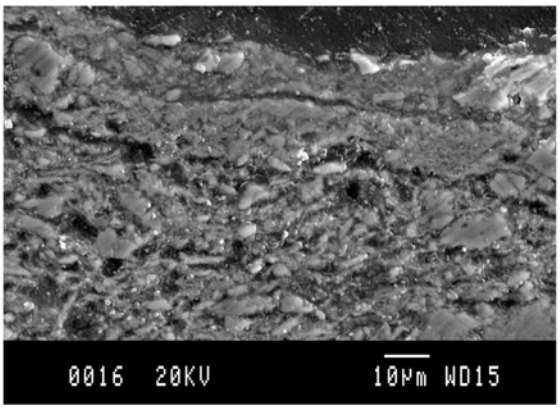

TRZ337 1000x

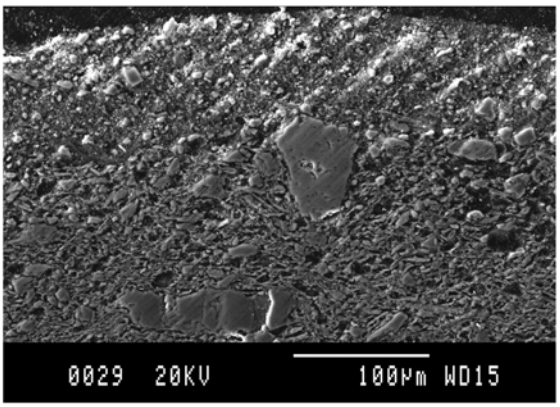

TRZ358 300x

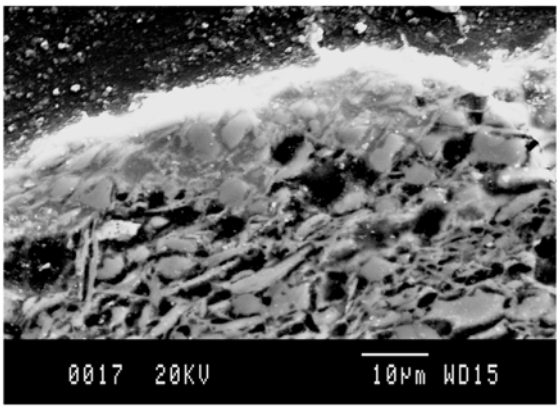

TRZ149 1300x

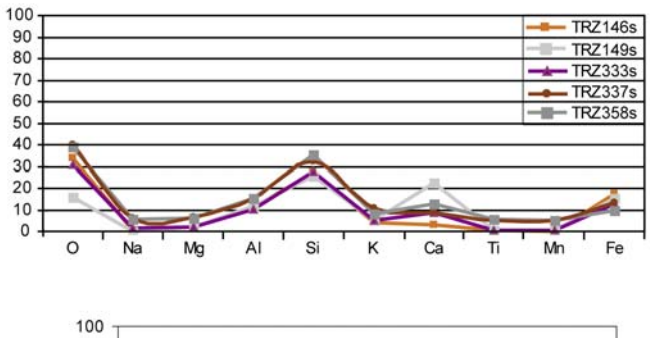

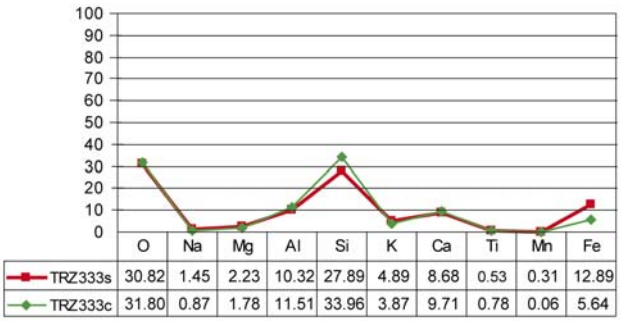

	O	Na	Mg	Al	Si	K	Ca	Ti	Mn	Fe
TRZ333s	30.82	1.45	2.23	10.32	27.89	4.89	8.68	0.53	0.31	12.89
TRZ333c	31.80	0.87	1.78	11.51	33.96	3.87	9.71	0.78	0.06	5.64

Figure 16: Graphics representing the normalised chemical composition obtained by SEM-EDS microanalysis of the slip (s) and clay (c) of the painted vessels TRZ146, TRZ149, TRZ333, TRZ337 and TRZ358 from sectors **AC1** and **AC2** (Termez)

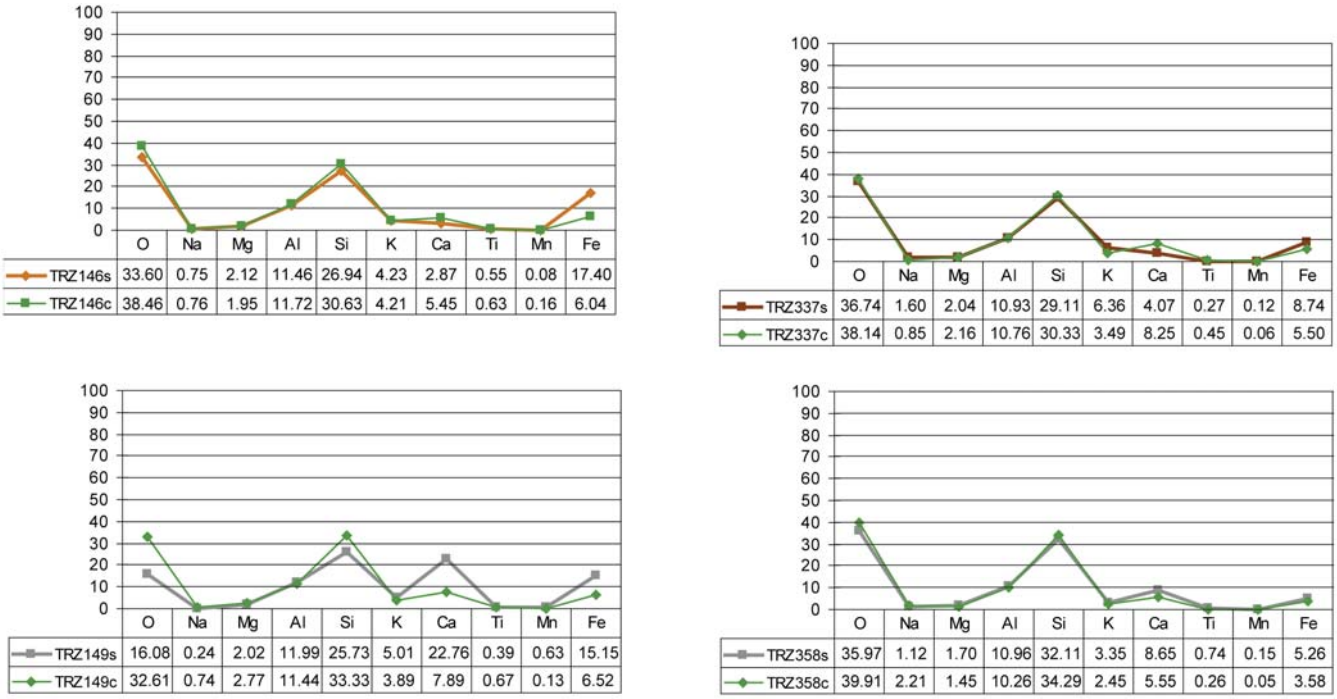

Figure 16: Graphics representing the normalised chemical composition obtained by SEM-EDS microanalysis of the slip (s) and clay (c) of the painted vessels TRZ146, TRZ149, TRZ333, TRZ337 and TRZ358 from sectors **AC1** and **AC2** (Termez)

5.2. Kampyr Tepe

From **Kampyr Tepe** a total number of 65 individuals, both typologically considered as Hellenistic and First Kushan has been analysed (TRZ209 to TRZ242 and TRZ365 to TRZ389). Some of them have been already presented in previous works (Martínez *et al*., 2009: 305). The analyzed material typologically is composed by cups, bowls, plates, craters and jars (Table 1). Most of them covered by a slip that varies in colour from reddish (TRZ210, TRZ211, TRZ212, TR213, TRZ214, TRZ215, TRZ218, TRZ219, TRZ222, TRZ223, TRZ224, TRZ226, TRZ228, TRZ230, TRZ232, TRZ365, TRZ375, TRZ381 and TRZ386), to orange (TRZ217, TRZ366 and TRZ376), brown (TRZ220, TRZ221, TRZ368, TRZ377), to grey (TRZ231 and TRZ380) and black (TRZ216, TRZ225, TRZ236, TRZ367 and TRZ374). Some of them also present relief decoration (grooves) or incised motifs, predominantly palms (TRZ231 and TRZ380).

5.2.1. Chemical composition (XRF analysis)

The normalised chemical composition of 65 individuals is given at Table 2. The CVM has been calculated over 65 samples from **Kampyr Tepe** (TRZ203 to TRZ242 and TRZ365 to TRZ389), using the subcomposition: Fe_2O_3 (as total Fe), Al_2O_3, TiO_2, MgO, CaO, Na_2O, K_2O, SiO_2, Ba, Rb, Th, Nb, Zr, Y, Sr, Ce, Ga, V, Zn, Cu, Ni and Cr. The total variation (vt) in this data set according to the CVM is relatively high 0.3433 that generally indicates a rather heterogeneous composition (Table 3b). The elements which introduce more than the 50% of the variability in this data set are CaO ($\tau_{.CaO}$ = 1.751), Sr ($\tau_{.Sr}$ = 1.733), Na_2O_3 ($\tau_{.Na2O3}$ = 1.017), Ce ($\tau_{.Ce}$ = 0.852), Cu ($\tau_{.Cu}$ = 0.775), Ni ($\tau_{.Ni}$ = 0.753), K_2O ($\tau_{.Ce}$ = 0.707) and Ba ($\tau_{.Ba}$ = 0.681).

As in the previous case, the high variability introduced by CaO, Ce and Ni might be associated to differences in the raw material composition. Nevertheless, crystallisation of secondary calcite (Buxeda and Cau, 1995; Cau, Day, Montana, 2002) in some samples, as it will be presented at petrographic analysis, could contribute to CaO variation. Chemical variation of Na_2O_3 and K_2O can be linked to analcime crystallisation ($Na[AlSi_2O_6]\cdot 6H_2O$) as it has been already described in detail in previous works (Tsantini *et al.,* 2007; Martínez *et a*l., 2008, 2009). For these reasons, the statistical evaluation of the chemical

data from **Kampyr Tepe** have been repeated without consider CaO, Na_2O, K_2O, Ba, Sr and Cu values. The CVM calculated for the new data set shows a vt =0.1245 value, that is sufficiently low to indicate a relatively homogeneous data set. The result of the data treatment are summarized in the dendrogram of the cluster analysis (Figure 17) performed using the Square Euclidean distance and the centroid algorithm over the logratio transformed subcomposition: Fe_2O_3 (as total Fe), Al_2O_3, TiO_2, MgO, CaO, SiO_2, Rb, Th, Nb, Zr, Y, Ce, Ga, V, Zn, Cu, Ni and Cr, using TiO_2 as a divisor.

Dendrogram in the Figure 17 shows that **TRZ373** (cooking ware) and **TRZ385** have significantly different chemical composition regarding to the rest of the shards and, for this reason, they are separated by a high ultrametrical distance. The chemical composition of these two individuals is given in Table 5. The cooking ware TRZ373 present significant chemical differences from the rest of the individuals as it can be seen at this table. At the same way, by looking at its chemical composition (Table 5), **TRZ385** is characterized by a very high CaO and Sr values. **TRZ385** is a medium coarse calcareous jar, with high Ni and low K_2O, Ba, Rb and Sr relative contents. The typology of these ceramics is given in Figure 18.

Individuals TRZ377, TRZ381, TRZ380, TRZ383, TRZ235, TRZ386 and TRZ229 stand at a marginal position respect to the rest of the pottery. **TRZ381** presents the highest MgO relative content in this data set, whereas **TRZ377** is characterised by high Na_2O, K_2O, and Zn (Table 5) concentrations. **TRZ380** have a higher relative concentration in Fe_2O_3, Rb, Sr and V. **TRZ383** presents a higher content in Al_2O_3, Rb, Cu and Ni. **TRZ235** is characterised by a higher V concentration whereas the values in Zr and Y are bigger in **TRZ386**. Finally, TRZ229 is different to the rest of the ceramics due to the higher concentration in SiO_2, Ba and Ce (Figure 18).

The major number of ceramics from **Kampyr Tepe** is grouped in a small ultrametrical distance, forming several subgroups (Figure 17) with slight chemical differences between them that can be confirmed by the mean chemical composition presented at Table 6. The typology of these ceramics is represen-ted in Figure 19. Individuals TRZ370 and TRZ204 are joined together in a small subgroup **KT-1**, which chemical composition differs because of the high TiO_2 and low Rb contents. One of the major subgroups, **KT-2** is formed by 15 individuals (TRZ203, TRZ208, TRZ209, TRZ210, TRZ211, TRZ212, TRZ213, TRZ214, TRZ215, TRZ219, TRZ222, TRZ228, TRZ230, TRZ232 and TRZ367) characterised by high Fe_2O_3, Al_2O_3 and Cr, and slightly lower CaO content than the rest of the ceramics analysed from **Kampyr Tepe.** Six individuals (TRZ206, TRZ233, TRZ239, TRZ384, TRZ388 and TRZ389) are grouped in **KT-3**, which composition shows high K_2O and low Zr content. The major chemical group, **KT-4**, is composed of 18 ceramics (TRZ205, TRZ207, TRZ220, TRZ221, TRZ224, TRZ225, TRZ226, TRZ227, TRZ231, TRZ234, TRZ236, TRZ238, TRZ240, TRZ241, TRZ242, TRZ372, TRZ376 and TRZ387) which present a slightly higher Zn and Ce concentration and lower Ga values. **KT-5** group is formed by two individuals (TRZ379 and TRZ382), which basically contains the highest Th, Zr and Y relatives values and lower V and Zn contents. Seven ceramic individuals (TRZ218, TRZ237, TRZ365, TRZ366, TRZ269, TRZ371 and TRZ375) are clustered together in **KT-6**, which present low Na_2O_3, Th and Sr values. Finally, **TRZ374** and **TRZ216** that correspond to black painted pottery are grouped in **KT-7** because of their high K_2O and the low Cu and Ni values.

The different ceramic groups identified at **Kampyr Tepe** should be considered as diverse PCRU's, whose provenance will be only established when the pottery workshops from the Hellenistic period will be located and excavated. At the vicinity of **Kampyr Tepe**, a pottery kiln was found and excavated some years ago by the archaeologists of the Oriental Museum of Moscow. However, so far, no archaeometrical analysis of the pottery associated to this kiln site has been carried out. Therefore, the chemical characteristics of the ceramic production from the Hellenistic period at **Kampyr Tepe** are still unknown.

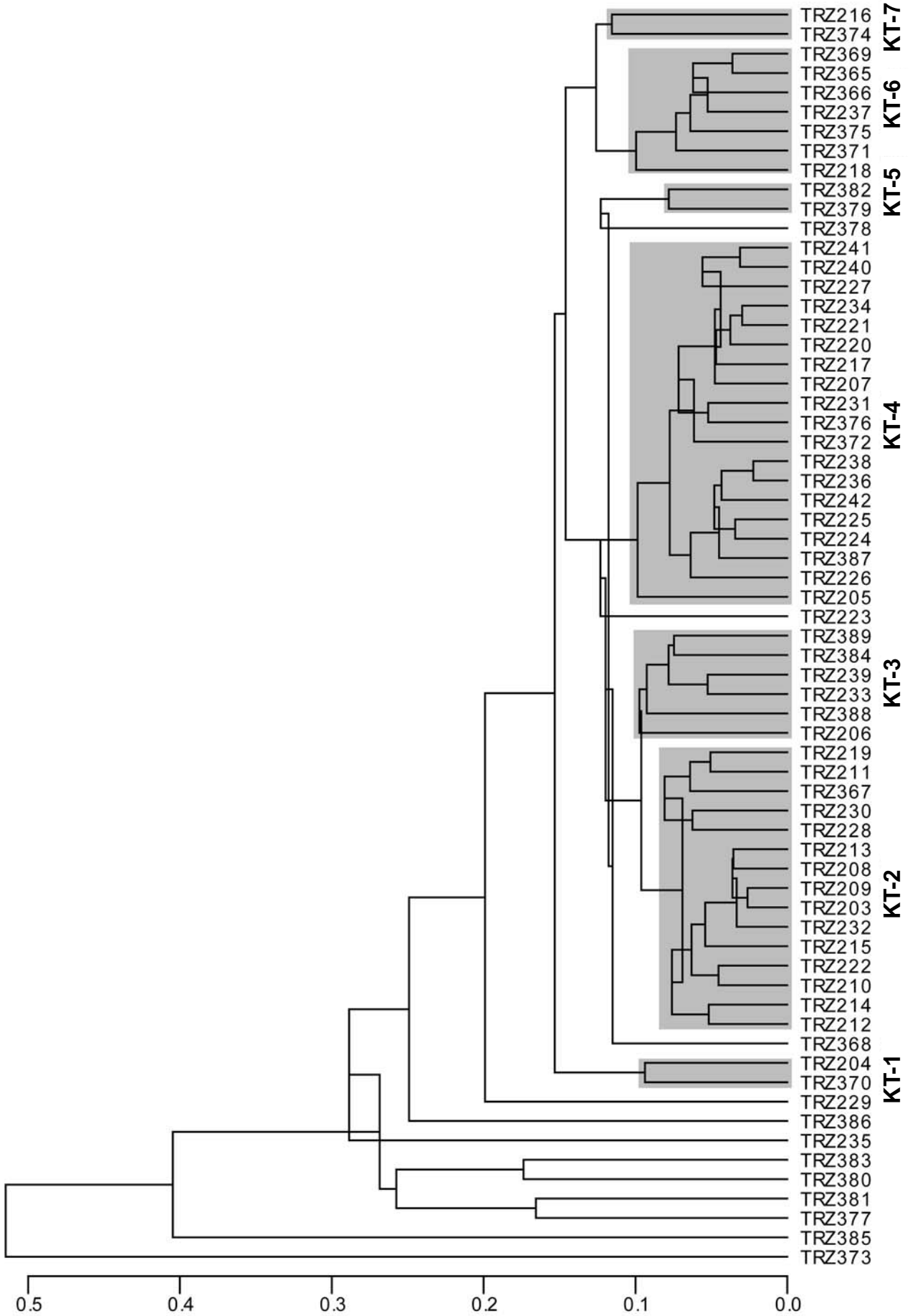

Figure 17: Dendrogram resulted from the cluster analysis performed on the subcomposition Fe2O3, Al2O3, MgO, CaO, SiO2, Rb, Th, Nb, Zr, Y, Ce, Ga, V, Zn, Cu, Ni and Cr, using TiO2 as a divisor, of 65 individuals sampled at sector **Kampyr Tepe**, using the Square Euclidean distance and the centroid algorithm

	TRZ373	TRZ385	TRZ377	TRZ381	TRZ380	TRZ383	TRZ235	TRZ386	TRZ229
Fe_2O_3 (%)	3.67	5.96	5.41	5.19	6.61	6.32	5.52	4.91	5.22
Al_2O_3 (%)	10.08	15.03	14.15	14.23	15.56	16.07	15.87	14.57	13.98
TiO_2 (%)	0.46	0.67	0.65	0.66	0.66	0.66	0.67	0.67	0.65
MgO (%)	1.91	3.55	4.95	6	4.45	4.07	2.72	2.76	3.25
CaO (%)	34.50	12.71	9.66	9.95	10.73	10.88	7.73	9.60	8.57
Na_2O (%)	1.16	2.16	3.55	1.73	2.41	1.71	2.12	1.63	2.19
K_2O (%)	2.61	2	3.78	3.72	3.69	3.67	3.42	3.69	3.37
SiO_2 (%)	45.46	57.77	57.68	58.37	55.69	56.42	61.78	61.99	62.60
Ba (ppm)	185	321	427	363	508	495	403	503	578
Rb (ppm)	93	75	120	117	141	145	132	133	115
Th (ppm)	10	17	14	16	14	17	12	13	15
Nb (ppm)	13	17	17	17	18	18	14	18	15
Zr (ppm)	144	179	170	190	166	163	155	198	194
Y (ppm)	17	27	25	25	29	27	24	29	26
Sr (ppm)	803	345	563	376	773	603	433	485	460
Ce (ppm)	33	54	60	58	56	45	64	72	80
Ga (ppm)	13	19	17	17	21	21	17	18	15
V (ppm)	78	98	90	108	114	89	116	96	96
Zn (ppm)	80	95	123	107	117	116	120	106	90
Cu (ppm)	17	28	25	24	25	40	24	24	20
Ni (ppm)	18	50	46	38	48	52	30	32	38
Cr (ppm)	48	70	74	72	76	73	67	68	74

Table 5: The raw normalised chemical compositions of the outliers: TRZ373, TRZ385, TRZ377, TRZ381, TRZ380, TRZ383, TRZ235, TRZ386 and TRZ229 from **Kampyr Tepe**

	KT-1 (n=2)		KT-2 (n= 15)		KT-3 (n= 6)		KT-4 (n= 18)		KT-5 (n= 2)		KT-6 (n= 7)		KT-7 (n= 2)	
	m	sd	m	sd	m	sd	m	sd	m	sd	m	sd	m	sd
Fe_2O_3 (%)	6.36	0.14	6.44	0.26	6.11	0.47	5.64	0.29	5.55	0.29	6.07	0.26	5.49	0.30
Al_2O_3 (%)	16.21	0.14	16.36	0.54	15.64	0.75	14.98	0.51	14.47	0.66	15.83	0.52	14.52	0.46
TiO_2 (%)	0.71	0.01	0.70	0.02	0.66	0.04	0.67	0.02	0.66	0.01	0.70	0.02	0.66	0.04
MgO (%)	3.76	0.16	3.49	0.19	3.41	0.32	3.20	0.23	3.21	0.44	3.32	0.20	3.28	0.04
CaO (%)	10.95	1.35	8.46	1.44	10.08	0.65	9.89	1.46	11.70	0.85	9.77	0.42	10.34	2.89
Na_2O (%)	2.33	0.44	1.55	0.16	1.80	0.20	1.77	0.28	1.96	0.40	1.61	0.19	1.92	0.12
K_2O (%)	2.35	0.07	3.77	0.22	3.87	0.48	3.67	0.35	2.97	0.14	3.55	0.16	3.92	0.28
SiO_2 (%)	57.16	1.42	59.06	1.43	58.26	1.95	60.00	1.35	59.31	2.50	59.00	1.24	59.69	1.66
Ba (ppm)	458	9	511	32	512	41	488	28	431	10	449	34	474	27
Rb (ppm)	98	10	139	7	133	9	123	7	115	6	133	8	124	8
Th (ppm)	15	1	14	1	16	2	13	1	17	0	12	1	13	1
Nb (ppm)	16	1	16	1	16	2	15	1	17	1	16	0	16	1
Zr (ppm)	164	2	161	7	156	9	180	8	195	7	170	11	184	1
Y (ppm)	27	0	26	1	26	2	26	1	29	0	26	1	27	2
Sr (ppm)	379	21	367	78	439	110	425	102	428	4	352	45	492	108
Ce (ppm)	67	5	64	10	62	5	69	5	70	0	53	6	65	2
Ga (ppm)	18	1	19	1	19	2	17	1	18	1	18	1	18	1
V (ppm)	104	2	107	6	103	9	94	7	89	5	97	5	97	8
Zn (ppm)	94	4	104	8	120	14	104	14	90	1	98	8	116	16
Cu (ppm)	30	2	31	3	32	4	26	3	26	3	28	3	24	3
Ni (ppm)	49	1	50	3	48	5	41	2	43	3	42	3	41	2
Cr (ppm)	76	6	78	4	74	3	68	4	65	1	69	2	70	6

Table 6: The mean chemical composition (m) and the standard deviation (sd) of **KT-1**, **KT-2**, **KT-3**, **KT-4**, **KT-5**, **KT-6** and **KT-7** PCRU's from **Kampyr Tepe** using normalised data

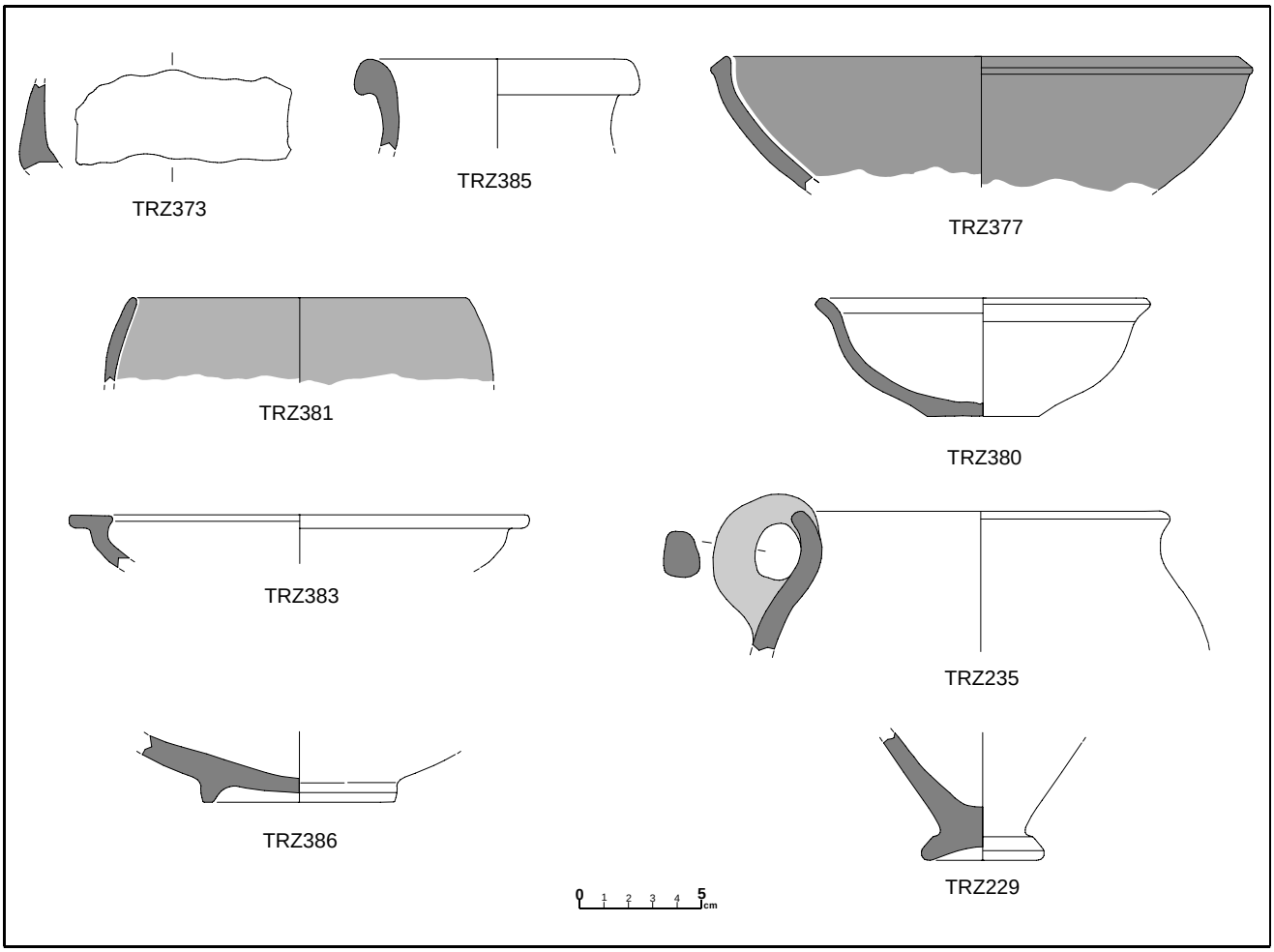

Figure 18: Typology of the ceramic outliers of **Kampyr Tepe**
(TRZ373, TRZ385, TRZ377, TRZ381, TRZ380, TRZ383, TRZ235, TRZ386 and TRZ229)

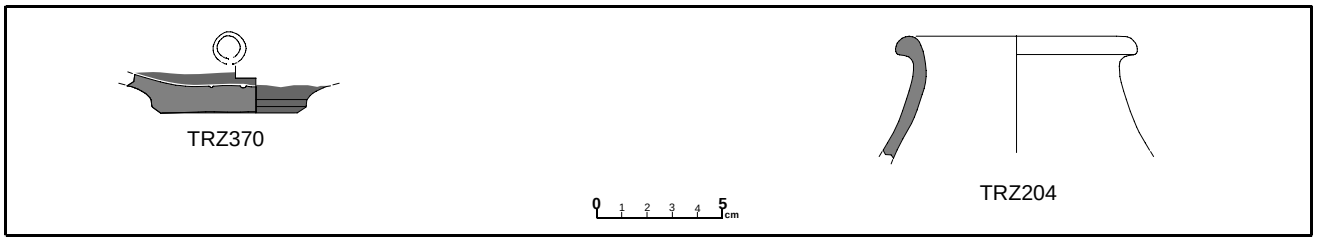

Figure 19a: Typology of the **KT1** group (TRZ370 and TRZ204)

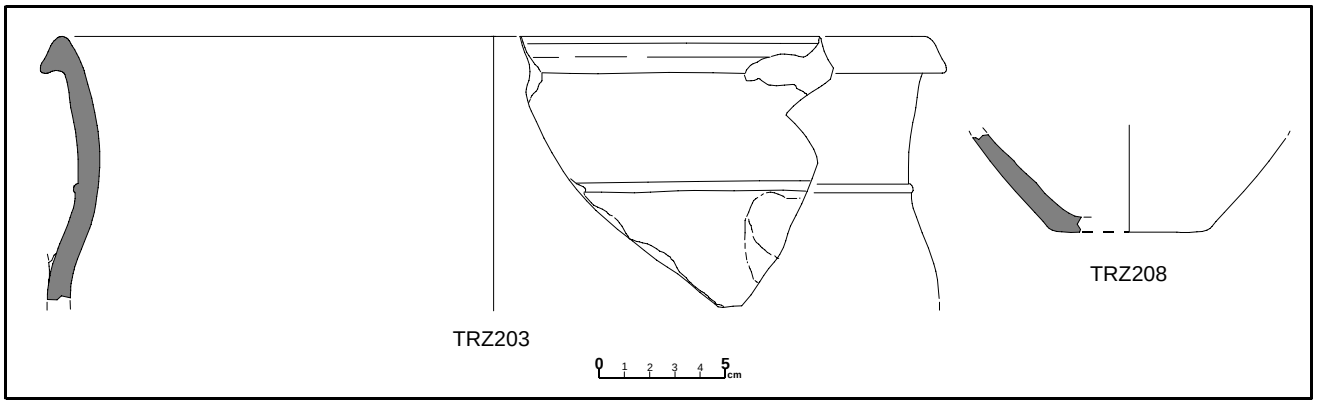

Figure 19b: Typology of the **KT2** group (TRZ203, TRZ208, TRZ209, TRZ210, TRZ211, TRZ212, TRZ213, TRZ214, TRZ215, TRZ219, TRZ222, TRZ228, TRZ230, TRZ232 and TRZ367)

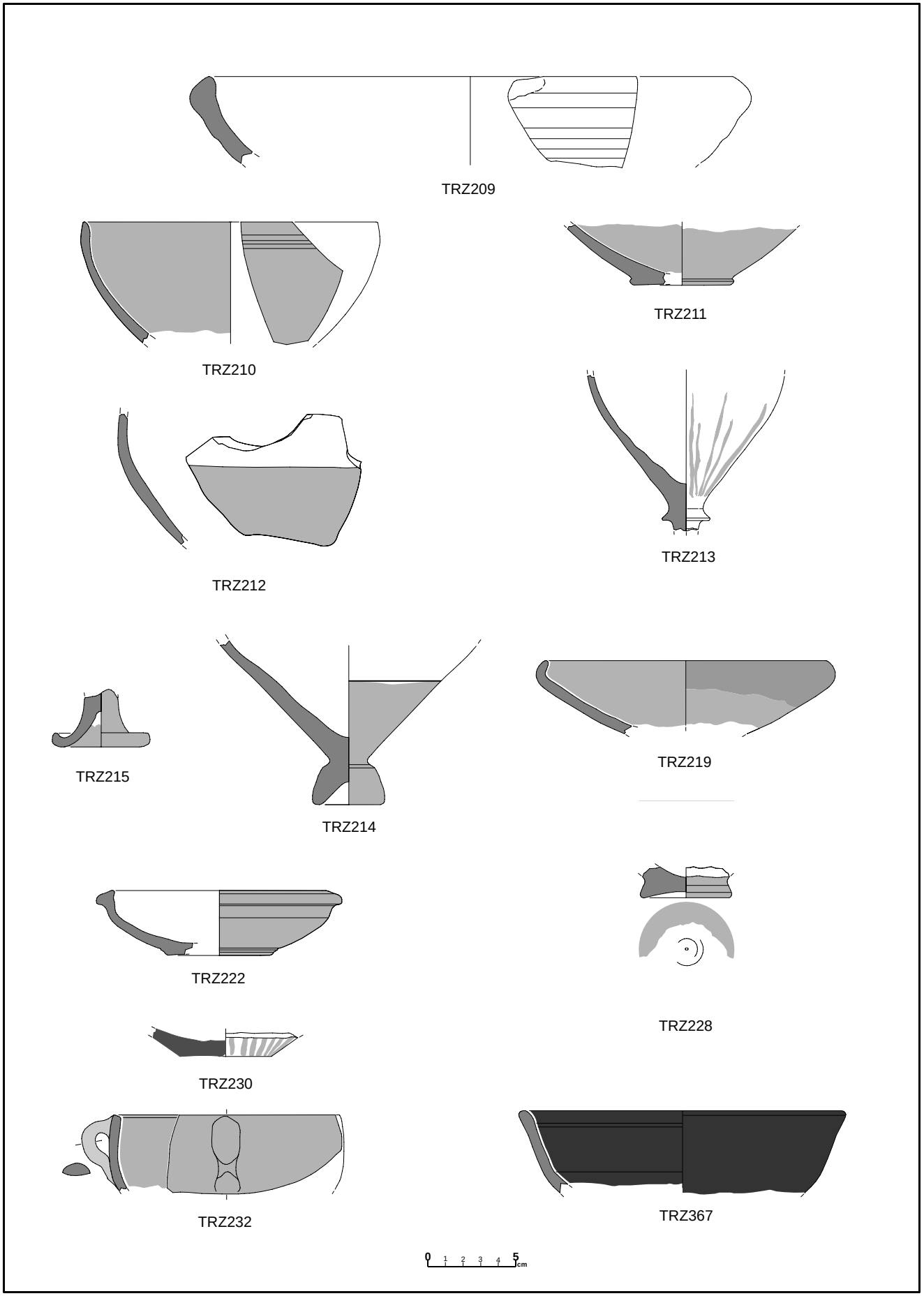

Figure 19b: Typology of the **KT2** group (TRZ203, TRZ208, TRZ209, TRZ210, TRZ211, TRZ212, TRZ213, TRZ214, TRZ215, TRZ219, TRZ222, TRZ228, TRZ230, TRZ232 and TRZ367)

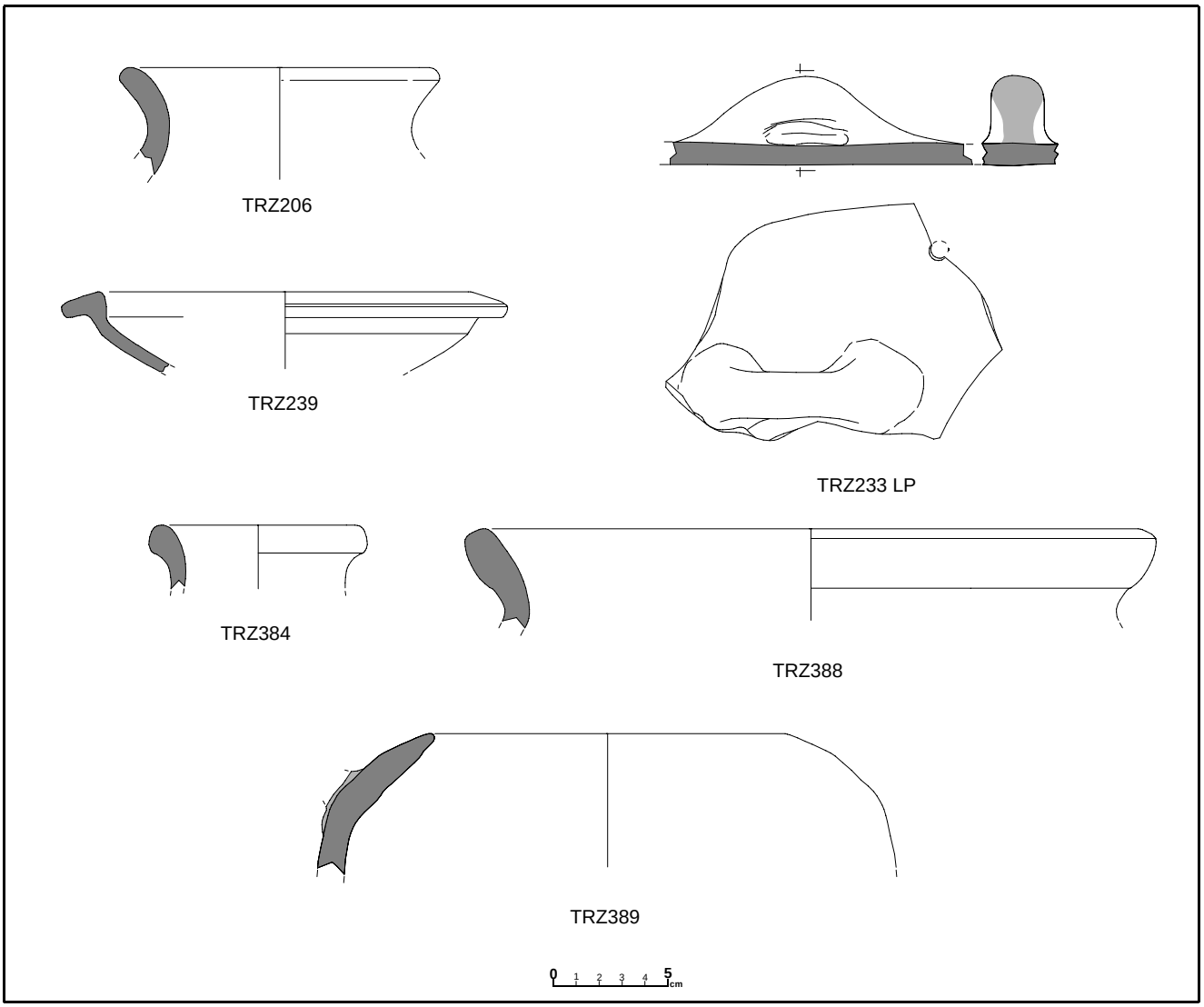

Figure 19c: Typology of the **KT3** group (TRZ206, TRZ233, TRZ239, TRZ384, TRZ388 and TRZ389)

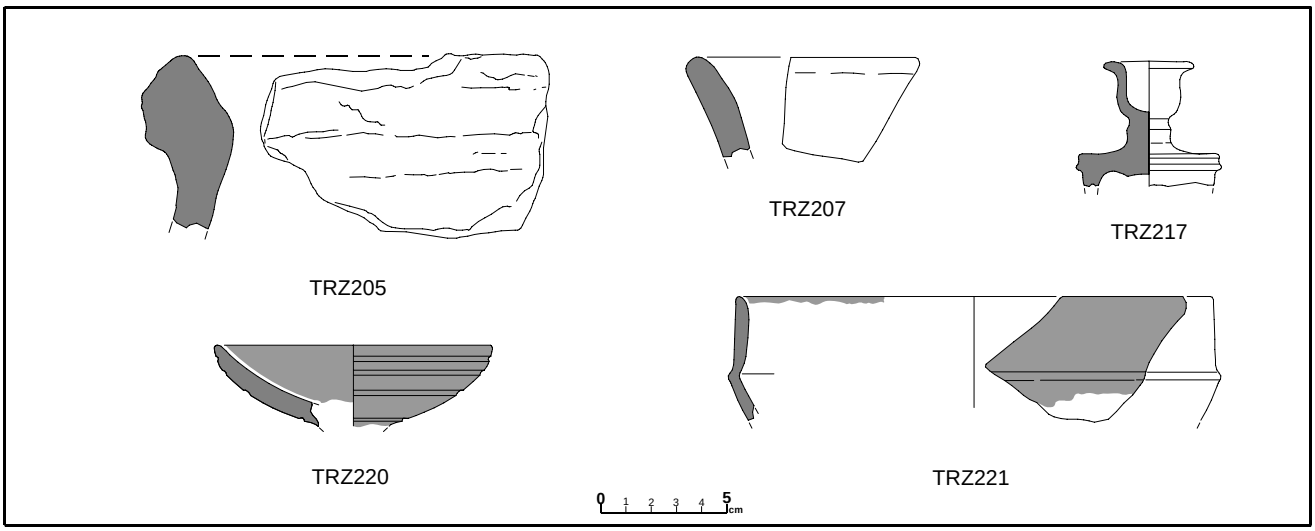

Figure 19d: Typology of the **KT4** group (TRZ205, TRZ207, TRZ220, TRZ221, TRZ224, TRZ225, TRZ226, TRZ227, TRZ231, TRZ234, TRZ236, TRZ238, TRZ240, TRZ241, TRZ242, TRZ372, TRZ376 and TRZ387)

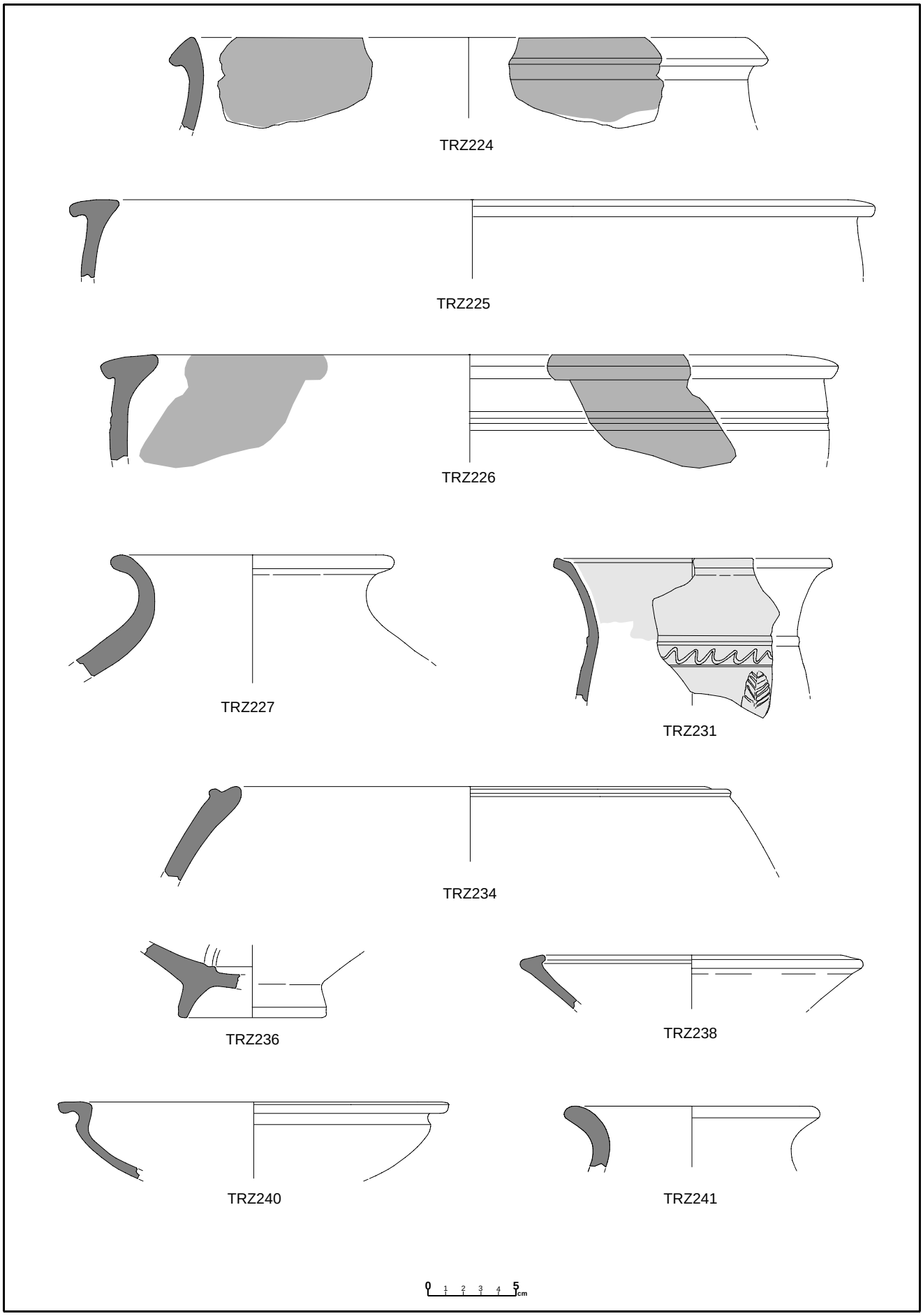

Figure 19d: Typology of the **KT4** group (TRZ205, TRZ207, TRZ220, TRZ221, TRZ224, TRZ225, TRZ226, TRZ227, TRZ231, TRZ234, TRZ236, TRZ238, TRZ240, TRZ241, TRZ242, TRZ372, TRZ376 and TRZ387)

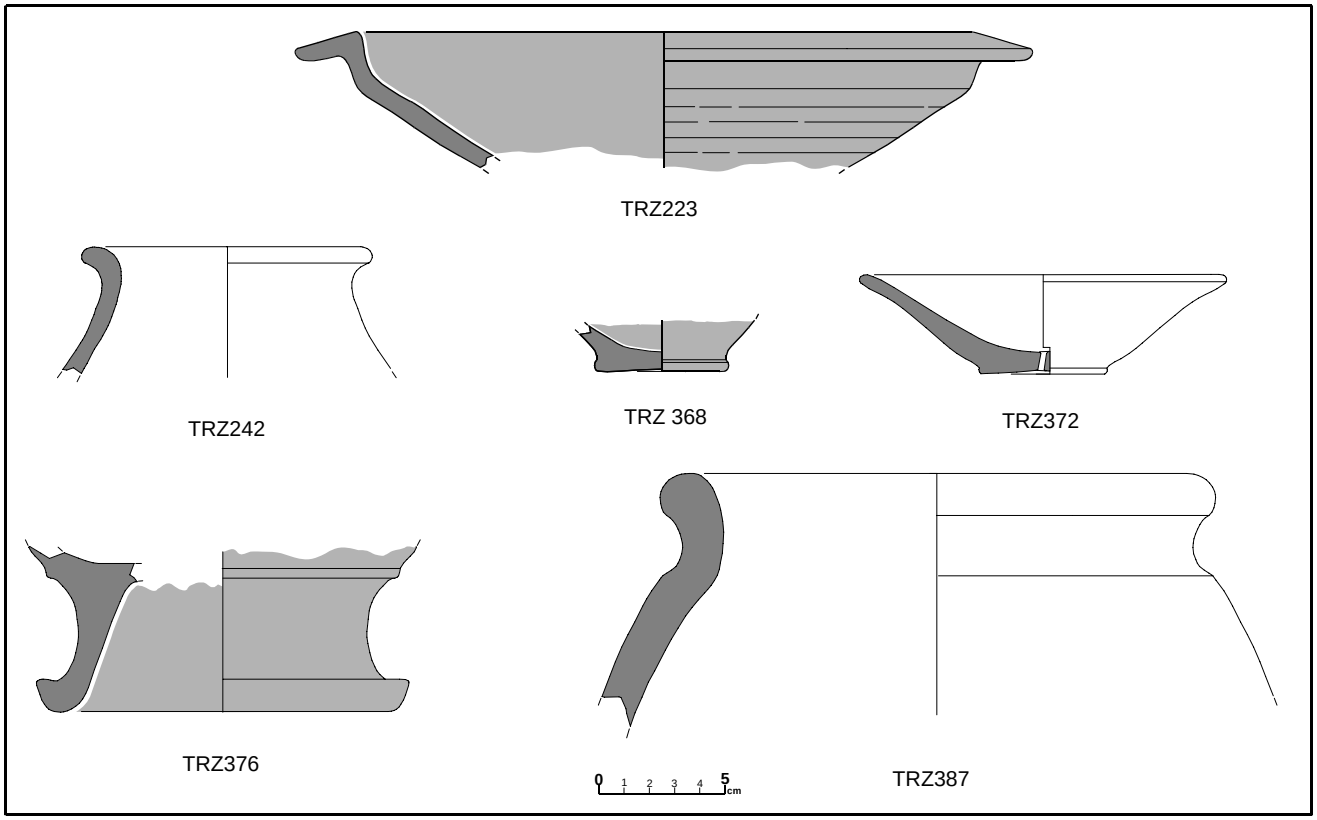

Figure 19d: Typology of the **KT4** group (TRZ205, TRZ207, TRZ220, TRZ221, TRZ223, TRZ224, TRZ225, TRZ226, TRZ227, TRZ231, TRZ234, TRZ236, TRZ238, TRZ240, TRZ241, TRZ242, TRZ368, TRZ372, TRZ376 and TRZ387)

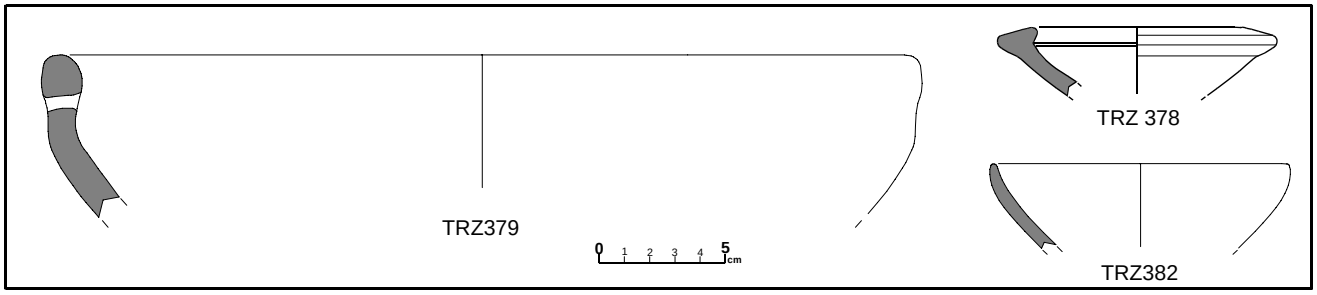

Figure 19e: Typology of the **KT5** group (TRZ378, TRZ379 and TRZ382)

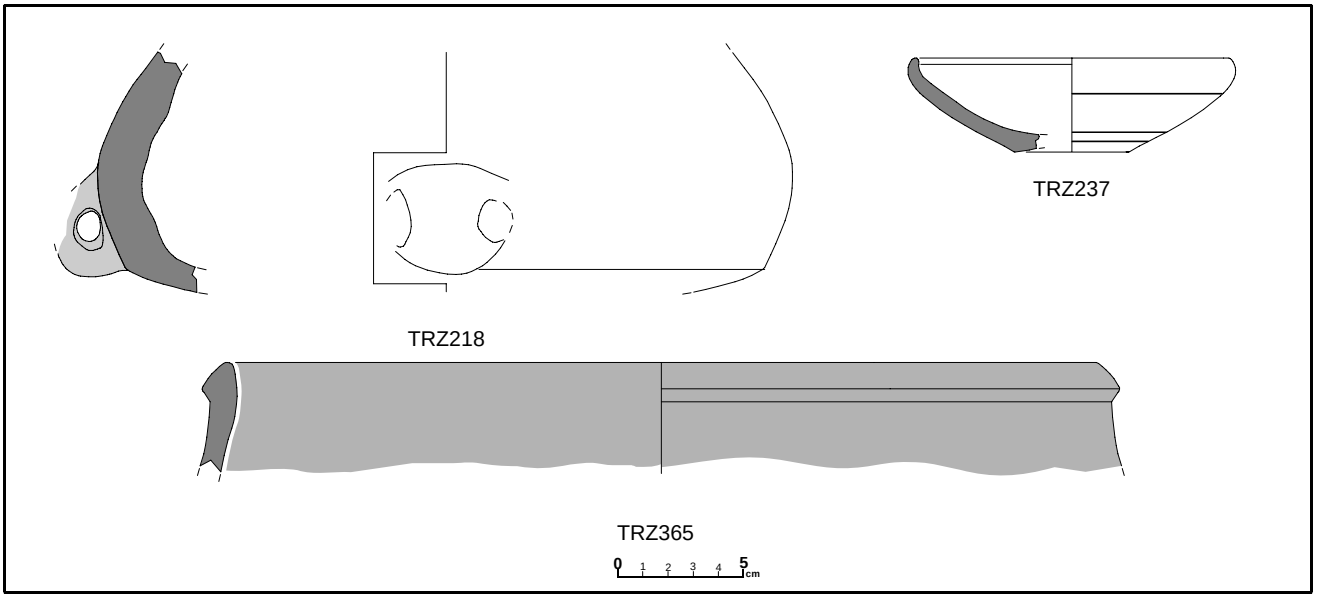

Figure 19f: Typology of the **KT6** group (TRZ218, TRZ237, TRZ365, TRZ366, TRZ269, TRZ371 and TRZ375)

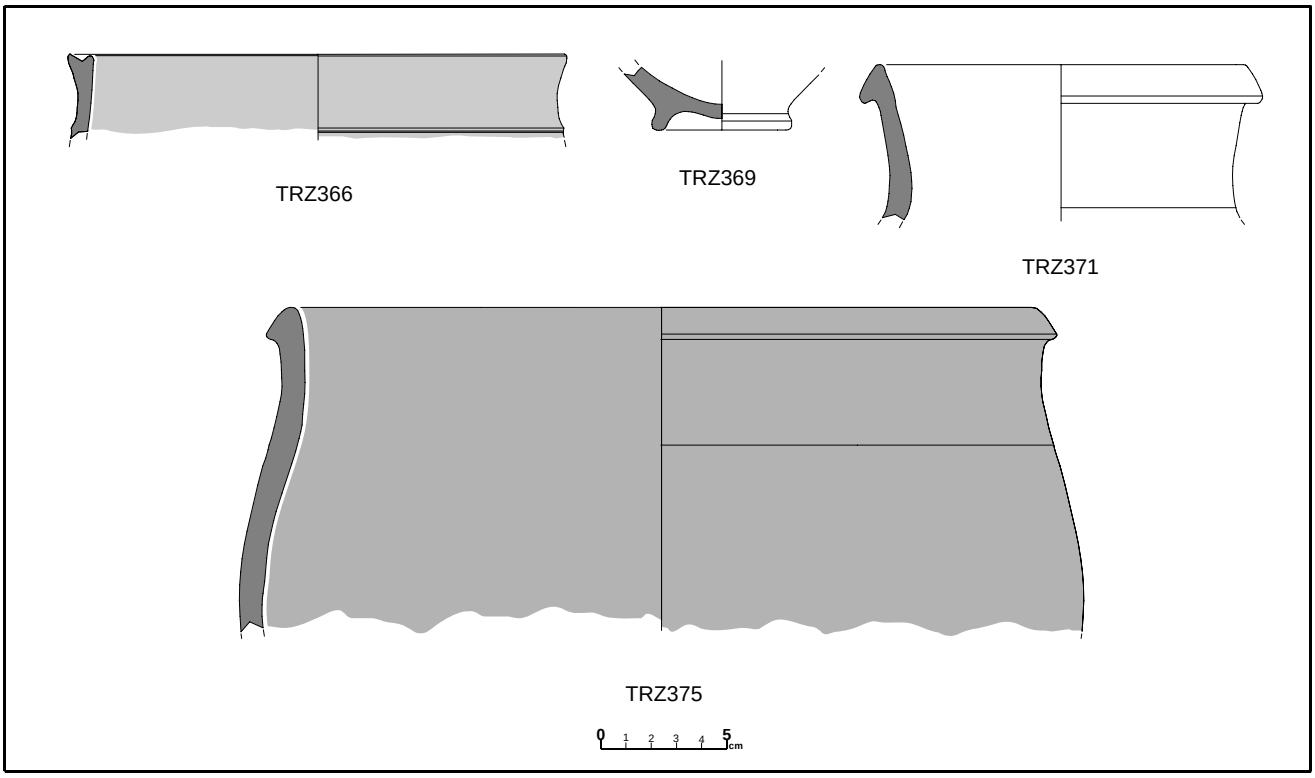

Figure 19f: Typology of the **KT6** group (TRZ218, TRZ237, TRZ365, TRZ366, 269, TRZ371 and TRZ375)

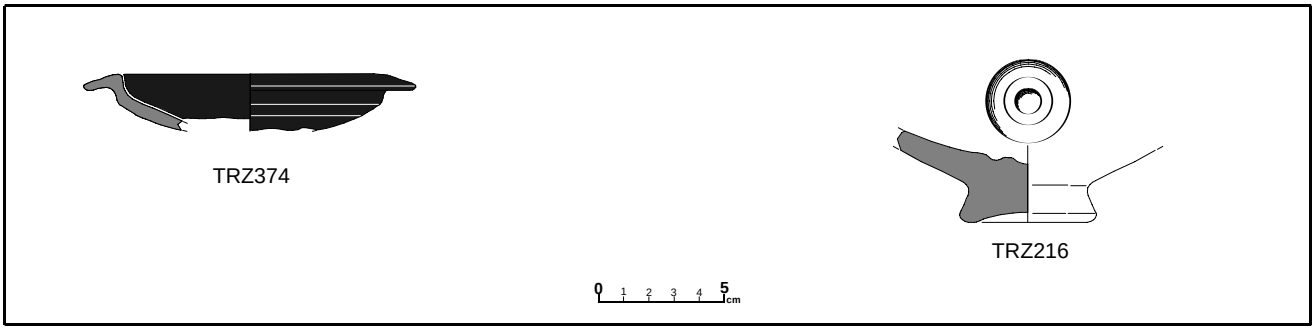

Figure 19g: Typology of the **KT7** group (TRZ216, TRZ374)

5.2.2. Petrographical composition (thin section analysis)

Petrographical analysis has been carried out upon 27 ceramics from **Kampyr Tepe.** The cooking ware **TRZ235**, which is a chemical outlier, is a medium-coarse calcareous fabric. Clay matrix: Fe-rich (+ Ca-rich clay lumps; poorly vitrified). Groundmass (relatively abundant): quartz, muscovite, opaques (dominant), micritic calcite, (accessory). Coarser inclusions (≤ 0.5 mm): moderately abundant, sub-rounded to sub-angular, moderately to poorly sorted, open-spaced (at times single-spaced), unimodal grain-size distribution. Predominant to dominant: quartz, biotite and muscovite; Dominant to frequent: quart-mica schist, mica schist and plagioclase crystals; Common to few: opaques, k-feldspar, amphiboles; Few to occasional: epidote, garnet, calcareous microfossils and micritic calcite. Micro-voids and meso-channels are relatively abundant (Figure 20).

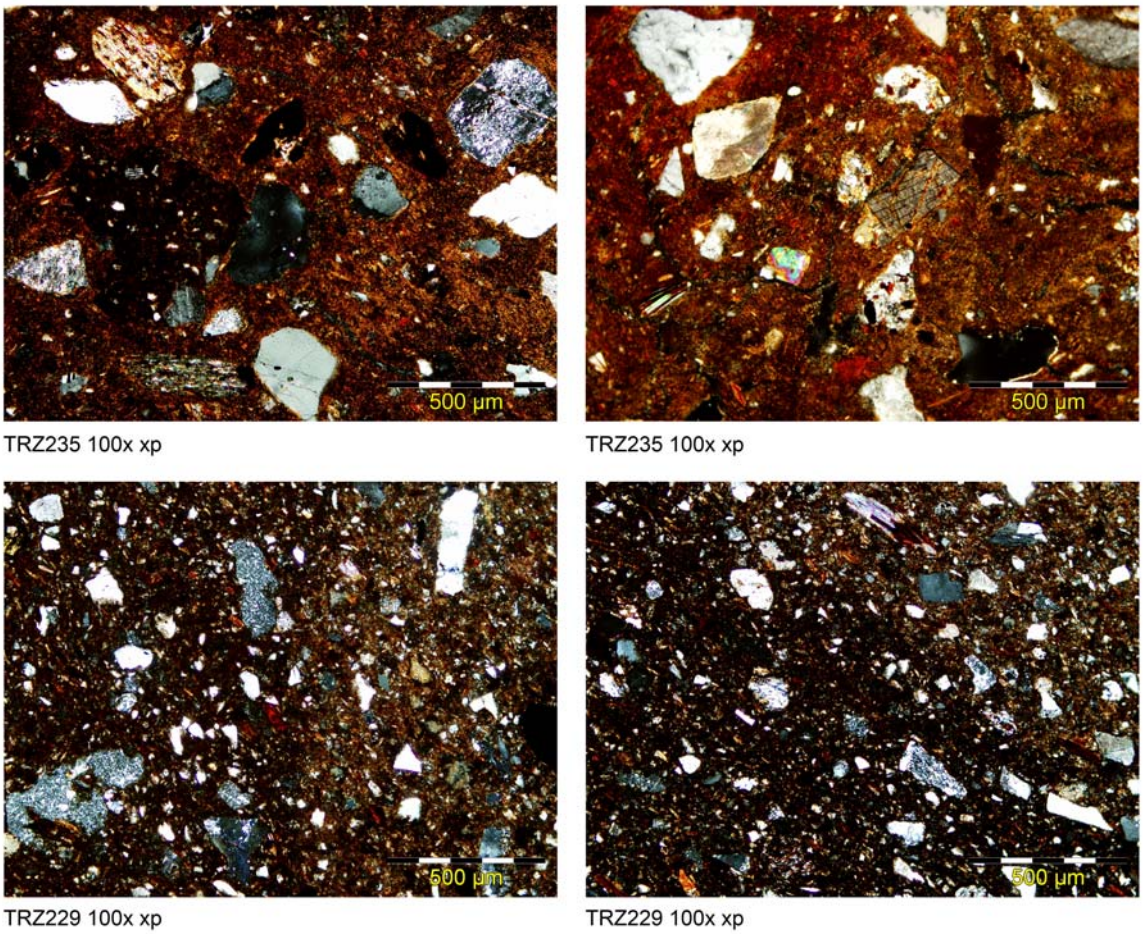

Figure 20: Microphotographs by crossed polars (xp) of the ceramics outliers TRZ235 and TRZ229 from **Kampyr Tepe**

The base of a bowl or cup **TRZ229**, which is a chemical outlier, has medium fine fabric. Clay matrix: Fe-rich (+ Ca-rich nodules of micritic calcite), semi-vitrified. Groundmass (abundant): quartz, muscovite (dominant). Coarser inclusions (< 0.5 mm): abundant but generally fine, sub-rounded to sub-angular, well sorted, unimodal grain-size distribution (Figure 20). Predominant to dominant: quartz, muscovite, micritic calcite, chert; Dominant to frequent: quartz-mica schist rocks; Dominant to frequent: k-feldspar, plagioclase; Common to few: amphibole, serpentinite. The carbonatic component must be originated by the semi-decomposition of calcareous microfossils during firing.

The bowl **TRZ216** from **KT-7** is painted with a black slip. In petrographical terms, it presents more fine fraction and less and smaller coarse fraction than TRZ235. Clay matrix is Ca-rich (semi-vitrified). Groundmass (abundant): quartz, micritic calcite, opaques (dominant), muscovite and amphibole (accessory). Coarser inclusions (≤ 0.5 mm): scarce, sub-angular to sub-rounded, well sorted, open-spaced (at

times single-spaced), unimodal grain-size distribution (Figure 20). Predominant to dominant: quartz, calcareous fossils, quartz-mica schist rocks; Dominant to frequent: plagioclase crystals, k-feldspar, quartzite, biotite and muscovite; Common to few: amphibole, epidote, calcite (sparite); Few to occasional: chert, garnet, pyroxene, gypsum. Voids are rare, mainly forming meso-vughs.

Petrographic fabric ***F-KT-A***: (**KT-2** and **KT-3** PCRU's)

The petrographical analysis of some shards from the chemical groups **KT-2** and **KT-3** reveals that they have a similar petrographical composition. However, the cooking ware **TRZ233** must be considered a subfabric because of differences in percentage and dimensions of the coarse fraction. The rest of the individuals (common wares TRZ203, TRZ214, TRZ219, TRZ222, TRZ232 and TRZ239) can be grouped in the mean petrographical fabric, ***F-KT-A*** (Figure 21). Clay matrix: Fe-rich (+ Ca-rich in TRZ203 and TRZ239), low to semi-vitrified. Groundmass (very scarce and very fine): quartz, muscovite (dominant). Coarser inclusions (generally ≤ 0.5 mm): scarce, sub-angular to sub-rounded, well sorted, open-spaced (at times single-spaced), bimodal grain-size distribution. Predominant to dominant: quartz, muscovite, mica-esquist and quartz-mica schist rocks; Dominant to frequent: granitic rock fragments, sandstone; Common to few: micritic calcite, plagioclase, amphibole, biotite and muscovite; Few to occasional: epidote, serpentinite, chert, basalt, garnet, opaques. Concerning TRZ203 and TRZ239, nodules of micritic calcite derives of calcareous microfossils decomposed during firing. Secondary calcite crystals have been observed inside the voids.

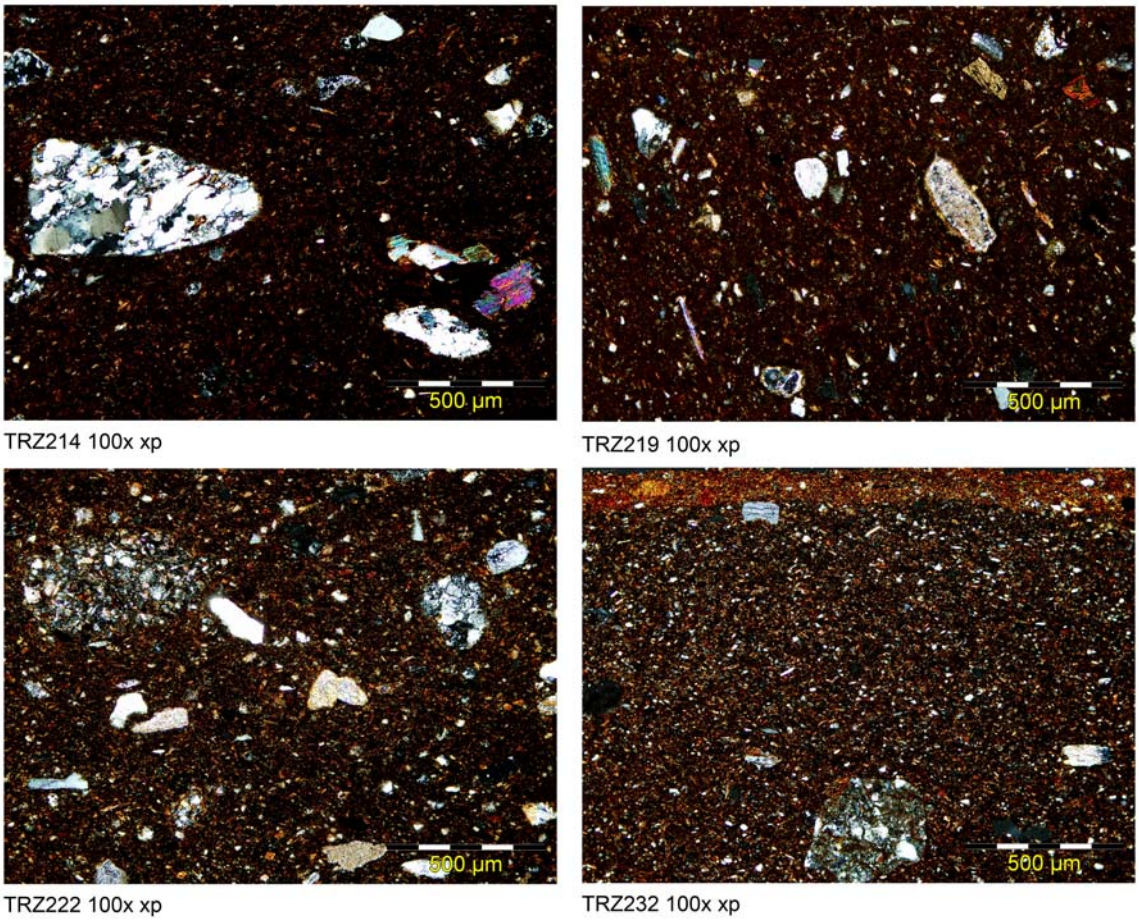

Figure 21: Microphotographs by crossed polars (xp) of the ceramics TRZ203, TRZ214, TRZ219, TRZ222, TRZ232, TRZ233 and TRZ239 belonging to fabric **F-KT-A**

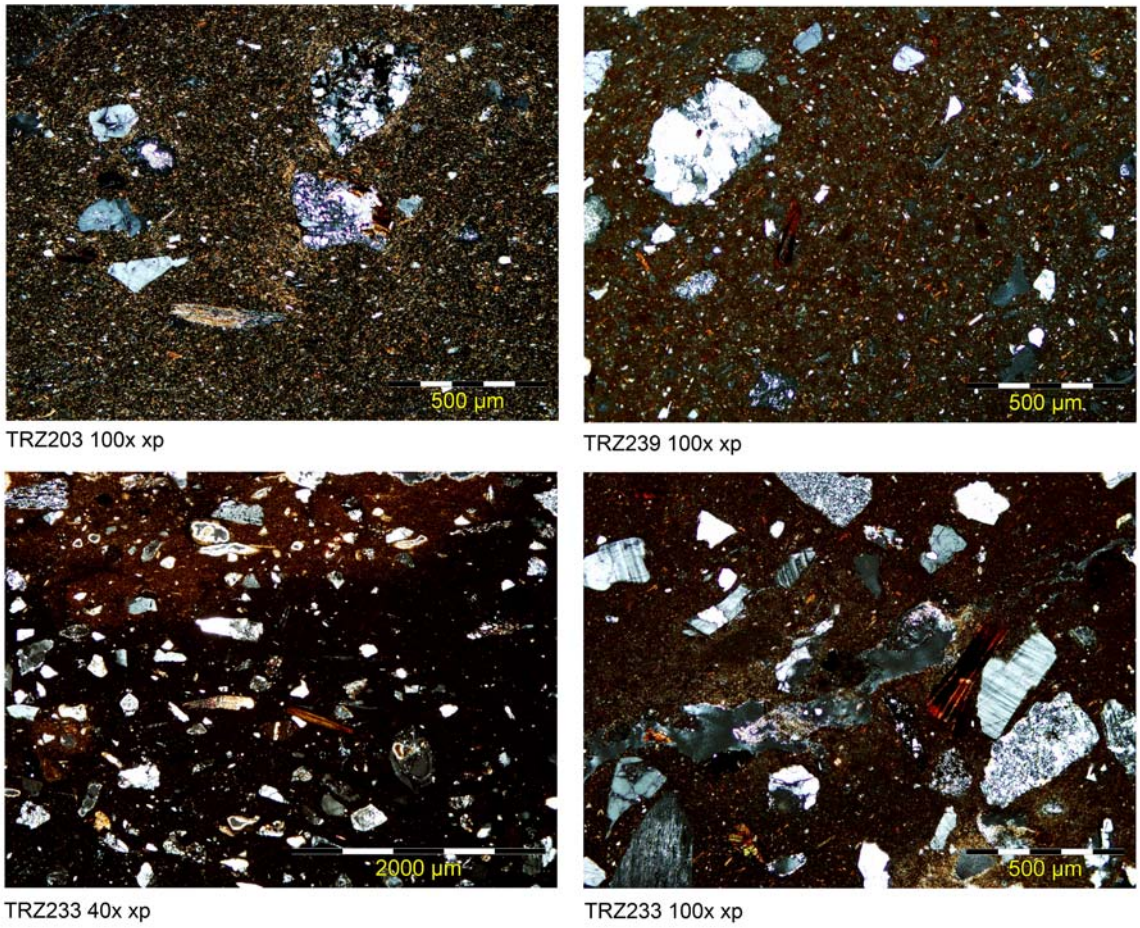

Figure 21 (b): Microphotographs by crossed polars (xp) of the ceramics TRZ203, TRZ214, TRZ219, TRZ222, TRZ232, TRZ233 and TRZ239 belonging to fabric **F-KT-A**

The cooking ware **TRZ233** associated to the chemical subgroup **KT-3** corresponds to a medium-coarse fabric. Clay matrix and micromass composition is very similar to the ceramics of ***F-KT-A*** fabric. However, non-plastic inclusions in **TRZ233** are more abundant and bigger. Clay matrix: Fe-rich (with few Ca-rich clay lumps; poorly vitrified). Micromass is heterogeneous, darker on the margins of the vessel walls. Groundmass (scarce and very fine): quartz, muscovite, opaques (dominant). Coarser inclusions (≤ 0.5 mm): moderately abundant, sub-rounded to sub-angular, moderately to poorly sorted, single-spaced (at times open-spaced or in contact), bimodal grain-size distribution. Predominant to dominant: quartz, plagioclase, muscovite and quartz-mica schist; Dominant to frequent: mica-schist, sandstones, amphiboles; Common to few: cherts, k-feldspars and epidote; Few to occasional: basalt, serpentinite, garnet, opaques. Porosity is basically constituted by few meso-vesicles and meso-vughs (Figure 21).

Petrographic fabric ***F-KT-B***: (**KT-4**, **KT-5** and **KT-6** PCRU's)

The rest of the analysed shards by thin section (TRZ223, TRZ224, TRZ225, TRZ226, TRZ227, TRZ231, TRZ236 and TRZ240), which belong to **KT-4** chemical group, can be assigned to the same petrographic fabric (***F-KT-B***) according to the similarity in composition, frequency and size of non plastic inclusions (Figure 22). Nevertheless, differences in the calcareous component of ceramics lead to distinguish two subfabrics:

- *F-KT-B1* (TRZ223, TRZ224, TRZ225, TRZ227, TRZ231 and TRZ240): Clay matrix: Fe-rich (+ Ca-rich nodules of micritic calcite), semi-vitrified and high vitrified in TRZ231. Groundmass (abundant): quartz, muscovite (dominant), amphibole, micritic calcite (accessory). Coarser inclusions (≤ 0.5 mm): moderately abundant, sub-rounded to sub-angular, well sorted, single-spaced, bimodal grain-size distri-

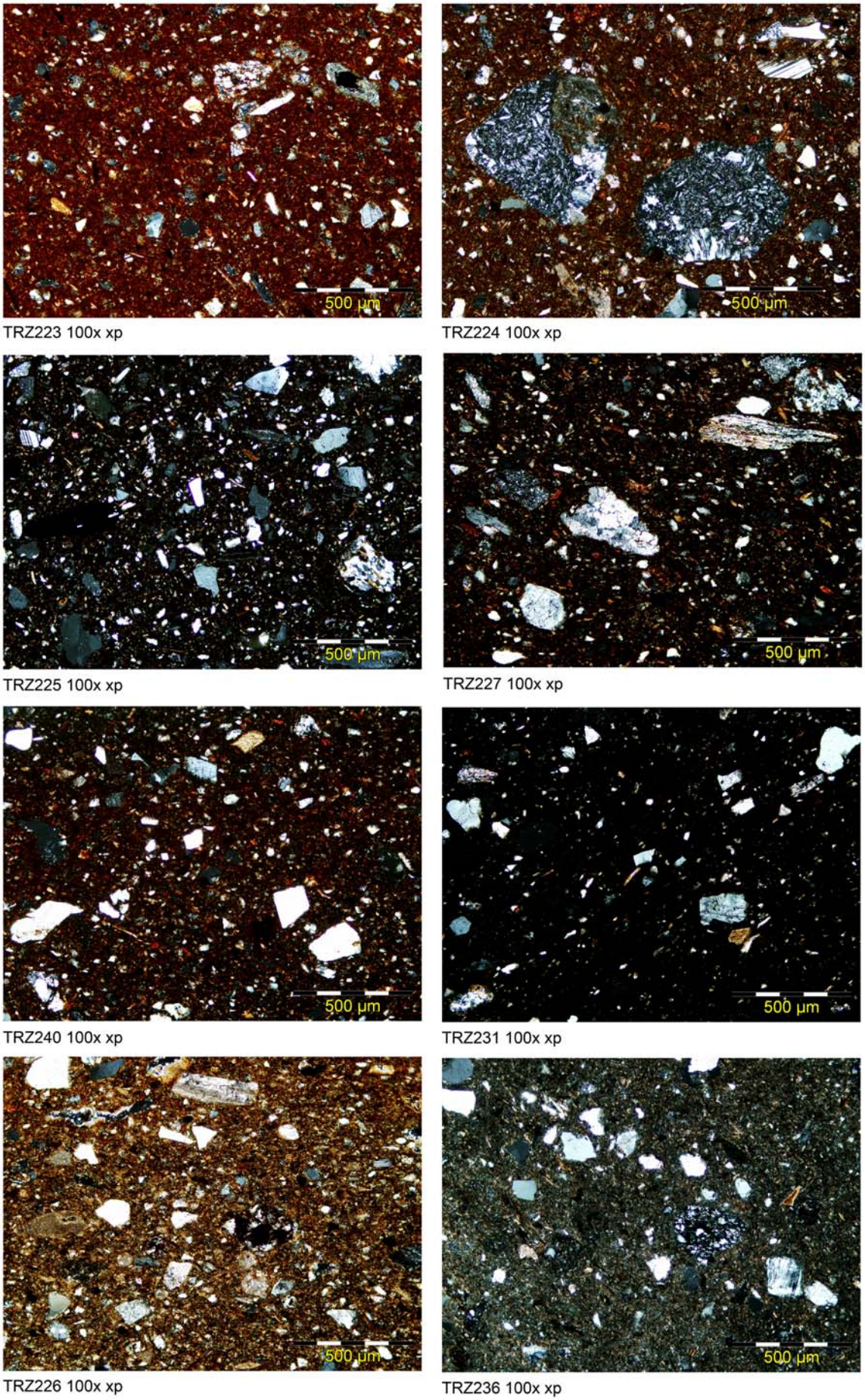

Figure 22: Microphotographs by crossed polars (xp) of the ceramics TRZ223, TRZ224, TRZ225, TRZ226, TRZ227, TRZ231, TRZ236 and TRZ240 belonging to fabric **F-KT-B**

bution. Predominant to dominant: quartz, plagioclase, muscovite; Dominant to frequent: acid rocks, quartz-mica schist, mica-schist; Common to few: amphiboles, claystones, chert, micritic calcite; Few to occasional: epidote, basalt, pyroxene, garnet, opaques. Voids are scarce, predominantly micro and meso-vesicles and meso-vughs.

- *F-KT-B2* (TRZ226 and TRZ236): Clay matrix: Ca-rich (semi-vitrified). Groundmass (abundant): quartz, micritic calcite (dominant), biotite, opaques (accessory). Coarser inclusions (≤ 0.5 mm): moderately abundant, sub-rounded to sub-angular, poorly sorted, single-spaced, bimodal grain-size distribution. Predominant to dominant: quartz, micritic calcite; Dominant to frequent: quartz-mica schist and mica-schist; Common to few: plagioclase, k-feldspar, chert, amphibole; Few to occasional: epidote, sparite calcite, pyroxene, biotite and muscovite, opaques.

5.2.3. Mineralogical composition (XRD analysis)

According to the mineralogical analysis, the 2 individuals representing the group **KT-1** (TRZ204 and TRZ370) are over fired ceramics. Their EFT can be estimated around 1000-1050/1110°C, due to the advanced decomposition of illite-muscovite and gehlenite and the total decomposition of calcite together to the increment of the pyroxenes (Figure 23). TRZ370 is also characterised by the presence of analcime crystals as secondary mineral phase due to post-depositional alteration and/or contamination processes.

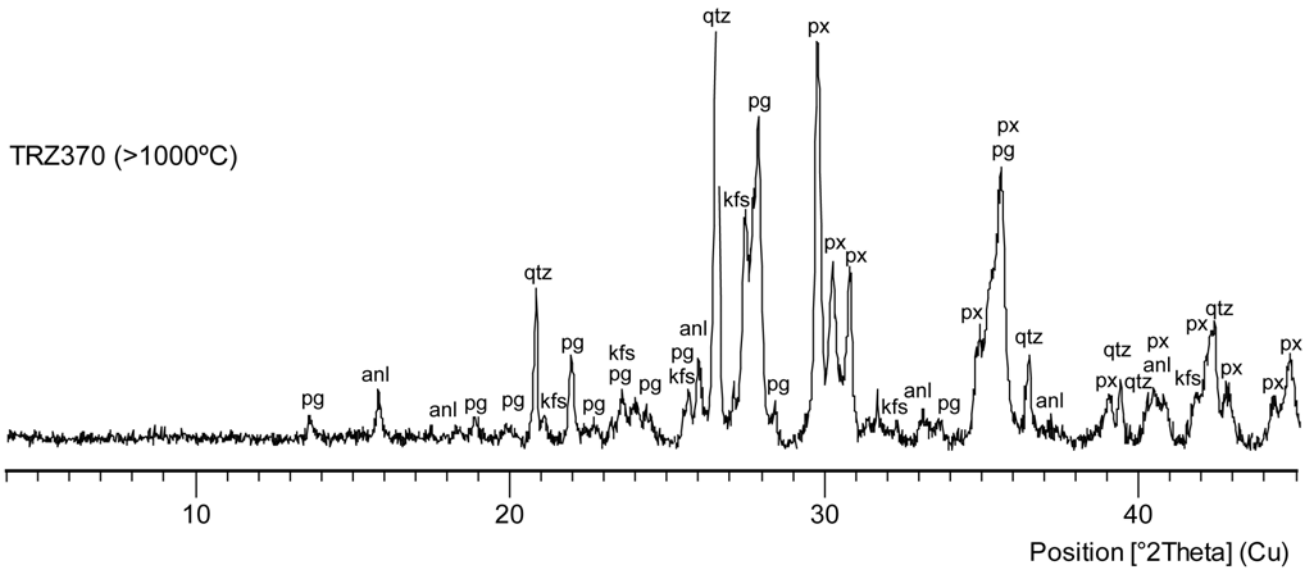

Figure 23: Diffractograms of the individual TRZ370 representing the chemical group **KT1**; anl: analcime, kfs: k-feldspar, pg: plagioclase, px: pyroxene, qtz: quartz

The 15 individuals that belong to **KT-2** correspond to four different mineralogical categories, associated to four different Equivalent Firing Temperatures (EFT's). The first category's EFT is estimated between 800-850°C, which correspond to low firing temperature, according to the presence of primary mineral phases and the total absence of clear firing phases and it contains the individuals: TRZ203, TRZ210, TRZ222 and TRZ228 (Figure 24a). In the second category, illite-muscovite and alkaline feldspars coexist with gehlenite and pyroxene which situates the EFT of this category around 850-950°C. This category is configured by: TRZ209, TRZ211, TRZ212, TRZ214, TRZ219 and TRZ232 (Figure 24b). In the third category (TRZ213, TRZ215 and TRZ228), the development of the firing phases is much more advanced but the existence of illite-muscovite in the diffractograms of the individuals in this category indicates a EFT between 950°C and 1000°C (Figure 24c). Finally, the last mineralogi-

cal category's ETF, estimated in the range of 1000-1050/1110°C, is represented by TRZ230 and TRZ367 shards (Figure 24d). It is characterised by the advanced decomposition of illite-muscovite and gehlenite and the total decomposition of calcite with the parallel clear increment of the pyroxenes.

Three different mineralogical categories can be observed in **KT-3**. Two shards (TRZ388 and TRZ389)

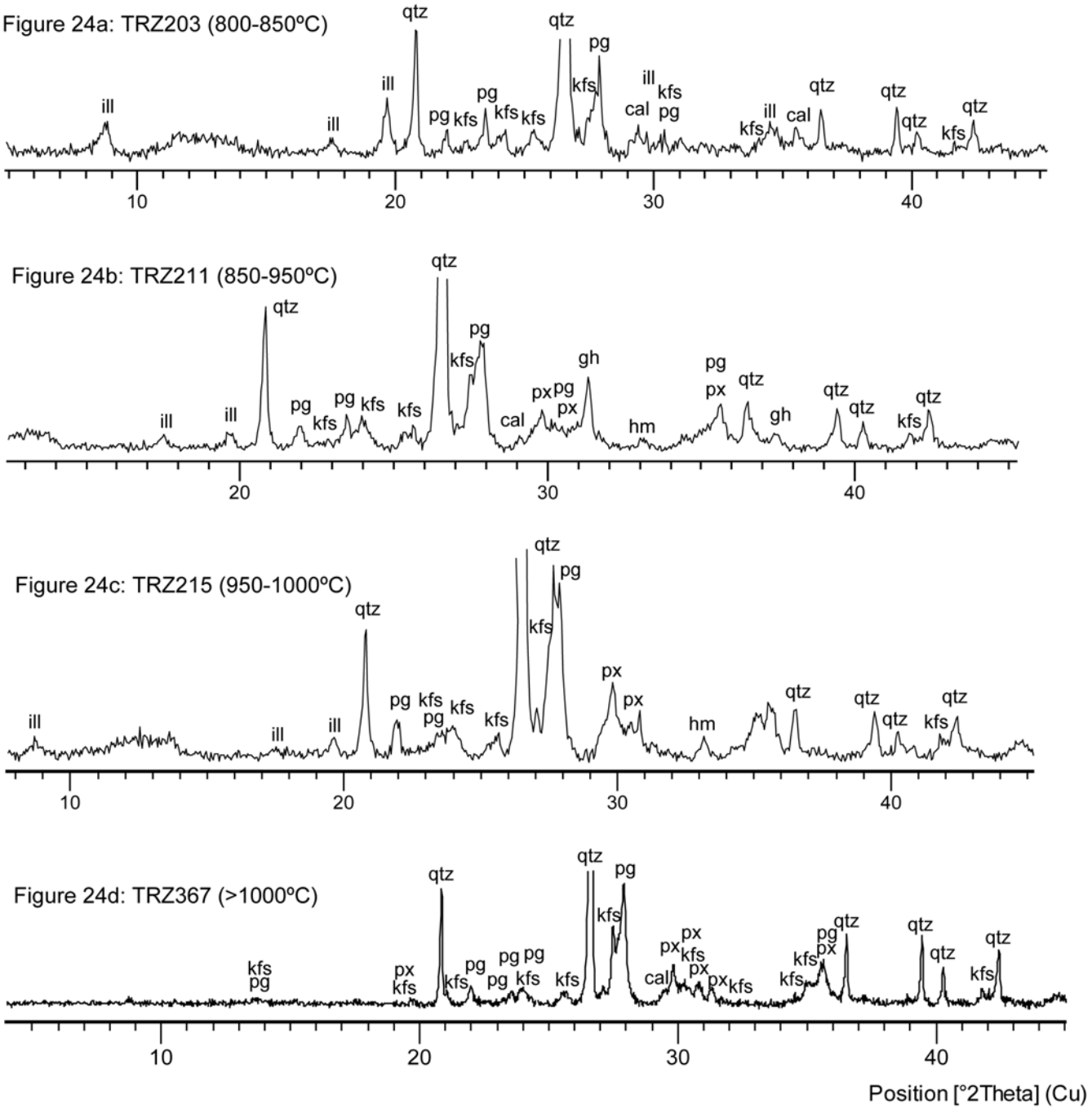

Figure 24: Diffractograms of the individuals TRZ203, TRZ211, TRZ215 and TRZ367 representing the chemical group **KT2**; cal: calcite, gh: gehlenite, hm: hematite, ill: illite-muscovite, kfs: k-feldspar, pg: plagioclase, px: pyroxene, qtz: quartz

present only primary phases (quartz, calcite, illite-muscovite, k-feldspar, plagioclase and few hematite) and EFT can be estimated around 800-850ºC (Figure 25a). TRZ206 and TRZ239 are characterised by the simultaneous presence of primary and firing phases (Figure 25b), which indicates relatively high firing temperature (850-900ºC). Finally, the diffractograms of TRZ233 and TRZ384 are similar to the previous mineralogical category but illite-muscovite shows advanced decomposition, whereas firing phases

are more developed (Figure 25c). Because of that, the EFT has been estimated around 950-1000°C.

Regarding the 20 ceramics from **KT-4**, four different mineralogical categories have been identified.

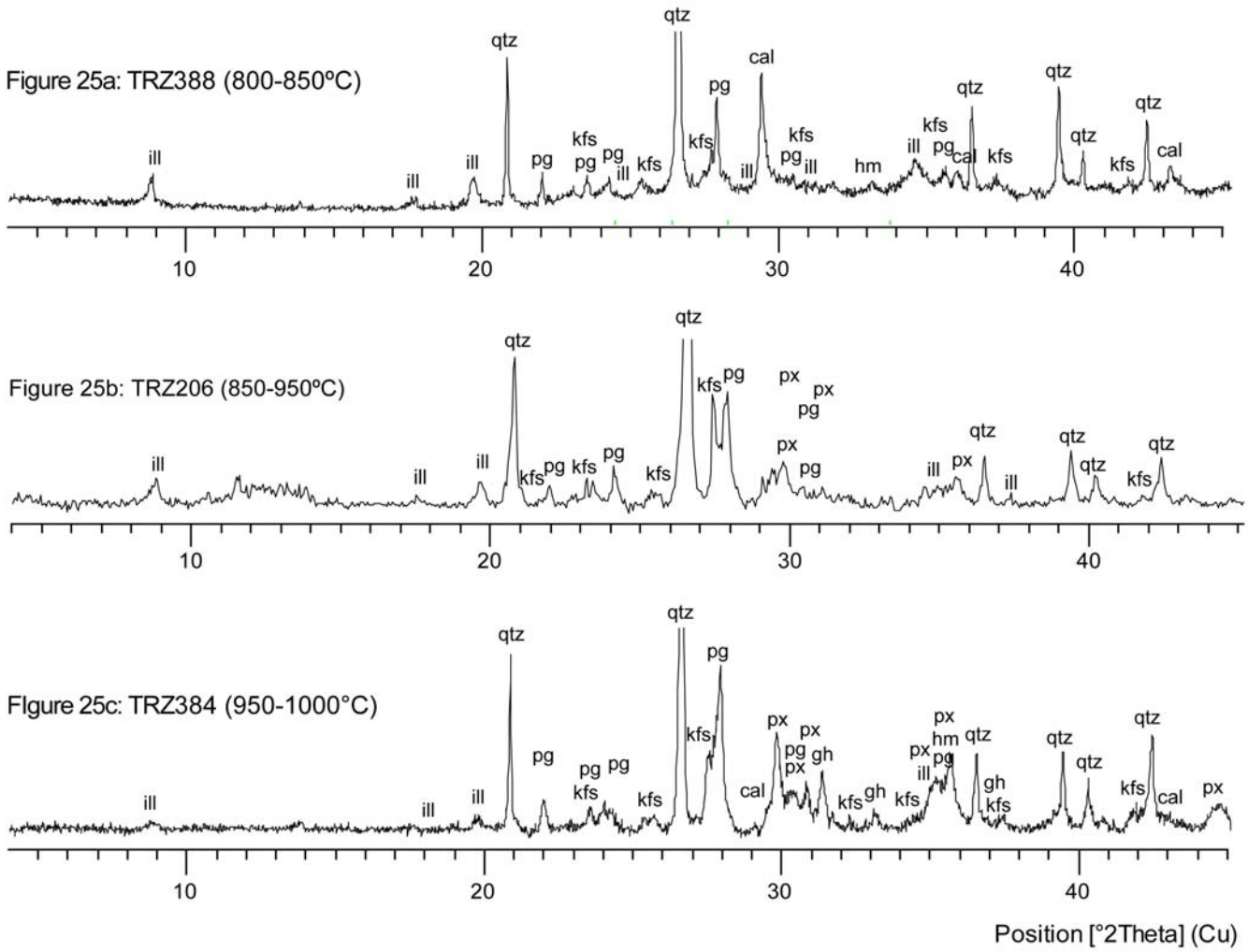

Figure 25: Diffractograms of the individuals TRZ388, TRZ206 and TRZ384 representing the chemical group **KT3**; cal: calcite, gh: gehlenite, hm: hematite, ill: illite-muscovite, kfs: k-feldspar, pg: plagioclase, px: pyroxene, qtz: quartz

Ceramics TRZ205, TRZ225, TRZ226 TRZ227 and TRZ387 have been fired at low temperature (800-850°C) owing to the presence of primary mineral phases and the total absence of clear firing phases (Figure 26a). In TRZ217, TRZ221, TRZ224, TRZ236 TRZ238 TRZ372 and TRZ376 ceramics, the coexistence of illite-muscovite and alkaline feldspars together with gehlenite and pyroxene leads to estimate a EFT around 900-950°C (Figure 26b). The development of the firing phases and the presence of illite-muscovite for TRZ207, TRZ220, TRZ223, TRZ234 and TRZ242 points to firing range around 950-1000°C (Figure 26c). Finally, the ETF of TRZ231 and TRZ241 can be estimated about 1000-1050/1110°C because of the advanced decomposition of illite-muscovite and gehlenite, with the parallel clear increment of the pyroxenes. Both can be considered as over fired ceramics.

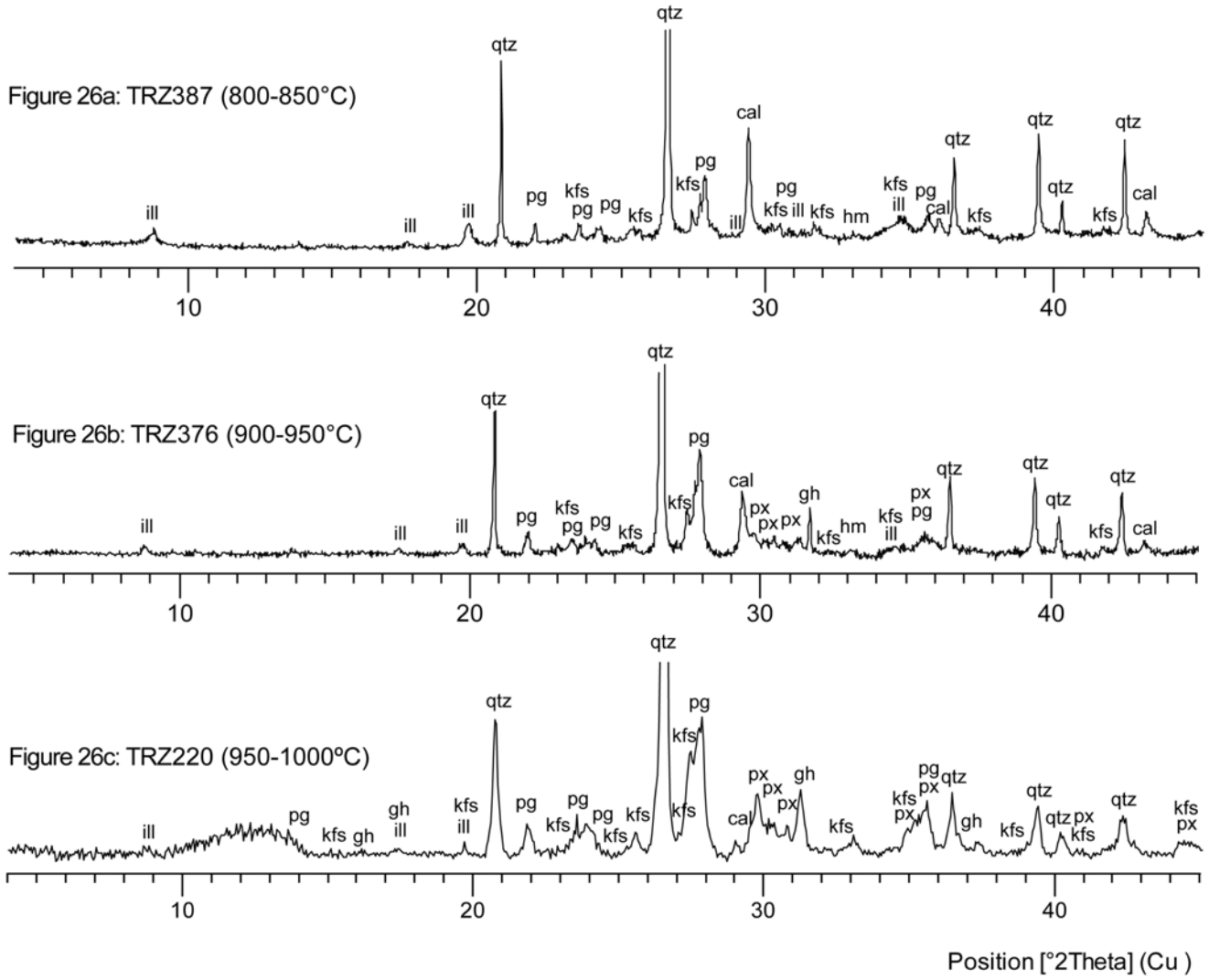

Figure 26: Diffractograms of the individuals TRZ387, TRZ376 and TRZ220 representing the chemical group **KT4**; cal: calcite, gh: gehlenite, hm: hematite, ill: illite-muscovite, kfs: k-feldspar, pg: plagioclase, px: pyroxene, qtz: quartz

The shards classified in **KT-5** are high fired ceramics (TRZ379 and TRZ382). However, a small percentage of illite-muscovite and calcite are still present in TRZ382 together with other primary phases (quartz, k-feldspar and plagioclase). Due to that the EFT of TRZ382 (Figure 27a) has been estimated around 950-1000ºC. The total decomposition of illite-muscovite in TRZ379 leads to consider an EFT higher than 1000ºC (Figure 27b).

KT-6 is separated into three different mineralogical categories. TRZ369 and TRZ375 are low fired (800-850ºC), because of the merely presence of primary phases (quartz, calcite, illite-muscovite, k-feldspar and plagioclase) (Figure 28a). TRZ365 and TRZ366 can be attributed to a slightly higher EFT (850/900-950ºC) due to the apparition of incipient firing phases (pyroxene, gehlenite and hematite) (Figure 28b). Finally, the total decomposition of illite-muscovite and the increment of the firing phases in TRZ371 indicate a temperature in the range of 1000-1050°C (Figure 28c).

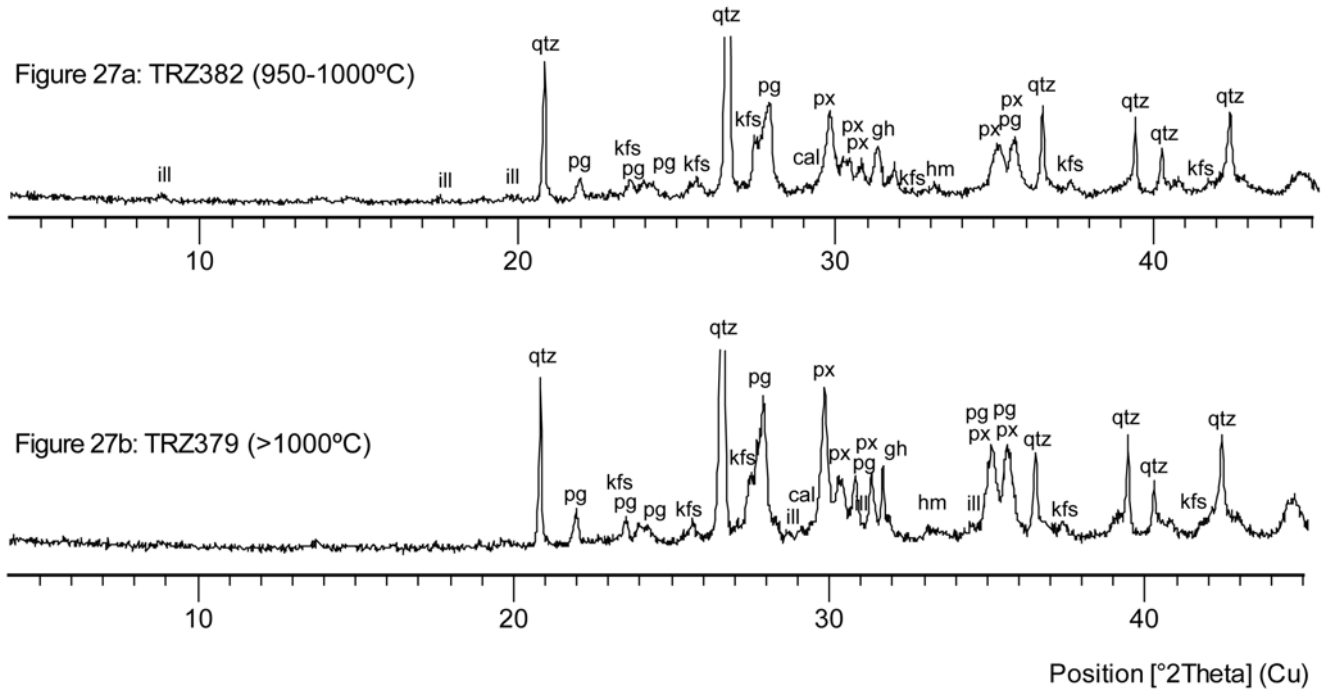

Figure 27: Diffractograms of the individuals TRZ382 and TRZ379 representing the chemical group **KT5**; cal: calcite, gh: gehlenite, hm: hematite, ill: illite-muscovite, kfs: k-feldspar, pg: plagioclase, px: pyroxene, qtz: quartz

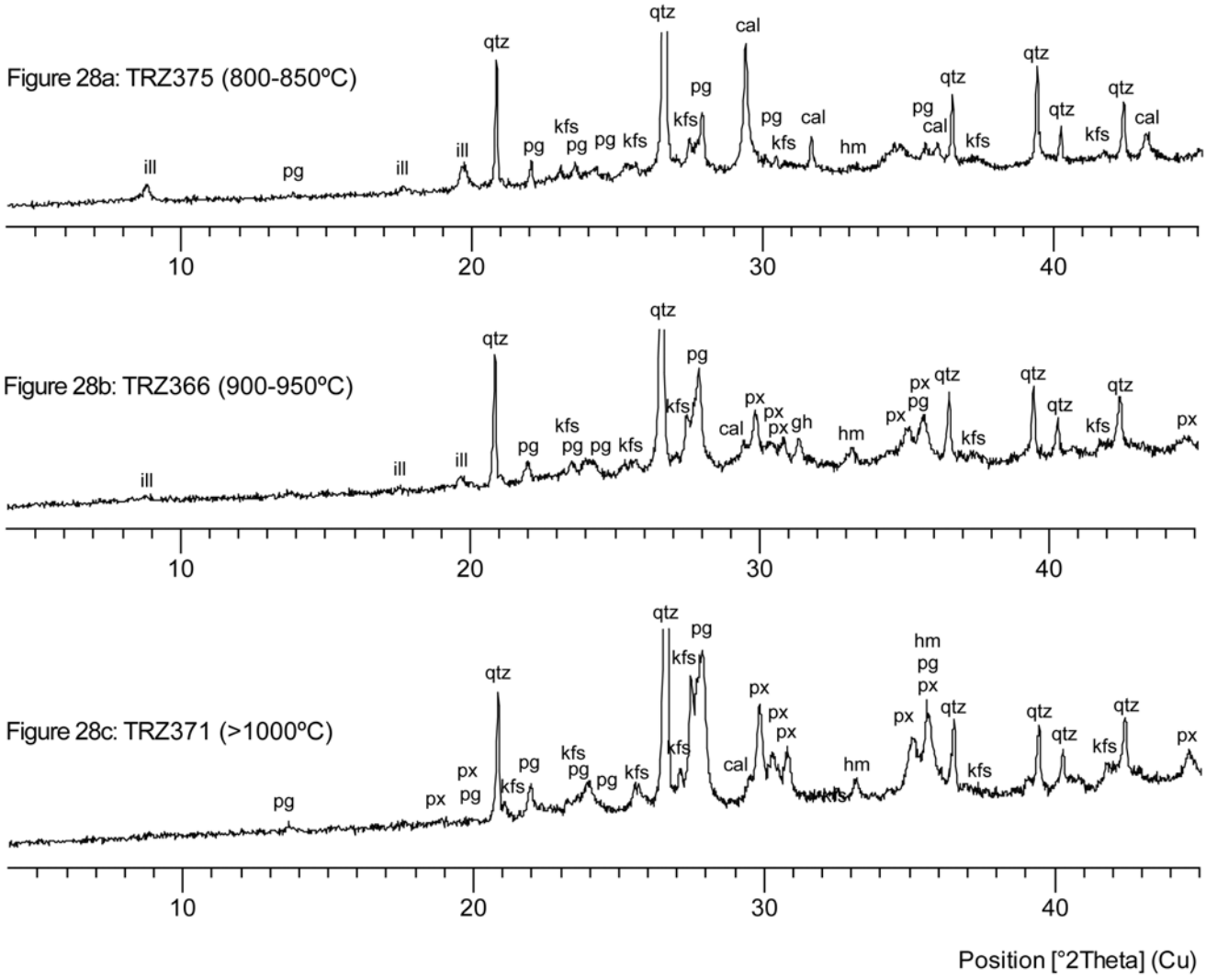

Figure 28: Diffractograms of the individuals TRZ375, TRZ366 and TRZ371 representing the chemical group **KT6**; cal: calcite, gh: gehlenite, hm: hematite, ill: illite-muscovite, kfs: k-feldspar, pg: plagioclase, px: pyroxene, qtz: quartz

The last chemical group from **Kampyr Tepe KT-7**, contains one low fired pottery (TRZ374) (Figure 29a) with EFT around 800-850ºC, owing to the exclusive presence of primary mineral phases, and a black slip painted bowl (TRZ216), fired at reduced atmosphere, under the rang of 900/950ºC, on account of the simultaneous presence of primary and firing phases (Figure 29b).

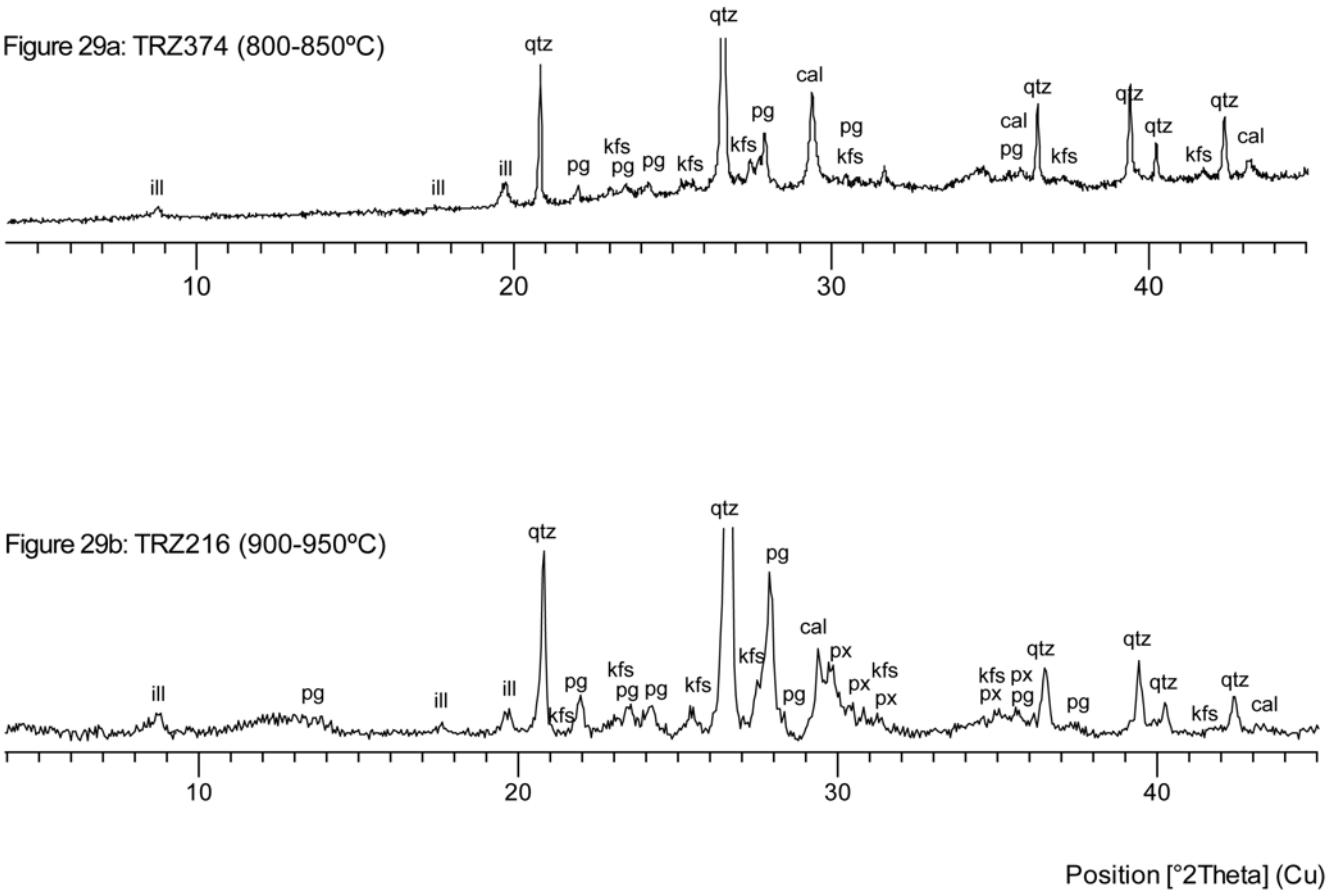

Figure 29: Diffractograms of the individuals TRZ374 and TRZ216 representing the chemical group **KT7**; cal: calcite, ill: illite-muscovite, kfs: k-feldspar, pg: plagioclase, px: pyroxene, qtz: quartz

The eight chemical outliers from **Kampyr Tepe** show different diffraction patterns to the previous ones. **TRZ373** represents a high calcareous pottery. Its diffractogram indicates the presence of primary phases (quartz, calcite, illite-muscovite and few k-feldspar and plagioclase) only, thus its EFT has been estimated around 800-850ºC (Figure 30).

TRZ377 is a well fired pottery (850/900-950ºC) which contains primary phases (quartz, calcite, illite-muscovite, k-feldspar, plagioclase and few hematite), firing phases (pyroxene and gehlenite) (Figure 30). **TRZ386** present a similar diffractogram to the previous one and can be attributed to the same range of firing temperature. Besides of primary and firing phases, sodium chloride is also present as secondary phase.

TRZ380, TRZ381 and **TRZ383** seem to be fired at slightly higher temperature (950-1000ºC) according to the advanced decomposition of illite-muscovite and calcite and the clear development of firing phases (pyroxene and gehlenite) (Figure 30).

Finally, **TRZ385** is an over fired ceramic (EFT upper than 1000ºC) in which primary phases (quartz, k-feldspar, plagioclase, hematite and alkali basalt) and firing phases (pyroxene and gehlenite) coexist. Analcime observed as secondary postdeposictional alteration and/or contamination face (Figure 30).

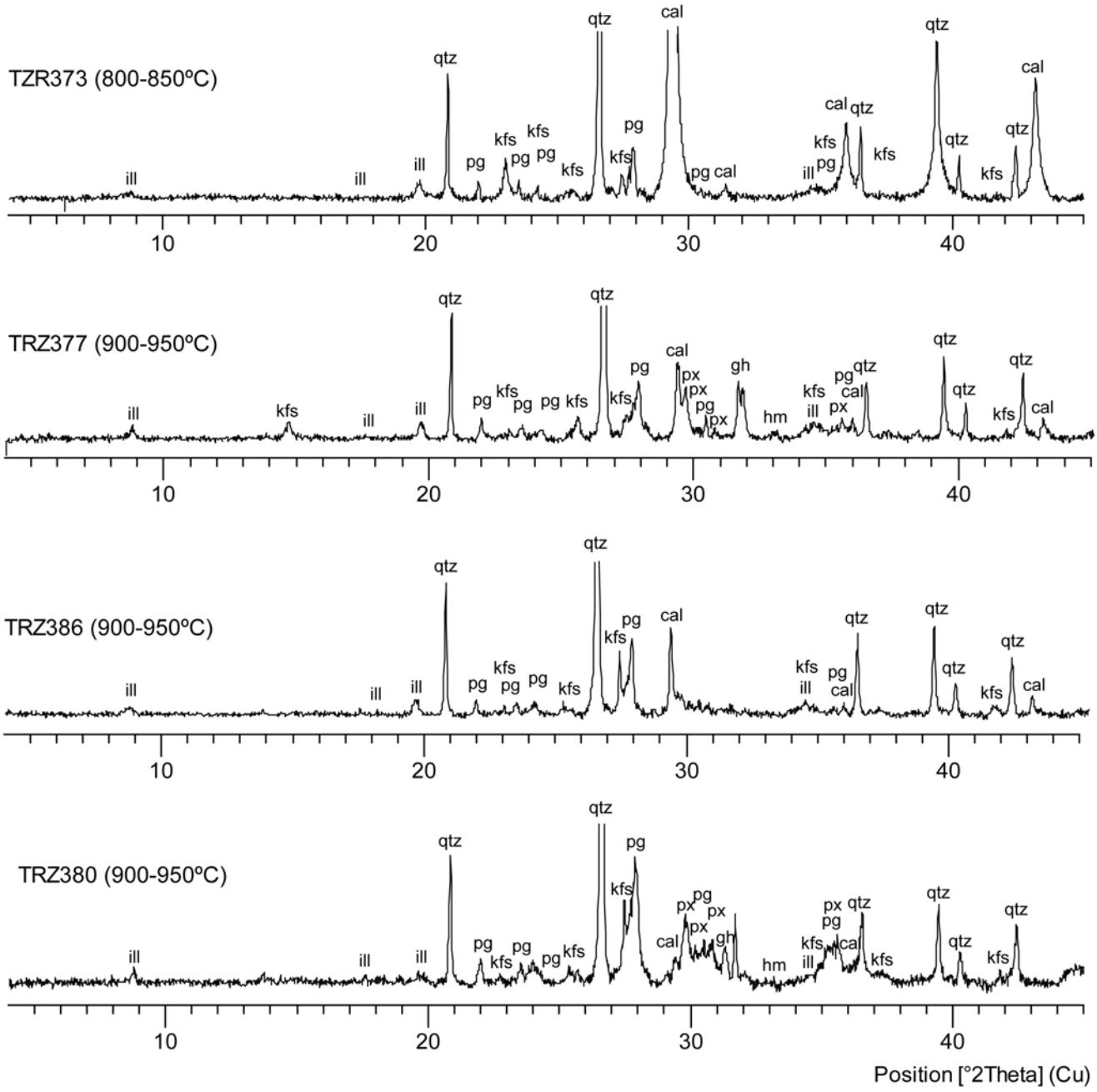

Figure 30: Diffractograms of the ceramic outliers from **Kampyr Tepe** (TRZ373, TRZ377, TRZ386, TRZ380, TRZ381, TRZ383 and TRZ385); cal: calcite, gh: gehlenite, hm: hematite, ill: illite-muscovite, kfs: k-feldspar, pg: plagioclase, px: pyroxene, qtz: quartz

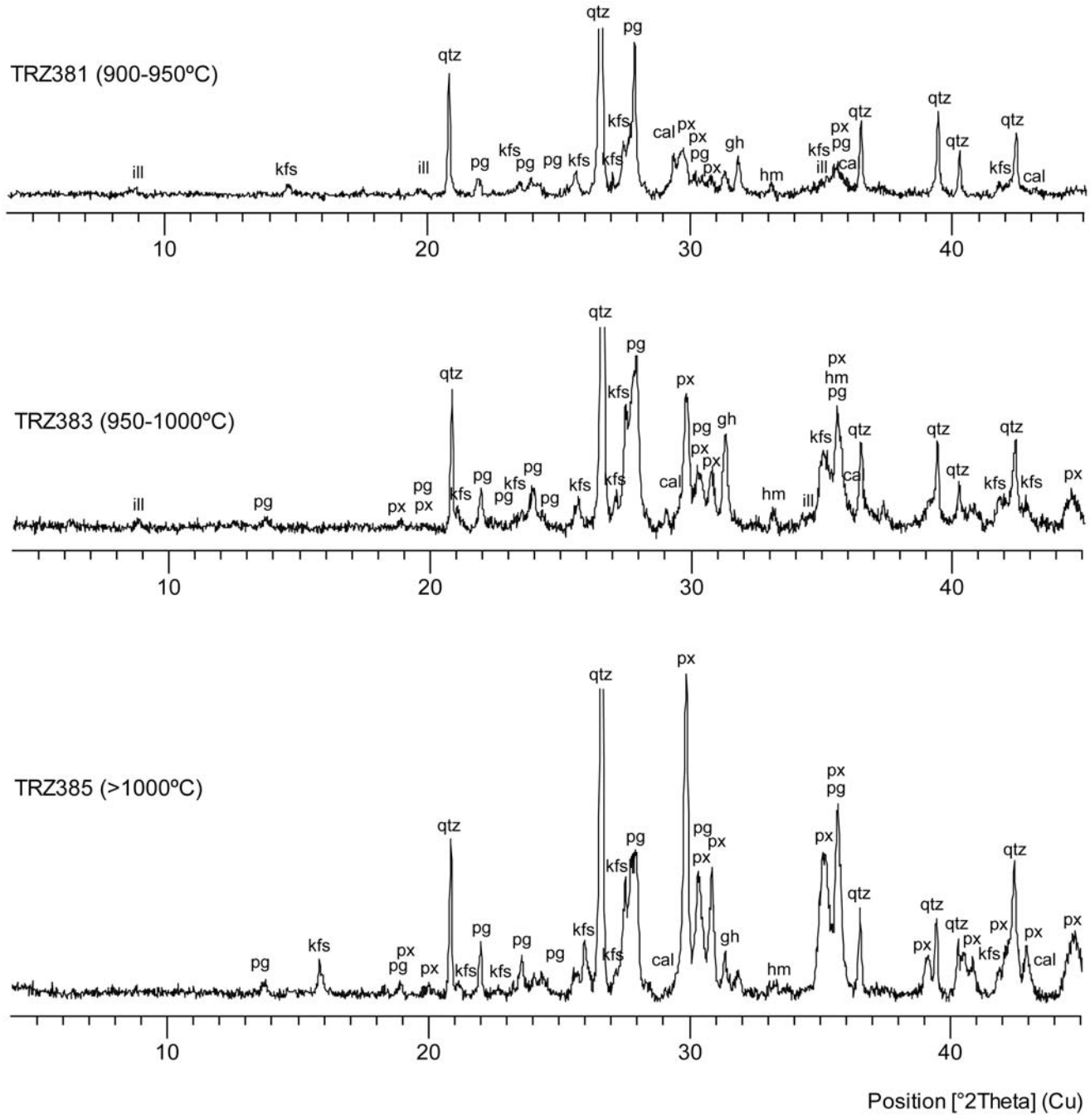

Figure 30: Diffractograms of the ceramic outliers from **Kampyr Tepe** (TRZ373, TRZ377, TRZ386, TRZ380, TRZ381, TRZ383 and TRZ385); cal: calcite, gh: gehlenite, hm: hematite, ill: illite-muscovite, kfs: k-feldspar, pg: plagioclase, px: pyroxene, qtz: quartz

5.2.4. Surface treatment (SEM analysis)

From **Kampyr Tepe**, six ceramics with two different kind of surface treatment have been analysed by MER-EDX (Figure 31). The only vessel fired in an oxidising atmosphere is **TRZ219**, which is a kind of small plate recovered with a red slip. The microphotographs of the polished section of this shard show an advanced vitrification state of both, the slip (Figure 32) and matrix, that indicates generally high firing temperatures. The interface between the clay and the slip layer is clear because of the different density of the material. The layer of red slip is homogeneous in the surface of the vessel and presents a 30-40µm thickness. The composition of the red slip, obtained by SEM-EDS microanalysis, has high Al, less Ca and a similar Fe composition, although is slightly inferior in the clay (Figure 33).

Figure 31: Photographs of the ceramics analysed by SEM-EDS from **Kampyr Tepe**

The other ceramics analysed by SEM-EDS were fired under reduction atmosphere and their slips show different degrees of greyish and black colours (TRZ216, TRZ231, TRZ367, TRZ384 and TRZ380). **TRZ216** is a base of a cup painted with black slip that has inhomogeneous colour and thickness. The microstructure of the matrix and the slip is very similar. They generally present the same vitrification state, however at some areas the glassy phase seems slightly more extended (Figure 32). The chemical similarity between the body and the slip can confirmed by the quantitative chemical microanalysis (Figure 33), though, the percentage of Fe on the slip composition is slightly higher than in the clay. This is also characteristic for the other three shards.

TRZ367 and **TRZ374** present a really shiny black slip over the surface. The aspect of the surface is similar to those of the black Hellenistic ceramics from Athens or the black Roman ceramics from Campania region. Concerning **TRZ367**, the slip layer (30 µm) is very homogeneous and clearly differs from the matrix of the body. The clay particles are seem to be sintered with respect to the ceramic body, (Figure 32). As we have a single firing, in this case, these differences are probably the consequence of the fact that using a finer fraction for the slip it reaches the state of sintering in lower temperatures than the body. The composition of the black slip of **TRZ367**, according to the chemical microanalysis, shows that the composition has less Ca and more Fe content than the matrix (Figure 33). The quantitative

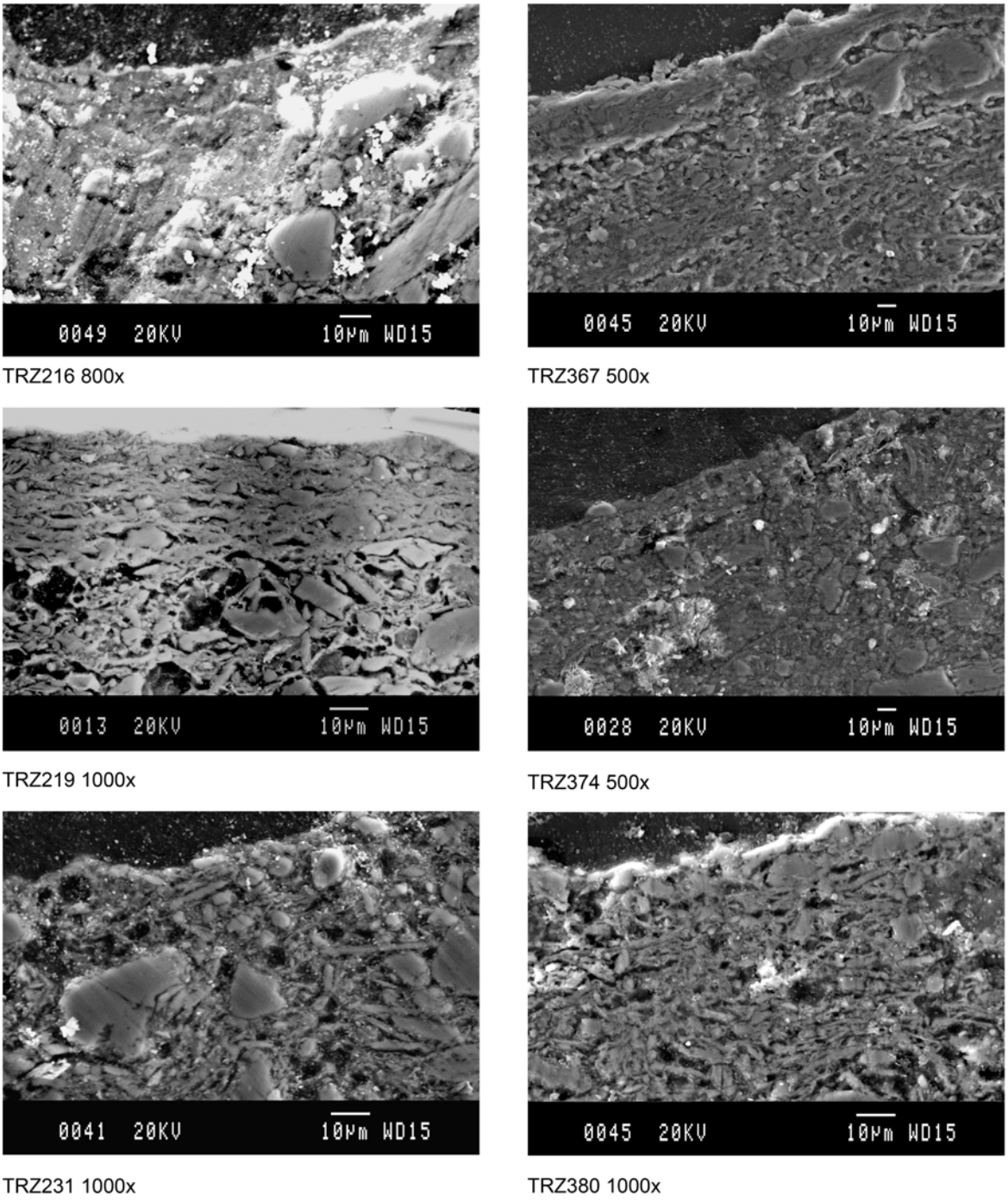

Figure 32: SEM photomicrographs of the polished sections of the slip and paste area observed in SEM-EDS upon the common wares TRZ216, TRZ219, TRZ231, TRZ367, TRZ374 and TRZ380 from **Kampyr Tepe**

microanalysis of the grey slip and the ceramic paste of **TRZ374**, that is a common ware, differ only in Fe relative content. Slip and body both present extended vitrification but the interface between the black slip and the clay matrix is clearly marked. The main chemical difference between the slip and the body of the individuals **TRZ367** and **TRZ374,** with an intense black slip, is the lower Ca content in the slip.

TRZ231 and **TRZ380** have not only a grey slip over the surface but also impressed motifs like palms. In both cases, no clear separation line could be observed between the slip and the body. That clearly indicates that these ceramics were fired just once, following biscuit and not glaze firing (Figure 32). The chemical composition indicates that the grey slip of **TRZ380** contains also less quantity of Ca and higher Si content, whereas the grey slip of **TRZ231** presents more K, less Si and no differences in Ca compared to the ceramic body (Figure 33).

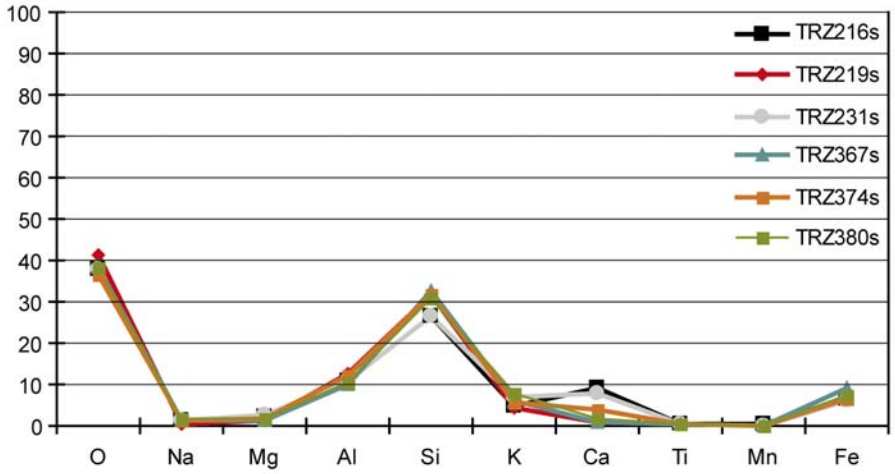

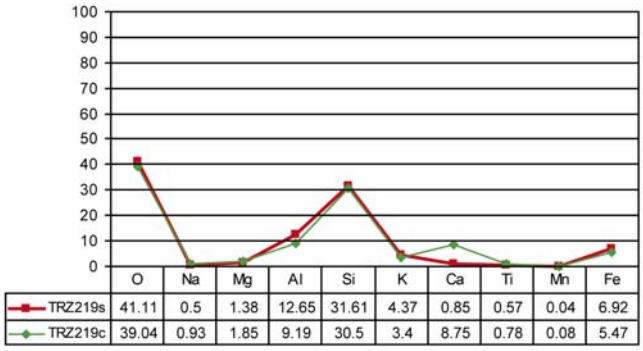

	O	Na	Mg	Al	Si	K	Ca	Ti	Mn	Fe
TRZ219s	41.11	0.5	1.38	12.65	31.61	4.37	0.85	0.57	0.04	6.92
TRZ219c	39.04	0.93	1.85	9.19	30.5	3.4	8.75	0.78	0.08	5.47

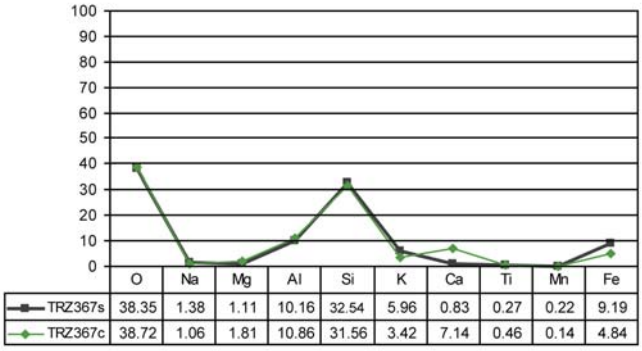

	O	Na	Mg	Al	Si	K	Ca	Ti	Mn	Fe
TRZ367s	38.35	1.38	1.11	10.16	32.54	5.96	0.83	0.27	0.22	9.19
TRZ367c	38.72	1.06	1.81	10.86	31.56	3.42	7.14	0.46	0.14	4.84

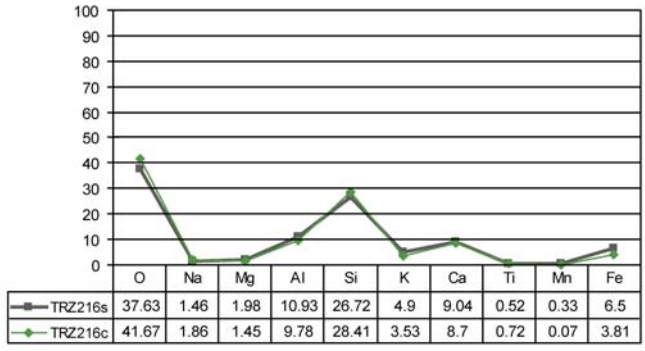

	O	Na	Mg	Al	Si	K	Ca	Ti	Mn	Fe
TRZ216s	37.63	1.46	1.98	10.93	26.72	4.9	9.04	0.52	0.33	6.5
TRZ216c	41.67	1.86	1.45	9.78	28.41	3.53	8.7	0.72	0.07	3.81

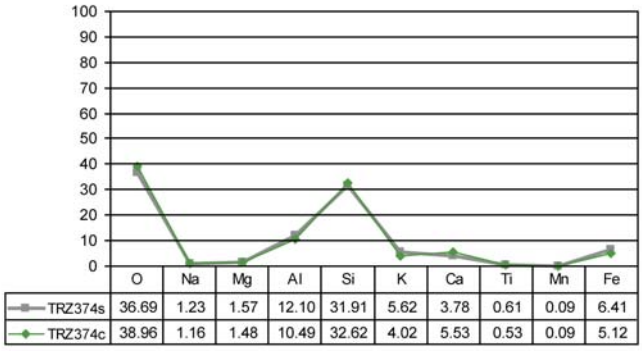

	O	Na	Mg	Al	Si	K	Ca	Ti	Mn	Fe
TRZ374s	36.69	1.23	1.57	12.10	31.91	5.62	3.78	0.61	0.09	6.41
TRZ374c	38.96	1.16	1.48	10.49	32.62	4.02	5.53	0.53	0.09	5.12

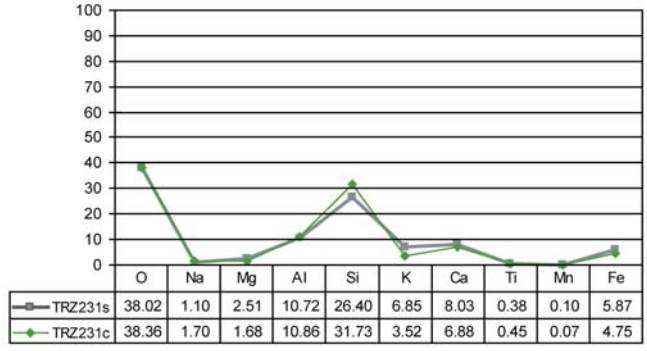

	O	Na	Mg	Al	Si	K	Ca	Ti	Mn	Fe
TRZ231s	38.02	1.10	2.51	10.72	26.40	6.85	8.03	0.38	0.10	5.87
TRZ231c	38.36	1.70	1.68	10.86	31.73	3.52	6.88	0.45	0.07	4.75

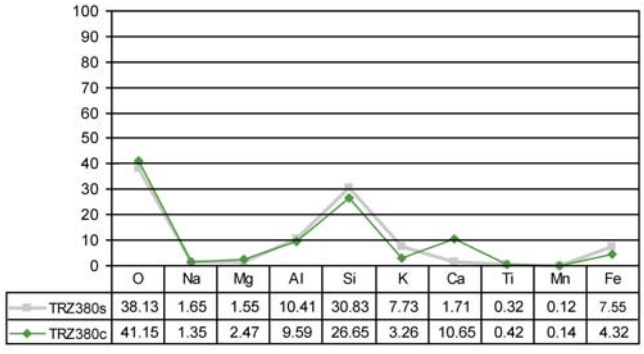

	O	Na	Mg	Al	Si	K	Ca	Ti	Mn	Fe
TRZ380s	38.13	1.65	1.55	10.41	30.83	7.73	1.71	0.32	0.12	7.55
TRZ380c	41.15	1.35	2.47	9.59	26.65	3.26	10.65	0.42	0.14	4.32

Figure 33: Graphics representing the normalised chemical composition obtained by SEM-EDS microanalysis of the slip (s) and clay (c) of the vessels TRZ216, TRZ219, TRZ231, TRZ367, TRZ374 and TRZ380 from **Kampyr Tepe**

5.3. Integrated data of Hellenistic-First Kushan ceramics from Termez and Kampyr Tepe

Crosschecking the archaemetrical results obtained of the 106 shards from **Termez** (sectors **AC1** and **AC2**) and **Kampyr Tepe** together with two clay sediments from sector **AC2** and three sediments from two domestic kilns from **Kampyr Tepe**, we can obtain important information on the regional production and diffusion of ceramics during the Hellenistic and First Kushan periods.

The Compositional Variation Matrix (CVM) has been calculated for the 111 samples considering the following elements: Fe_2O_3 (as total Fe), Al_2O_3, TiO_2, MgO, CaO, Na_2O, K_2O, SiO_2, Ba, Rb, Th, Nb, Zr, Y, Sr, Ce, Ga, V, Zn, Cu, Ni and Cr. The total variation (vt) in this data set according to the CVM is 0.3759, which generally, indicates a relatively heterogeneous geochemical character for all the analysed material (Table 3c). The variability introduced by the majority of the elements is relatively low except for the Na_2O, CaO, Cu, Sr, Th, Ce and Ba.

Part of the variability that CaO, Cu, Sr and Ba introduce is probably due to natural variability but also due to post-depositional contaminations. Finally, Na_2O is altered almost in the whole data set because of the presence of NaCl (salt) crystals and analcime ($Na[AlSi_2O_6]\cdot 6H_2O$) as secondary phases, as it has been already explained in previous works (Tsantini *et al.,* 2007, Martínez *et al.,* 2008, 2009).

Repeating the CVM, upon the subcomposition Fe_2O_3 (as total Fe), Al_2O_3, TiO_2, MgO, SiO_2, Rb, Th, Nb, Zr, Y, Ce, Ga, V, Zn, Ni and Cr, leaving out the above mentioned elements, to avoid the possible chemical differences introduced by the alterations and/or contaminations dominate the statistical treatment, the vt is much more lower, in fact, is equal to 0.1186. A total variation of this range indicates, in mathematical terms, a monogenetic data set (Buxeda and Kilikoglou, 2003) representing probably one single production. However, in geochemical terms, regarding to the restricted geological variation at the geographical area where **Termez** and **Kampyr Tepe** are located, this total variation can point towards the use of clay deposits in pottery production of a very similar geochemical origin.

The chemical results of the 111 ceramics and geological samples are summarized in the dendrogram of Figure 34, resulting from the cluster analysis performed using Square Euclidean distance and the centroid algorithm. The subcomposition Fe_2O_3 (as total Fe), Al_2O_3, TiO_2 as divisor, MgO, K_2O, SiO_2, Rb, Nb, Zr, Y, Ce, Ga, V, Zn, Ni and Cr was transformed into logratios using Al_2O_3. Looking at the dendrogram, only few direct associations can be established between analysed shards from **Termez** (Ancient Military Quarters) and **Kampyr Tepe.**

At the left side of the dendrogram, the cooking ware **TRZ373** and the reddish painted common wares **TRZ377** and **TRZ381** are located somehow separated from the rest of the ceramics on account of some differences in their chemical composition (Table 2 and Table 5). These chemical differences are important enough to indicate that these vessels stands out chemically from the rest of the analysed individuals but only a future petrographical study could confirm different origin for these ceramics.

As mentioned previously, two vessels from **Kampyr Tepe**, the unpainted common ware **TRZ204** and the brown-grey painted common ware **TRZ370**), belongs to the same URCP **(KT-1)**. On the other hand, in the dendrogram (Figure 34), the jar **TRZ385** from **Kampyr Tepe** and the reddish common ware **TRZ339** from **AC2** are also joined to this group due to important similarities in their chemical composition (Table 2). The group formed by all the above mentioned individuals is named **TRZ-1** in the dendrogram of Figure 34 and it can be considered as one of the PCRU's of Hellenistic and First Kushan periods for the whole area. As this group cannot be associated archaeologically to a kiln, the only way to make infe-rences upon its origin is a future petrographic study.

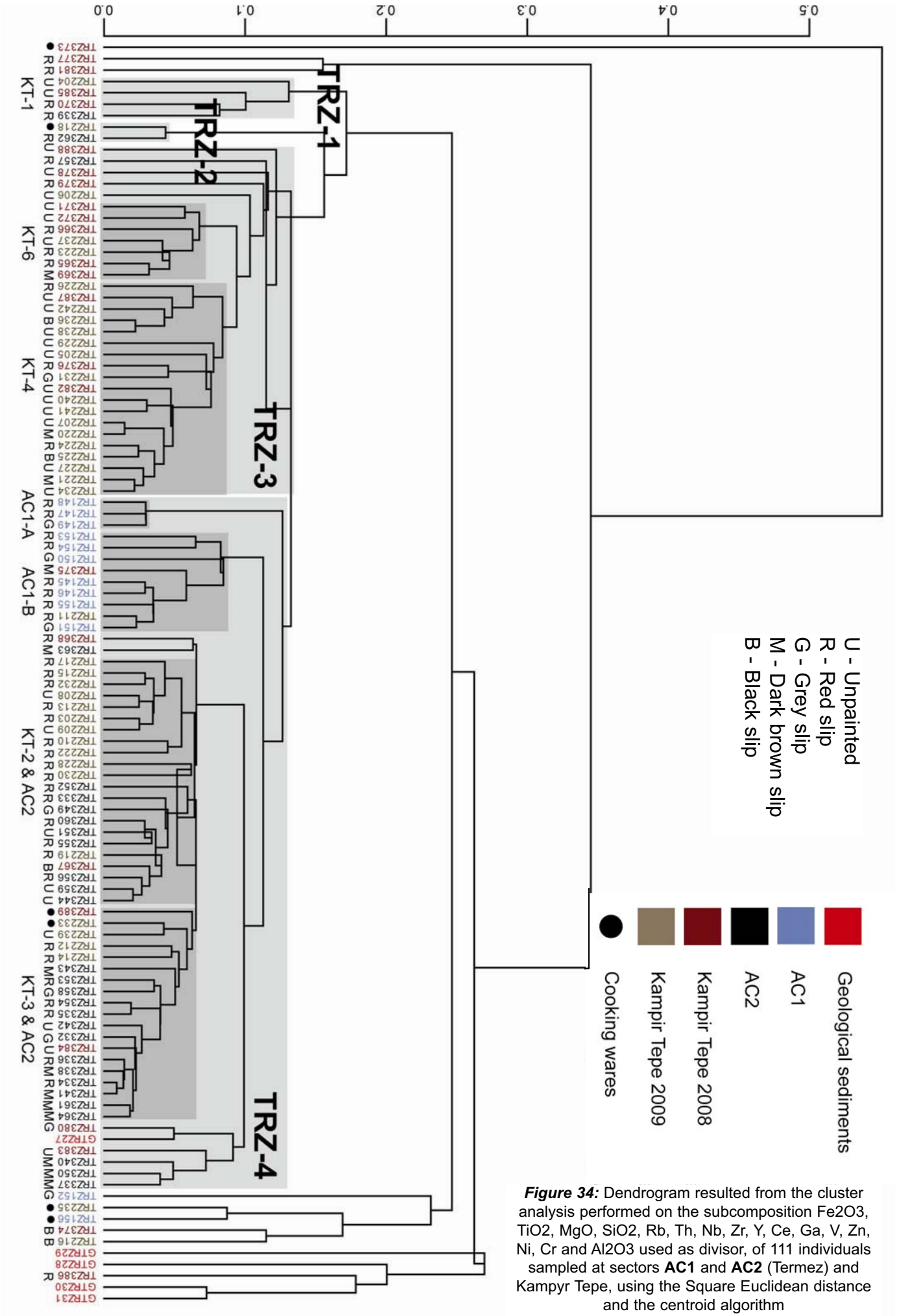

Figure 34: Dendrogram resulted from the cluster analysis performed on the subcomposition Fe2O3, TiO2, MgO, SiO2, Rb, Th, Nb, Zr, Y, Ce, Ga, V, Zn, Ni, Cr and Al2O3 used as divisor, of 111 individuals sampled at sectors **AC1** and **AC2** (Termez) and Kampyr Tepe, using the Square Euclidean distance and the centroid algorithm

Next to the above group (Figure 34) the cooking ware **TRZ218** from **Kampyr Tepe** and the common ware **TRZ362** from **AC2** are located. Typologically both correspond to similar red slip common wares. They are joined together in a small ultrametrical distance which might indicate that both belong to the same ceramic production. According to their chemical similarities (Table 2), they have been classified in one single PCRU called **TRZ-2**. The local regional character of the production is possible. Nevertheless it has to be confirmed by petrographical analysis in the near future.

The individuals from **Kampyr Tepe** belonging to **KT-4**, **KT-5** and **KT-6** that have been identified as URCP's, expose very similar chemical composition, that is why they appear mixed in dendrogram of Figure 34. All these shards are common wares from **Kampyr Tepe**. 16 of them are unpainted common wares (TRZ205, TRZ207, TRZ227, TRZ229, TRZ232, TRZ234, TRZ237, TRZ240, TRZ241, TRZ242, TRZ371, TRZ372, TRZ378, TRZ382, TRZ387, TRZ388), 11 are common wares with a reddish-brown slip (TRZ220, TRZ221, TRZ223, TRZ224, TRZ226, TRZ357, TRZ365, TRZ366, TRZ369, TRZ376, TRZ379),1 of them is a grey ware (TRZ231) and 2 of them are black painted wares (TRZ225 and TRZ236). As mentioned above in the petrographical description (Figure 22), they might correspond to variants of the same ceramic production (**TRZ-3** that includes petrographic fabrics ***F-KT-B1*** and ***F-KT-B2***). An important new data is the association of one chemical outlier from **AC2**, the reddish pain-ted common ware **TRZ357**, to these wider group **TRZ-3** (Figure 34), which might indicates a regional diffu-sion of the *Hellenistic* ceramics at the area.

Up to know, no archaeologically recovered kiln site can be associated to these production, however the geochemical compatibility with the area together with the existence of a pottery kiln in the vicinity of **Kampyr Tepe** could indicate a local provenance. Nonetheless and again we must to enlarge the petro-graphic analysis to prove this hypothesis. On the other hand, as according to the chronology they are all Hellenistic, this group **TRZ-3** (Figure 34) probably represents another Hellenistic production, char-acte-ristic for the area.

The dendrogram of Figure 34 also confirms the existence of another Hellenistic ceramic production **TRZ-4,** composed by both, individuals coming from **Kampyr Tepe** and from **Termez** (**AC2**). This broa-der group unifies the previously identified chemical subgroups **KT-2** and **KT-3**. Typologically, the indivi-duals sampled at **Kampyr Tepe** belonging to this group correspond to 2 unpainted common wares (TRZ208 and TRZ209) and 7 reddish painted common wares (TRZ203, TRZ210, TRZ213, TRZ215, TRZ217, TRZ222 and TRZ232).The other 9 shards classified into this group are characterised typolo-gically in the following way: 3 are unpainted common wares (TRZ344, TRZ351 and TRZ359), 5 are red-dish painted common wares (TRZ333, TRZ352, TRZ355, TRZ356 and TRZ360) and one is grey pain-ted common ware (TRZ349). Moreover, it is important to point out that one red slip plate (TRZ219) and a black slip bowl (TRZ367) from **Kampyr Tepe** seem to present chemical similarities with this wider group. Finally, two reddish-brown painted common wares (TRZ363 from **AC2** and TRZ368 from **Kampyr Tepe**) are also chemically related to this group. Despite of the small differences between the individuals classified into **TRZ-4** (Figure 34), their significant general chemical similarity indicates for them the same or at least common geo-chemical origin.

Despite of the small differences between the individuals classified into **TRZ-4** (Figure 34), their sig-nificant general chemical similarity indicates the same or at least common geo-chemical origin for them. Additionally, in the dendrogram of Figure 34, the red clay G-TRZ-27 sampled at the Antique Quarters (AC) is classified into this main chemical group (**TRZ-4**) evidencing important chemical similarities between the pottery shards and this specific clay, indicating the same geological origin for both the pot-tery and this specific clay. Consequently the raw materials used for the manufacture of the pottery clas-sified into **TRZ-4** might come from the same clay bed that is clearly points toward a local origin. The lack of recovered kiln to associate this production with, however, no permits actually to identify the workshop they were manufactured.

The PCRU's **AC1-A** and **AC1-B** in Figure 34 can be still distinguished by slight differences. Nevertheless, they form part of the wider group **TRZ-4** and by checking on the chemical similarities (Table 4), these two groups must be subgroups of the same pottery production. Typologically, **AC1-A** is represented by 2 red slip common wares (TRZ147 and TRZ148) and one grey slip ware (TRZ149).

These ceramics have a very homogeneous chemical composition and belong also to the same petrographic fabric ***F-AC1-A*** (Figure 8). The same affirmation can be made for **AC1-B** (TRZ145, TRZ146, TRZ150, TRZ151, TRZ153, TRZ154 and TRZ155) that correspond to the petrographic fabric ***F-AC1-B*** (Figure 9). Moreover, two common wares (the base of a common ware with a red slip TRZ211 and the cratera with red slip TRZ375) from **Kampyr Tepe** seem to be associated, in chemical terms, to ***AC1-B*.** Typologically, all individuals classified into **AC1-B** are reddish-brown slip common wares, except TRZ150 and TRZ151, which are grey wares. Finally, we could observe that the chemical composition of **AC1-B** is much more similar to **KT-2** identified at **Kampyr Tepe** than to **AC1-A** indentified for the **Antic Quarters**. Both for **AC1-A** and **AC1-B** the inexistence of recovered pottery kilns from this period, make impossible the identification of the provenance area of production.

Finally, some shards (TRZ380, TRZ383, TRZ337, TRZ340 and TRZ350) seem to be chemically related to this last fourth big set of subproductions: main group **TRZ-4** (Figure 34) even though according to their chemical composition (Table 2) Between them there are one grey slip ware (TRZ380) and an undecorated common ware (TRZ383) from **Kampyr Tepe** and 3 brownish slip common wares from **AC2** (TRZ337, TRZ340 and TRZ350).

It is important to stress that the reddish clay have been chemically analysed, **G-TRZ-27** (Table 2), sampled at **AC2** sector that have similar chemical composition with **AC2** and the subgroup of **Kampyr Tepe** that are integrated in the main group **TRZ-4** (Figure 34). This evidences a common geo-chemical origin for the clay and for the pottery grouped in TRZ-4. The chemical similarity between the production identified for **Kampyr Tepe** and Antique Quarters also indicates that the low geological variability in the area. Therefore it is very probable that the raw materials used for the fabrication of these PCRU's came from the same o very similar clay deposit. The limitation in the access to adequate clay sources probably leaded to a log lasting local/regional ceramic tradition, where the explored raw material recourses were the same, even though there are differences in the production processes, typology and maybe chronology.

At the right part of the dendrogram (Figure 34), some isolated individuals appear to be linked to **TRZ-1**, **TRZ-2**, **TRZ-3** and **TRZ-4** at high ultrametrical distance. For the storage jar or cooking ware TRZ152 from **AC1** and the cooking ware TRZ235 from **Kampyr Tepe,** the thin section analysis points toward local origin. On the other hand, no concrete origin by petroraphic analysis can be assigned to the cooking ware TRZ156, also sampled at the sector **AC1**. The aplastic inclusions of this pot are mainly composed of shell fragments and argillaceous and sedimentary rocks, which are a very common temper used in cooking wares from the Neolithic Period. Other cooking wares dated on the Kushan-Sassanian period, already described in previous studies (Tsantini *et al*. 2007., Martínez *et al*., 2008, 2009) are also characterised by the presence of calcareous shell fragments as main temper. To be able to identify an origin for the rest of the ungrouped individuals, a petrographic study has been scheduled for the near future.

6. Ceramics from the Kushan-Sassanian period. Integrated results of archaeometrical analysis.

6.1. Termez: Tchinguiz Tepe

Analysed pottery from **Tchinguiz Tepe** comes from the sectors RF, RC and RB. At sector RF, a pottery workshop, dated to the Kushan-Sassanian period was excavated in 2008. Pottery from this sector were recovered inside a kiln structure, in the accumulation levels of filing materials due to the collapse of the kiln structures and the discard of household trash, once the kiln was no longer performing its primary function, but was used as a trash heap instead (Martínez, 2008). The 20 individuals analysed from RF correspond to cooking wares (TRZ187, TRZ189 and TRZ292) and to a large variety of painted and unpainted common wares (Table 1) such as plates (TRZ190, TRZ192, TRZ193, TRZ194, TRZ196 and TRZ197), sometimes with impressed motifs, jars (TRZ198, TRZ202), bowls (TRZ184, TRZ185, TRZ186, TRZ191, TRZ199, TRZ200 and TRZ291) and cups (TRZ188 and TRZ195). The superficial prospection carried out at sector RF in 2007 proportioned 6 individuals also for this analytical work (TRZ067 to TRZ072).

From the rest of the ceramics from **Tchinguiz Tepe,** 79 shards come from a domestic building area that is in contact with the fortified wall excavated during 2007, 2008 and 2009 (Ariño,Martínez *et al*., 2009: 121, in this volume). They are predominantly big plates (TRZ051, TRZ053, TRZ065, TRZ077, TRZ079, TRZ082, TRZ083, TRZ087, TRZ0157, TRZ0158, TRZ0173, TRZ0174, TRZ0177, TRZ0180, TRZ296, TRZ297, TRZ300, TRZ301, TRZ303 and TRZ306), bowls (TRZ052, TRZ056, TRZ057, TRZ058, TRZ059, TRZ064, TRZ066, TRZ076, TRZ080, TRZ086, TRZ0121, TRZ0164, TRZ0167, TRZ0168, TRZ0175, TRZ0178, TRZ302 and TRZ304), jars (TRZ054, TRZ055, TRZ081, TRZ166 and TRZ181), cups (TRZ063, TRZ075, TRZ078, TRZ095, TRZ160, TRZ165, TRZ176, TRZ307, TRZ310, TRZ311 and TRZ312), lamps (TRZ159 and TRZ169), a terracotta (TRZ308) and a big container (TRZ179). Some cooking wares have been also analysed (TRZ061, TRZ086, TRZ161, TRZ162, TRZ163, TRZ170, TRZ171, TRZ172, TRZ182, TRZ183, TRZ293, TRZ294, TRZ295, TRZ298, TRZ305 and TRZ309).

6.1.1. Chemical composition (XRF analysis)

The chemical concentrations of 101 ceramic individuals from **Tchinguiz Tepe** (**TT**) determined by XRF (Table 2) were treated statistically according to the proposals of Aitchison (1986) and Buxeda (1999). The first step of the statistical evaluation was to calculate the Compositional Variation Matrix (CVM) which shows a vt = 0.6177 (Table 7a). This value is relatively high and indicates a polygenic origin of the data set. The main variability is introduced by the elements: CaO ($\tau_{\cdot CaO}$ = 7.228), Sr ($\tau_{\cdot Sr}$ = 1.985), Cr ($\tau_{\cdot Cr}$ = 1.465), Na_2O_3 ($\tau_{\cdot Na2O3}$ = 1.305), Ce ($\tau_{\cdot Ce}$ = 1.131), V ($\tau_{\cdot V}$ = 1.089), Cu ($\tau_{\cdot Cu}$ = 1.066), Ba ($\tau_{\cdot Ba}$ = 1.050) and K_2O ($\tau_{\cdot K2O}$ = 0.938). Repeating the calculation of the CVM without to consider that might introduce variability due to postdepositional alterations in the data set (Na_2O, K_2O, Ba, Sr, and Cu), the value of the total variation (vt= 0.4459) remains still high, that indicates that chemical variability is not only reflecting perturbations due to postdeposicional alteration and/or contamination processes, but also, differences in raw material composition between the analysed shards.

The chemical data of the analysed shards from **Tchinguiz Tepe** has been transformed into logratios using Ga as divisor because, as according to the second CVM, is the element less contributing to the chemical variability. The chemical results are summarized in the dendrogram of Figure 35 resulting from the cluster analysis performed upon the subcomposition Fe_2O_3 (as total Fe), Al_2O_3, TiO_2, MgO, CaO, SiO_2, Rb, Th, Nb, Zr, Y, Ce, Ga, V, Zn, Ni and Cr, using the Square Euclidean distance and the centroid algorithm.

At the right side of the dendrogram, six cooking wares (TRZ163, TRZ170, TRZ293, TRZ294, TRZ295 and TRZ309) from RC sector are jointed together forming **TT-A** group. The cooking ware TRZ163 comes from the stratigraphical unit 4, TRZ170 and TRZ193 were recovered in the stratigraphical unit 5, TRZ294 and TRZ295 come from the s.u. 18 and TRZ309 from the s.u. 28. These cooking wares were produced with a very low calcareous paste and exhibit high chemical values in K_2O, SiO_2 and in some trace elements. Their chemical differences compared to the rest of the analysed material in this dendrogram are important enough to indicate that they correspond to one single production (Table 2) **TT-A.**

(TT)	Fe_2O_3	Al_2O_3	TiO_2	MgO	CaO	Na_2O	K_2O	SiO_2	Ba	Rb	Th	Nb	Zr	Y	Sr	Ce	Ga	V	Zn	Cu	Ni	Cr
$\tau_{\cdot i}$	0.653	0.670	0.704	0.902	7.228	1.305	0.938	0.734	1.050	0.872	0.823	0.728	0.792	0.743	1.985	1.131	0.668	1.089	0.815	1.066	0.818	1.465
$vt/\tau_{\cdot i}$	0.946	0.923	0.877	0.685	0.085	0.474	0.658	0.841	0.588	0.708	0.751	0.849	0.780	0.832	0.311	0.546	0.924	0.567	0.758	0.580	0.755	0.422
$r\ v,\tau$	1.000	0.999	0.998	0.994	-0.370	0.997	0.996	0.997	0.983	0.994	0.998	0.998	0.995	0.997	0.788	0.995	0.999	0.981	0.998	0.977	0.992	0.981
vt	0.618																					

Table 7a: Compositional Variation Matrix (CVM) calculated upon the 101 ceramics from the Kushan-Sassanian period sampled at **Tchinguiz Tepe** (Termez)

(ZT)	Fe_2O_3	Al_2O_3	TiO_2	MgO	CaO	Na_2O	K_2O	SiO_2	Ba	Rb	Th	Nb	Zr	Y	Sr	Ce	Ga	V	Zn	Cu	Ni	Cr
$\tau_{\cdot i}$	0.417	0.400	0.377	1.008	1.070	2.384	0.680	0.420	1.514	0.454	0.503	0.385	0.444	0.381	1.204	0.769	0.448	0.516	0.452	0.544	0.441	0.428
$vt/\tau_{\cdot i}$	0.830	0.865	0.918	0.344	0.324	0.145	0.509	0.825	0.229	0.762	0.688	0.900	0.781	0.910	0.288	0.450	0.773	0.671	0.767	0.637	0.785	0.809
$r\ v,\tau$	0.995	0.994	0.997	0.941	0.939	0.724	0.911	0.989	0.941	0.989	0.994	0.997	0.988	0.996	0.913	0.988	0.993	0.986	0.988	0.985	0.990	0.996
vt	0.346																					

Table 7b: Compositional Variation Matrix (CVM) calculated upon the 48 ceramics from the Kushan-Sassanian period sampled at **Zar Tepe**

(TT&ZT)	Fe_2O_3	Al_2O_3	TiO_2	MgO	CaO	Na_2O	K_2O	SiO_2	Ba	Rb	Th	Nb	Zr	Y	Sr	Ce	Ga	V	Zn	Cu	Ni	Cr
$\tau_{\cdot i}$	0.640	0.636	0.657	1.068	5.323	2.263	1.046	0.685	1.270	0.790	0.780	0.699	0.736	0.708	1.885	1.079	0.660	0.986	0.768	0.976	0.785	1.195
$vt/\tau_{\cdot i}$	0.910	0.917	0.886	0.546	0.109	0.257	0.557	0.850	0.459	0.738	0.747	0.833	0.792	0.823	0.309	0.540	0.882	0.591	0.758	0.597	0.742	0.488
$r\ v,\tau$	0.997	0.998	0.997	0.988	0.036	0.959	0.974	0.995	0.982	0.994	0.998	0.997	0.994	0.996	0.766	0.994	0.997	0.983	0.995	0.975	0.984	0.983
vt	0.583																					

Table 7c: Compositional Variation Matrix (CVM) calculated upon the 149 ceramics from the Kushan-Sassanian period sampled at **Tchinguiz Tepe** (Termez) and at **Zar Tepe**.

Figure 35: Dendrogram resulted from the cluster analysis performed on the subcomposition Fe_2O_3, Al_2O_3, TiO_2, MgO, CaO, SiO_2, Rb, Th, Nb, Zr, Y, Ce, Ga, V, Zn, Ni, Cr and Ga used as divisor, of 101 individuals sampled at **Tchinguiz Tepe** (Termez), using the Square Euclidean distance and the centroid algorithm

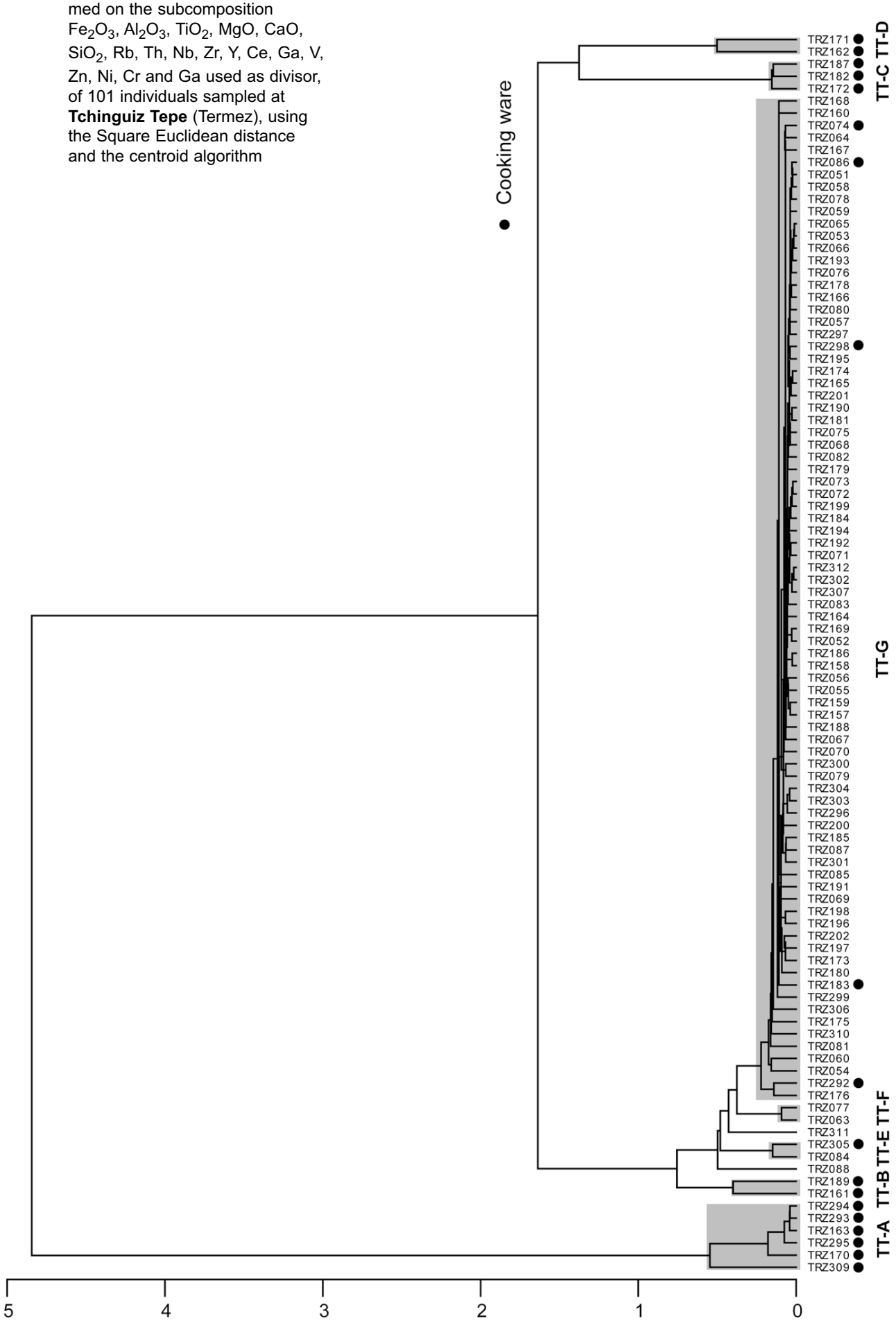

However, this group shares some typological characteristics (Figure 36) with the rest of the material analysed from **Tchinguiz Tepe**. The mean chemical composition and the standard deviation of **TT-A** group are given in Table 8.

Two other cooking wares (TRZ161 from s.u. 2 of RC grid and TRZ189 from s.u. 20 of RF grid) present several chemical (Table 8) and petrographical (Figure 45) similarities between them that leads us to consider them both as one single pottery production (**TT-B**) (Figure 37). The common chemical difference that they present respect to the rest of the individuals of this data set is higher relative concentration in CaO, as both have the highest CaO value within the analysed shard from **Tchinguiz Tepe.** At the same time, their concentrations in Fe_2O_3, Al_2O_3, TiO_2, SiO_2, Nb, Zr, Ga and Cr are lower (Table 8).

At the right side of the dendrogram, three cooking wares are linked at small ultrametrical distance in **TT-C** group (Figure 35). Two of them (TRZ172 and TRZ182) have been sampled at the sector RC (stratigraphical units 5 and 21 respectively) and the other (TRZ187) comes from the stratigraphical unit 11 of the sector RF (Figure 38). This group is border calcareous with significant differences in Ce, Cu and Cr compared to the rest of the analysed material (Table 8). Specifically, the very high Cr concentration that characterise them regarding to the rest of the ceramic material is an indication of the possible foreign character of this production. From a macroscopic and microscopic point of view (Figure 46), these three vessels from **TT-C** present calcareous shell fragments as dominant aplastic inclusions due to which they are similar in technological terms to the cooking ware TRZ156 recovered at the sector **AC1** (Figure 5, 10b).

Another clear chemical group is **TT-D** which contains two cooking wares: TRZ162 from s.u. 3 and TRZ171 from s.u. 5 both sampled at RC sector. These two shards are linked in a major ultrametrical distance than the previous ones. Beside slight chemical differences between them, the common chemical aspect that they present regarding to the rest of the material are high content in SiO_2 and Zr and low MgO, CaO, Na_2O_3, Ba, th, Nb, Cu and Ni relative concentrations. The petrographic analysis that will be presen-ted bellow (Figure 47) is also sustains that they can be two variants of the same ceramic production. The mean chemical composition and the standard deviation of the group **TT-D** is given at Table 8 and the typology of the group is in Figure 39.

At the left side of the dendrogram, the cooking ware TRZ305 from u.s. 25 of sector RC is grouped together with the painted common ware TRZ084 from u.s. 5 of the same sector at a small ultrametrical distance (Figure 35). The significant similarities of their chemical composition between them, such as high values in K_2O and Sr and low concentrations in Zn (Martínez *et al*., 2009: 258) indicates that they represent the same production. The mean chemical composition and standard deviation of this production **TT-E** is given at Table 8. The typology of these vessels is presented in figure 40.

Some common wares placed at the left side of the dendrogram of Figure 35 show chemical differences with the rest of the analysed material from **Tchinguiz Tepe**. On the one hand, there is a small group (**TT-F**) of two common wares TRZ063 and TRZ077 (Figure 41). TRZ063 comes from the u.s. 10 from the grid RC whereas TRZ077 was recovered during the superficial prospecting works carried out at the grid RF. These are both calcareous ceramics, with the highest MgO concentration in this data set. The chemical similarities indicate that they correspond to the same production **TT-F**. In Table 8 where the mean chemical composition of **TT-F** is given a generally higher content of CaO and other small differences in trace elements (Zn, v, Ni, Cr) compare to the other chemical groups identified for common wares can be seen.

On the other hand, two other common wares (TRZ088 and TRZ311) appear isolated at the left side of the dendrogram of Figure 35. Even though the chemical composition indicates a possible local/regional character, they can not be clearly classified into none of the above identified productions and to identify their origin, a deep petrographic analysis is needed. TRZ311, from u.s. 28 of RC grid (Figure 42), that is a jar with the surface dark brownish slip it's a border calcareous with high Sr and low Th and V contents. TRZ088, from u.s. 5 of RB grid, that is a base of a decorated common ware, with painted motives at the outside, has high Fe_2O_3, Ba and Ni values and low Ce and V concentrations (Table 8).

	TT-A (n=6)		TT -B (n= 2)		TT -C (n= 3)		TT -D (n= 2)		TT -E (n= 2)		TT -F (n= 2)		TT -G (n= 82)		TRZ088	TRZ311
	m	sd	m	sd	m	sd	m	sd	m	sd	m	sd	m	sd	nc	nc
Fe_2O_3 (%)	6.07	0.26	5.56	0.20	6.16	0.23	5.82	0.28	5.99	0.12	6.63	0.19	6.33	0.31	6.64	6.01
Al_2O_3 (%)	17.26	0.33	13.98	1.16	16.86	0.42	16.34	0.37	16.13	0.47	16.23	0.17	16.04	0.53	16.73	15.41
TiO_2 (%)	0.75	0.02	0.59	0.04	0.74	0.02	0.74	0.01	0.72	0.02	0.68	0.03	0.68	0.03	0.72	0.68
MgO (%)	3.71	0.03	2.87	0.06	3.18	0.44	2.35	0.32	3.09	0.06	3.94	0.02	3.77	0.33	3.57	4.40
CaO (%)	1.29	0.50	21.27	4.43	6.25	0.50	3.73	1.41	6.21	0.49	11.60	0.05	10.63	1.12	8.30	6.43
Na_2O (%)	1.55	0.08	1.94	0.02	1.56	0.86	1.44	0.08	1.73	0.00	2.32	0.02	1.40	0.16	1.92	1.50
K_2O (%)	4.27	0.05	3.60	0.56	3.59	0.11	3.66	0.07	4.15	0.39	2.16	0.33	3.39	0.22	3.64	3.65
SiO_2 (%)	64.95	0.93	50.03	2.43	61.48	0.62	65.79	1.47	61.80	1.54	56.29	0.03	57.58	1.21	58.31	61.75
Ba (ppm)	449	43	408	13	469	78	307	11	540	45	517	12	561	68	609	493
Rb (ppm)	147	4	121	7	158	5	138	9	127	9	77	6	130	9	132	101
Th (ppm)	15	1	15	1	14	1	13	1	12	2	15	1	15	2	14	13
Nb (ppm)	18	1	14	0	17	0	14	1	17	1	15	0	16	1	16	16
Zr (ppm)	188	2	140	4	172	4	184	6	166	1	155	3	153	7	156	152
Y (ppm)	32	1	23	0	26	2	26	1	25	1	26	1	26	1	24	26
Sr (ppm)	159	21	527	77	364	23	348	63	476	237	313	1	379	51	421	540
Ce (ppm)	76	5	53	9	74	9	59	10	62	10	66	9	62	8	32	48
Ga (ppm)	19	1	17	1	19	0	18	0	17	0	19	0	18	1	18	16
V (ppm)	123	6	100	7	220	14	127	3	106	10	100	7	103	6	96	92
Zn (ppm)	123	8	103	1	116	5	95	7	70	7	110	1	104	8	93	106
Cu (ppm)	34	2	28	4	20	2	21	1	25	0	35	5	35	3	35	31
Ni (ppm)	49	5	40	3	45	2	28	2	46	1	53	0	51	4	52	46
Cr (ppm)	91	7	61	1	226	32	96	12	78	2	74	2	77	6	78	80

Table 8: The mean chemical composition (m) and the standard deviation (sd) using normalised data of **TT-A**, **TT-B**, **TT-C**, **TT-D**, **TT-E**, **TT-F** and **TT-G** chemical groups and the raw normalised chemical composition (nc) of the ceramic outliers TRZ088 and TRZ311 from **Tchinguiz Tepe**

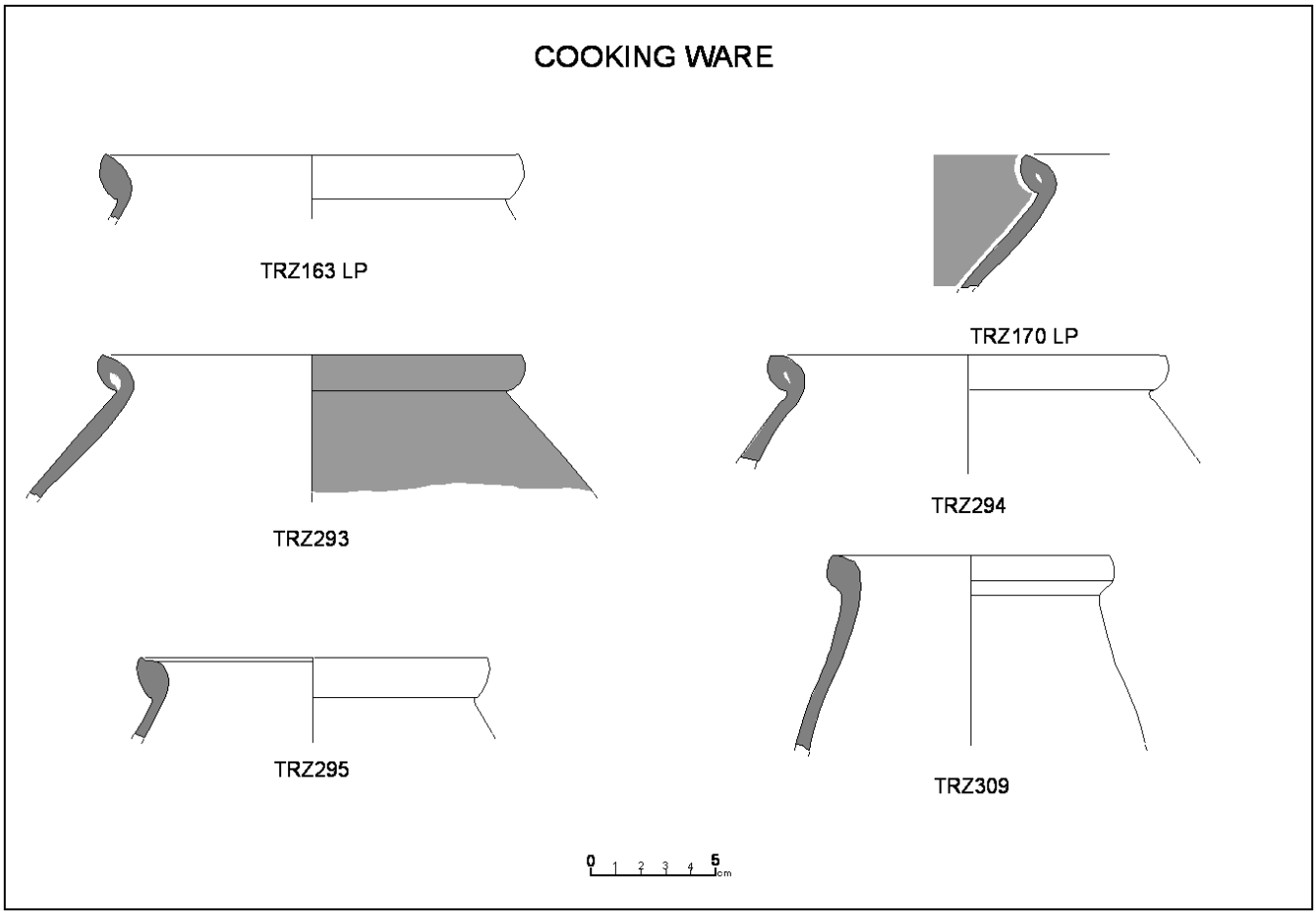

Figure 36: Typology of the cooking wares belonging to **TT-A** group (TRZ163, TRZ170, TRZ293, TRZ294, TRZ295 and TRZ309)

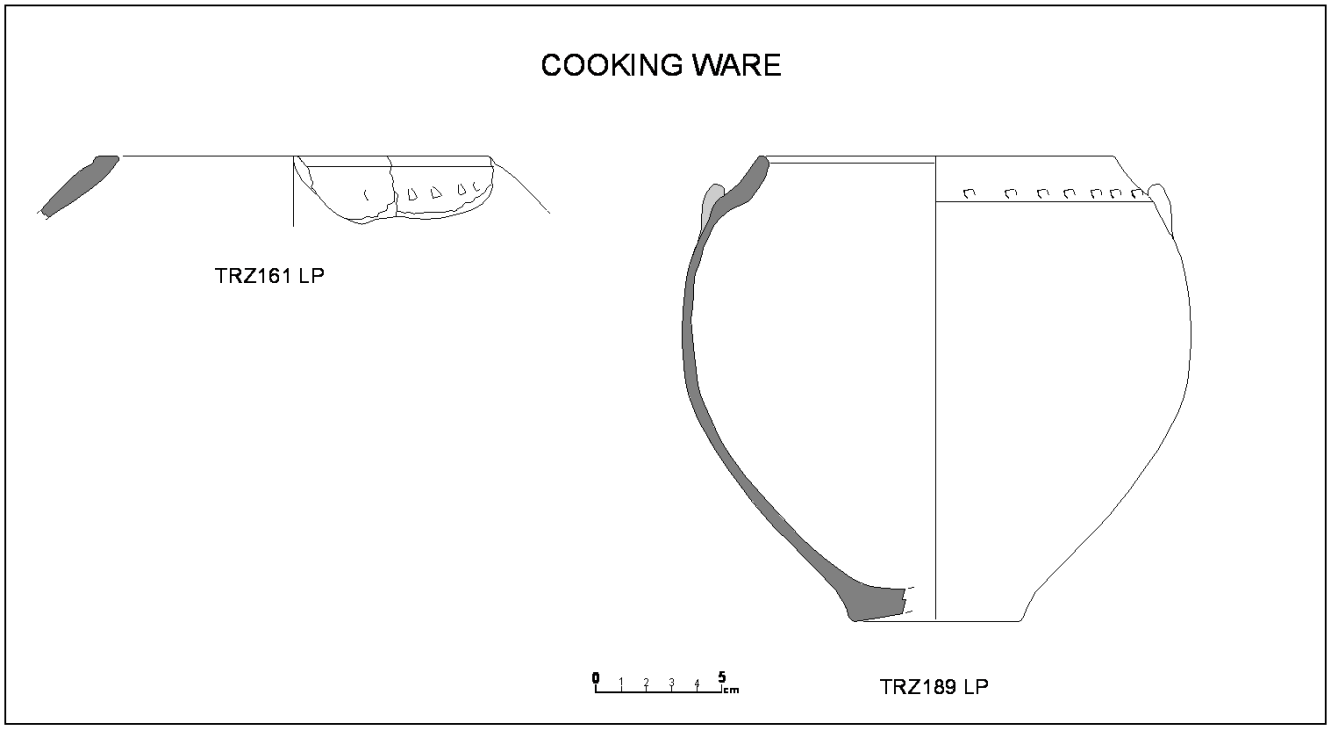

Figure 37: Typology of the cooking wares belonging to **TT-B** group (TRZ161 and TRZ189)

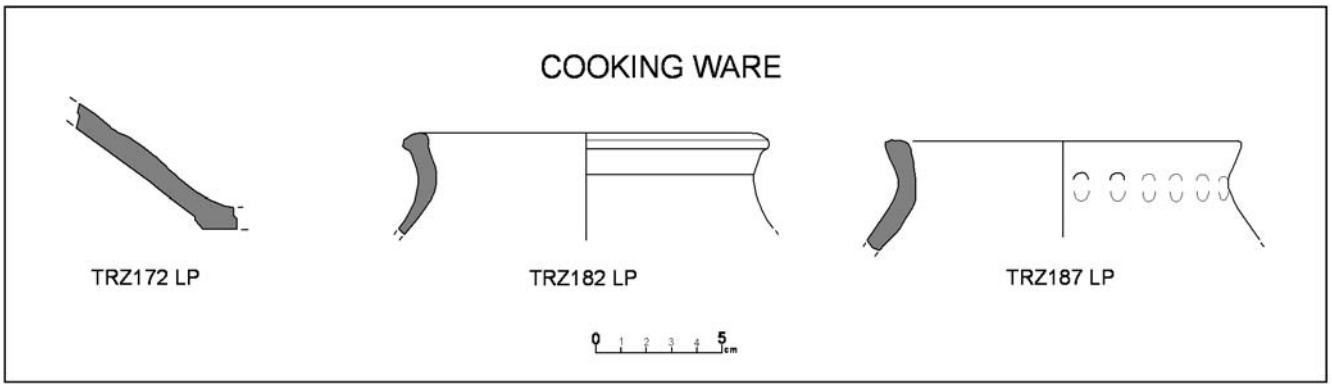

Figure 38: Typology of the cooking wares belonging to **TT-C** group (TRZ172, TRZ182 and TRZ187)

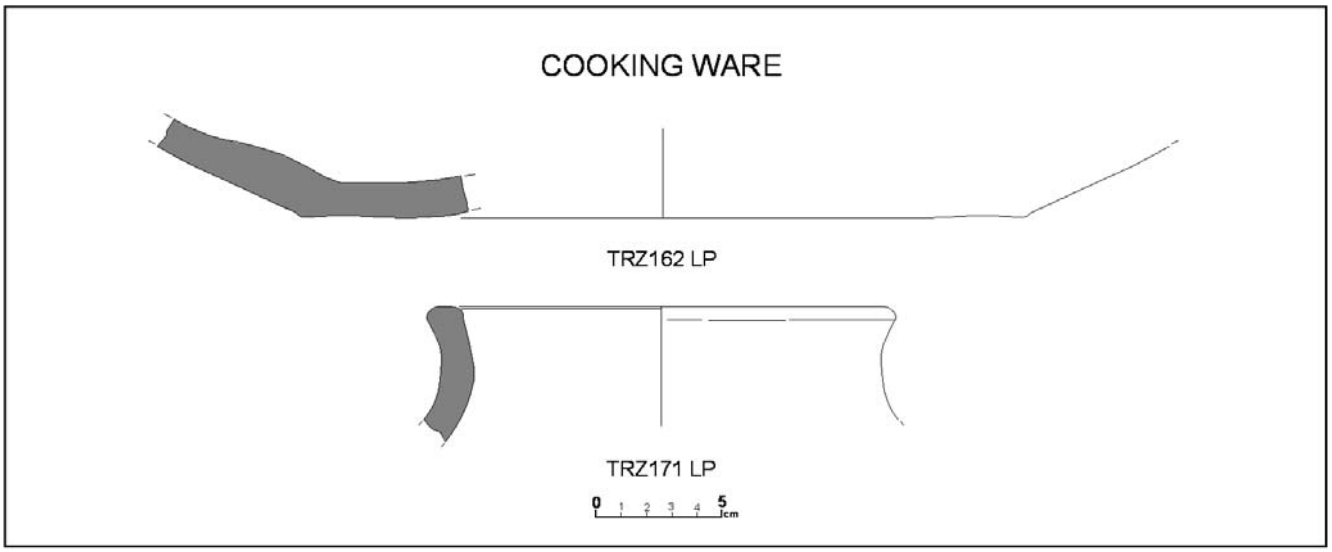

Figure 39: Typology of the cooking wares belonging to **TT-D** group (TRZ162 and TRZ171)

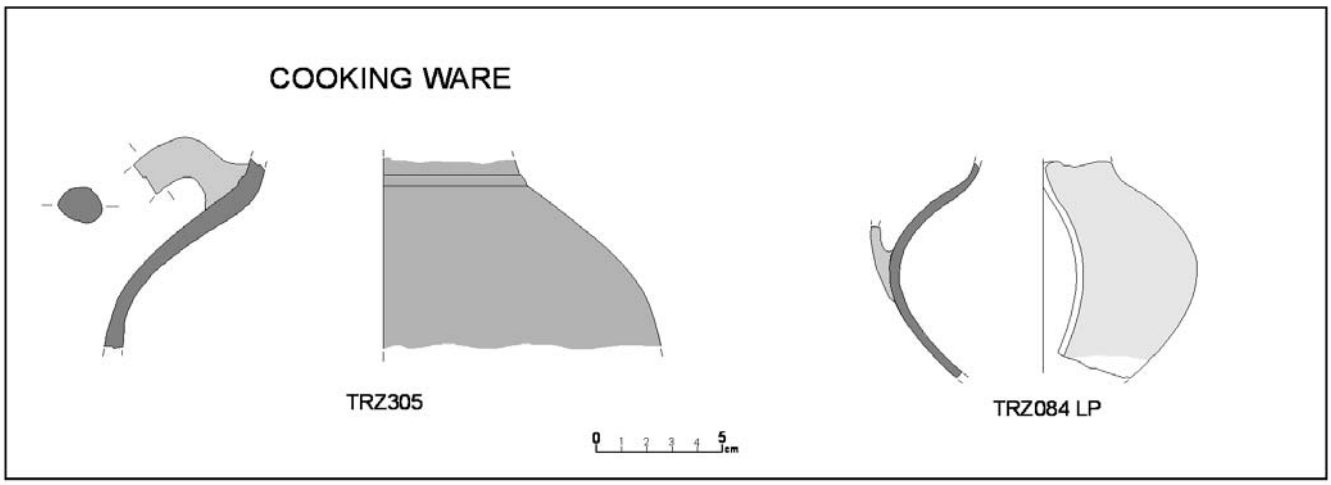

Figure 40: Typology of the cooking ware TRZ305 and the common ware TRZ084 belonging to **TT-E** group

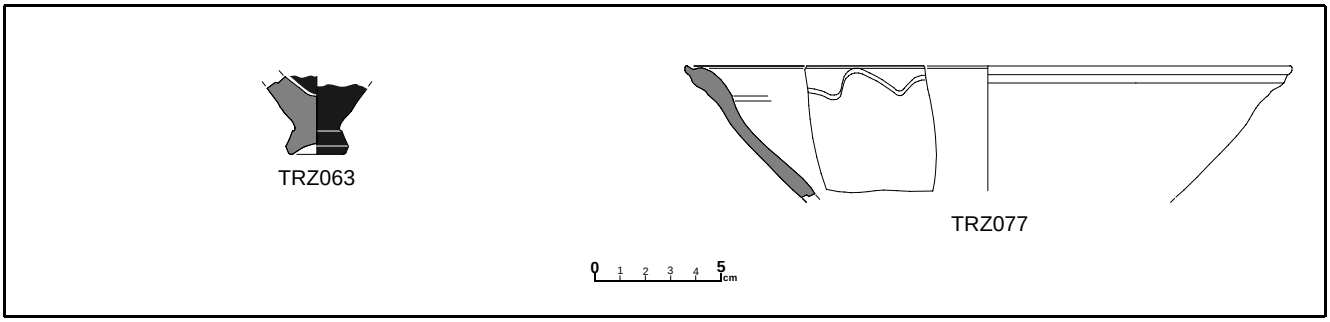

Figure 41: Typology of the **TT-F** group (TRZ063 and TRZ077)

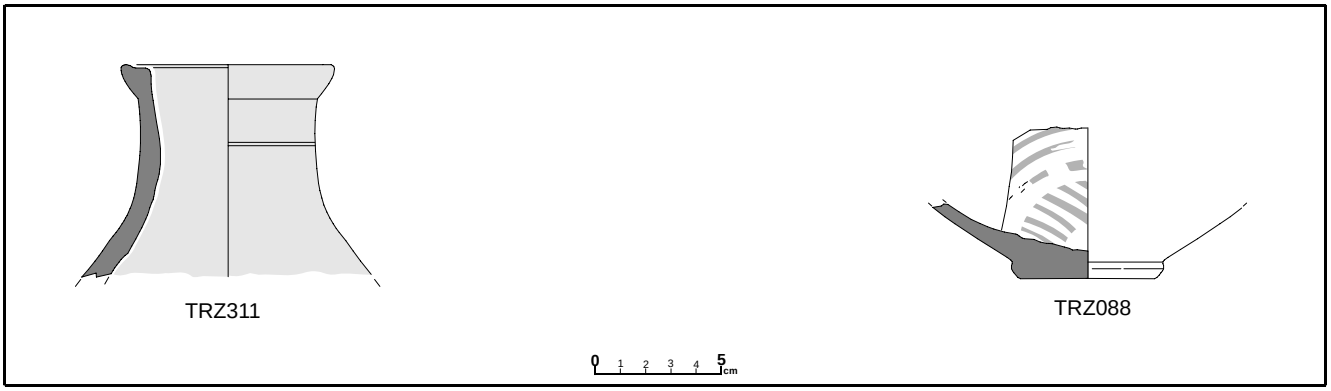

Figure 42: Typology of the common wares TRZ311 and TRZ088

The rest of the pottery from Tchinguiz Tepe, that correspond to the majority of the analysed shards, (TRZ051, TRZ052, TRZ053, TRZ054, TRZ055, TRZ056, TRZ057, TRZ058, TRZ059, TRZ060, TRZ064, TRZ065, TRZ066, TRZ067, TRZ068, TRZ069, TRZ070, TRZ071, TRZ072, TRZ073, TRZ074, TRZ075, TRZ076, TRZ078, TRZ079, TRZ080, TRZ081, TRZ082, TRZ083, TRZ085, TRZ086, TRZ087, TRZ157, TRZ158, TRZ159. TRZ160, TRZ164, TRZ165, TRZ166, TRZ167, TRZ168, TRZ169, TRZ173, TRZ174, TRZ175, TRZ176, TRZ178, TRZ179, TRZ180, TRZ181, TRZ183, TRZ184, TRZ185, TRZ186, TRZ188, TRZ190, TRZ191, TRZ192, TRZ193, TRZ194, TRZ195, TRZ196, TRZ197, TRZ198, TRZ199, TRZ200, TRZ201, TRZ202, TRZ292, TRZ296, TRZ297, TRZ298, TRZ299, TRZ300, TRZ301, TRZ302, TRZ303, TRZ304, TRZ306, TRZ307, TRZ310 and TRZ312) is grouped together in **TT-G** (Figure 35) at the centre of the dendrogram. **TT-G** is composed by 82 calcareous pottery shards with significant chemical similarities and a low total variation according to the CVM calculated for the group that indicate that they represent the same production. The mean chemical composition and the standard deviation of **TT-G** are given at Table 8. It is interesting that, according to this table, the whole group present lower Na_2O concentration regarding to the rest of the analysed material. As the all individuals sampled at the kiln site (RF) of Tchinguiz Tepe are classified into this last group, as well, **TT-G** might be associated, with high probability, to the ceramic production of this pottery workshop (sector RF) recovered at **Tchinguiz Tepe**. That is why **TT-G** has been considered as the Reference Group (RG) of this specific kiln.

Three shards from **TT-G** group are cooking wares from the sector RC (TRZ085, TRZ183) whereas one comes from RF sector (TRZ292). The rest of the ceramics corresponds to two oil lamps (TRZ159 and TRZ169 from RC sector) and several painted and unpainted common wares from RC and RF sectors (Figure 43). Special mention should be made of the typology of these ceramics. They are predominantly bowls, big plates, plates and jars and usually a reddish-brownish slip was added over the inner and/or the outer surfaces.

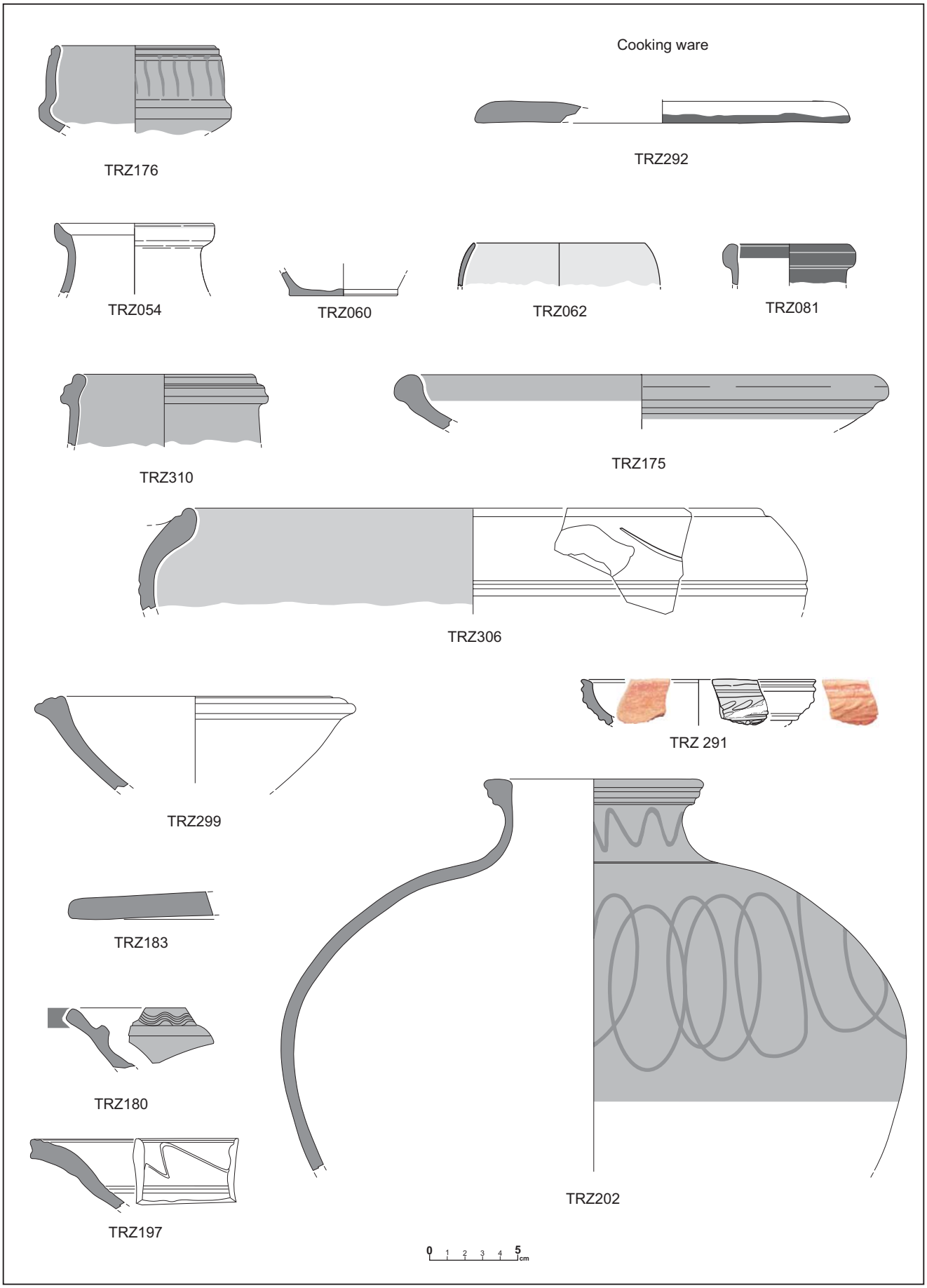

Figure 43: Typology of the **TT-G** group

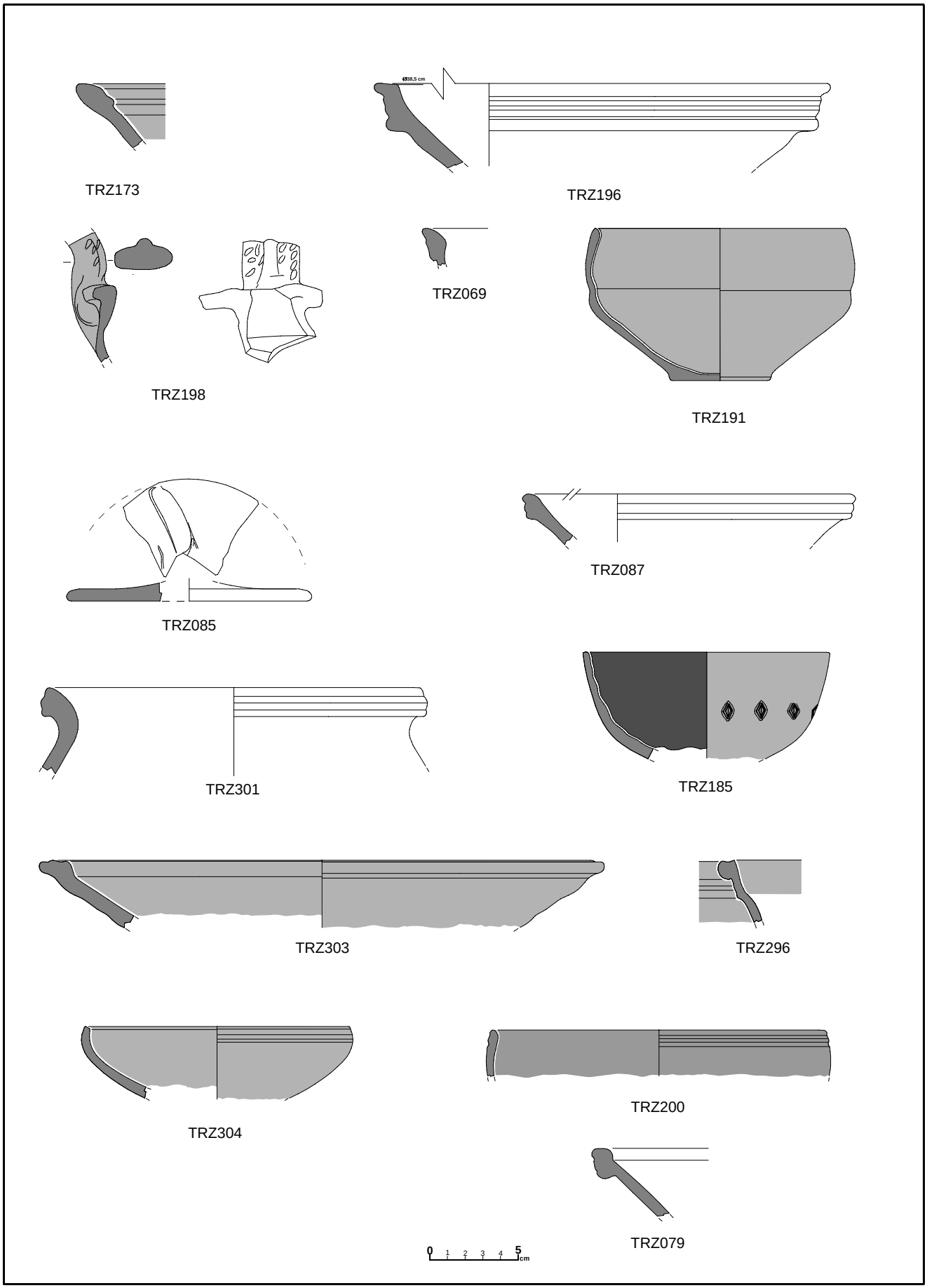

Figure 43: Typology of the **TT-G** group

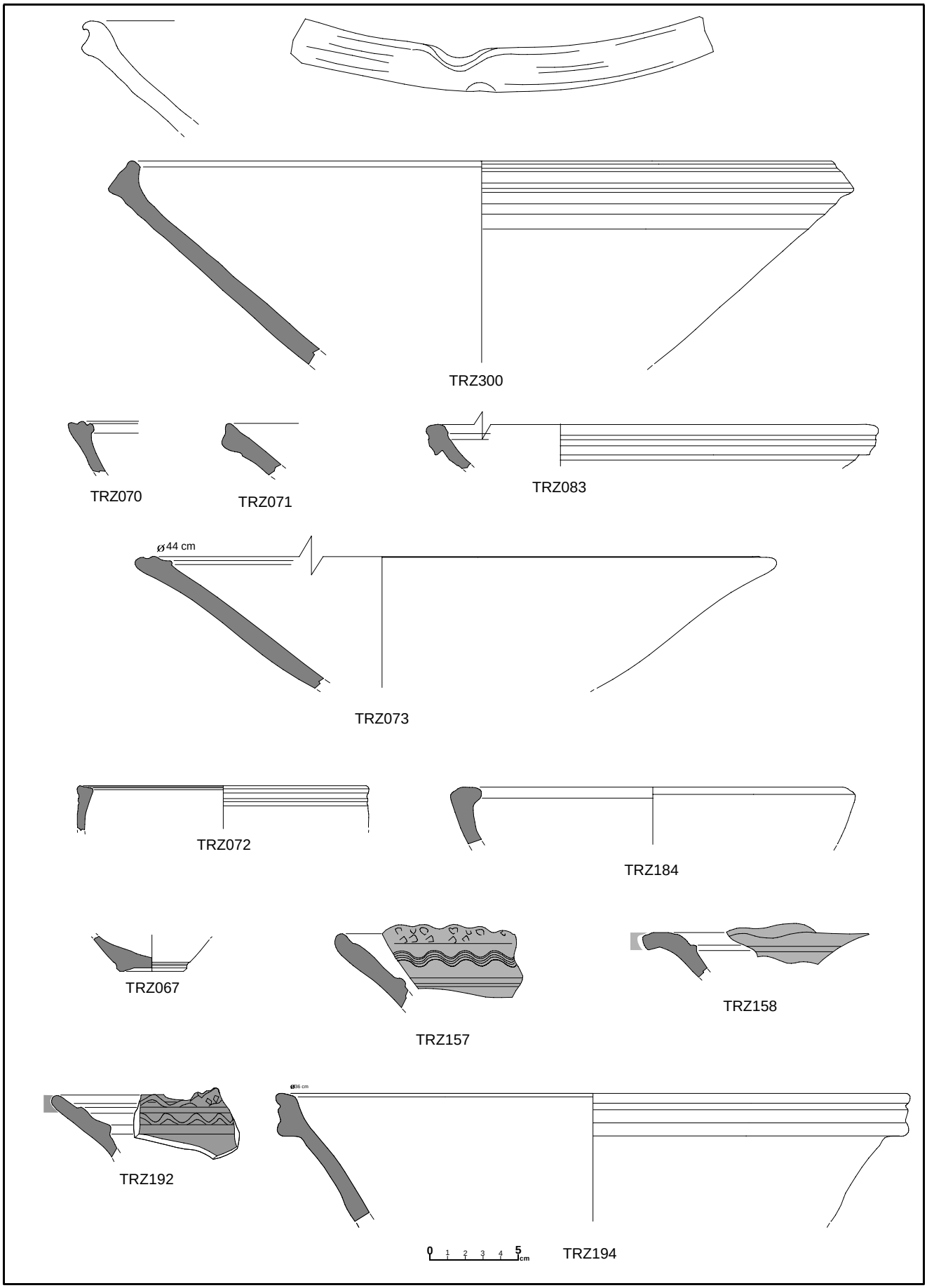

Figure 43: Typology of the **TT-G** group

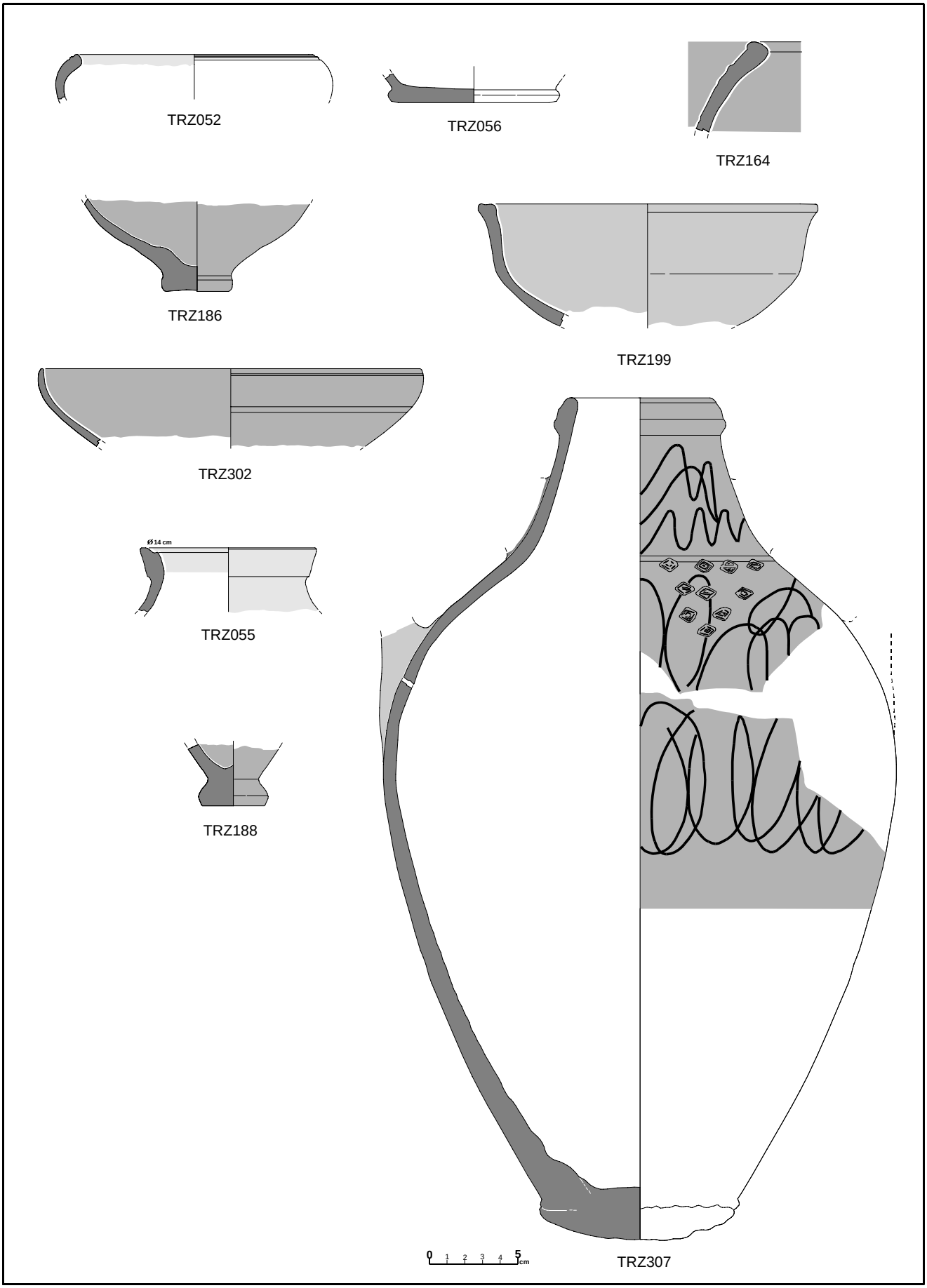

Figure 43: Typology of the **TT-G** group

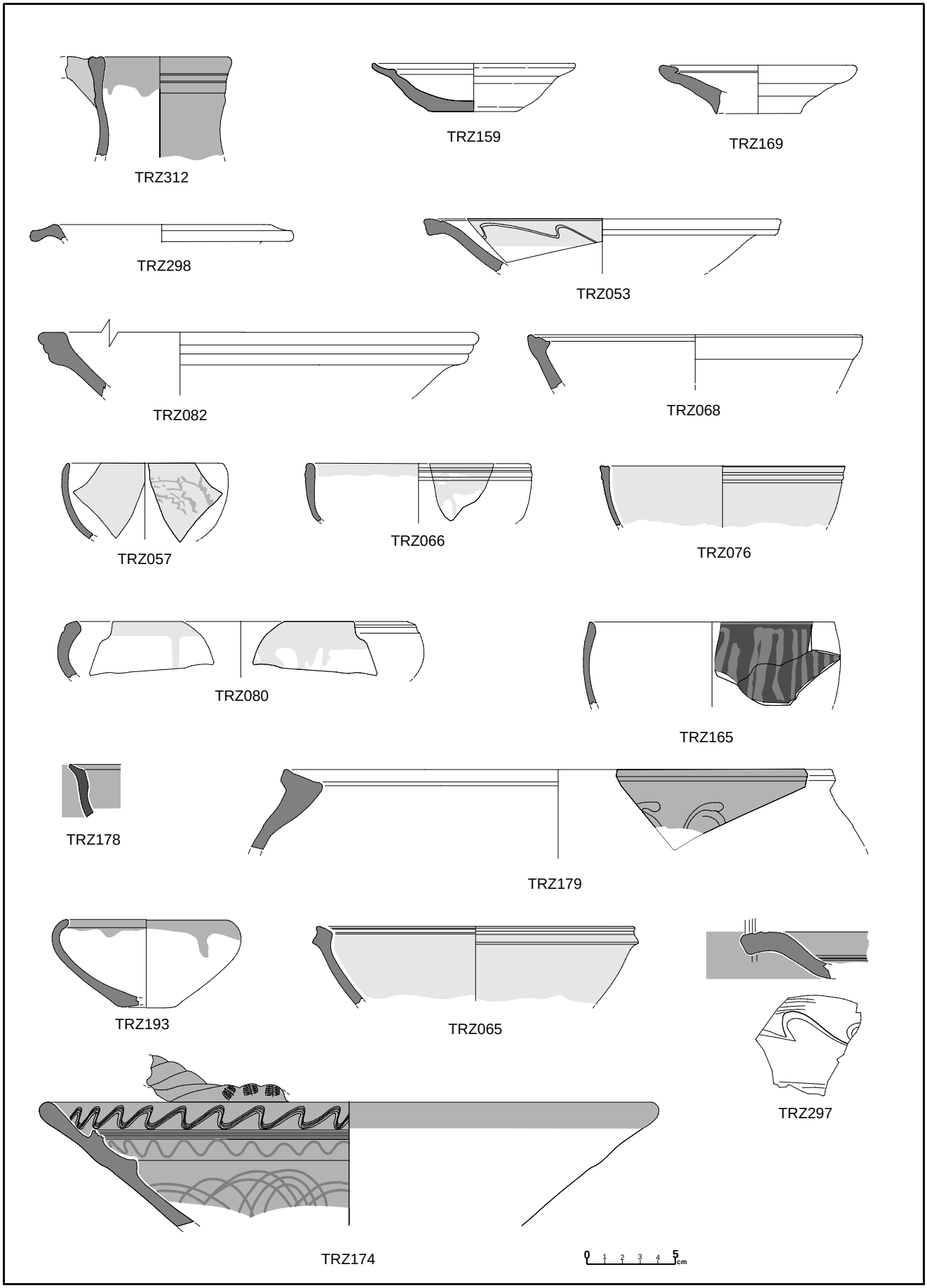

Figure 43: Typology of the **TT-G** group

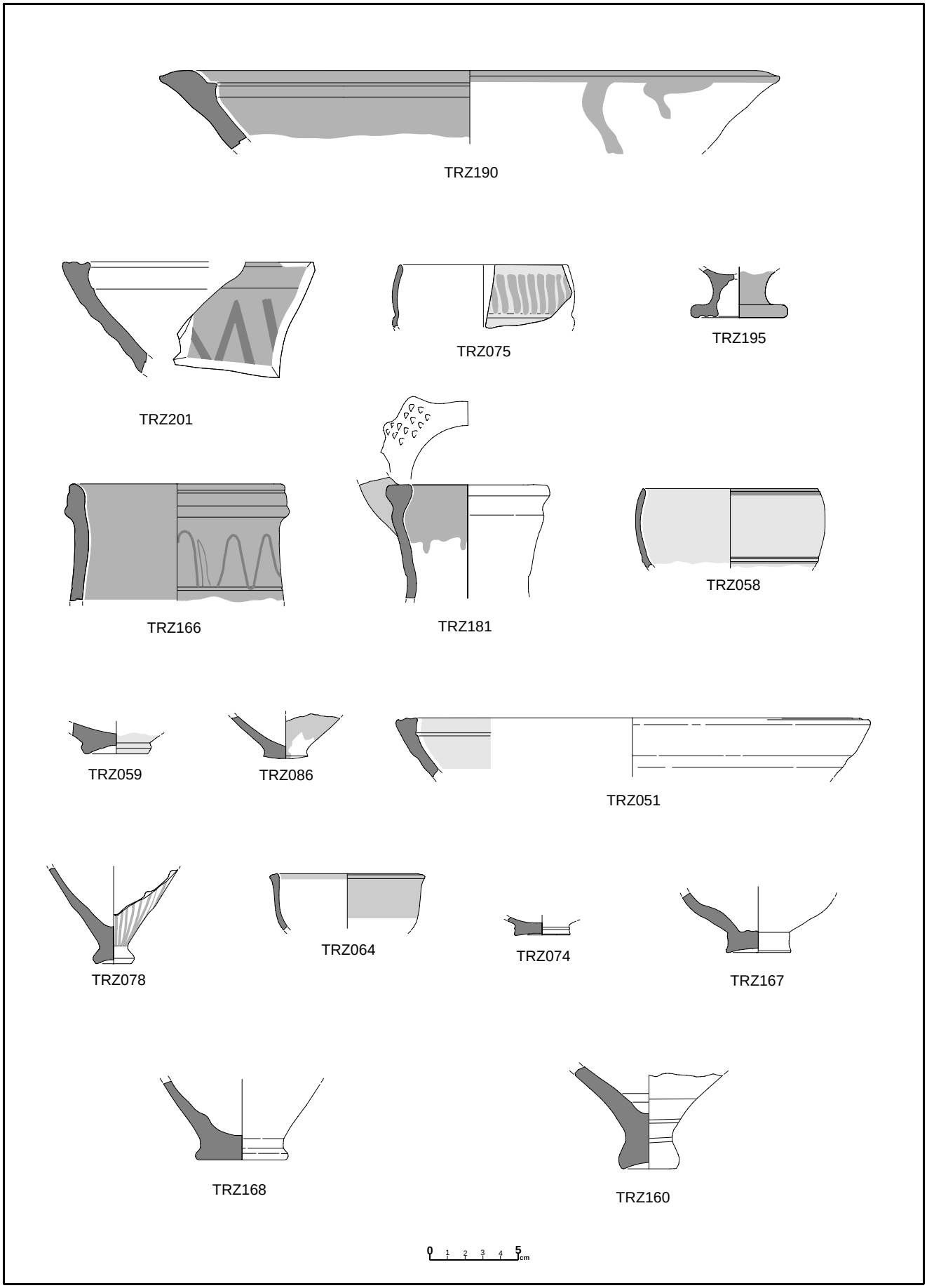

Figure 43: Typology of the **TT-G** group

From **RC** sector, 13 unpainted common wares form part of **TT-G** group. They are six plates (TRZ073, TRZ079, TRZ082, TRZ087, TRZ300, TRZ087, TRZ300), five bases (TRZ056, TRZ060, TRZ074, TRZ167 and TRZ168) and two bowls (TRZ298 and TRZ299) together with one jar (TRZ301). But most of the ceramics are decorated with a slip. They are ten big plates (TRZ051, TRZ157, TRZ173,TRZ174, TRZ175, TRZ180, TRZ201, TRZ297, TRZ303, TRZ306), 19 small plates and bowls (TRZ052, TRZ053, TRZ057, TRZ058, TRZ059, TRZ060, TRZ064, TRZ065, TRZ066, TRZ074, TRZ076, TRZ080, TRZ158, TRZ164,TRZ165, TRZ178, TRZ296, TRZ302, TRZ304), 8 jars (TRZ054, TRZ055, TRZ081, TRZ166, TRZ181, TRZ307, TRZ310, TRZ312), 4 cups (TRZ075, TRZ078, TRZ160, TRZ176) and one big container storage jar (TRZ179)

Finally, the rest of common wares joined in **TT-G** group come from the prospection works carried out in 2007 over the surface of **RF** sector and from the pottery kiln stratigraphy excavated in 2008. They are five unpainted plates (TRZ1069, TRZ070, RZ071, TRZ194, TRZ196) one base (TRZ067) and 3 unpainted bowls (TRZ068, TRZ072, TRZ184). The rest are slip vessels: two big plates (TRZ190, TRZ192), five small plates and bowls (TRZ185, TRZ186, TRZ191, TRZ193, TRZ200), two jars (TRZ198, TRZ202) and two cups (TRZ188, TRZ195)

6.1.2. Petrographical composition (thin section analysis)

From a petrographic point of view, cooking wares from **TT-A** group (TRZ163, TRZ170, TRZ293, TRZ294, TRZ295 and TRZ309) are characteristics of a medium-fine fabric (Figure 44). Clay matrix: Fe-rich (semi-vitrified). Groundmass (relatively abundant and fine): quartz and muscovite (dominant). Coarser inclusions (≤ 0.5 mm): scarce, moderately to well sorted, sub-rounded to sub-angular, double-spaced, bimodal grain-size distribution. Predominant to dominant: quartz, k-feldspars, plagioclase, quartz-mica schist; Dominant to frequent: muscovite, mica-schist; Common to few: quartzite, chert; Few to occasional: epidote, opaques, micritic calcite. Few voids are present, consisting of rare elongate macro-vughs, orientated in a parallel axis to the vessel margins. They are partially filled by secondary micritic calcite. Some differences in the calcareous component are observed, being TRZ163 richer in Fe oxides then TRZ170.

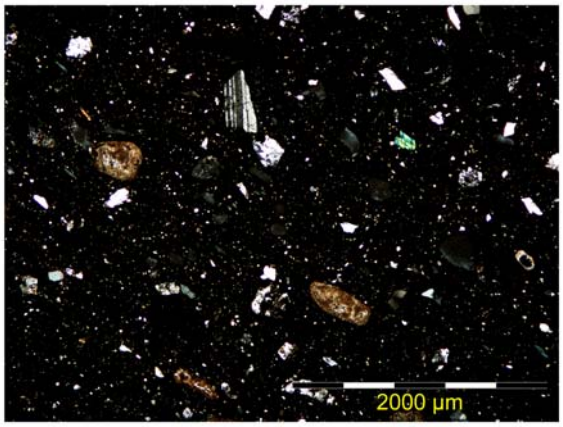

TRZ170 40x xp

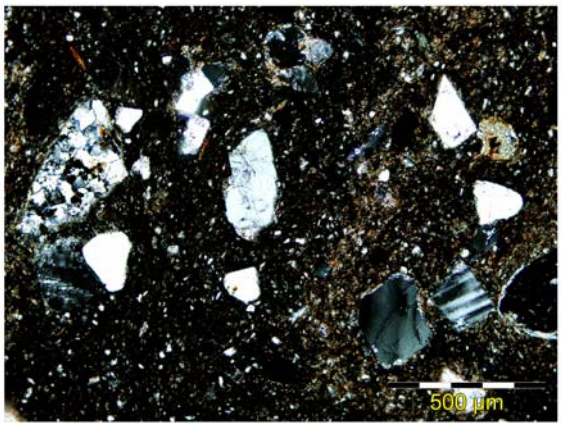

TRZ170 100x xp

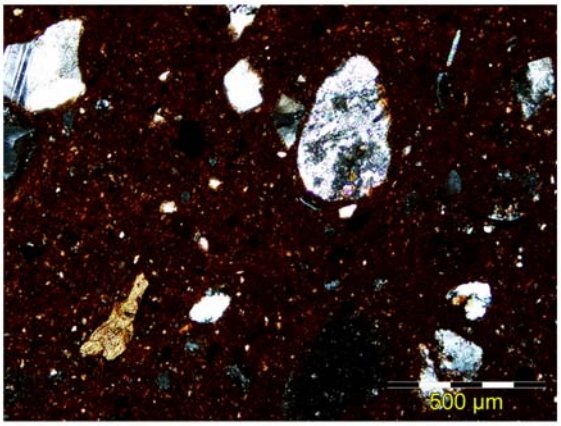

TRZ163 100x xp

Figure 44: Microphotographs by crossed polars (xp) of the ceramics TRZ163 and TRZ170 from **TT-A** (Tchinguiz Tepe)

In petrographical terms, the cooking wares TRZ161 and TRZ189 from **TT-B** chemical group correspond to a coarse fabric with dominant shell-fragments inclusions (Figure 45). To this fabric can be attributed the cooking ware TRZ061 analysed only by thin section analysis (Martínez *et al.*, 2009: 256). Clay matrix: Fe-rich (+ Ca-rich shell and fossils; poorly vitrified). Groundmass (relatively abundant and fine): quartz and muscovite (dominant); calcite (micrite and sparite), opaques (accessory). Coarser inclusions (≤ 1.5 mm): relatively abundant, moderately well sorted, rounded to sub-angular, single-spaced, bimodal grain-size distribution. Predominant to dominant: shell macrofossils and calcareous

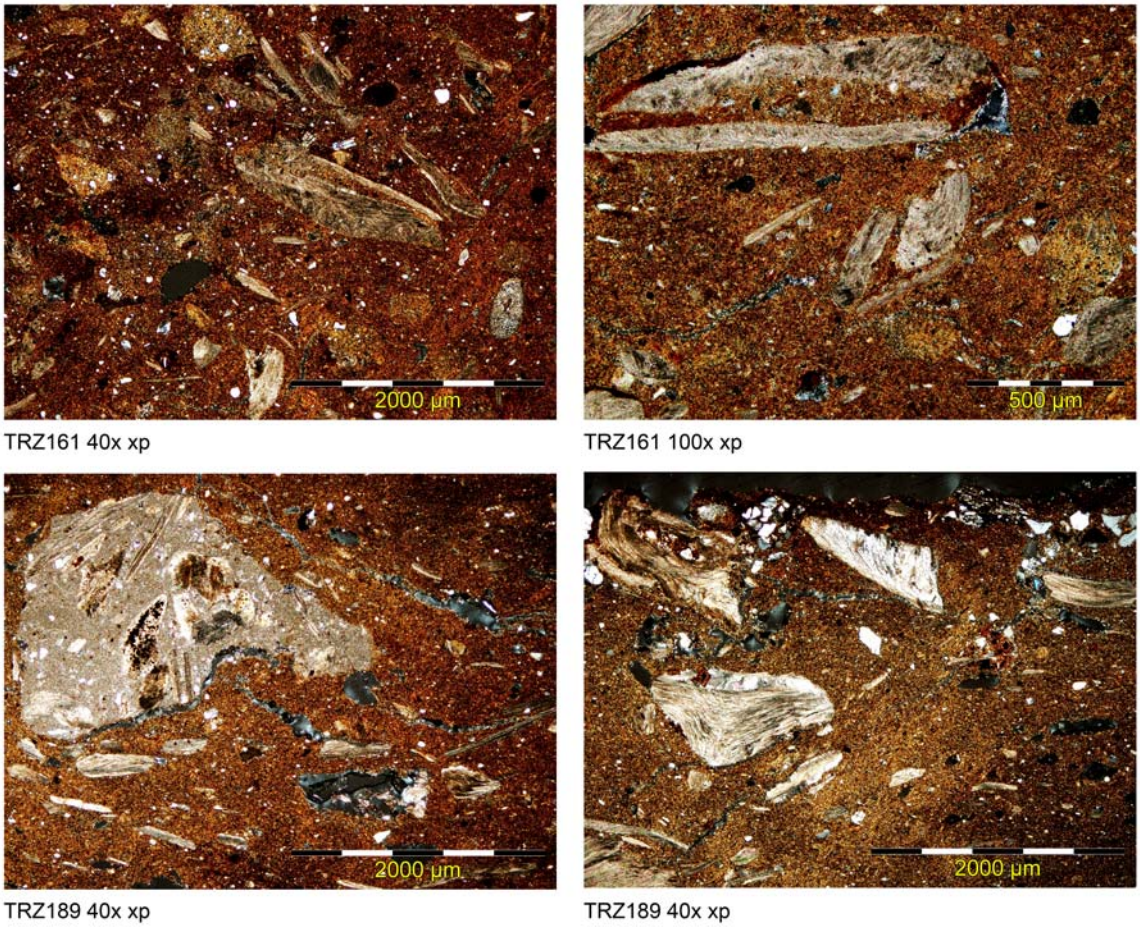

Figure 45: Microphotographs by crossed polars (xp) of the ceramics TRZ161 and TRZ189 from **TT-B** (Tchinguiz Tepe)

sedimentary rock fragments (fine-grained sandstone). Some of these rocks have become in a silicate rock altogether with spathic calcite crystals forming the sedimentary rocks; quartz, calcite (micrite); Common to few: quartz-mica schist; Few to occasional: volcanic-glass. Voids are common, corresponding to mesovughs, sometimes partially filled with secondary calcite (Cau *et al.*, 2002) and orientated following the vessel margins.

In thin section, the three cooking wares from **TT-C** chemical group (TRZ172, TRZ182 and TRZ187) present various similarities between them and they are very different to the previous two groups of cooking wares **TT-A** and **TT-B**. The main characteristic of this coarse fabric is the presence of shell fragments which measures 3 mm as maximum long axis dimension (Figure 46). In the three samples there are also frequent microfossils, some of which have been decomposed during the firing process becoming micritic calcite (Cau *et al.*, 2002). Macrovughs are more frequents in TRZ182 as the consequence of decomposition of calcite from shell fragments due to the high firing temperature. However, several differences in the type of aplastic inclusions point at the existence of various sub-fabrics. Clay matrix: Fe-rich (+ Ca-rich shell and fossils; poorly vitrified). Groundmass (relatively abundant, more scarce and fine in TRZ172 and TRZ182): quartz and muscovite (dominant); calcite (micrite) and opaques (acces-

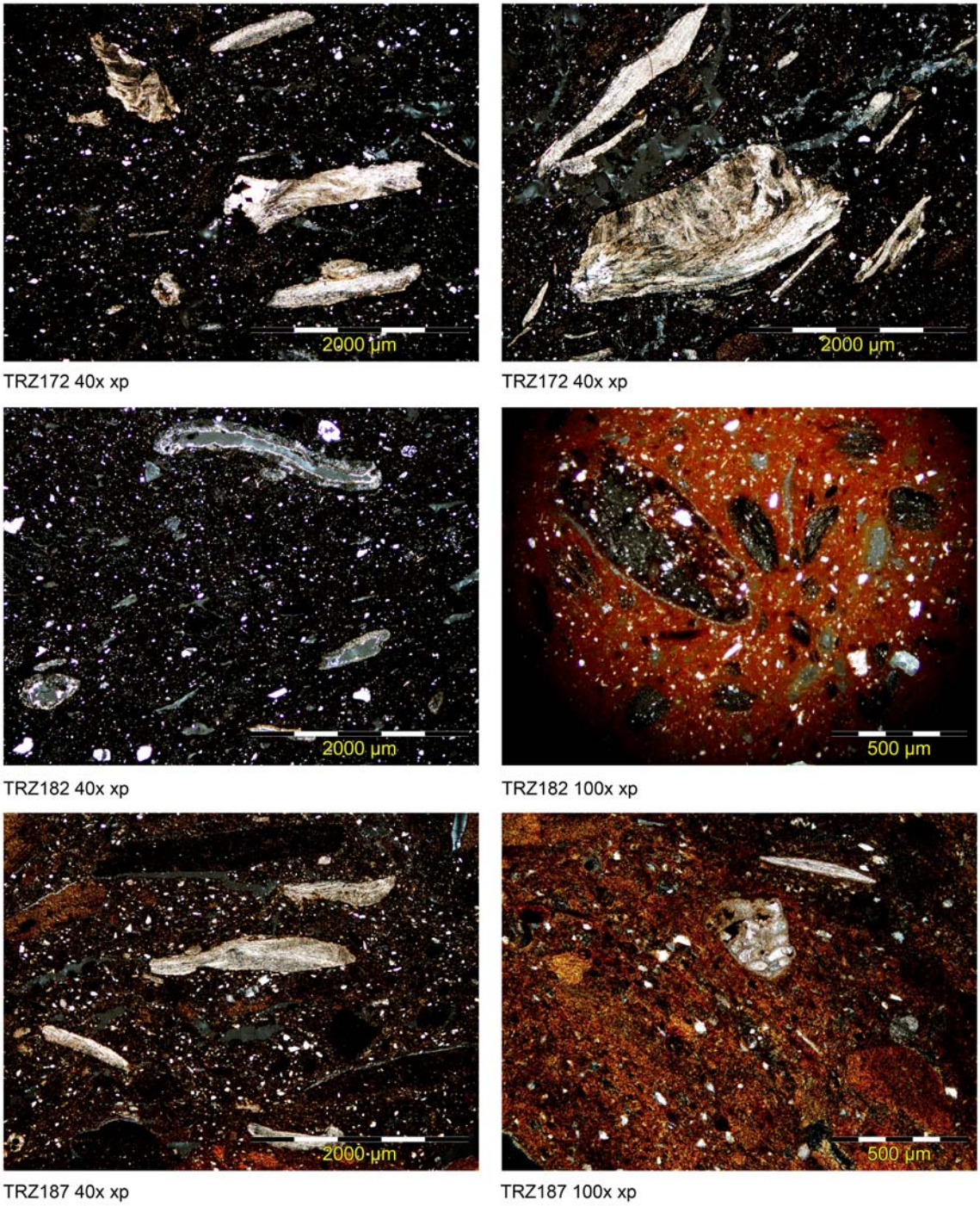

Figure 46: Microphotographs by crossed polars (xp) of the ceramics TRZ172, TRZ182 and TRZ187 from **TT-C** (Tchinguiz Tepe)

sory). Coarser inclusions (≤ 3 mm): relatively abundant, moderately well sorted, sub-rounded, elongate, single-spaced, bimodal grain-size distribution.

– In TRZ172: Predominant to dominant: calcareous microfossils and shell fragments.

– In TRZ182: Predominant to dominant: calcareous microfossils and shell fragments, sedimentary rocks as sandstones and siltstones. Dominant to frequent: quartz-mica schist, muscovite; Common to few: quartz, plagioclase; Few to occasional: amphibole, epidote and opaques.

– In TRZ187: Predominant to dominant: calcareous microfossils and shell fragments, sedimentary rocks as sandstones and siltstones. Dominant to frequent: muscovite.

Another coarse fabric (**TT-D**) is formed by TRZ162 and TRZ171 cooking wares coming from s.u. 3 and s.u. 5 respectively of RC sector of the **Tchinguiz Tepe**. However, differences in composition

between both ceramics leads to divided in two subfabrics (Figure 47). Clay matrix: Fe-rich (+ Ca-rich shell and fossils; semi-vitrified). Groundmass is moderately abundant, homogeneous with low optical activity: quartz and muscovite (dominant); calcite (micrite) (accessory). Coarser inclusions (≤ 2.5 mm): relatively abundant, moderately well sorted, sub-rounded, elongate, single-spaced, sometimes in contact, bimodal grain-size distribution. Predominant to dominant: sedimentary rocks (quartzarenite, siltstones); Dominant to frequent: calcareous microfossils and shell fragments; Common to few: quartz, muscovite and opaques; Few to occasional: chert, plagioclase, amphibole, epidote. The sub-fabric re-

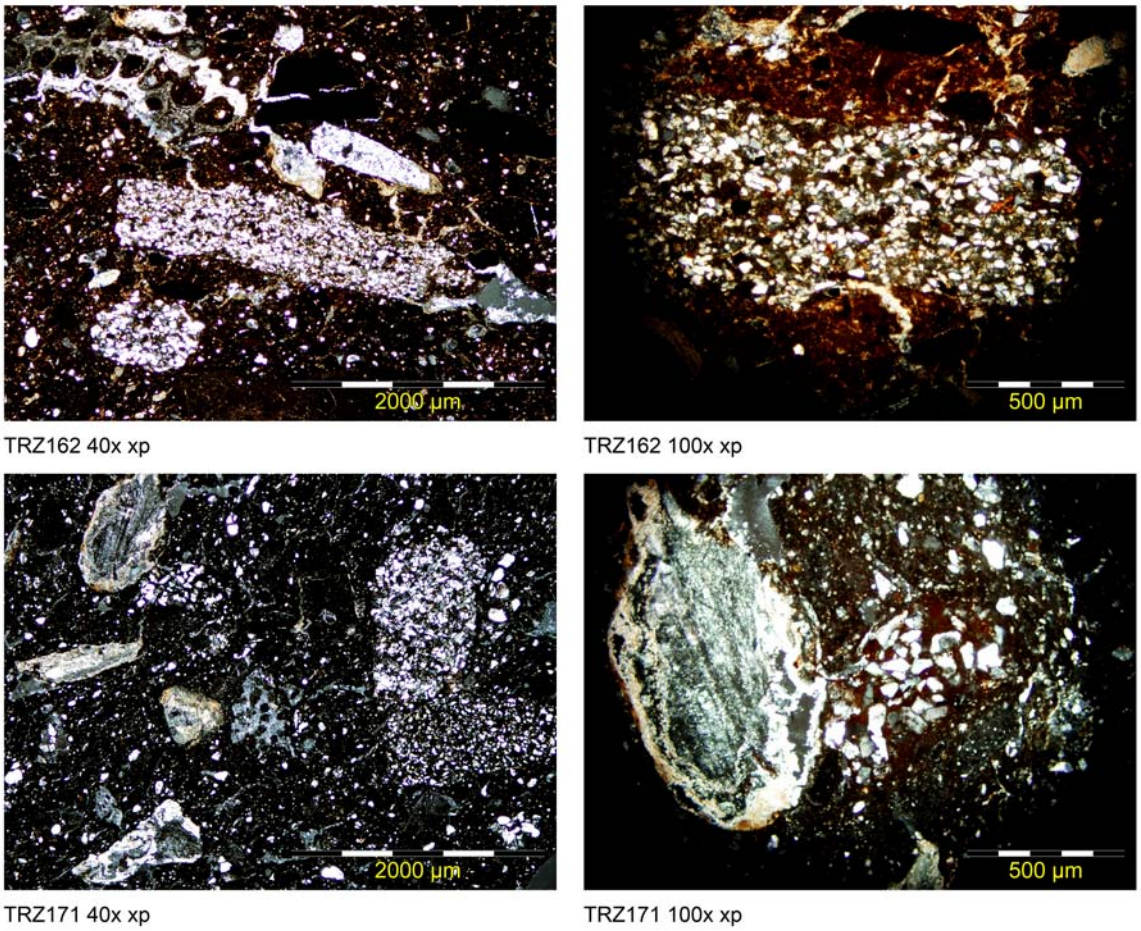

Figure 47: Microphotographs by crossed polars (xp) of the ceramics TRZ162 and TRZ171 from **TT-D** (Tchinguiz Tepe)

presented by the individual **TRZ171** is also characterised by the presence of sandstones and frequent nodules of secondary micritic calcite derived from calcareous shell fragments. Nevertheless, no cherts, plagioclases, amphiboles nor epidotes are present. Frequent voids in both subfabrics can be observed, corresponding mainly to macro-vughs and meso-vughs, sometimes partially or totally filled with secondary calcite, created by a non total decomposition of calcareous shells or due to the reprecipitation of carbonate inclusions (Cau *et al.*, 2002).

Regarding **TT-E** chemical group, only the painted jar TRZ084, from s.u. 5 of RC sector, has been examined by thin section analysis (Figure 48). Clay matrix: Fe-rich (+ Ca-rich nodules), homogeneous, and the optical activity is medium-low (semi-vitrified). Groundmass (abundant): quartz and muscovite (dominant); plagioclase, k-feldspar, opaques (accessory). Coarser inclusions (≤ 1.5 mm): relatively abundant, moderate to well sorted, sub-rounded, elongate, open-spaced to single-spaced, bimodal grain-size distribution. Predominant to dominant: quartz, quartz-mica schist fragments, muscovite; Dominant to frequent: plagioclase, k-feldspar; Common to few: amphibole, epidote and biotite; Few to occasional: quartzite, quartzarenite, opaques. Voids are rare, predominantly meso-vughs.

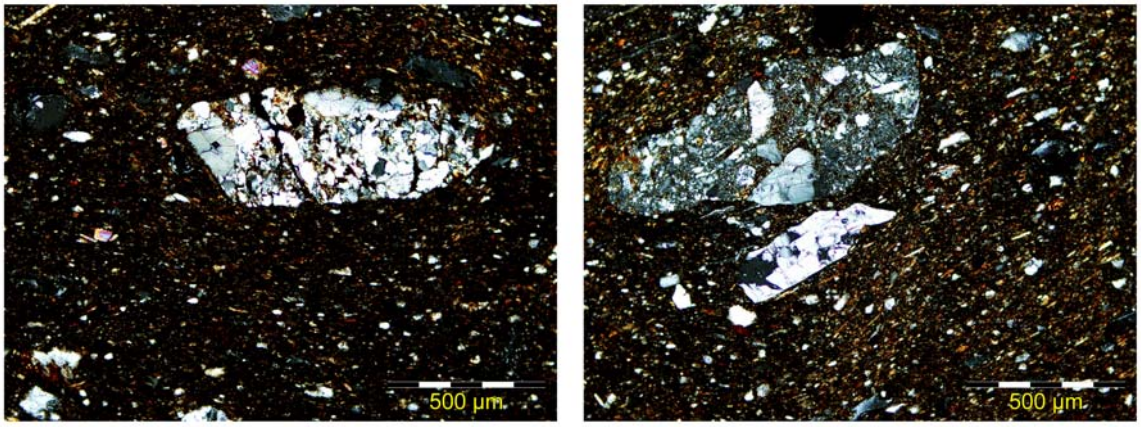

TRZ084 100x xp TRZ084 100x xp

Figure 48: Microphotographs by crossed polars (xp) of the ceramic TRZ084 from **TT-E** (Tchinguiz Tepe)

In the case of two common wares from **TT-F** chemical group (TRZ063 and TRZ077), no thin section analysis has been realised until now. Because of that, we don't know the petrographical composition of these wares. However, the chemical similarity with ceramics from **TT-G** group leads to consider a similar provenance area inside ancient **Termez**.

Finally, the major group of cooking wares and common wares is represented by chemical group **TT-G**. In petrographic terms, the analysed vessels (TRZ060, TRZ065, TRZ067, TRZ068, TRZ076, TRZ085, TRZ183 and TRZ188) have been divided in five main petrographical fabrics because of differences in frequency and dimensions of non-plastic inclusions.

- ***F-TT-G1***: Common wares TRZ060, TRZ065, TRZ076 and TRZ085 can be grouped in a fine subfabric (Figure 49). Clay matrix: Fe-rich (semi-vitrified). Groundmass (relatively abundant, very fine): quartz and muscovite (dominant). Coarser inclusions (≤ 0.5 mm): scarce, well sorted, sub-angular to sub-rounded, open-spaced, unimodal grain-size distribution. Predominant to dominant: quartz, muscovite; Dominant to frequent: plagioclase, k-feldspar; quartzite, quart-mica schist; Common to few: granites, phyllite, calcareous microfossils; Few to occasional: sandstone, chert, amphibole, nodules of micri-tic calcite, opaques. Microfossils seem to be present in the calcareous clay which was added and mixed with a ferric one. Voids (few meso-vesicles) are partially filled with secondary calcite.

- ***F-TT-G2***: Common ware TRZ067, from the surface prospected in RF sector. Clay matrix: Fe-rich and the micromass of the totally fired matrix is optically inactive. It is noticeably over-fired and can be characterized as '*waster*' (Figure 50). Groundmass (relatively abundant): quartz and muscovite (dominant). Coarser inclusions (≤ 500-700 µm): relatively abundant, well sorted, sub-rounded to sub-angular, open-spaced, bimodal grain-size distribution. The majority of inclusions show strong alteration due to the high temperature of firing. Predominant to dominant: Monocrystalline and polycrystalline quartz, quartz-mica schist, sandstone; Dominant to frequent: chert; Common to few: plagioclase, k-feldspar; Few to occasional: muscovite and biotite.

- ***F-TT-G3***: Common ware TRZ188 from the kiln found in RF sector. Clay matrix: Ca-rich (vitrified). High firing temperature can be deduced by only slightly optically active matrix and because of the decomposition process suffered by the carbonate rocks and the degree of alteration of non-plastic inclusions. Groundmass (scarce, very fine): quartz and muscovite (dominant). Coarser inclusions (≤ 500 µm) are smaller and less frequent than in TRZ085 and TRZ183 but similar in size and frequency to the ones of ***F-TT-G1*** fabric (Figure 50). Coarser inclusions are well sorted, sub-rounded to sub-angular, single-spaced, bimodal grain-size distribution. Predominant to dominant: monocrystalline and polycrystalline quartz, muscovite; Dominant to frequent: quartz-mica schist, plagioclase, K-feldspar; Common to few: biotite; Few to occasional: chert, opaques. Voids are frequents, as micro-vesicles and micro-vughs.

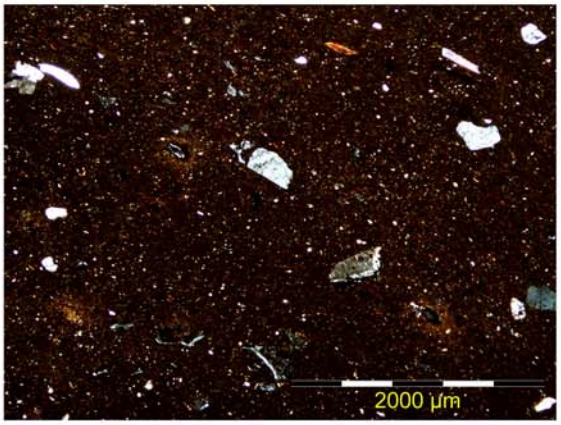

TRZ060 40x xp

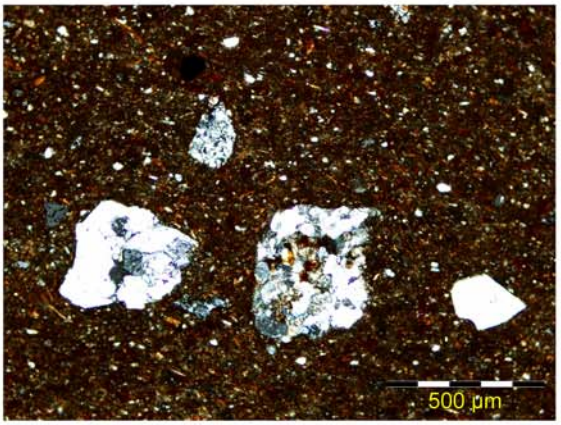

TRZ060 100x xp

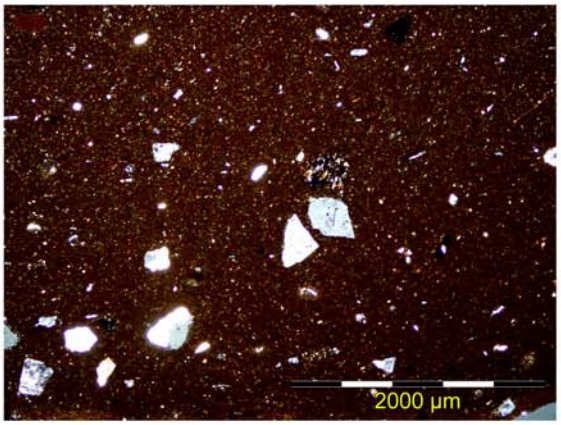

TRZ068 40x xp

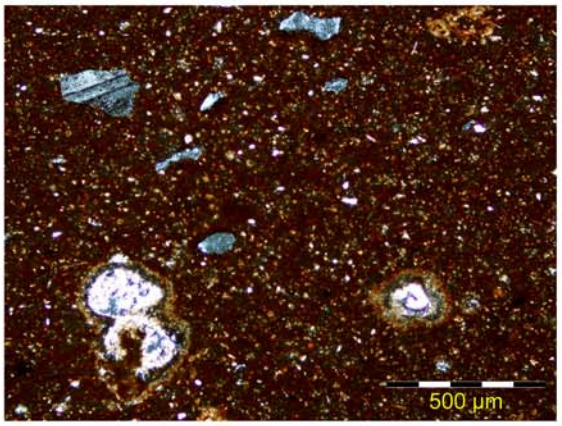

TRZ068 100x xp

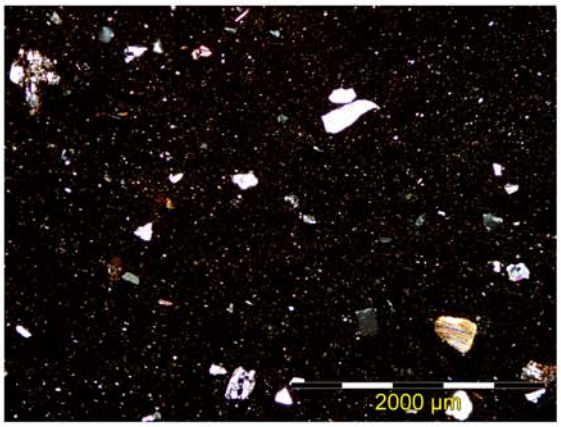

TRZ076 40x xp

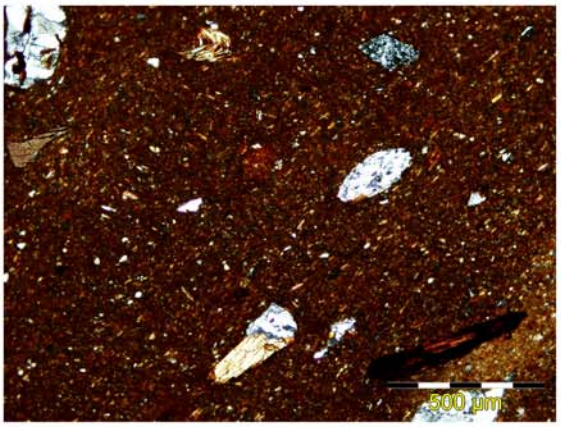

TRZ076 100x xp

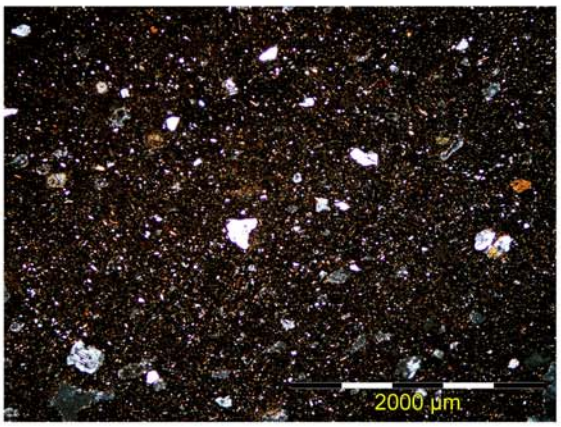

TRZ065 40x xp

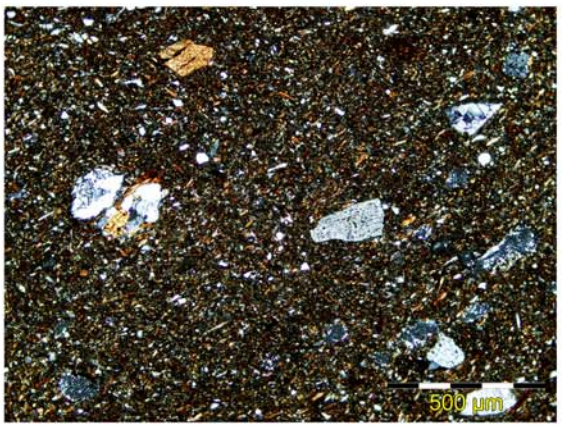

TRZ065 100x xp

Figure 49: Microphotographs by crossed polars (xp) of the ceramics TRZ060, TRZ065, TRZ068 and TRZ076 from **F-TT-G1** petrographic subfabric from **TT-G** (Tchinguiz Tepe)

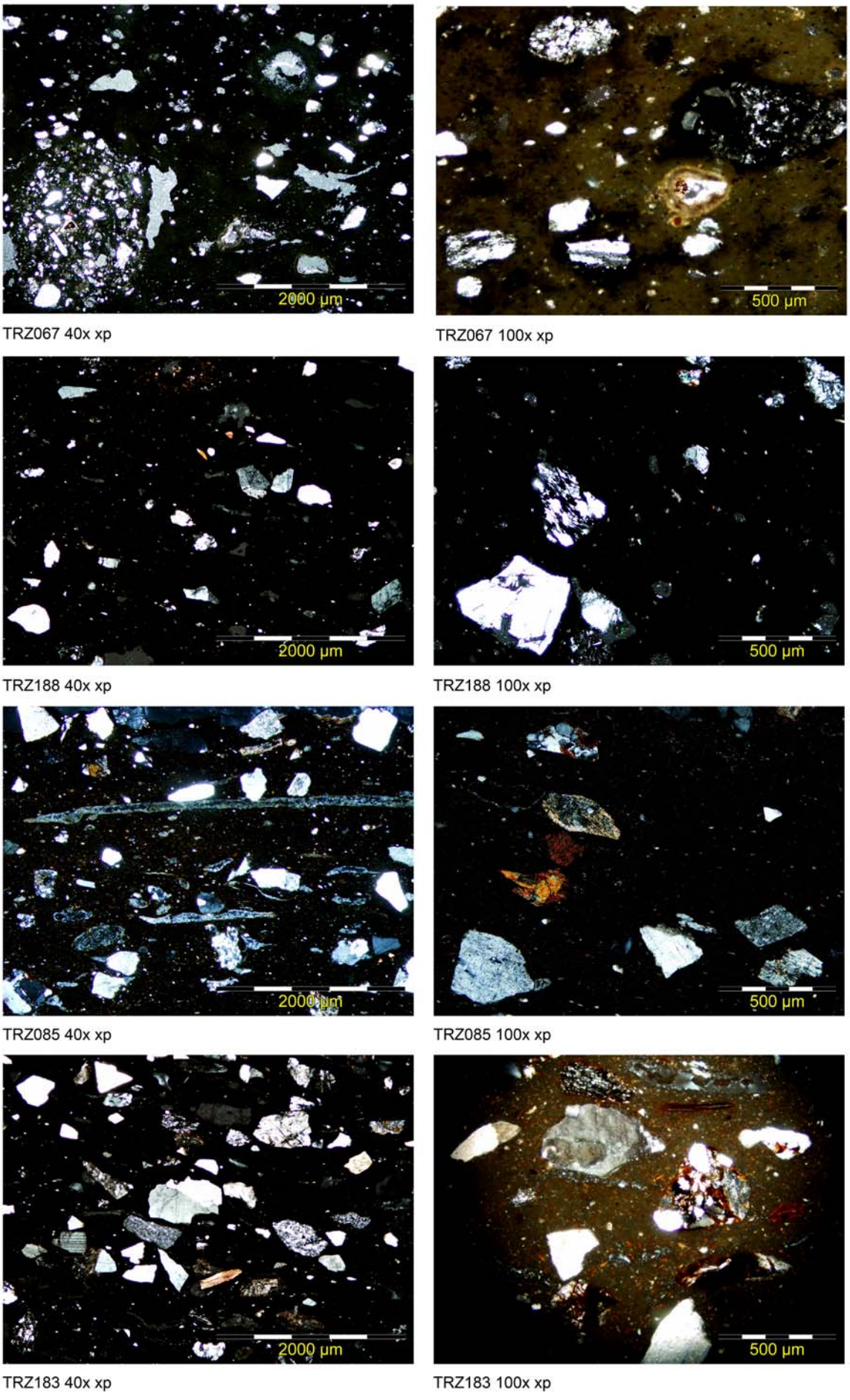

Figure 50: Microphotographs by crossed polars (xp) of the **F-TT-G2** (TRZ067), **F-TT-G3** (TRZ188), **F-TT-G4** (TRZ085) and **F-TT-G5** (TRZ183) petrographic subfabrics from **TT-G** (Tchinguiz Tepe)

- ***F-TT-G4***: Common ware TRZ085 from s.u. 5 of RC sector, considered as medium-coarse fabric. Clay matrix: Fe-rich (+ Ca-rich nodules). The matrix is only slightly optically active (semi-vitrified), suggesting a generally higher firing temperature. Groundmass (relatively abundant, very fine): quartz and muscovite (dominant); amphibole and epidote (accessory). Coarser inclusions (≤ 500-700µm): abundant, well sorted, sub-rounded to sub-angular, single-spaced, bimodal grain-size distribution (Figure 50). Predominant to dominant: quartz, quartz-mica schist, calcareous shell fragments; Dominant to frequent: muscovite, plagioclase and k-feldspar from granite rocks or gneiss; Common to few: amphibole; Few to occasional: basalt and epidote. Is evident that coarser fraction contains calcareous microfossils remains and shell fragments, some of them up to 2mm long axis dimension. Firing process has altered the calcareous component of microfossils, favouring the decomposition of primary calcite and the formation of secondary micritic calcite within the closed pores (Cau *et al*., 2002).

- ***F-TT-G5***: Cooking ware TRZ183 from s.u. 21 of RC sector. Clay matrix: Fe-rich (+ Ca-rich nodules). The clay is rich in iron oxides but includes rests of carbonates that can be the consequence of calcareous shell decomposition, latter altered to secondary micritic calcite (Cau *et al*., 2002). Firing temperature was high, as evidenced by the optically inactive micromass, the degree of alteration, the bloating suffered by non-plastic inclusions and the decomposition process suffered by the calcareous shell fragments (Figure 50). Groundmass (scarce, very fine): quartz and muscovite (dominant). Coarser inclusions (≤ 500µm): abundant, moderately to well sorted, sub-rounded to sub-angular, single-spaced, sometimes in contact, bimodal grain-size distribution. Predominant to dominant: quartz, muscovite, quartz-mica schist, phyllite; Dominant to frequent: plagioclase, k-feldspar, quartzite; Common to few: calcareous microfossils, sandstones, chert; Few to occasional: amphibole, epidote, biotite, opaques; Voids are very frequents with predominant meso-vughs and macro-vughs orientated parallel to the vessel margins.

6.1.3. Mineralogical composition (XRD analysis)

6.1.3.1. TT-A PCRU (TRZ163, TRZ170, TRZ293, TRZ294, TRZ295 and TRZ309)

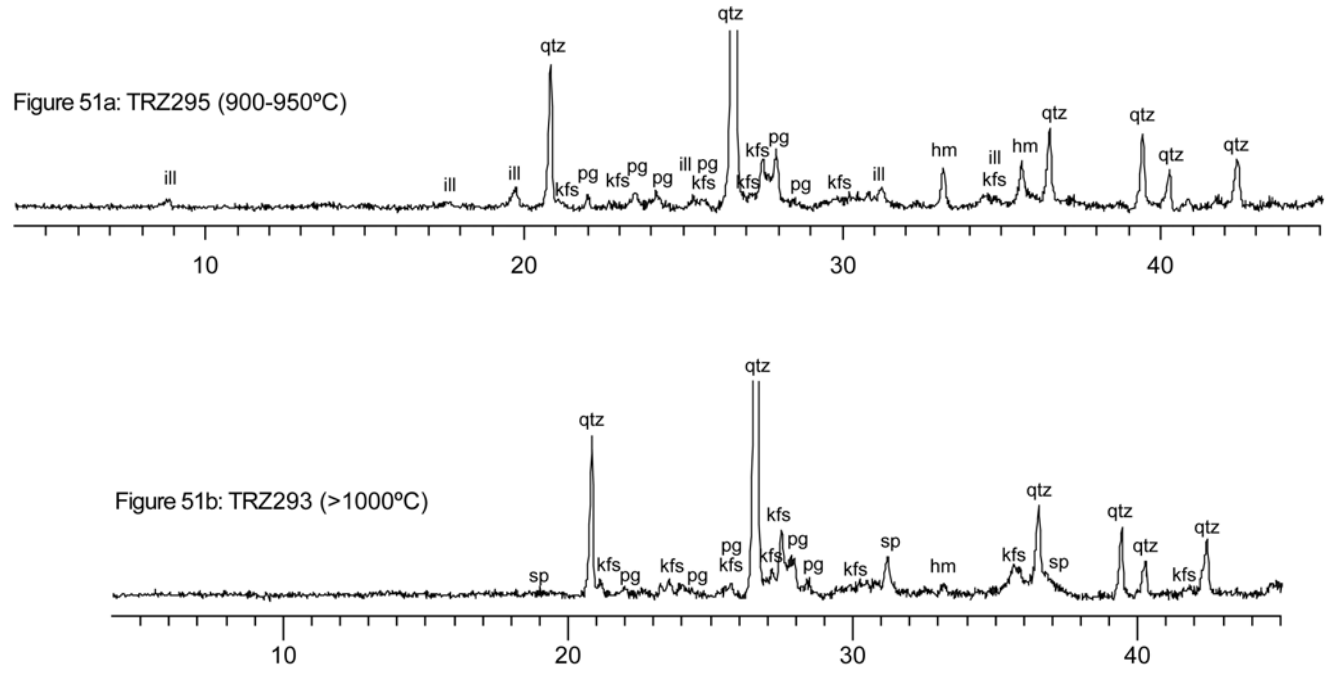

Figure 51: Diffractograms of the individuals TRZ295 and TRZ293 representing the chemical group **TT-A**; hm: hematite, ill: illite-muscovite, kfs: k-feldspar, pg: plagioclase, qtz: quartz, sp: spinel

The low calcareous ceramics TRZ294, TRZ295 and TRZ309 are well fired (Figure 51a), the scarce presence of illite-muscovite points to Equivalent Firing Temperature (EFT) around (850/900-950ºC). TRZ163 is characterised by the simultaneous presence of primary (illite-muscovite) and firing phases (spinel) which indicates relatively high firing temperature. Despite of the presence of illite-muscovite in the diffractogram of this individual, the 10 Å peak of this crystalline phase is already inexistent. The partial descomposition of illite-muscovite, and the obvious presence of spinel under an advanced stage of development, indicates an EFT in the range of 950/1000°C that is because micas withstand relatively high temperatures. The total decomposition of illite-muscovite in the diffractogram of TRZ293 and TRZ170 (Figure 51b) and the even sharper peaks of spinel situate the EFT of these individuals over 1000°C, possibly between 1050°C and 1100°C.

6.1.3.2. TT-B PCRU (TRZ161 and TRZ189)

This group represented by two cooking wares (TRZ161 and TRZ189) with calcareous shell fragments as main temper, shows a diffractogram very different to the previous ceramics. Only primary phases (quartz, calcite, illite-muscovite, plagioclase, k-feldspar) are present, indicating an EFT around 800-850ºC. It must to be noted the predominance of quartz and calcite in these shards, whereas hematite is not present (Figure 52).

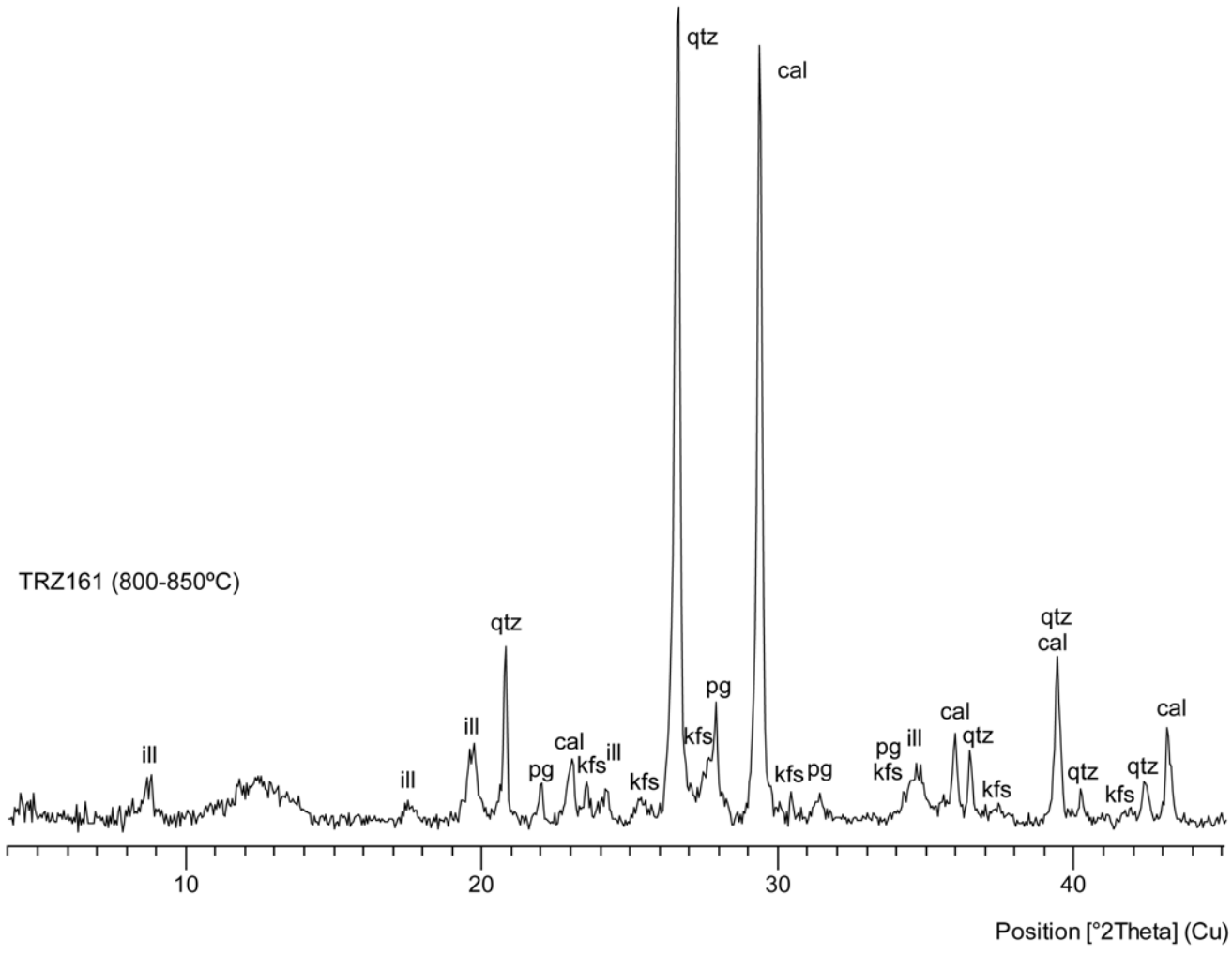

Figure 52: Diffractogram of the individuals TRZ161 representing the chemical group **TT-B**; cal: calcite, ill: illite-muscovite, kfs: k-feldspar, pg: plagioclase, qtz: quartz

6.1.3.3. TT-C PCRU (TRZ172, TRZ182 and TRZ187)

The three individuals belong to this group correspond to two different mineralogical category associated to two different Equivalent Firing Temperature (EFT). On the one hand, TRZ172 and TRZ187 both are characterised by the presence of clear primary phases (illite-muscovite, alkaline feldspars and, according to petrography, plagioclase here is primary) but not clear firing phases (gehlenite or pyroxene) which indicates low firing temperature (Figure 53a). The EFT of both individuals can be estimated in the range of 800/850°C. On the other hand, diffractogram of TRZ182 shows the total decomposition of the illites-muscovite, which in these fabrics correspond mostly to micas (see petrographical description). These phyllosilicates decompose at higher temperature compared to the clay which decomposed at 950/1000°C. Moreover, the sharp peaks of pyroxene with the additional absence of intermediate firing phases like gehlenite that has already decomposed situate the EFT of this individual over 1000°C, possibly between 1050°C and 1100°C (Figure 53b).

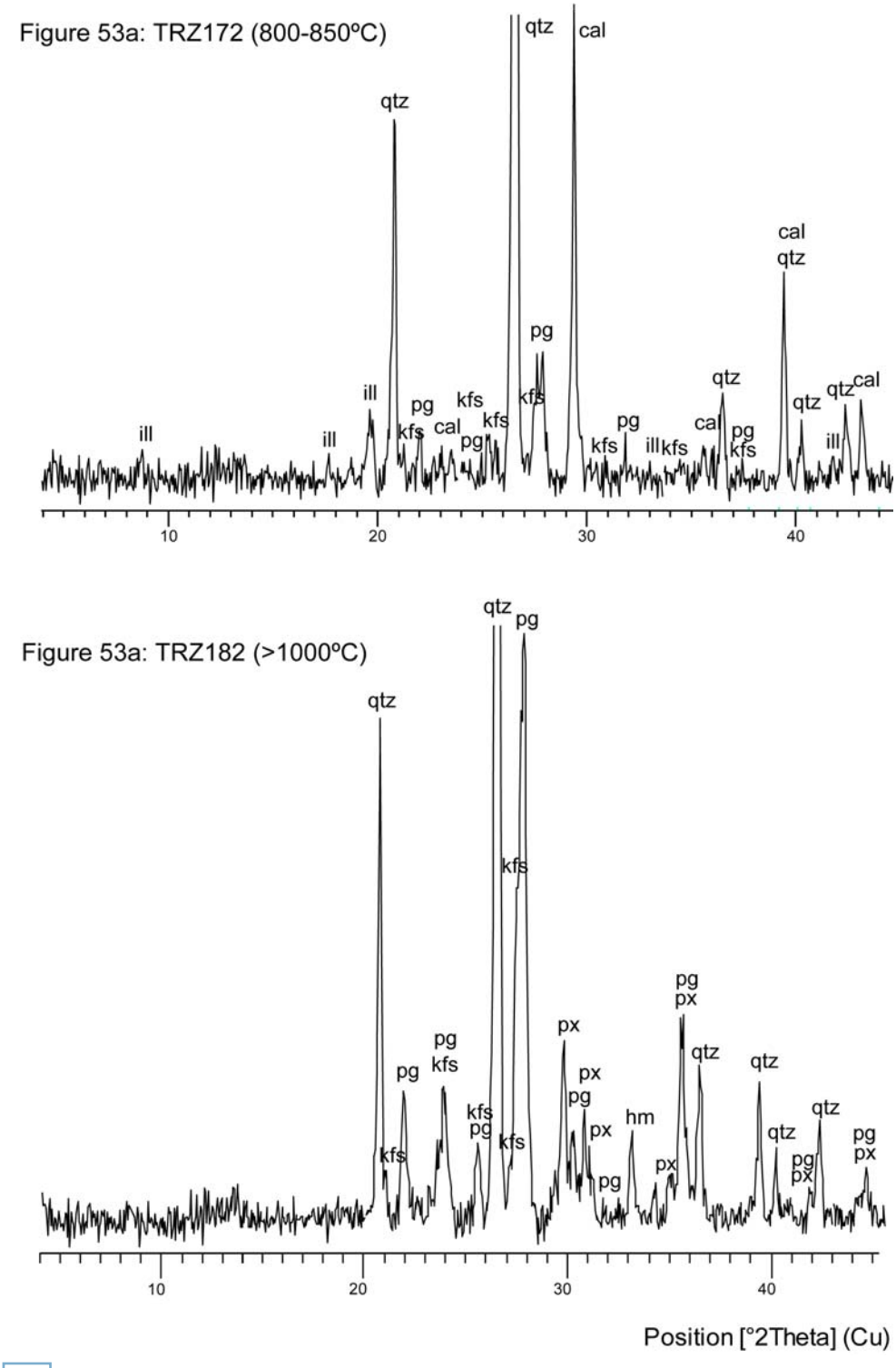

Figure 53: Diffractograms of the individuals TRZ172 and TRZ182 representing the chemical group TT-C; cal: calcite, hm: hematite, ill: illite-muscovite, kfs: k-feldspar, pg: plagioclase, px: pyroxene, qtz: quartz.

*6.1.3.4. **TT-D*** PCRU (TRZ162 and TRZ171)

TRZ162 and TRZ171 are low calcareous ceramics were fired at very high temperature (>1000ºC) because of the presence of firing phases (spinel) together with the absence of illite-muscovite (Figure 54).

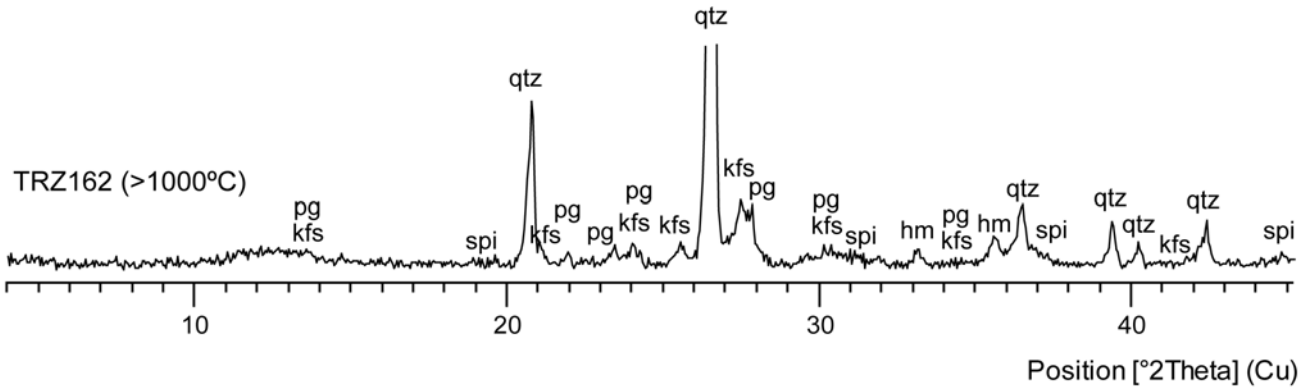

Figure 54: Diffractogram of the individual TRZ162 representing the chemical group **TT-D**; hm: hematite, ill: illite-muscovite, kfs: k-feldspar, pg: plagioclase, qtz: quartz, spi: spinel

*6.1.3.5. **TT-E*** PCRU (TRZ084 and TRZ305)

In the diffractogram of TRZ084 and TRZ305 individuals can be observed the presence of primary phases (calcite, quartz, illite-muscovite, microcline and plagioclase) and also firing phases such as pyroxene and gehlenite in its initial phase of formation (Figure 55), that is why the EFT of this fabric can be estimated around 850/900°C.

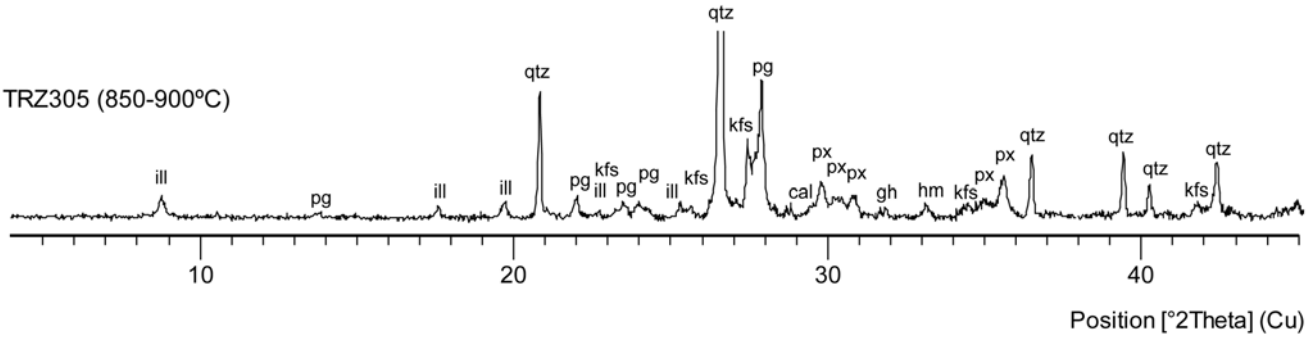

Figure 55: Diffractogram of the individual TRZ305 representing the chemical group **TT-E**; cal: calcite, gh: gehlenite, hm: hematite, ill: illite-muscovite, kfs: k-feldspar, pg: plagioclase, px: pyroxene, qtz: quartz

*6.1.3.6. **TT-F*** PCRU (TRZ063 and TRZ077)

Both individuals from TT-F group are characterised by the partial decomposition of illite-muscovite, calcite and gehlenite and the clear increment of the pyroxenes as a firing phases of a high temperature (Figure 56a). The ETF can be estimated over 950-1000°C. However, TRZ077 is over fired because it diffractogram show the total decomposition of phyllosilicates together with the advanced decomposition of some firing phases as gehlenite but the increment of other ones (pyroxene). Moreover, show the presence of a characteristic postdepositional alteration related to the formation of the Na-zeolite analcime ($Na[AlSi_2O_6]\cdot 6H_2O$) (Figure 56b).

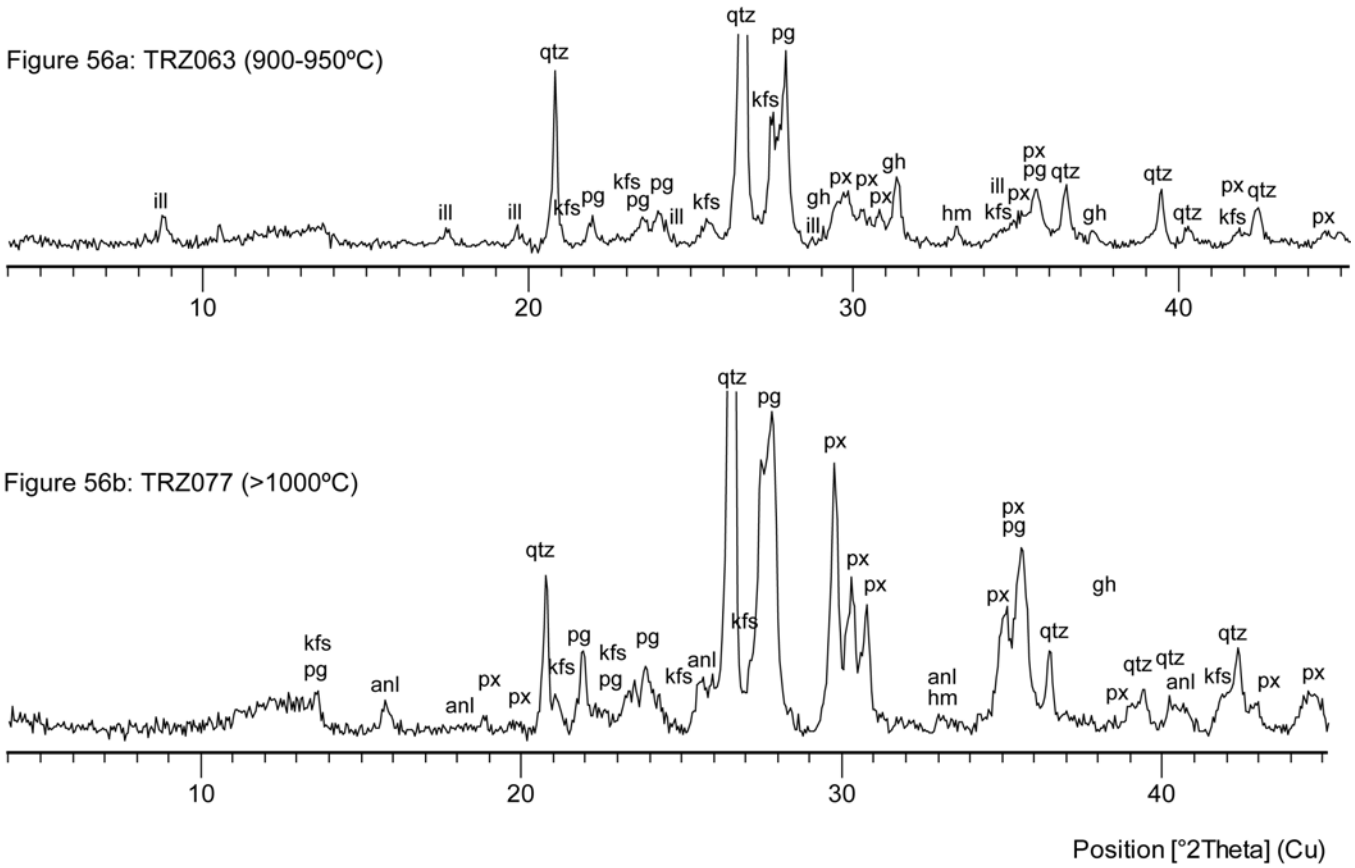

Figure 56: Diffractograms of the individuals TRZ063 and TRZ077 representing the chemical group **TT-F**; anl: analcime, gh: gehlenite, hm: hematite, ill: illite-muscovite, kfs: k-feldspar, pg: plagioclase, px: pyroxene, qtz: quartz

6.1.3.7. TT-G PCRU

According to the mineralogical analysis, the 82 individuals representing the group **TT-G** can be divided into four mineralogical categories.

The first contains the individuals: TRZ080, TRZ166, TRZ179, TRZ184, TRZ191 and TRZ202 and it is characterised by the presence of primary mineral phases and the total absence of clear firing phases. The EFT estimated for this category is 800-850°C, which corresponds to a low firing temperature.

In the second category, the coexistence of primary phases, like illite-muscovite and alkaline feldspars, and firing phases in the initial phase of development, like gehlenite and pyroxenes can be observed (Figure 57a). Therefore, the EFT of this category is around 850-950°C. This category is configured by TRZ051, TRZ052, TRZ054, TRZ055, TRZ057, TRZ064, TRZ068, TRZ085, TRZ086, TRZ160, TRZ164, TRZ169, TRZ178, TRZ186, TRZ302, TRZ303 and TRZ304.

In the third category, the development of the firing phases is much more advanced but the existence of illite-muscovite in the diffractograms of the individuals in this category indicate a EFT between 950°C and 1000°C (Figure 57b).The individuals that belong to this fabric are: TRZ053, TRZ058, TRZ065, TRZ066, TRZ070, TRZ078, TRZ093, TRZ126, TRZ128, TRZ129, TRZ130, TRZ133, TRZ143, TRZ157, TRZ158, TRZ173, TRZ174, TRZ175, TRZ181, TRZ190, TRZ192, TRZ193, TRZ195, TRZ196, TRZ197, TRZ198, TRZ199, TRZ201, TRZ296, TRZ297, TRZ301, TRZ307, TRZ310 and TRZ312.

Finally, the last mineralogical category is characterised by the advanced decomposition of illite-muscovite and gehlenite and the high degree of decomposition of calcite with the parallel clear increment of the pyroxenes as a firing phase of a high temperature (Figure 57c). Consequently, this fabric represents over fired ceramics. Its ETF can be estimated in the rang between 1000-1050/1110°C and it includes TRZ056, TRZ059, TRZ060, TRZ067, TRZ069, TRZ071, TRZ072, TRZ073, TRZ074, TRZ075, TRZ076,

TRZ079, TRZ081, TRZ082, TRZ083, TRZ087, TRZ165, TRZ167, TRZ168, TRZ176, TRZ180, TRZ183, TRZ185, TRZ188 (reduction atmosphere), TRZ194, TRZ200, TRZ300 and TRZ306. Moreover, TRZ056, TRZ069, TRZ071, TRZ079, TRZ083, TRZ183 and TRZ200 present also analcime ($Na[AlSi_2O_6]\cdot 6H_2O$) in their diffractogram.

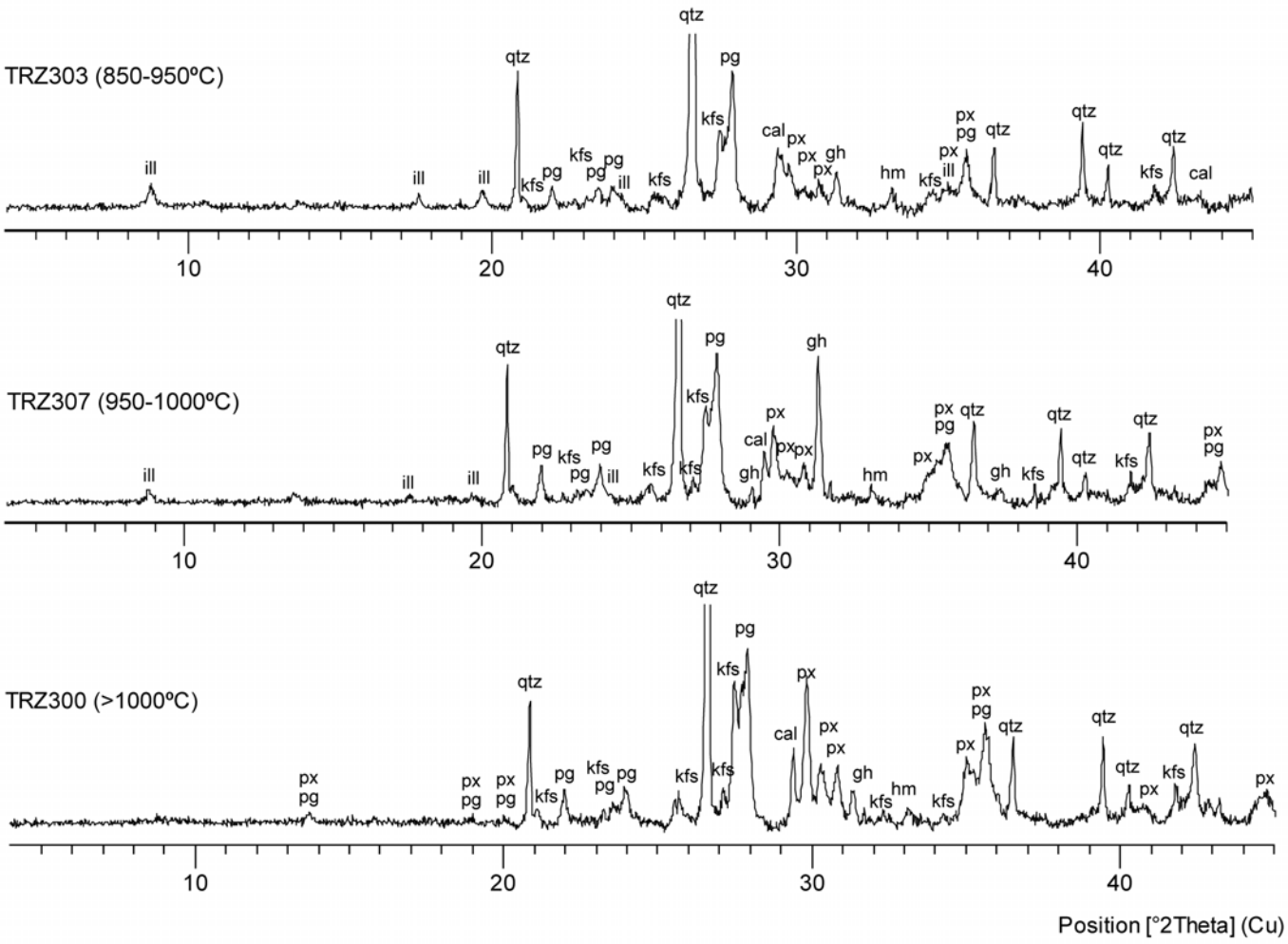

Figure 57: Diffractograms of the individuals TRZ303, TRZ307 and TRZ300 representing the chemical group **TT-G**; cal: calcite, gh: gehlenote, hm: hematite, ill: illite-muscovite, kfs: k-feldspar, pg: plagioclase, px: pyroxene, qtz: quartz

No clear differences are observed in the firing process between painted and unpainted common wares (Figure 60). Painted kushan-sassanian ceramics from **Tchinguiz Tepe** appears in all ranges of estimated temperatures. Bowls were normally fired around 850-950ºC whereas big plates and coups were fired up to 950ºC.

6.1.4. Surface treatment (SEM analysis)

The study of the reddish-orange slip that covers some of the common wares was performed on TRZ074 and TRZ084 shards from **Tchinguiz Tepe** (Figure 58). The quantitative micro-chemical analysis that carried out by SEM-EDS in 3 different points of the slip and different areas of the body at 2 different shards reveal slight differences between TRZ074 and TRZ084 ceramics (Figure 59). Clay of TRZ074 is richer in Si and Ca whereas the clay matrix of TRZ084 is richer in Al and K. In both cases, the clay matrix and the red slip have similar composition but Al and K values are higher in the slip of TRZ074 whereas on the case of TRZ084, the Si content is higher in the slip. The similarity in the composition between clays and slip in both cases probably means that a finer fracture of the clay used to fabricate the pots was applied to produce the red slip.

The microphotographs of the polished sections show a fine and homogeneous layer of an irregular thickness, from 150 to 450µm, on the ceramic body's surface. Looking at the interface between the red slip and the clay matrix, no clear separation line could be observed but the existence of a 10 to 50µm insertion zone. That clearly indicates a biscuit, just fired at ones, and no glaze firing.

Figure 58: Photographs of the painted ceramics analysed by SEM-EDS from **Tchinguiz Tepe** (sector RC)

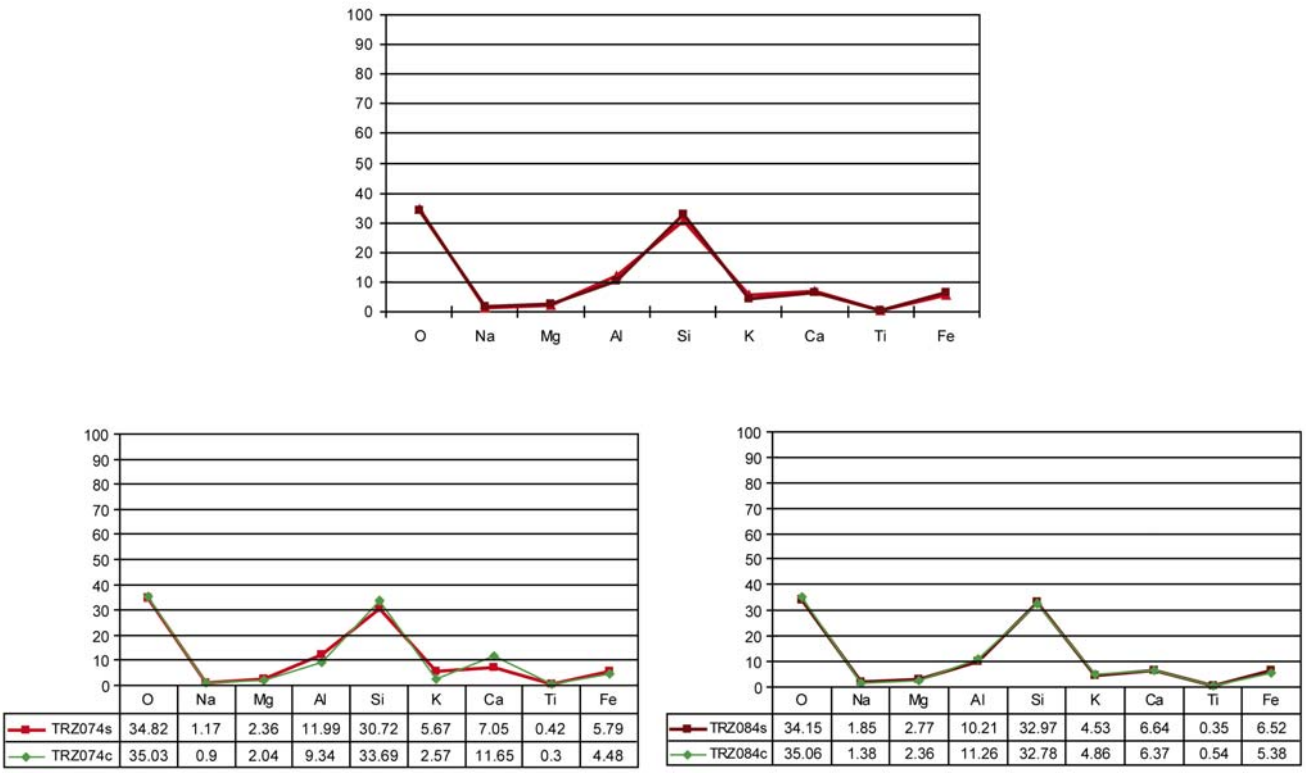

	O	Na	Mg	Al	Si	K	Ca	Ti	Fe
TRZ074s	34.82	1.17	2.36	11.99	30.72	5.67	7.05	0.42	5.79
TRZ074c	35.03	0.9	2.04	9.34	33.69	2.57	11.65	0.3	4.48

	O	Na	Mg	Al	Si	K	Ca	Ti	Fe
TRZ084s	34.15	1.85	2.77	10.21	32.97	4.53	6.64	0.35	6.52
TRZ084c	35.06	1.38	2.36	11.26	32.78	4.86	6.37	0.54	5.38

Figure 59: Graphics representing the normalised chemical composition obtained by SEM-EDS microanalysis of the slip (s) and clay (c) of the painted vessels TRZ074 and TRZ084 from **Tchinguiz Tepe** (sector RC)

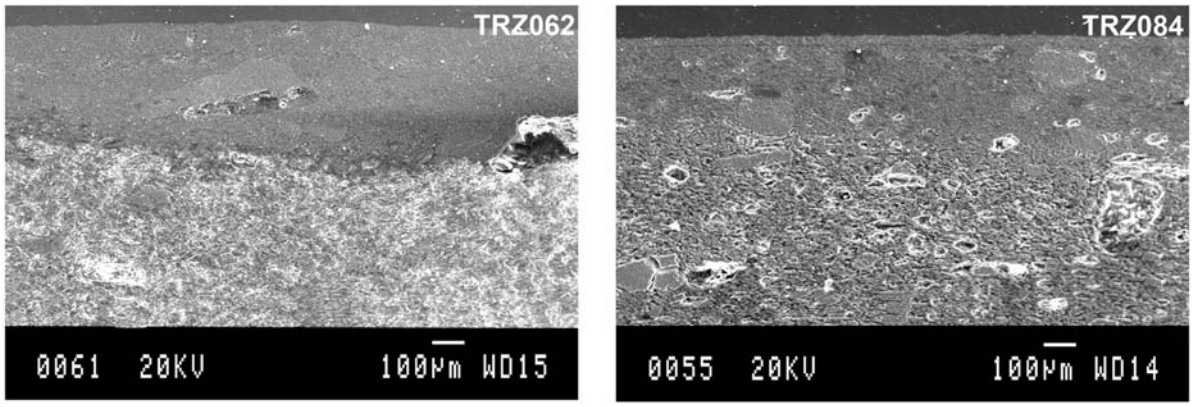

Figure 60: SEM photomicrographs of the polished sections of the slip and paste area observed in SEM-EDS upon the common wares TRZ062 and TRZ084 from **Tchinguiz Tepe** (sector RC)

6.2. Zar Tepe

Ceramics from **Zar Tepe** correspond to several variants of typologies of coarse wares, medium coarse wares and fine wares. From the 48 shards analysed, 18 belong to the first category. They are four possible cooking wares (TRZ245, TRZ271, TRZ272 and TRZ284) and a cover or tap (TRZ281). There are also five shards corresponding to plane bases which can be related to cooking wares or storage jars (TRZ286, TRZ287, TRZ288, TRZ289 and TRZ290) and two shards corresponding to big storage jars or *dolia* (TRZ275 and TRZ275). But few big plates (TRZ247, TRZ250 and TRZ252) and big jars (TRZ253 and TRZ266) from **Zar Tepe** present also a coarse fraction as temper (Martínez *et al*., 2009: 322).

Most of ceramics from **Zar Tepe** are related to a medium coarse common wares from which jars are the type most representative (TRZ246, TRZ249, TRZ255, TRZ256, TRZ259, TRZ260, TRZ261, TRZ262, TRZ263, TRZ264, TRZ265, TRZ269 and TRZ283) together with some big plates and bowls (TRZ244, TRZ251, TRZ254, TRZ257 and TRZ280). However, one *dolia* (TRZ273) and one cover or tap (TRZ277) can be also associated to a medium coarse fabric.

The last 11 ceramics are fine common wares of different typology and painted with a slip in some cases. The fine ceramics are predominantly jars (TRZ267, TRZ268, TRZ270, TRZ282 and TRZ285) but also big plates (TRZ243 and TRZ276), bowls (TRZ248) and other unknown types (TRZ258, TRZ278, TRZ279, TRZ282 and TRZ285).

6.2.1. Chemical composition (XRF analysis)

At first site, the same observations than in the above described cases can be made on the data set. All the analysed material is calcareous without any exception and the Na_2O concentrations are clearly high in all the individuals as there are salt (NaCl) contaminations in all the samples of **Zar Tepe** and in two cases (TRZ283 and TRZ246) the presence of analcime ($Na[AlSi_2O_6]\cdot 6H_2O$) could be observed by XRD analysis (Tsantini *et al*., 2007; Martínez *et al*., 2008, 2009).

The CVM calculated for **Zar Tepe's** data set can be seen in Table 7b. It has been calculated without considering the elements: Mo, Sn, Co, W, MnO P_2O_5 and Pb. As we have already explained, the two elements have been left out in the cause of analytical imprecision, as both of them are under their regression limits in ceramics. MnO is an element with analytical accuracy problems. Co and W have been left out from the statistical treatment because of the possibility that can be contaminated due to the sample preparation process and, the last two above mentioned elements (P_2O_5 and Pb) because they are elements very susceptible to suffer post-depositional contaminations, therefore they can introduce a false high variability in the data set.

The total variation (vt) in this data set, according to the CVM is 0.3463 which generally indicates a polygenetic data (the presence of more than one production in the data set). But it is sufficiently low to point to a similar or common geochemical origin of the raw materials used for their manufacture.

The variability introduced by the majority of the elements is relatively low. The elements which introduce more than the 50% of the variability in this data set are Na_2O, Ba, Sr, CaO, and Ce. From these elements, in the case of Na_2O ($\tau_{.Na2O}$ = 0.2384), the high variability is due to post-depositional contaminations as already mentioned. The presence of NaCl (salt) and in some cases (TRZ246 and TRZ283) and the presence of analcime ($Na[AlSi_2O_6]\cdot 6H_2O$), affect the composition of specific individuals altering the Na_2O and also the K_2O and Rb concentrations. By looking at the chemical data, it can be observed the values of Ba are variable but without being clear if there are some individuals possibly contaminated. On the other hand, in the CVM can be observed the highest value in the column of Ba that is the one of this element with Na_2O, which indicates that the contamination in Na_2O element affects probably Ba values. Therefore, to avoid the chemical differences introduced by the above mentioned alterations and/or contaminations dominate the statistical treatment, we ignored Na_2O, K_2O, Ba and Rb in the rest of the process.

In the new CVM, the vt is equal to 0.1741 and the elements which introduce now more than the 50% of the variability in the data set are: Sr, CaO, MgO and Ce. All of them are chemically associated elements with generally high natural variability in calcareous raw material sources. A total variation of this range indicates a very homogeneous data set representing probably one single production. At the same way as in the case of **Termez** and **Kampyr Tepe**, in geochemical terms, this vt might point towards a very similar geochemical origin of the raw materials used for the production of all the analysed individuals. It might be due to the fact that this area is very invariable geologically.

In continuation, the chemical data were transformed into logratios following the consideration of Aitchison (1986) and Buxeda (1999) on compositional data. The logratio transformation was performed upon the subcomposition: Fe_2O_3, Al_2O_3, TiO_2, MgO, CaO, SiO_2, Nb, Zr, Ce, Ga, V, Nb, Zn, Ni and Cr of the 48 analysed individuals from **Zar Tepe** where Y was used as divisor, as according to the CVM it was the element less contributing to the chemical variability. Sr, Th and Cu have been excluded from logratio transformation to avoid the domination of a possible natural variability upon the multivariate analysis. The chemical results are summarized in the dendrogram of Figure 61, resulting from the cluster analysis performed upon the previous subcomposition, using the Square Euclidean distance and the centroid algorithm. Although the chemical variability indicates a homogeneous geo-chemical composition for 48 ceramics from **Zar Tepe,** in this dendrogram four different subgroups can be distinguished (**ZT-A**, **ZT-B**, **ZT-C** and **ZT-D**). These differences indicate the existence of 4 subproductions.

In Table 9 where the mean chemical composition and the standard deviation for this subgroups is presented, can be observed that **ZT-A,** formed by the coarse wares TRZ272 and TRZ275 and the fine wares TRZ279 and TRZ282) presents lower values in Al_2O_3 and V to consider it as a separate subgroup. The typological characteristics of these vessels are presented in Figure 62.

ZT-B PCRU's is formed by three shards corresponding to one jar (TRZ262), one big plate (TRZ252) and a coarse jar (TRZ271) (Figure 63). In Table 9, the mean chemical composition and the standard deviation of this group is given and the differences in Cu and Na_2O are clear. Nevertheless the differences in Na_2O might only reflect a specific perturbation problem in analcime as it has been explained explicitly before.

The subgroups **ZT-C** and **ZT-D** seem to be chemically very similar to each other as it can be seen from their mean chemical composition presented at Table 9. However, this table also indicates slight differences in the concentrations of Al_2O_3, Na_2O, Ba, Sr, V and Cr. The typological aspects of these subgroups can be seen at Figure 65 and Figure 66.

It is important to stress out that, in general, the differences between these subgroups are not sufficiently important to consider them as different productions thus they only indicate the existence of

slightly different subproductions in this archaeological site. These chemical differences according to DRX might be owed to small differences in the firing temperatures. For these reason, all of these subgroups must reflect a common geological origin or common clay source for the raw materials (the same uncertainty zone) and might represent the same local ceramic production with four slightly different subproductions or variants of the same production.

ZT-C is composed by two painted common wares TRZ253 and TRZ26, two plates (TRZ247 and TRZ250), two bowls (TRZ254, TRZ257), one coarse storage jar (TRZ274) two plane bases (TRZ284, TRZ289), one big plate (TRZ251), one bowl (TRZ268) five jars (TRZ259, TRZ267, TRZ249 TRZ269 and TRZ344), two big bowls or plates (TRZ243 and TRZ248, the first one is painted) other three bases, one belonging to a common jar (TRZ283) and two belonging to a big wares (TRZ287 and TRZ290). Another base of one bowl (TRZ280), one cover or tap (TRZ281) one handle (TRZ246), one painted plate (TRZ250), one painted jar (TRZ245), another medium-coarse plate (TRZ276) and, finally, three big bowls or big storage jars (two painted TRZ258 and TRZ270 and one unpainted TRZ260) (Figure 64). On the other hand, **ZT-D** is composed by two coarse storage jars (TRZ255 and TRZ273), one plane base (TRZ286), one cover or tap (TRZ277) and one painted hang (TRZ278) (Figure 65).

Finally, four individuals located in a marginal position at the left side of the dendrogram (TRZ285, TRZ265, TRZ288 and TRZ266) can be distinguished. The typology of these ceramics is given at Figure 66. TRZ285 that is a small painted base presents a high MgO and a lower Cr content. The jar TRZ265 is the more calcareous and has lower values in SiO_2, Ba and Rb. The plane base TRZ288 presents slights differences in most of the major and trace elements. For example, it contains more SiO_2, Ba, Sr and Ce and less Fe_2O_3, MgO, Nb, Zr, Y, Zn, Cu and Ni (Table 9). At last, the jar TRZ266 contains more Fe_2O_3, Al_2O_3, TiO_2, K_2O and Rb but lower Ce. Despite this, TRZ266 assimilates fairly to **ZT-C** and **ZT-D** (Table 9). Owed to these chemical differences, these four ceramic individuals can be considered as the ceramics outliers in this data set.

Because non pottery worshop has been identified up to now at Zar Tepe settlement, we must consider all of those pottery subproductions as PCRU (Paste compositional Reference Units)

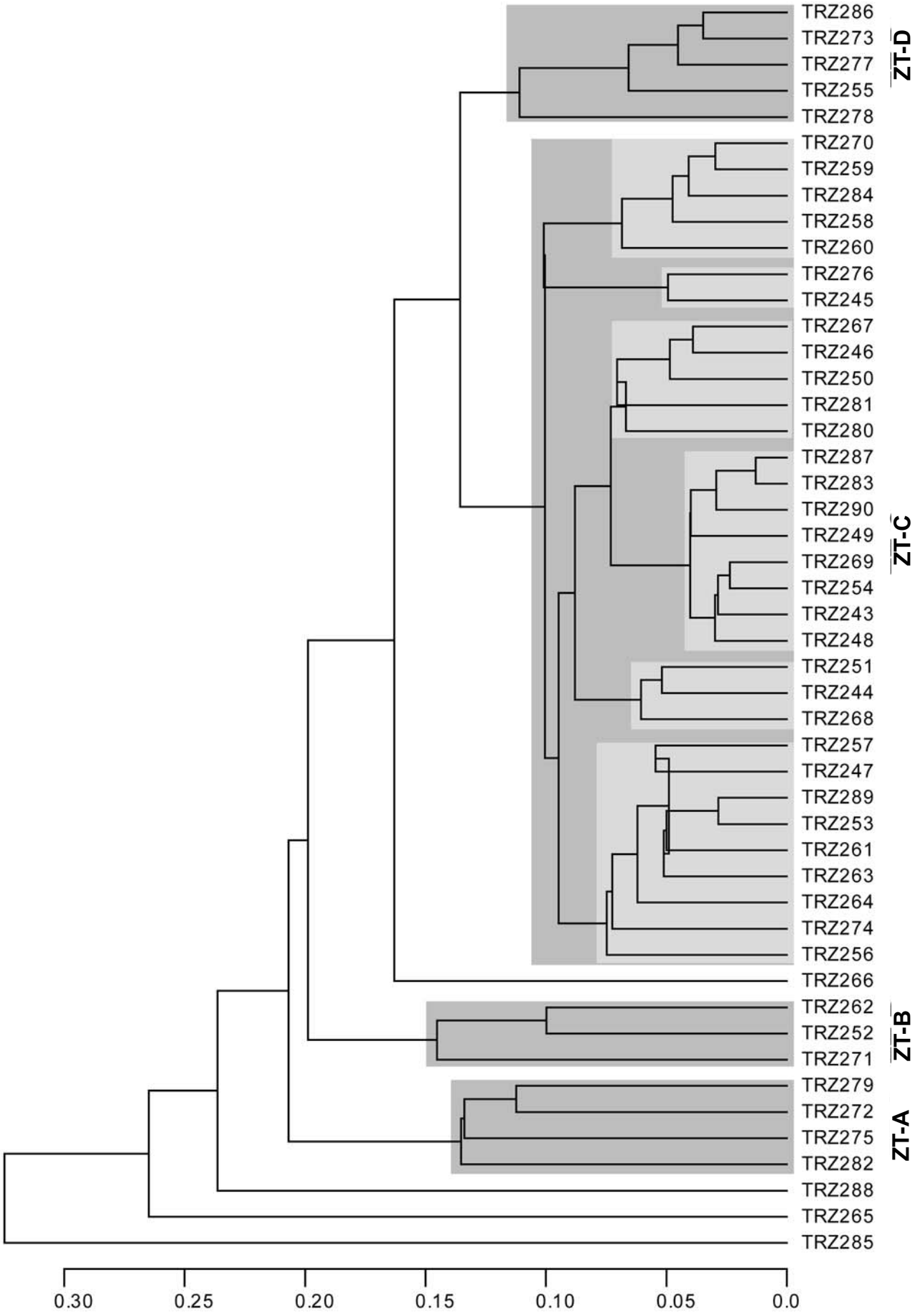

Figure 61: Dendrogram resulted from the cluster analysis performed on the subcomposition Fe_2O_3, Al_2O_3, TiO_2, MgO, CaO, SiO_2, Nb, Zr, Ce, Ga, V, Nb, Zn, Ni, Cr and Y used as divisor, of 48 individuals sampled at **Zar Tepe**, using the Square Euclidean distance and the centroid algorithm

Elements	ZT-A (n=4)		ZT-B (n=3)		ZT-C (n= 32)		ZT-D (n= 5)		TRZ285	TRZ265	TRZ288	TRZ266
	m	sd	m	sd	m	sd	m	sd	nc	nc	nc	nc
Fe_2O_3 (%)	5.45	0.26	5.87	0.10	6.01	0.40	6.41	0.20	6.03	5.88	5.08	6.42
Al_2O_3 (%)	14.67	0.43	15.26	0.14	15.96	0.91	16.69	0.46	15.46	15.32	15.76	16.78
TiO_2 (%)	0.61	0.04	0.64	0.01	0.66	0.03	0.69	0.01	0.68	0.64	0.60	0.71
MgO (%)	3.53	0.43	5.50	0.40	4.04	0.55	5.15	0.36	6.83	4.77	2.76	4.04
CaO (%)	11.17	1.39	9.45	1.78	8.06	0.92	6.62	0.63	6.51	11.32	6.79	6.68
Na_2O (%)	1.70	0.41	2.41	0.81	2.24	0.68	1.43	0.25	2.26	2.07	2.24	1.93
K_2O (%)	3.75	0.62	3.87	0.11	4.13	0.54	3.91	0.17	4.39	4.38	4.38	4.56
SiO_2 (%)	58.96	0.86	56.82	1.47	58.71	1.68	58.90	0.93	57.66	55.45	62.18	58.69
Ba (ppm)	530	29	558	109	570	149	769	49	546	463	767	670
Rb (ppm)	123	5	124	4	133	11	138	5	127	116	134	143
Th (ppm)	13	1	13	1	14	2	14	1	14	12	13	14
Nb (ppm)	14	1	15	1	14	0	15	1	15	15	13	16
Zr (ppm)	153	11	147	3	151	8	152	5	153	146	134	156
Y (ppm)	24	2	25	1	24	1	25	1	25	22	21	25
Sr (ppm)	420	92	430	15	428	104	361	11	409	575	601	407
Ce (ppm)	59	4	46	4	60	8	60	10	54	61	63	45
Ga (ppm)	16	1	16	1	18	1	19	1	17	15	17	18
V (ppm)	89	5	93	4	98	9	114	1	104	93	91	109
Zn (ppm)	91	11	102	8	98	7	104	6	101	103	78	97
Cu (ppm)	29	4	35	4	31	3	33	6	30	29	26	28
Ni (ppm)	42	4	47	3	45	3	50	3	51	45	37	50
Cr (ppm)	77	11	78	3	75	4	82	3	71	72	74	79

Table 9: The mean chemical composition (m) and the standard deviation (sd) using normalised data of **ZT-A**, **ZT-B**, **ZT-C** and **ZT-D** chemical groups an the raw normalised chemical composition (nc) of the ceramics outliers TRZ285, TRZ265, TRZ288 and TRZ266 from **Zar Tepe**

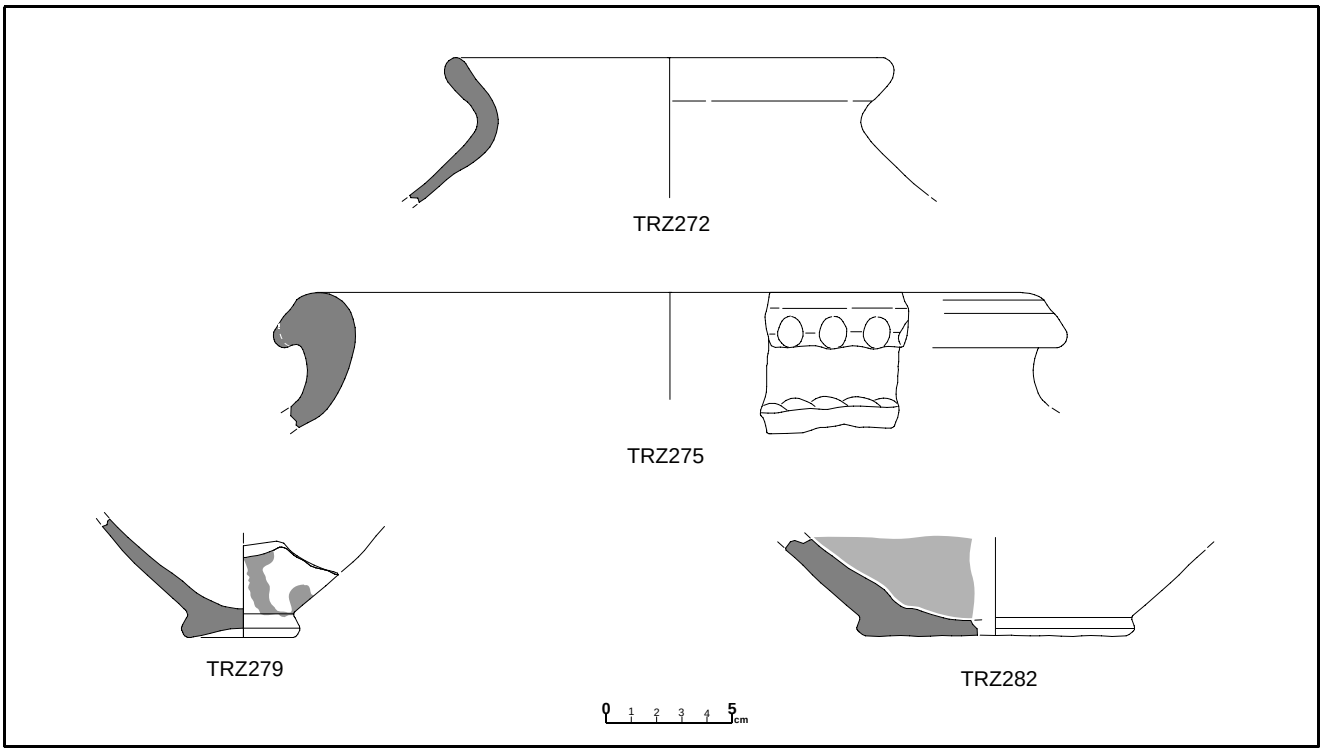

Figure 62: Typology of the **ZT-A** group (TRZ272, TRZ275, TRZ279 and TRZ282)

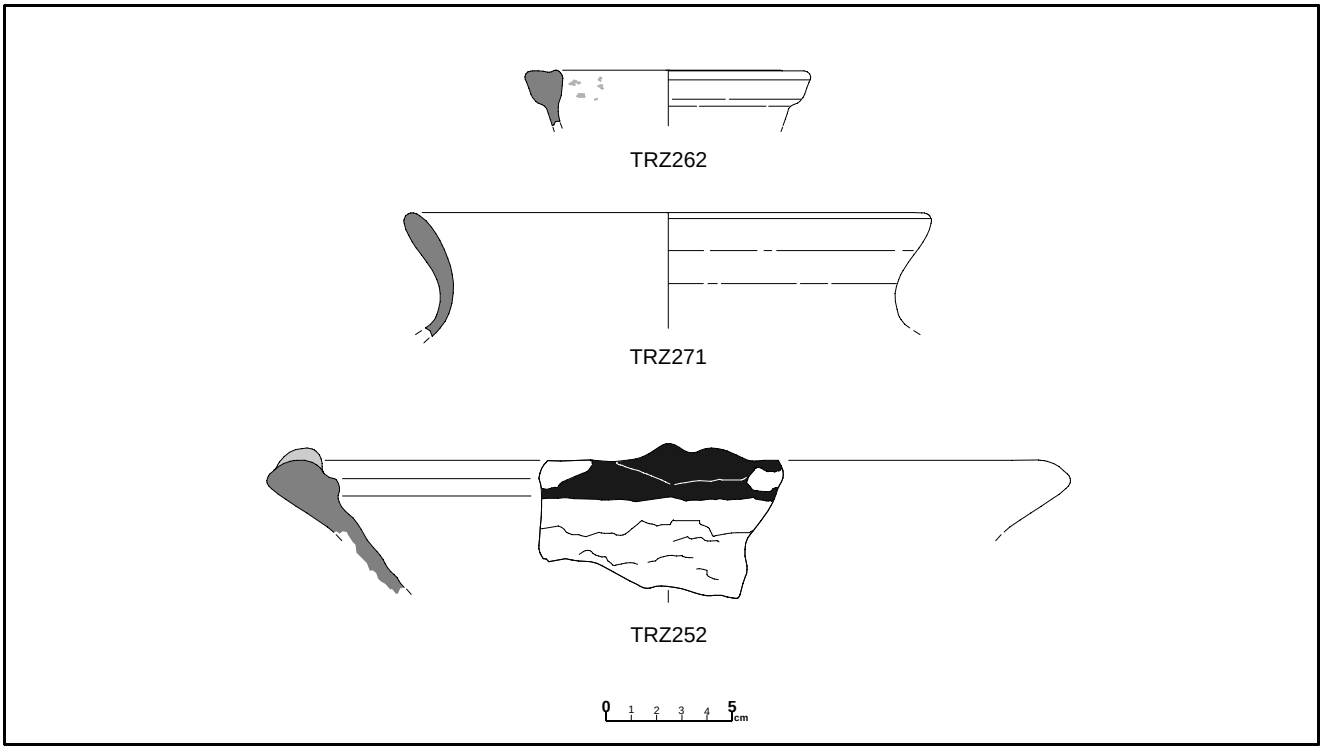

Figure 63: Typology of the ZT-B group (TRZ262, TRZ271 and TRZ252)

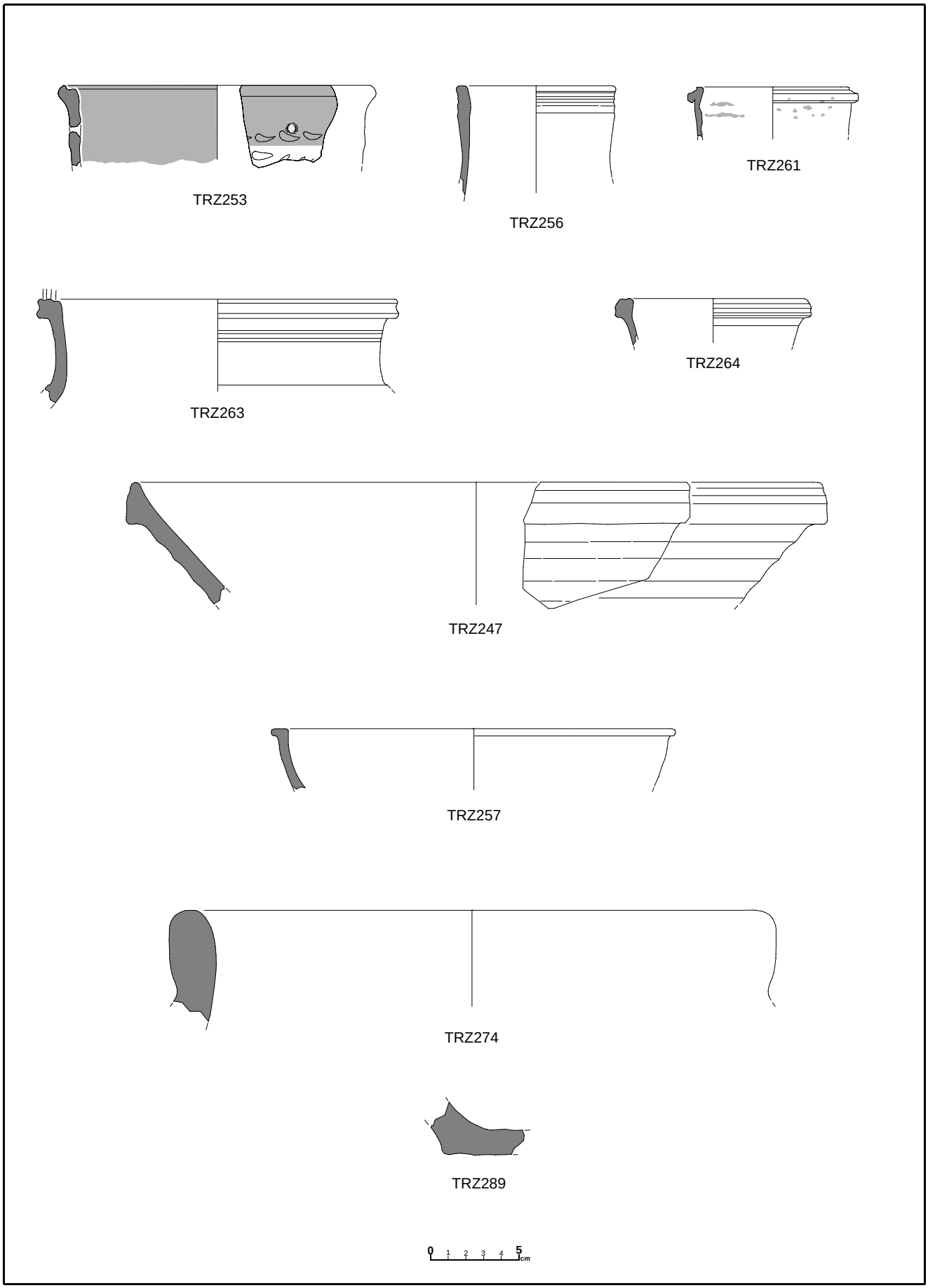

Figure 64a: Typology of the **ZT-C1** group
(TRZ253, TRZ256, TRZ261, TRZ263, TRZ264, TRZ247, TRZ257, TRZ274 and TRZ289)

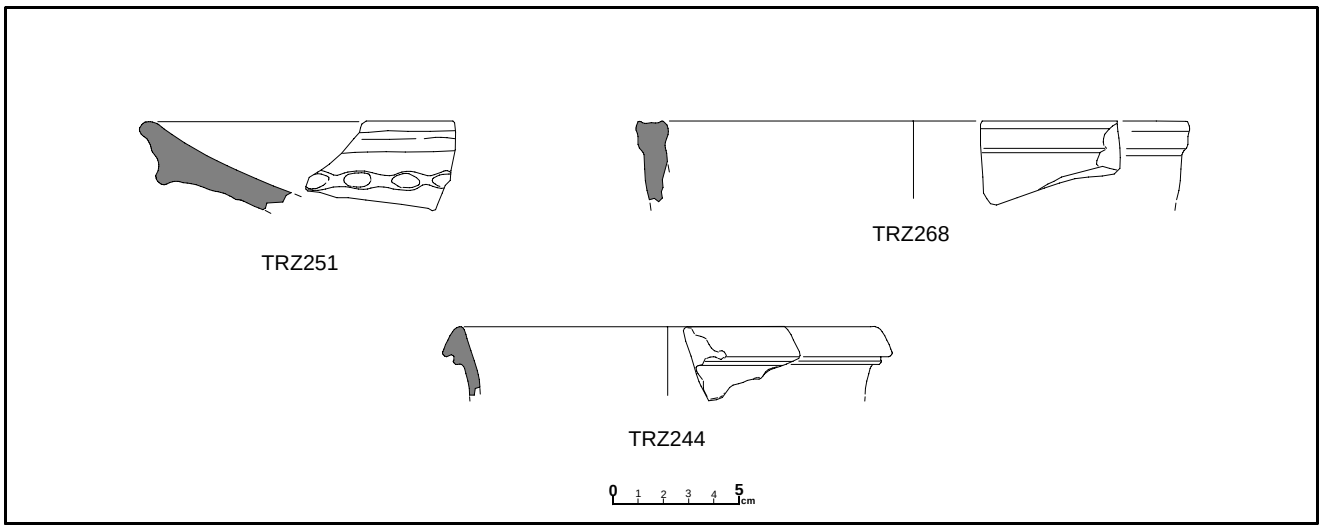

Figure 64b: Typology of the **ZT-C2** group (TRZ251, TRZ268 and TRZ244)

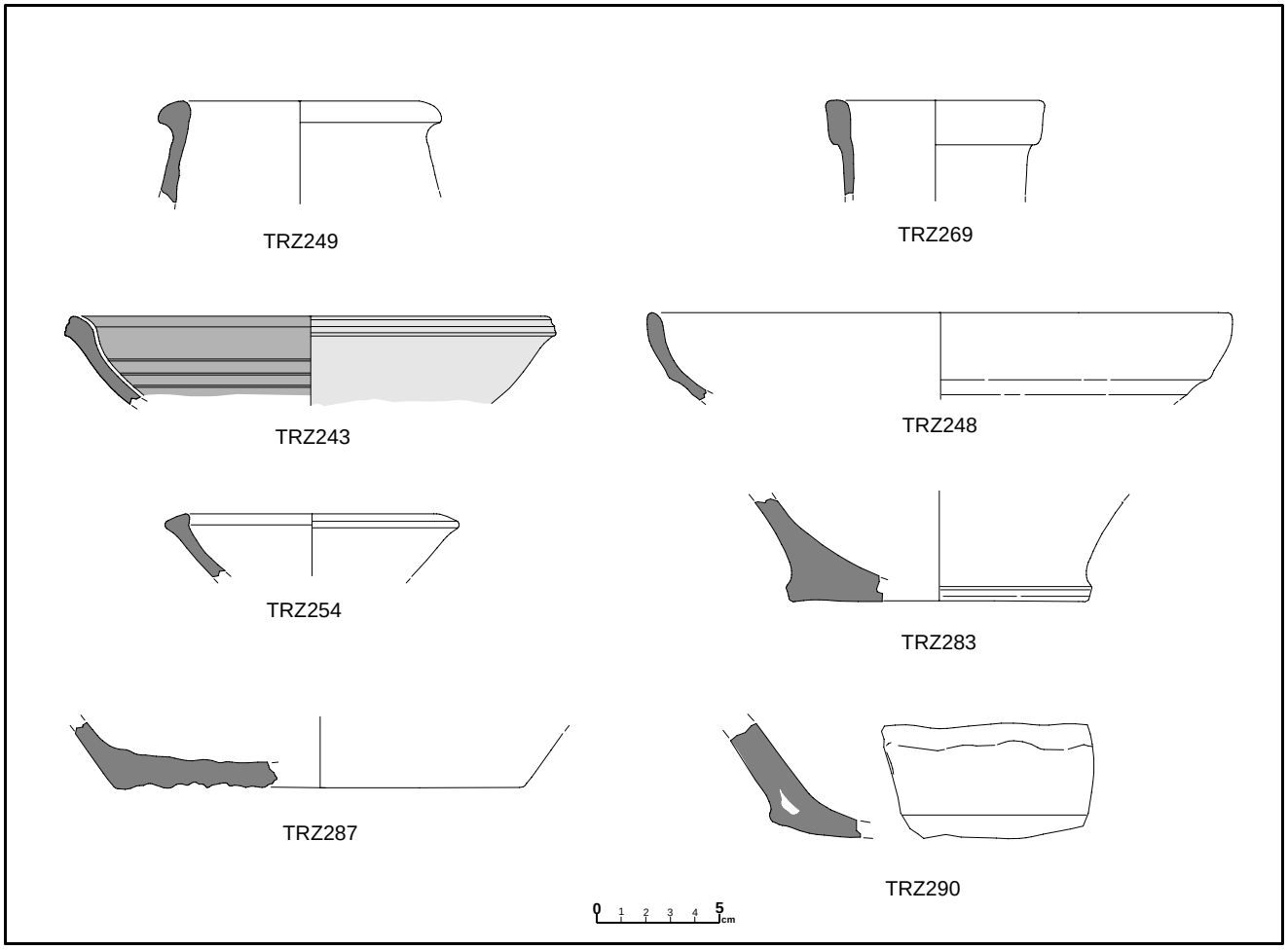

Figure 64c: Typology of the **ZT-C3** group (TRZ249, TRZ269, TRZ243, TRZ248, TRZ254, TRZ283, TRZ287 and TRZ290)

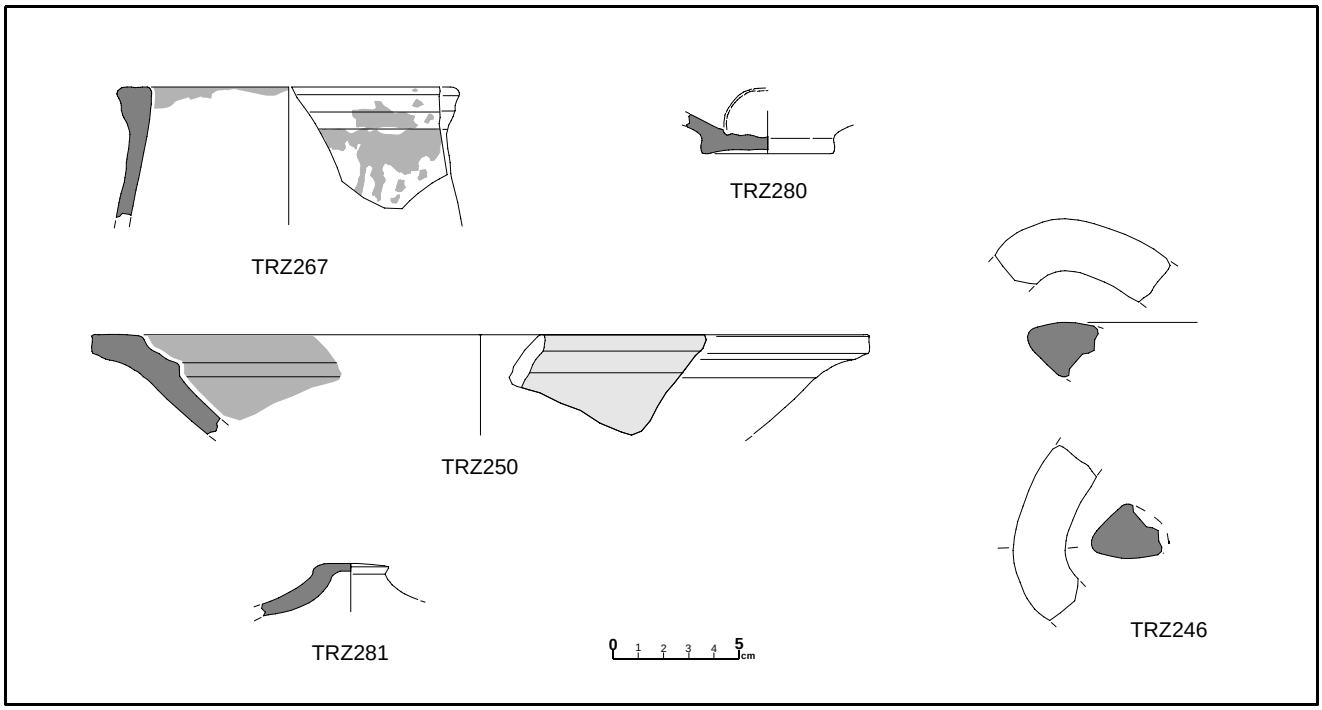

Figure 64d: Typology of the **ZT-C4** group (TRZ267, TRZ280, TRZ250, TRZ281 and TRZ246)

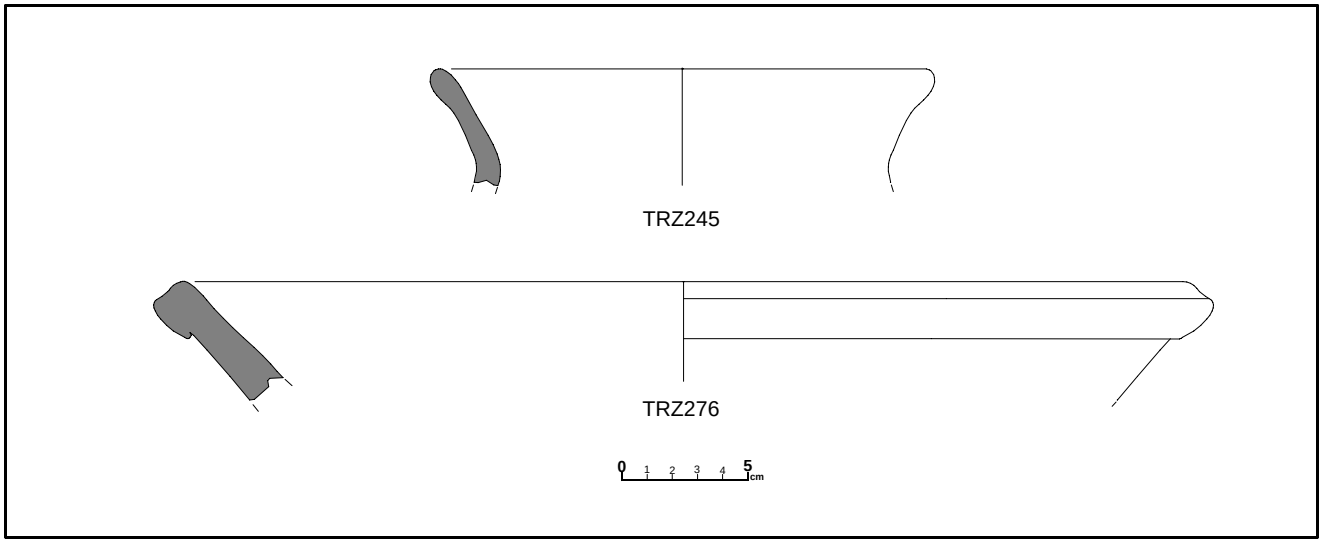

Figure 64e: Typology of the **ZT-C5** group (TRZ245 and TRZ276)

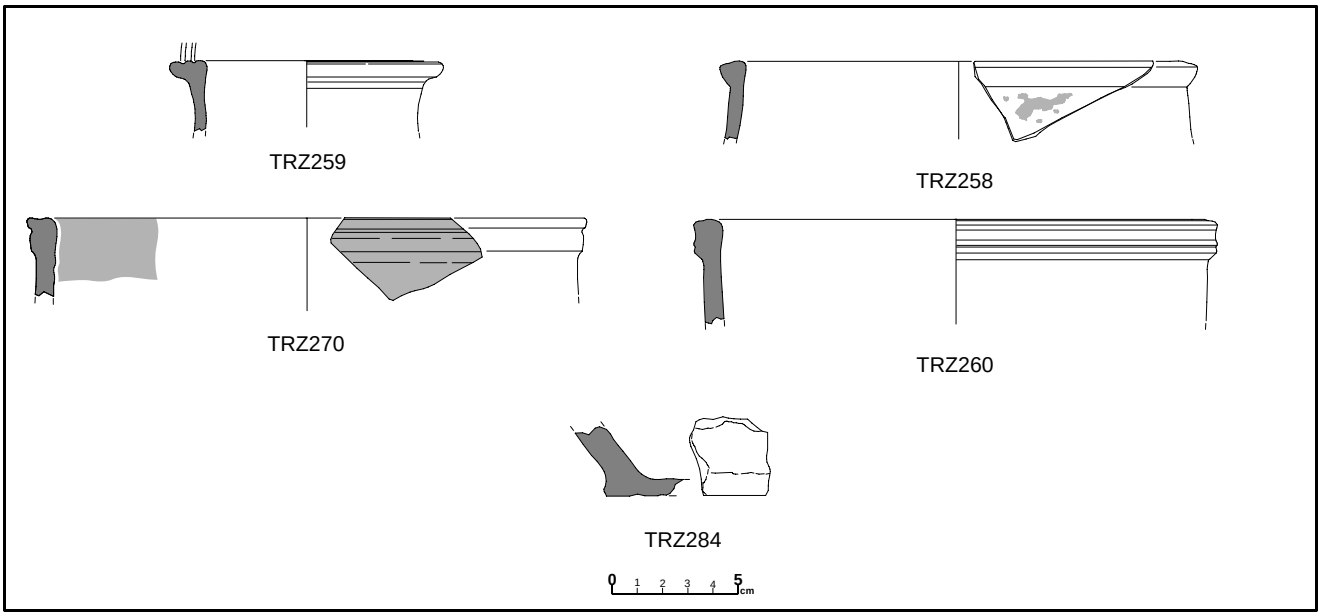

Figure 64f: Typology of the **ZT-C6** group (TRZ259, TRZ258, TRZ270, TRZ260 and TRZ284)

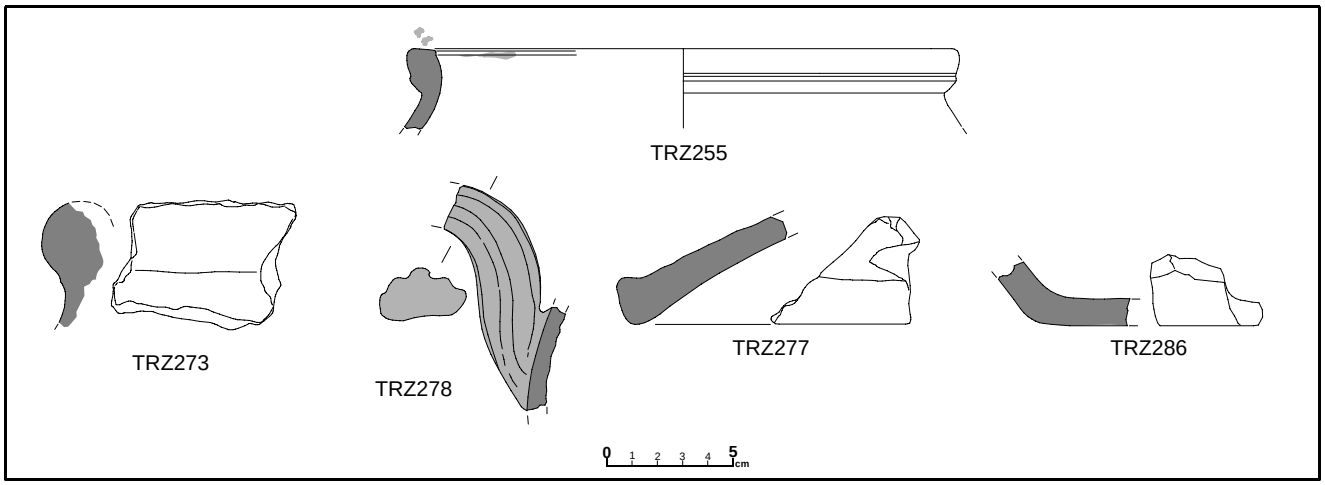

Figure 65: Typology of the **ZT-D** group (TRZ255, TRZ273, TRZ278, TRZ277 and TRZ286)

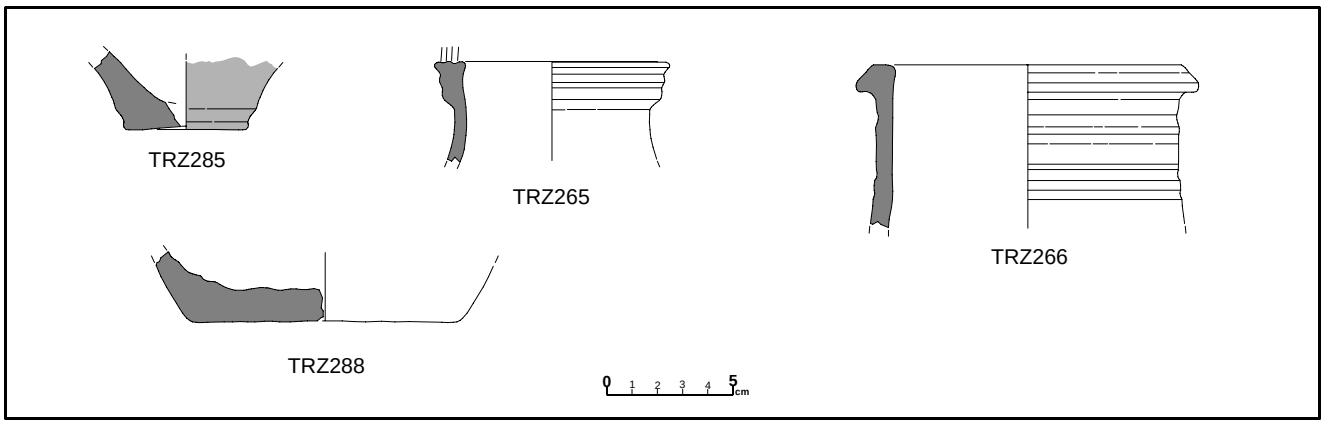

Figure 66: Typology of the ceramic outliers TRZ285, TRZ265, TRZ288 and TRZ266 from **Zar Tepe**

6.2.2. Petrographical composition (thin section analysis)

Examination of 12 ceramics from ***Zar Tepe*** using petrographic analysis shows few differences in composition in relation to the pottery from ***Kampyr Tepe*** and ***Termez.***

The slightly chemical differences observed in the case of four shards from **ZT-A PCRU**, comparing with shards from the others PCRU, are still more obvious when we look at section analysis. Two shards have been analysed by petrographical analysis (the coarse ware TRZ272 and the base of a common ware TRZ279). Although some constituents are present in both ceramic individuals, dimensions of aplastic inclusions points at two different petrographical fabrics which probably represent two different ceramic productions from neighbouring areas.

TRZ272: Coarse ware. Clay matrix: Fe-rich (+ Ca-rich nodules, probably derived of microfossils decomposition during firing), homogeneous, semi-vitrified. Groundmass (relatively abundant, fine): quartz and muscovite (dominant); calcite (micrite), plagioclase and k-feldspar (occasional). Coarser inclusions (≤ 750µm): abundant, moderately to well sorted, sub-rounded to sub-angular, equant to elongate, single-spaced, sometimes in contact, bimodal grain-size distribution (Figure 67). Predominant to dominant: granitic fragments and crystals detached of these rocks (quartz, plagioclase, k-feldspar altered to sericite and muscovite) and schist; dominant to frequent: quartzite, quartz-mica schist, calcareous sandstones; common to few: calcite (micrite), amphibole, opaques; Few to occasional: epidote, basalt, garnet and serpentinite. Porosity is diverse, mainly formed by few meso-vughs, macro-vughs and meso-vesicles.

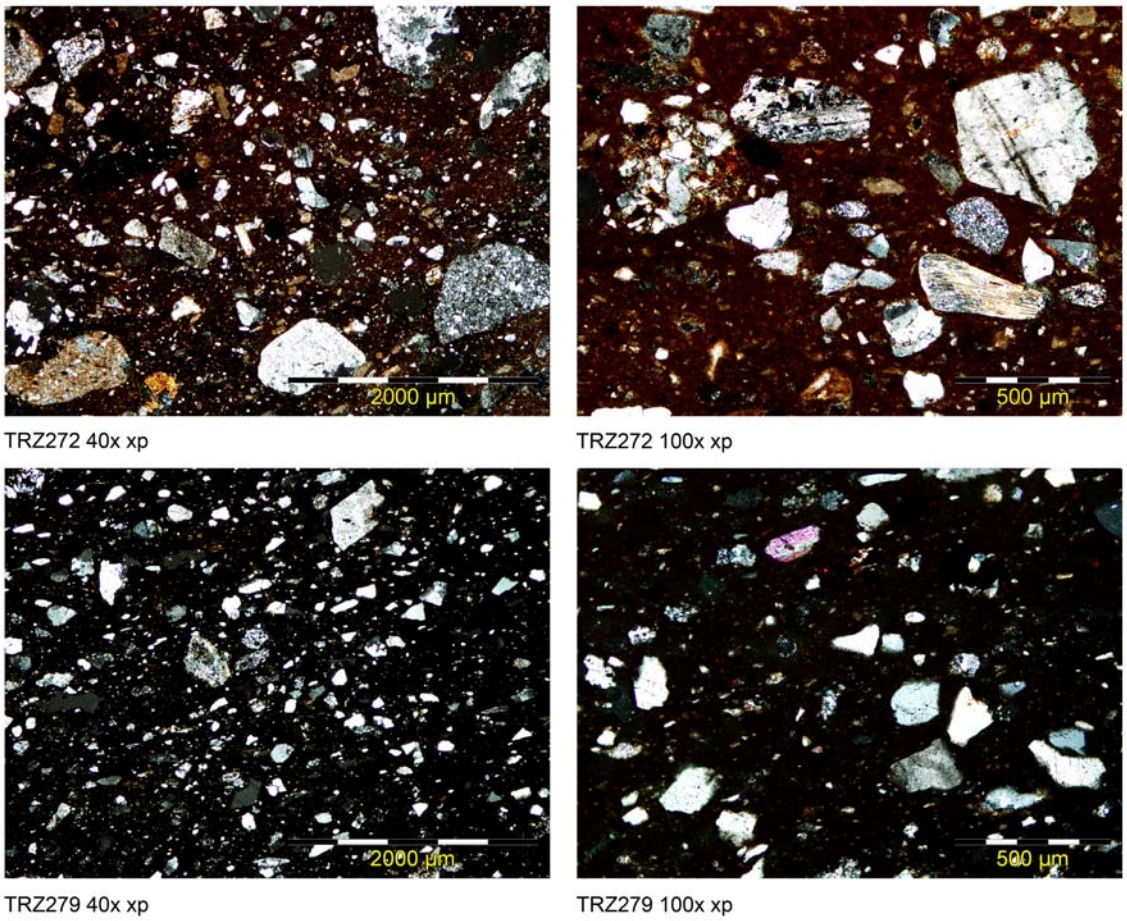

Figure 67: Microphotographs by crossed polars (xp) of the ceramics TRZ272 and TRZ279 belonging to **ZT-A**

TRZ279: Clay matrix: Ca-rich, heterogeneous, vitrified. Groundmass (relatively abundant, fine): quartz and muscovite, calcite (micrite) (dominant); plagioclase, k-feldspar (occasional). Coarser inclusions (≤ 300μm): abundant, moderately to well sorted, sub-angular to sub-rounded, equant, single-spaced to double-spaced, unimodal grain-size distribution (Figure 67). Predominant to dominant: quartz, plagioclase, k-feldspar and muscovite; Dominant to frequent: quartz-mica schist, chert; Common to few: sandstone, amphibole; Few to occasional: basalt, opaques. Voids are predominantly meso-vesicles and meso-vughs.

Concerning ceramics from **ZT-B PCRU**, thin section analysis of two shards (the plate TRZ252 and the coarse jar TRZ271) leads to distinguish two petrographic fabrics because of differences in coarse fraction dimension.

TRZ252: Clay matrix: Ca-rich, heterogeneous, high vitrified. Groundmass (moderately abundant, fine): quartz and muscovite, calcite (micrite) (dominant). Coarser inclusions (≤ 500μm): scarce, well sorted, sub-angular to sub-rounded, elongate, double-spaced, unimodal grain-size distribution (Figure 68). Predominant to dominant: quartz, muscovite, quartz-mica schist; Dominant to frequent: plagioclase, k-feldspar, calcareous sedimentary rocks; Common to few: amphibole, opaques; Few to occasional: garnet, basalt. Voids are meso-vesicles.

TRZ271: Coarse fabric. Clay matrix: Fe-rich (+ Ca-rich nodules), semi-vitrified. Groundmass (moderately abundant, fine): quartz and muscovite and calcite (micrite) (dominant); plagioclase, k-feldspar (occasional). Coarser inclusions (≤ 1.5 mm): abundant, poorly sorted, sub-rounded to sub-angular, equant and elongate, single-spaced, bimodal grain-size distribution (Figure 68). Predominant to dominant: granitic fragments and crystals detached of these rocks (quartz, plagioclase, k-feldspar altered to sericite and muscovite) and quartz-feldspat rocks; Dominant to frequent: quartz-mica schist; Common to few: sandstones, opaques; Few to occasional: amphibole, basalt. Porosity is very scarce, mainly formed by few meso-vesicles.

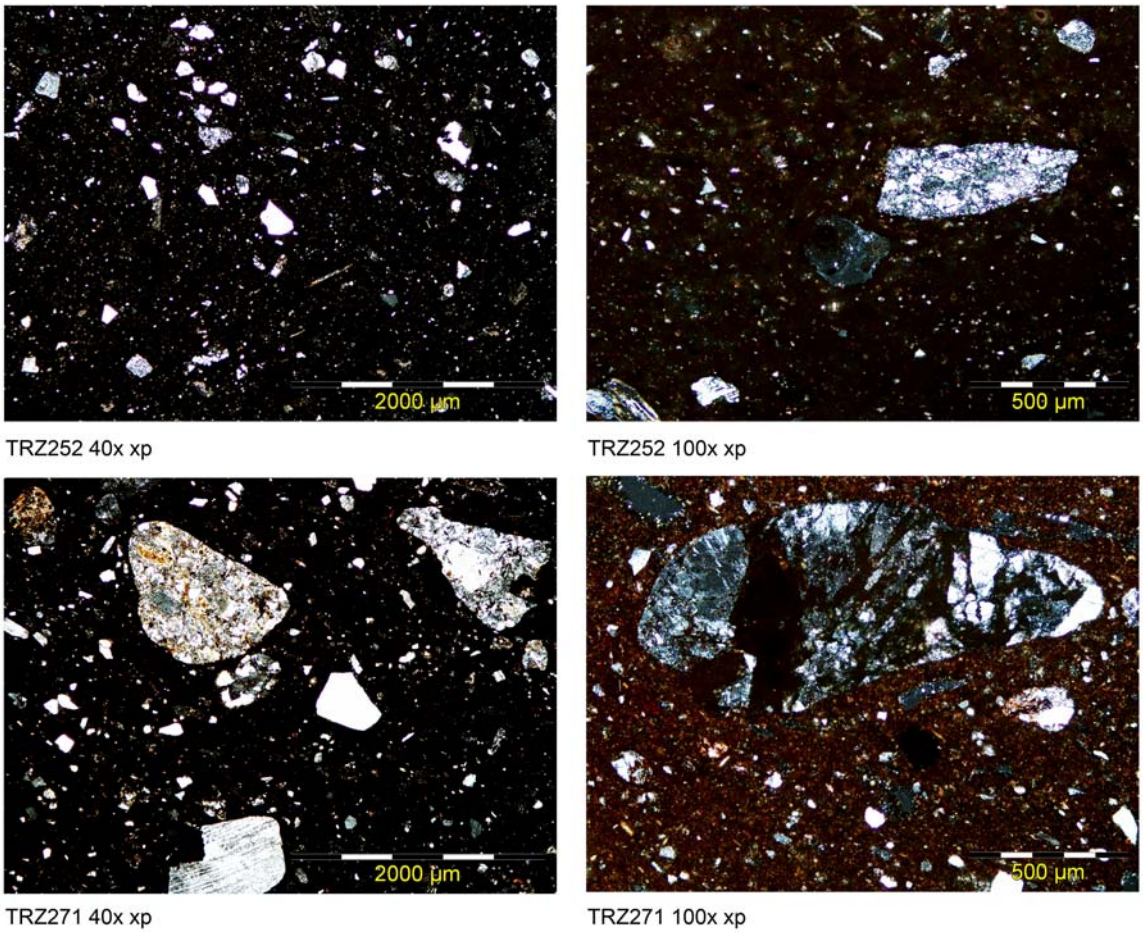

TRZ252 40x xp | TRZ252 100x xp

TRZ271 40x xp | TRZ271 100x xp

Figure 68: Microphotographs by crossed polars (xp) of the ceramics TRZ252 and TRZ271 belonging to **ZT-B**

The rest of the pottery analysed by thin section can be associated to the same petrographic fabric and to the same ceramic production except the chemical outlier **TRZ266**. This jar represents by itself a petrographic fine fabric. Clay matrix: Fe-rich (+ Ca-rich nodules), semi-vitrified (Figure 69). Groundmass (scarce, very fine): quartz and muscovite; (dominant); plagioclase, k-feldspar and calcite (micrite) (occasional). Coarser inclusions (≤ 500 μm): moderately abundant, well sorted, sub-rounded to sub-angular, equant and elongate, double-spaced to single-spaced, bimodal grain-size distribution. Predominant to dominant: granitic rocks and crystals derived of these rocks (quartz, plagioclase, k-feldspar and muscovite); Dominant to frequent: quartz-mica schist, quartzite; Common to few: biotite, basalt, amphibole; Few to occasional: serpentinite, titanite, chert, calcite (micrite). The process of clay mixing is evident in some textural features and it appears as clots of Fe-rich clay. There are abundant meso-vughs and meso-vesicles.

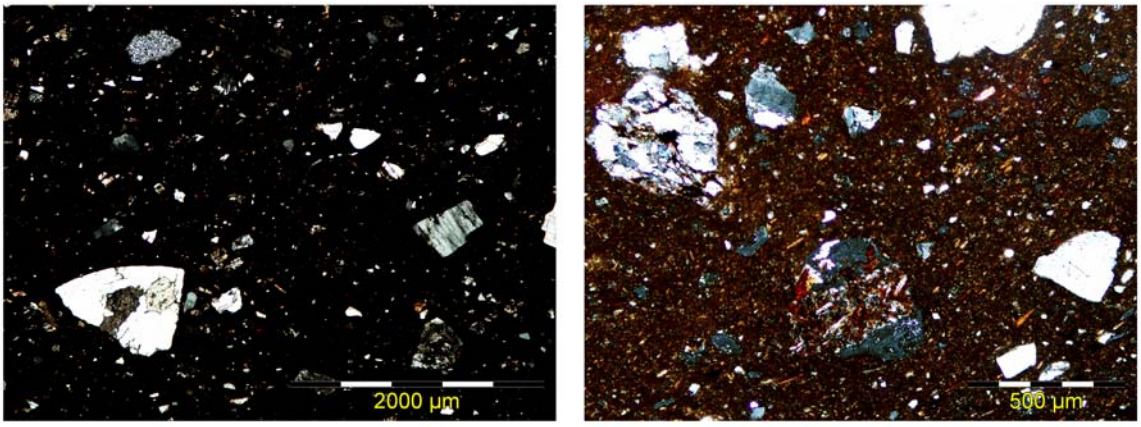

Figure 69: Microphotographs by crossed polars (xp) of the ceramic outlier TRZ266 from **Zar Tepe**

The individuals from **ZT-C** and **ZT-D PCRU's** examined by thin section analysis (TRZ243, TRZ247, TRZ248, TRZ250, TRZ263, TRZ276 and TRZ277) can be grouped to the same petrographic fabric although the existence of few differences concerning the percentage of fine and coarse inclusions (Figure 70). Clay matrix: Fe-rich (+ Ca-rich nodules), vitrified. TRZ248 is fired at reduced atmosphere. Groundmass (scarce, very fine): muscovite and quartz; (dominant); plagioclase, k-feldspar, amphibole and opaques (occasional). Coarser inclusions (≤ 500 μm): moderately abundant (high percentage of aplastic inclusions in TRZ250 and TRZ276), moderately to well sorted, sub-angular to sub-rounded, equant, single spaced (sometimes in contact), bimodal grain-size distribution. Predominant to dominant: quartz, plagioclase, k-feldspar and muscovite derived of granitic rocks; Dominant to frequent: quartz-feldspar rocks, sandstone and chert; Common to few: granite, quartz-mica schist, amphibole, garnet, opaques and calcite (micrite); Few to occasional: epidote, serpentinite and titanite.

Characteristics of matrix and aplastic inclusions evidence the use of very fine Fe-rich clay. Temper used in order to prepare the ceramic paste contains a small percentage of calcium carbonate, probably derived of calcareous microfossils. That indicates a maritime origin from some of the raw materials of the temper.

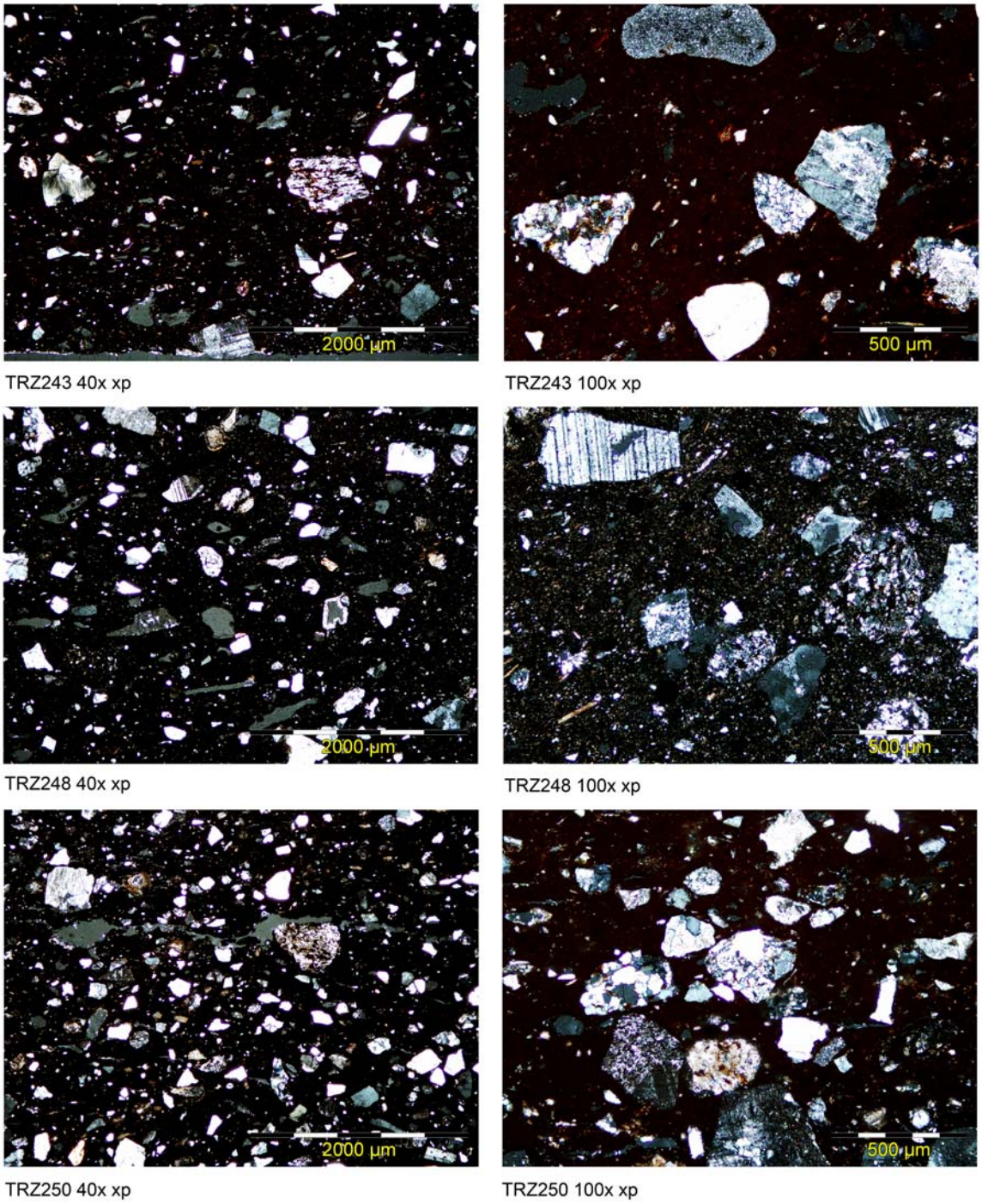

Figure 70: Microphotographs by crossed polars (xp) of the TRZ247, TRZ263, TRZ276, TRZ277, TRZ243, TRZ248 and TRZ250 belonging to **ZT-C** and **ZT-D**

6.2.3. Mineralogical composition (XRD analysis)

Ceramics from **ZT-A** can be divided into two different mineralogical categories. The coarse ceramic TRZ272 is low fired (800/850ºC) as in its diffractogram no clear firing phases can be observed (Figure 71a). However, TRZ275, TRZ279 and TRZ282 can be considered as over fired ceramics (EFT between 1050/1100ºC) because of the advanced decomposition of illite-muscovite and gehlenite and the total decomposition of calcite with the parallel clear increment of the pyroxenes (Figure 71b).

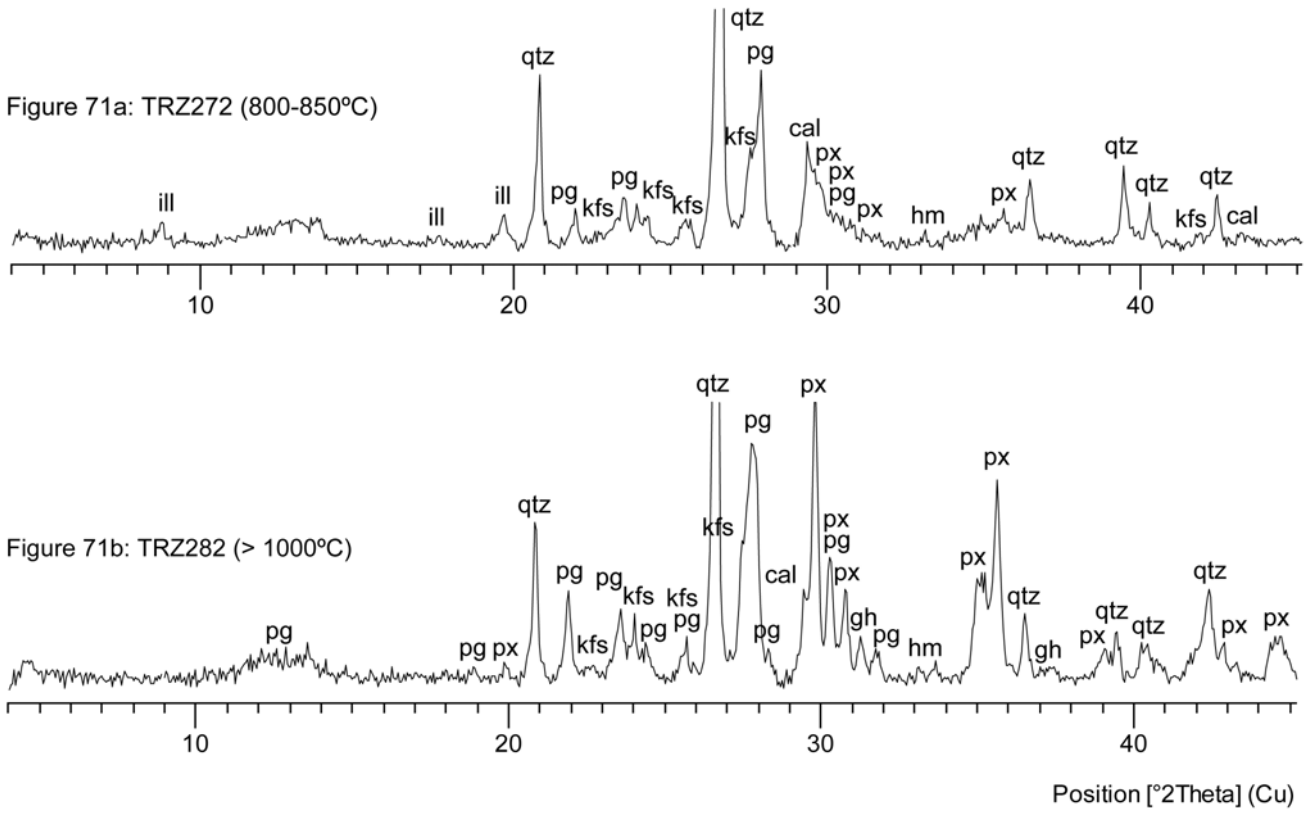

Figure 71: Diffractograms of the individuals TRZ272 and TRZ282 representing the chemical group **ZT-A**; cal: calcite, gh: gehlenite, hm: hematite, ill: illite-muscovite, kfs: k-feldspar, pg: plagioclase, px: pyroxene, qtz: quartz

ZT-B includes over fired ceramics (TRZ252, TRZ262 and TRZ271). Their diffractograms show an advanced decomposition of illite-muscovite and gehlenite and the total decomposition of calcite with the parallel clear increment of the pyroxenes. The EFT must be estimated around 1050/1100ºC (Figure 72).

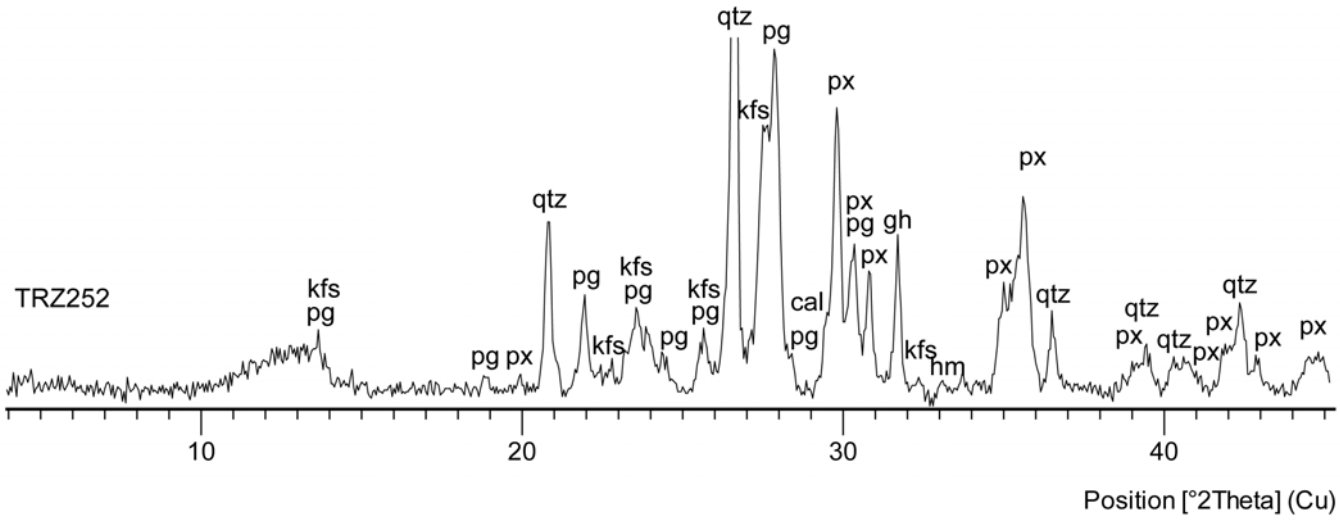

Figure 72: Diffractogram of the individual TRZ252 representing the chemical group **ZT-B**; cal: calcite, gh: gehlenite, hm: hematite, kfs: k-feldspar, pg: plagioclase, px: pyroxene, qtz: quartz

ZT-C can be separated into two mineralogical categories. One represents well fired and the other one high/over fired ones. The shards TRZ248, TRZ253, TRZ261, TRZ263, TRZ264, TRZ245, TRZ260, TRZ259, TRZ251, TRZ243, TRZ247, TRZ250, TRZ258, TRZ257, TRZ268, TRZ270, TRZ276, TRZ281 TRZ274, TRZ289 and TRZ284 present clear firing phases (gehlenite and pyroxenes) under advanced

state of development, but the coexistence of illite-muscovite, calcite and other primary phases points to an EFT around 950/1000ºC (Figure 73a). The individuals TRZ246, TRZ249, TRZ254, TRZ256, TRZ269, TRZ280, TRZ283, TRZ287, TRZ290 and TRZ282 present an advanced decomposition of illite-muscovite and gehlenite and the total decomposition of calcite with the parallel clear increment of the pyroxenes which indicates higher firing temperature, specifically an EFT around 1050/1100ºC. TRZ246 is also characterised by the presence of analcime crystals as secondary mineral phase due to post-depositional alteration and/or contamination processes (Figure 73b). Interesting in this case is that the over fired ceramics are predominantly bowls (TRZ248, TRZ254, TRZ280 and TRZ283).

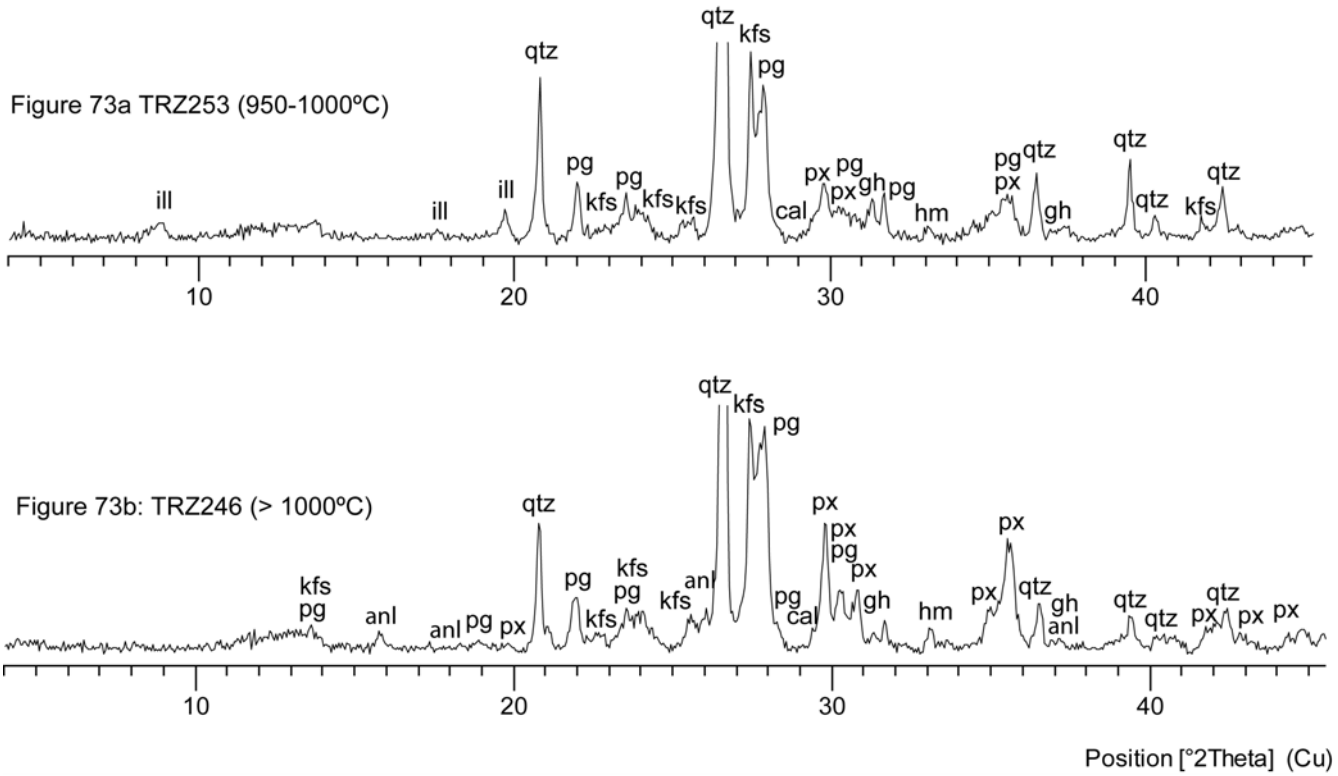

Figure 73: Diffractograms of the individuals TRZ253 and TRZ246 representing the chemical group **ZT-C**; anl: analcime, cal: calcite, gh: gehlenite, hm: hematite, ill: illite-muscovite, kfs: k-feldspar, pg: plagioclase, px: pyroxene, qtz: quartz

Three mineralogical categories related to three different EFT's can be established for five ceramics from **ZT-D.** The coarse storage jar TRZ273 seems to be fired at low temperature (800/850ºC) because in its diffractogram can not be identified any clear firing phase (Figure 74a). For the painted handle TRZ278 (Figure 74b) the clear development of some firing phases together with an advanced decomposition of calcite indicates a higher firing temperature (950/1000ºC). Finally, the EFT`s for the tap TRZ277 and the plane base TRZ286 must be estimated around 1050/1100ºC because of the almost total absence of primary phases and the pronounced peaks of pyroxenes in its XRD spectra (Figure 74c).

The jar TRZ266 and the painted base TRZ285 that have been chemically identified as outliers are fired in the range of 950/1000ºC, due to the clear development of some firing phases (gehlenite, pyroxenes) and the partial decomposition of gehlenite in their diffractograms (Figure 75a). Finally the jar TRZ265, also a chemical outlier, is over fired (>1000ºC) as in its diffractogram the phyllosilicates are absent and firing phases are clearly developed (Figure 75b).

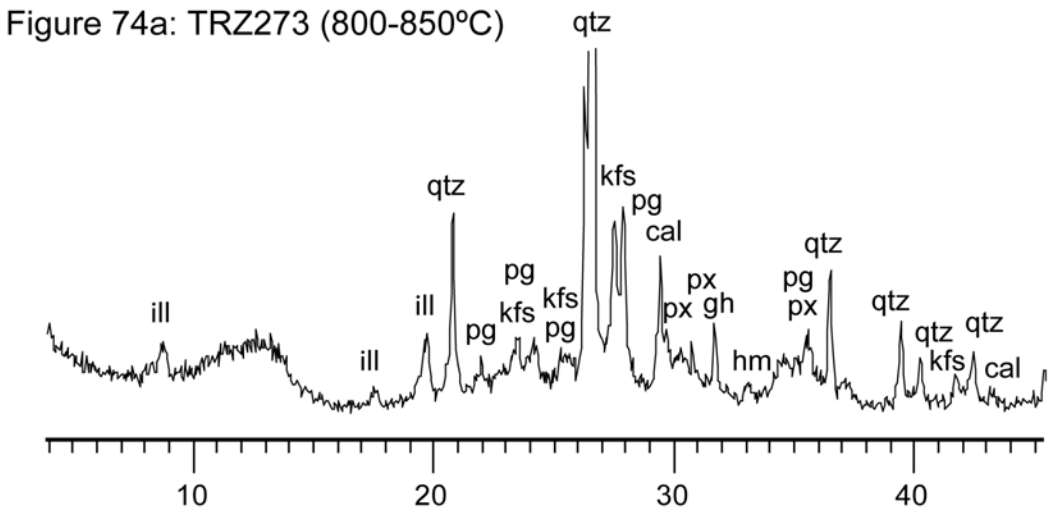

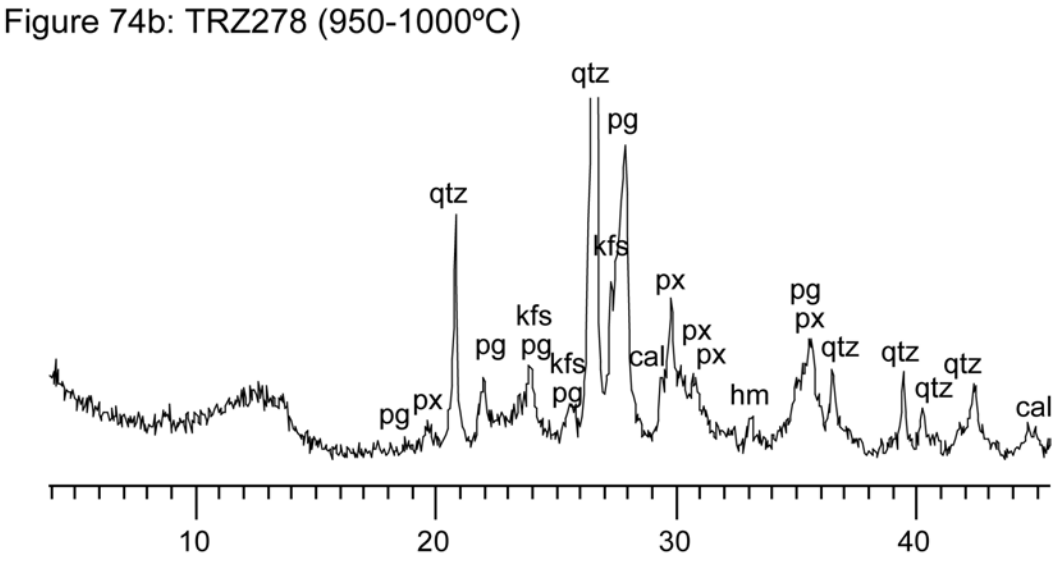

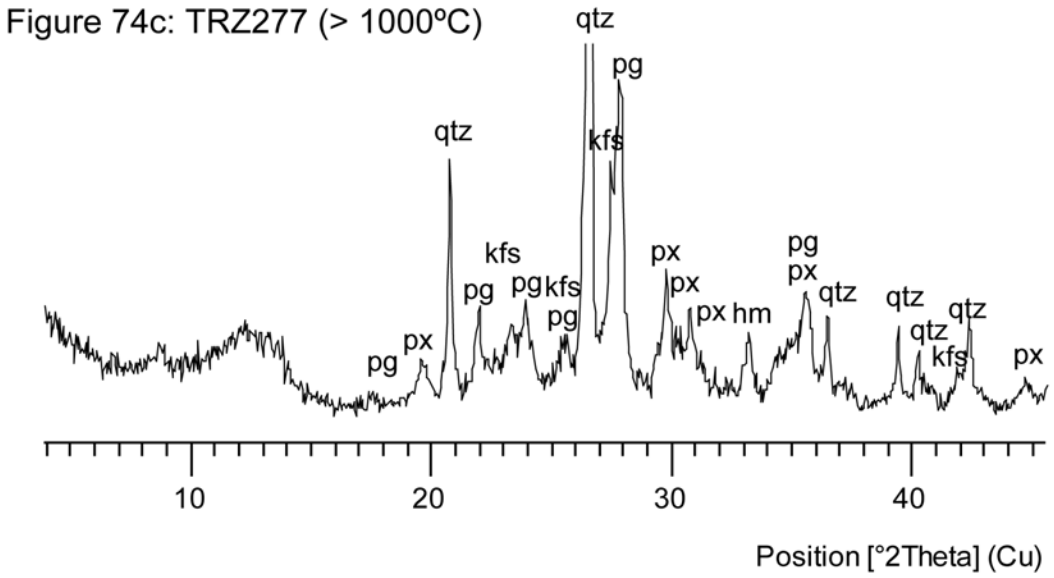

Figure 74: Diffractograms of the individuals TRZ273, TRZ278 and TRZ277 representing the chemical group **ZT-D**; cal: calcite, gh: gehlenite, hm: hematite, ill: illite-muscovite, kfs: k-feldspar, pg: plagioclase, px: pyroxene, qtz: quartz

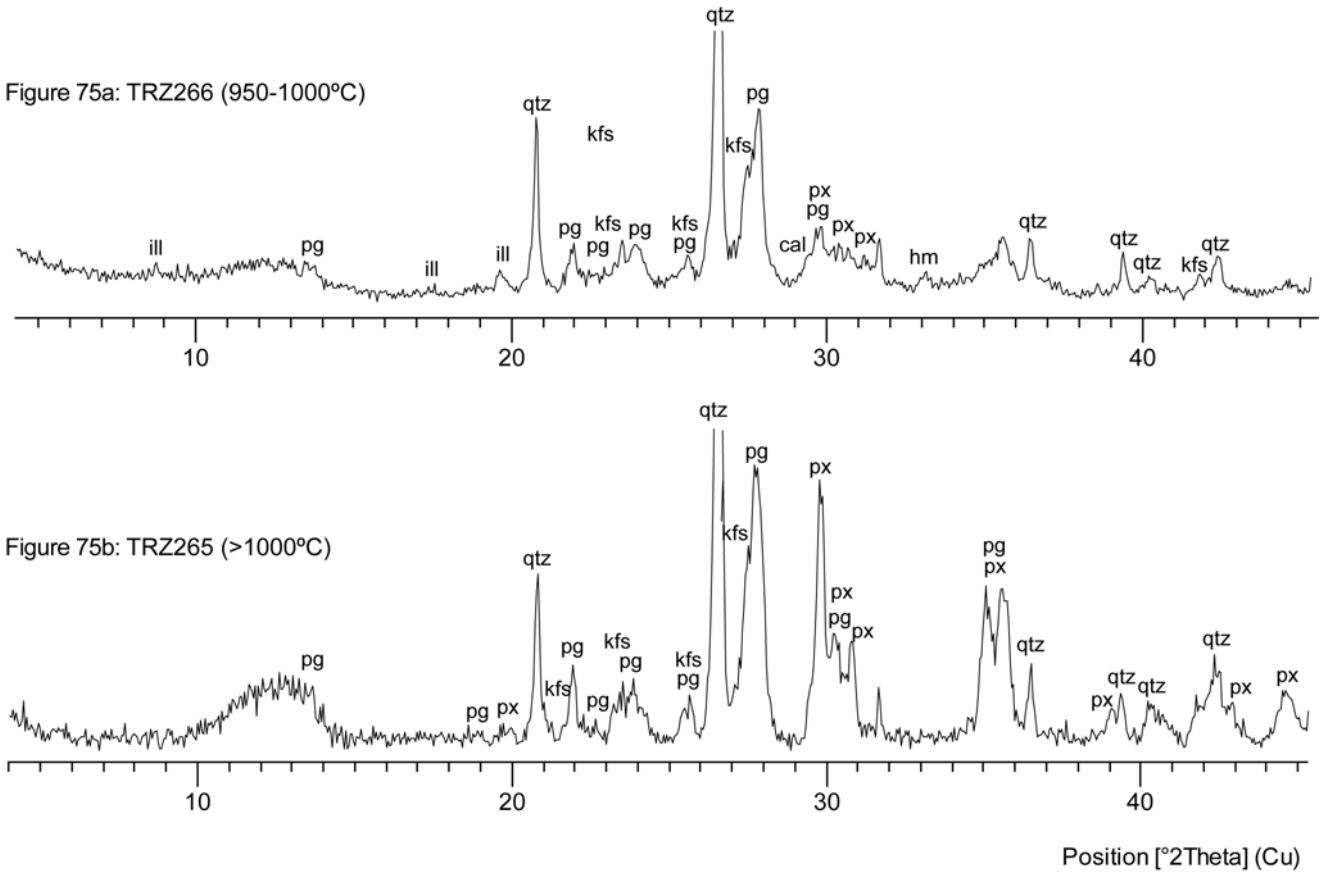

Figure 75: Diffractograms of the individuals TRZ265 and TRZ266; cal: calcite, hm: hematite, ill: illite-muscovite, kfs: k-feldspar, pg: plagioclase, px: pyroxene, qtz: quartz

6.3. Integrated data of Kushan-Sassanian ceramics from Termez and Zar Tepe

The chemical composition of ceramics from **Tchinguiz Tepe** and **Zar Tepe** have been compared in order to try to establish economical and commercial relations between both sites during the Kushan-Sassanian period. For that, the chemical concentrations of 149 shards from **Tchinguiz Tepe** and **Zar Tepe** determined by XRF were treated statistically according to the proposals of Aitchison (1986) and Buxeda (1999). The Compositional Variation Matrix (CVM) have been calculated upon the following chemical subcomposition: Fe_2O_3 (as total Fe), Al_2O_3, TiO_2, MgO, CaO, Na_2O, K_2O, SiO_2, Ba, Rb, Th, Nb, Zr, Y, Sr, Ce, Ga, V, Zn, Cu, Ni and Cr (Table 7c). Some elements, P_2O_5, Pb, MnO, Co and W, were not considered for reasons mentioned above. The CVM obtained offers a high total variation (vt = 0.583), which probably indicates a polygenic origin for the analysed shards. The variability introduced by some of these elements is due to differences in raw material composition (MgO, CaO, Ce and Cr), as has already been shown by the chemical and petrographical analysis. Nevertheless, the chemical variability of some elements also partly corresponds to several alteration and contamination processes (CaO, Na_2O, K_2O, Ba, Sr and Cu) as it has been already explained, and those elements have been excluded from the statistical evaluation of the chemical data.

To continue, a cluster analysis using the Square Euclidean distance and the centroid algorithm with S-plus2000 (MathSoft 1999) and applying Fe_2O_3 as divisor in logratio transformation was preformed on the previous mentioned subcomposition. The resulting dendrogram (Figure 76) shows several groups that generally correspond to the previously identified ones for **Tchinguiz Tepe** and **Zar Tepe**

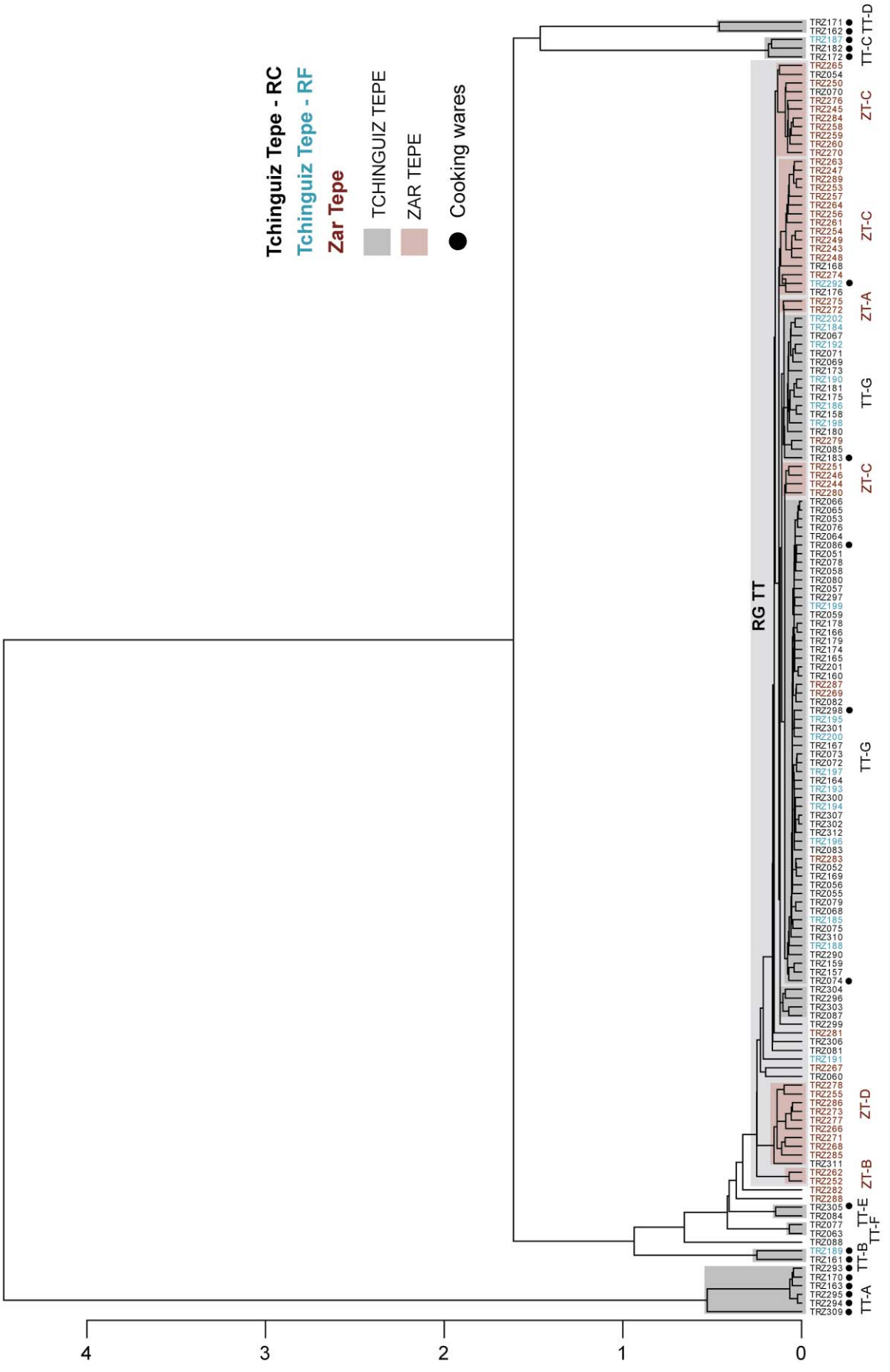

Figure 76: Dendrogram resulted from the cluster analysis performed on the subcomposition Al_2O_3, TiO_2, MgO, SiO_2, Rb, Th, Nb, Zr, Y, Ce, Ga, V, Zn, Ni, Cr and Fe_2O_3 used as divisor, of 149 individuals sampled at **Tchinguiz Tepe** and **Zar Tepe**

The groups **TT-A**, **TT-B**, **TT-C** and **TT-D** only including cooking wares from **Tchinguiz Tepe** remain separate from the rest of the material, as well the other two grups **TT-E** and **TT-F** mainly composed by common wares. The cooking wares represent several typologies which can be correlated to different petrographic fabrics. From the 17 cooking wares analysed by XRF, XRD and thin section analysis from **Tchinguiz Tepe** and **Zar Tepe**, 7 can be related to pastes containing shell fragments and microfossils (**TT-B**, **TT-C** and **TT-D** petrographic fabrics). All these pottery shards share a basic technological aspect which is the addition of coarse shell fragments as main temper in rich iron oxide clay. However, according to some differences in petrographic composition, they can be separate into tree different productions. **TT-B** is similar to **TT-C** because the major temper is composed by shell fragments and claystone, whereas the main inclusions in **TT-D** group are big fragments of shell and quartzarenite. The specific provenance of these ceramics remains still uncertain. Nevertheless, the same shell fragments were identified in some pottery classified into **TT-G** ,where there are also individuals sampled at the kiln located at sector RF of **Tchinguiz Tepe** (e.g. the tap TRZ085).

As already mentioned, the geological substrate of **Tchinguiz Tepe** is formed by sandstone, however the presence of limestone have been observed on the hillside of **Tchinguiz Tepe**, they correspond to the remains of architectural structures and their provenance is unknown. Petrographic analysis carried out on a limestone fragment (Figure 3) detected substantial differences in the petrographic composition between the limestone fragments and the type of carbonate-sedimentary rocks identified in pottery pastes. Thus, actually we have no sufficient data to precise the origin of these cooking wares. The cooking wares from **TT-A** in contrary, could have local origin (**Tchinguiz Tepe**) because the correspondent ceramic fabric is compatible with the geological environment of **Tchinguiz Tepe.** The pottery shards classified in **TT-A** fabric share the same typological characteristics.

Most pottery shards from **Tchinguiz Tepe** are grouped together at the centre of the dendrogram, configuring the chemical group **TT-G** (Figure 76). In chemical terms, however, they are more similar to the individuals coming from **Zar Tepe** than to the previous cooking wares. The pottery sampled at the kiln site of **Tchinguiz Tepe** (RF sector) is highly represented inside the chemical group **TT-G** that leads to the hypothesis that this group is the Reference Group of **Tchinguiz Tepe kiln's** production. They correspond mainly to common wares although three cooking wares of different typology can be also associated to this reference group. Moreover, one rim of jar (TRZ269) and two bases (TRZ283 and TRZ287) from **Zar Tepe** belong to this same group, which indicates, moreover, that pottery produced at **TchinguizTepe** was distributed to other settlements of the broader area of Surkhan Darya valley.

Beside the chemical compatibilities, the petrographic examination confirms some similarities in composition between most ceramics coming from **Zar Tepe** and **Tchinguiz Tepe** (Figure 76). Nevertheless, also different pottery productions have been identified for the pottery sampled at **Zar Tepe,** as it has been already demonstrated in the previous petrographical analysis. Looking at the dendrogram, the individuals from **Zar Tepe** form chemical groups with slight differences already described above. It is important to mention that only few vessels from **Tchinguiz Tepe** (TRZ054, TRZ70, TRZ168 and TRZ176 from RC sector and TRZ292 from RF sector) appear associated to ceramics from **Zar Tepe**.

This study clearly shows the compositional similarity between the kushan-sassanian common wares from **Tchinguiz Tepe** and **Zar Tepe**, especially in the cases in which pottery from both sites are mixed in the same cluster. According to this background, we might suggest the possible existence of other ceramic workshops installed in the territory in addition to the already known and excavated ones at **Tchinguiz Tepe**. However, it seems that these production centres use the same or very similar raw materials and most probably, coming from common geological formations.

Only the location and excavation of new ceramic production centres at the Surkhan Darya Valley and the expansion of the archaeometrical study with new ceramics from these production centres will lead to the establishment of reliable reference groups representing the local and regional ceramic production during the Kushan-Sassanian period.

7. Medieval pottery from *Tchurobkurgan*: *Integrated results of archaeometrical analysis*

With the aim of expanding knowledge on the ceramics produced and diffused in Uzbekistan along its history, a set of materials dating from the VI c. AD from **Tchurobkurgan**, have been included in the archaeometrical study (Table 1). **Tchurobkurgan** is a medieval settlement located nearby to the Hellenistic settlement of **Kampyr Tepe**. The nine analyzed shards correspond mainly to common wares and most them are covered with a reddish (TRZ391 and TRZ395) or dark brown slip (TRZ392 and TRZ393). Three of them are, however, unpainted (TRZ394, TRZ396 and TRZ399) while ceramics TRZ397 and TRZ398 are cooking wares.

7.1. Chemical composition (XRF analysis)

The normalised chemical composition of 9 analysed ceramics from **Tchurobkurgan** (Table 2) was treated statistically according to the proposals of Aitchison (1986) and Buxeda (1999). The first step of the statistical evaluation was to calculate the Compositional Variation Matrix (CVM) in order to know the total variation and the variability that each element introduces in the data set. The CVM has been calculated without considering Mo, Sn, Co, W, P_2O_5 and Pb for reasons that have been already explained. The CVM obtained for the rest of the chemical subcomposition (Fe_2O_3 (as total Fe), Al_2O_3, TiO_2, MgO, CaO, Na_2O, K_2O, SiO_2, Ba, Rb, Th, Nb, Zr, Y, Sr, Ce, Ga, V, Zn, Cu, Ni and Cr) shows very high total variation (vt = 1.2848), which indicates a roughly polygenic origin for the analysed shards (Table 10a). It also indicates that the main variability is introduced by the following elements: CaO ($\tau_{.CaO}$ = 14.135), Cr ($\tau_{.Cr}$ = 5.555), V ($\tau_{.V}$ = 5.449), Na_2O_3 ($\tau_{.Na2O3}$ = 3.034), MgO ($\tau_{.MgO}$ = 2.290), Sr ($\tau_{.Sr}$ = 2.138), Cu ($\tau_{.Cu}$ = 2.073) and Ba ($\tau_{.Ba}$ = 1.787).

The variability introduced by some of these elements must be due to differences in raw material composition. However, since we know the presence of some secondary alterations in some ceramics from Uzbekistan, we will repeat the statistical treatment without considering Na_2O_3, Sr, Ba and Cu. The vt of the new CVM is much more lower (vt= 0.1096) but it is still indicative of a polygenetic set of ceramics (Buxeda and Kilikoglou, 2003). CaO, MgO, V and Cr are still the responsible for most of the existing variability in the data set.

The cluster analysis has been performed under the previous subcomposition (Fe_2O_3 , Al_2O_3, TiO_2, MgO, CaO, K_2O, SiO_2, Rb, Th, Nb, Zr, Y, Ce, Ga, V, Ni and Cr) using Zn as divisor in the logratio transformation and the Square Euclidean distance and the centroid algorithm with S-plus2000 (MathSoft, 1999). In the dendrogram obtained (Figure 77), ceramics are distributed forming two main groups (**TRK-A** and **TRK-B**) that we might consider as two chemical trends rather than two chemical groups. The main chemical difference between these two trends is that the fist contains all the calcareous pottery from this data set and the second the low calcareous ones (Table 2). Beside CaO, also some differences in MgO and V can be observed between these two tendencies. Inside each trend, various chemical groups or PCRU's can be identified, as it is impossible to identify the provenance zone for this material, since they don't come from any pottery workshop. Nevertheless, according to these chemical results, the existence of several ceramic productions for these common and cooking wares is possible.

At the right side of the dendrogram of Figure 77, the trend **TRK-A** brings together only common wares, four of which are painted (TRZ391, TRZ392, TRZ393 and TRZ395) and three are unpainted (TRZ394, TRZ396 and TRZ399). **TRK-A,** according the value of the total variation (vt = 0.1038) of the CVM calculated for this group, indicative of a very homogeneous set of ceramics, thus it represents one single production. Small compositional differences between TRZ396 (Table 11) and the rest of the common wares could indicate that this specific individual is a chemical outlier of this specific group (Figure 78). Specifically it could be a more calcareous variant of **TRK-A2**. The main chemical composition and the standard deviation **TRK-A2** and the chemical composition of **TRZ396 (TRK-A1)** are given in Table 11. Besides though the differences in CaO and Sr, there are other slighter differences between TRZ396 and the rest of the common wares (Table 11) that are related to MgO, K_2O, Nb, Zn, Cu and Ni. In con-

(TB)	Fe_2O_3	Al_2O_3	TiO_2	MgO	CaO	Na_2O	K_2O	SiO_2	Ba	Rb	Th	Nb	Zr	Y	Sr	Ce	Ga	V	Zn	Cu	Ni	Cr
$\tau_{\cdot i}$	1.409	1.393	1.499	2.290	14.13	3.034	1.482	1.340	1.787	1.452	1.500	1.340	1.479	1.364	2.138	1.459	1.334	5.449	1.327	2.073	1.665	5.555
$vt/\tau_{\cdot i}$	0.912	0.922	0.857	0.561	0.091	0.423	0.867	0.958	0.718	0.884	0.856	0.959	0.868	0.942	0.601	0.880	0.963	0.236	0.967	0.620	0.771	0.231
$r\ v,\tau$	0.987	0.986	0.974	0.762	0.834	0.995	0.997	0.998	0.919	0.986	0.996	0.997	0.995	0.993	0.988	0.999	0.994	0.883	0.996	0.860	0.941	0.883
vt	1.284																					

Table 10a: Compositional Variation Matrix (CVM) calculated upon the 9 ceramics from the medieval period sampled at **Tchurobkurgan**

(AC)	Fe_2O_3	Al_2O_3	TiO_2	MgO	CaO	Na_2O	K_2O	SiO_2	Ba	Rb	Th	Nb	Zr	Y	Sr	Ce	Ga	V	Zn	Cu	Ni	Cr
$\tau_{\cdot i}$	3.838	4.077	3.950	6.513	10.26	4.390	6.375	3.915	4.888	24.12	4.484	3.812	4.142	5.058	4.660	5.605	11.42	4.078	5.505	22.29	6.881	4.478
$vt/\tau_{\cdot i}$	0.916	0.863	0.890	0.540	0.343	0.801	0.552	0.898	0.719	0.146	0.784	0.922	0.849	0.695	0.755	0.627	0.308	0.862	0.639	0.158	0.511	0.785
$r\ v,\tau$	0.993	0.964	0.976	0.888	0.856	0.988	0.900	0.974	0.945	0.946	0.913	0.982	0.979	0.889	0.974	0.860	0.653	0.977	0.940	0.750	0.894	0.979
vt	3.517																					

Table 10b: Compositional Variation Matrix (CVM) calculated upon the 22 ceramics from the Islamic period sampled at Ancient Military Quarters sector 2 (**AC2**) at Termez.

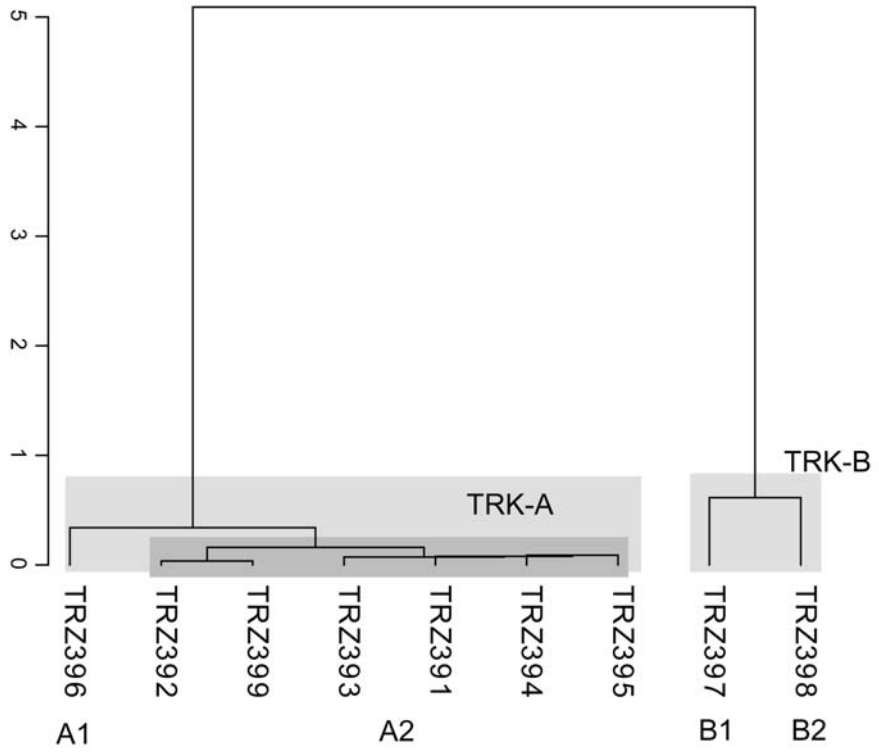

Figure 77: Dendrogram resulted from the cluster analysis performed on the subcomposition Fe_2O_3, Al_2O_3, TiO_2, MgO, CaO, K_2O, SiO_2, Rb, Th, Nb, Zr, Y, Ce, Ga, V, Ni and Cr and Zn used as divisor, of 9 individuals sampled at **Tchurobkurgan**, using the Square Euclidean distance and the centroid algorithm

Elements	TRK-A2 (n= 6)		TRK-A1 (TRZ396)	TRK-B1 (TRZ397)	TRK-B2 (TRZ398)
	m	sd	nc	nc	nc
Fe_2O_3 (%)	6.12	0.29	6.46	7.66	7.00
Al_2O_3 (%)	15.84	0.43	15.45	19.17	18.42
TiO_2 (%)	0.67	0.02	0.69	0.87	0.85
MgO (%)	3.69	0.41	3.74	2.51	2.32
CaO (%)	9.04	1.03	12.60	1.43	2.34
Na_2O (%)	1.55	0.65	1.71	1.84	1.50
K_2O (%)	3.62	0.27	2.91	3.33	3.55
SiO_2 (%)	59.29	1.08	56.28	62.98	63.84
Ba (ppm)	512	63	569	445	380
Rb (ppm)	144	4	123	164	167
Th (ppm)	16	2	20	19	18
Nb (ppm)	17	1	19	19	20
Zr (ppm)	170	13	166	186	192
Y (ppm)	29	1	29	34	32
Sr (ppm)	400	79	276	358	329
Ce (ppm)	60	6	62	57	72
Ga (ppm)	20	1	20	24	23
V (ppm)	103	7	93	329	227
Zn (ppm)	97	4	104	105	114
Cu (ppm)	32	2	47	26	26
Ni (ppm)	49	5	61	43	42
Cr (ppm)	77	6	74	184	244

Table 11: The mean chemical composition (m) and the standard deviation (sd) using normalised data of **TRK-A2** and the raw normalised chemical composition (nc) of the ceramics outliers **TRZ396**, **TRZ397**and **TRZ398** from **Tchurobkurgan**.

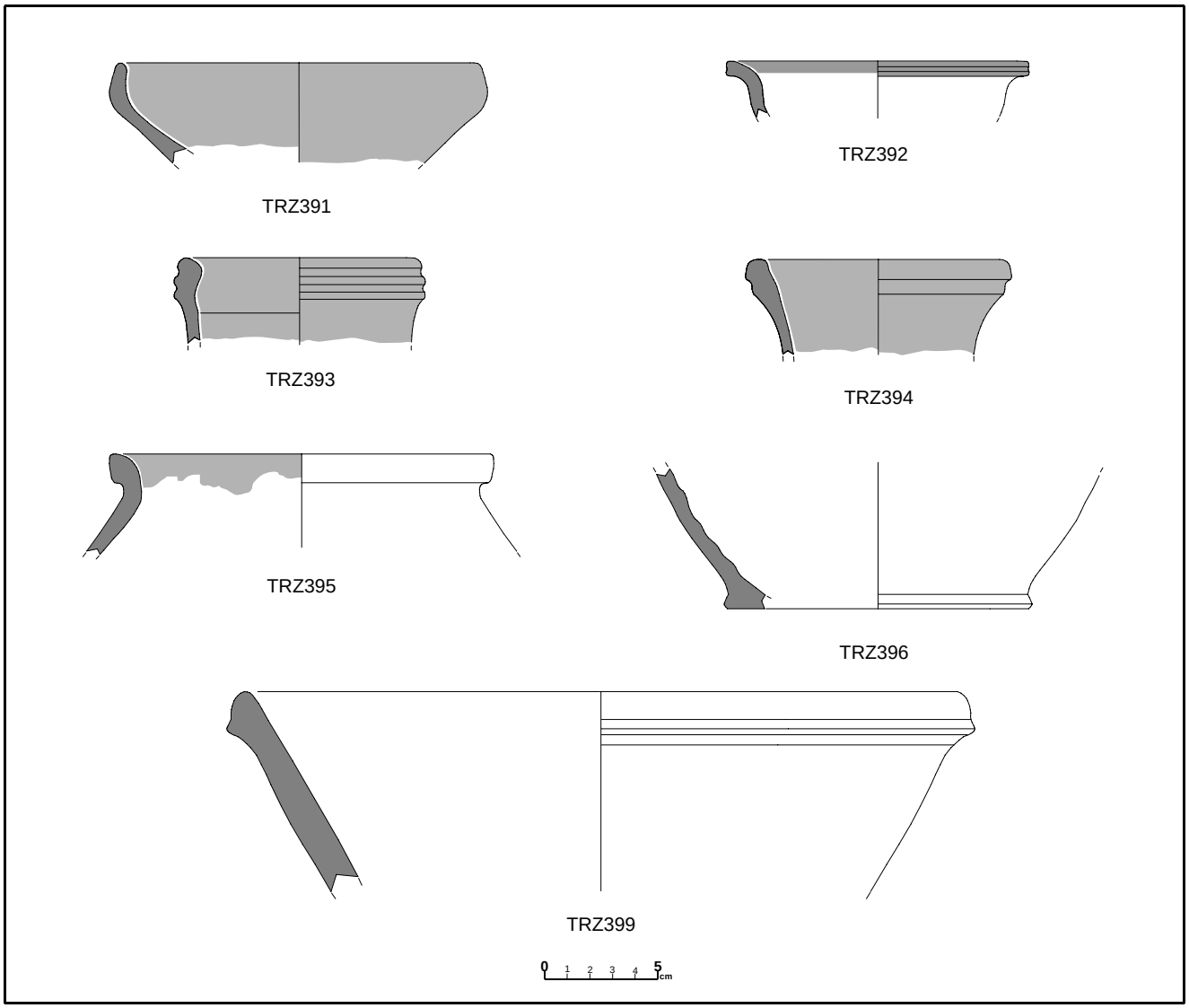

Figure 78: Typology of the **TRK-A** group (TRZ391, TRZ392, TRZ393 TRZ394, TRZ395, TRZ396 and TRZ399)

crete **TRZ396** besides being more calcareous, present higher relative concentrations of Ba, Nb, Zn, Cu and Ni and lower K_2O and Sr contents. Therefore, it might represent another production. Both **TRK-A1 (TRZ396)** and **TRK-A2** must be considered as PCRU's (Paste Compositional Reference Units) of medieval pottery production of **Tchurobkurgan** due to the actual impossibility to associate them to a specific kiln site.

At the left side of the dendrogram, the trend **TRK-B** contains only two individuals TRZ397 and TRZ398, both are cooking wares (Figure 79). Regarding to the chemical aspects, on the one hand, **TRZ397** present the lowest CaO content in the whole data set but also high values in Fe_2O_3, Al_2O_3, TiO_2 and in most of the trace elements except Cu and Ni (Table 11). The main difference of **TRZ398** respect to **TRZ397** is obviously higher Cr concentrations, although it has higher Rb, Zr, Ce, and Zn contents and lower V content. For these reasons, **TRK-B1** and **TRK-B2** correspond to two different PCRU's and represent two different of medieval cooking ware productions of **Tchurobkurgan**. Nevertheless, the general chemical aspects of both indicate similar geo-chemical origin.

The lack of archaeological documentation of pottery type's characteristics of the 6th c. AD as well as the lack of pottery production sites prevents to get further conclusions about ceramic production and diffusion during the medieval period.

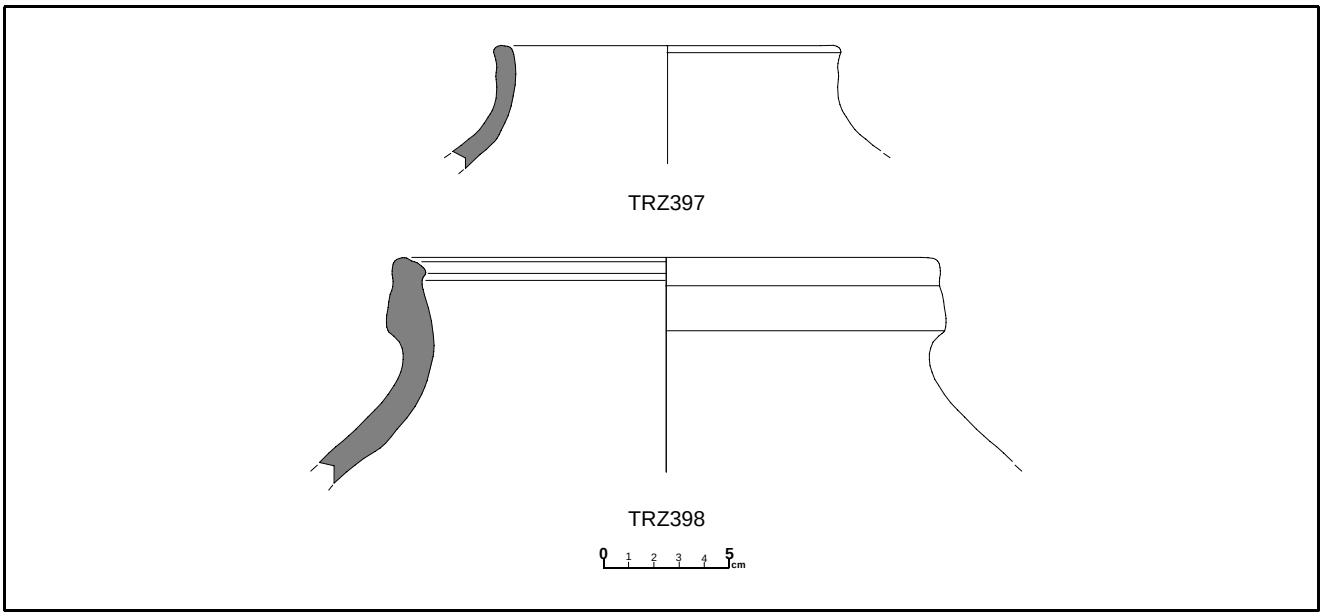

Figure 79: Typology of the **TRK-B** group (TRZ397 and TRZ398)

7.2. Mineralogical composition (XRD analysis)

The examination of diffractogram of **TRZ396** (**TRK-A1**) points out a very high firing temperature (> 1000ºC) because of the presence of primary phases (quartz, k-feldspars and plagioclase) and pyroxene very developed as a firing phase (Figure 80).

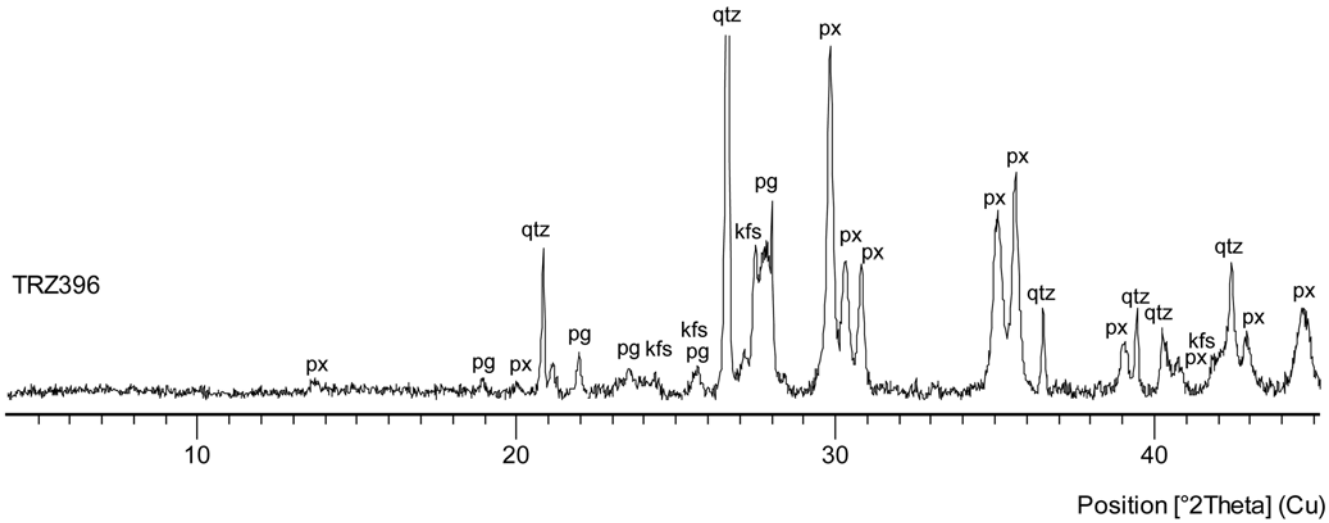

Figure 80: Diffractogram of the individual TRZ396; kfs: k-feldspar, pg: plagioclase, px: pyroxene, qtz: quartz

The six shards classified in **TRK-A2** can be divided in two different EFT and mineralogical categories. On the one hand, the diffractograms of TRZ391, TRZ393, TRZ394 and TRZ399 reflect firing temperature around 900-950ºC, according to the presence of both primary phases (quartz, calcite, illite-muscovite, k-feldspars, plagioclase and hematite) and firing phases, such as pyroxene and gehlenite (Figure 81a). On the other hand, TRZ392 and TRZ395 (both sliped wares) represent a second category of over fired pottery, as their diffractograms show the total decomposition of illite-muscovite and the partial decomposition of calcite. Moreover, firing phases such as pyroxenes, gehlenite and hematite are under an advanced state of development, which leads to estimate an EFT higher than 1000ºC (Figure 81b) for both.

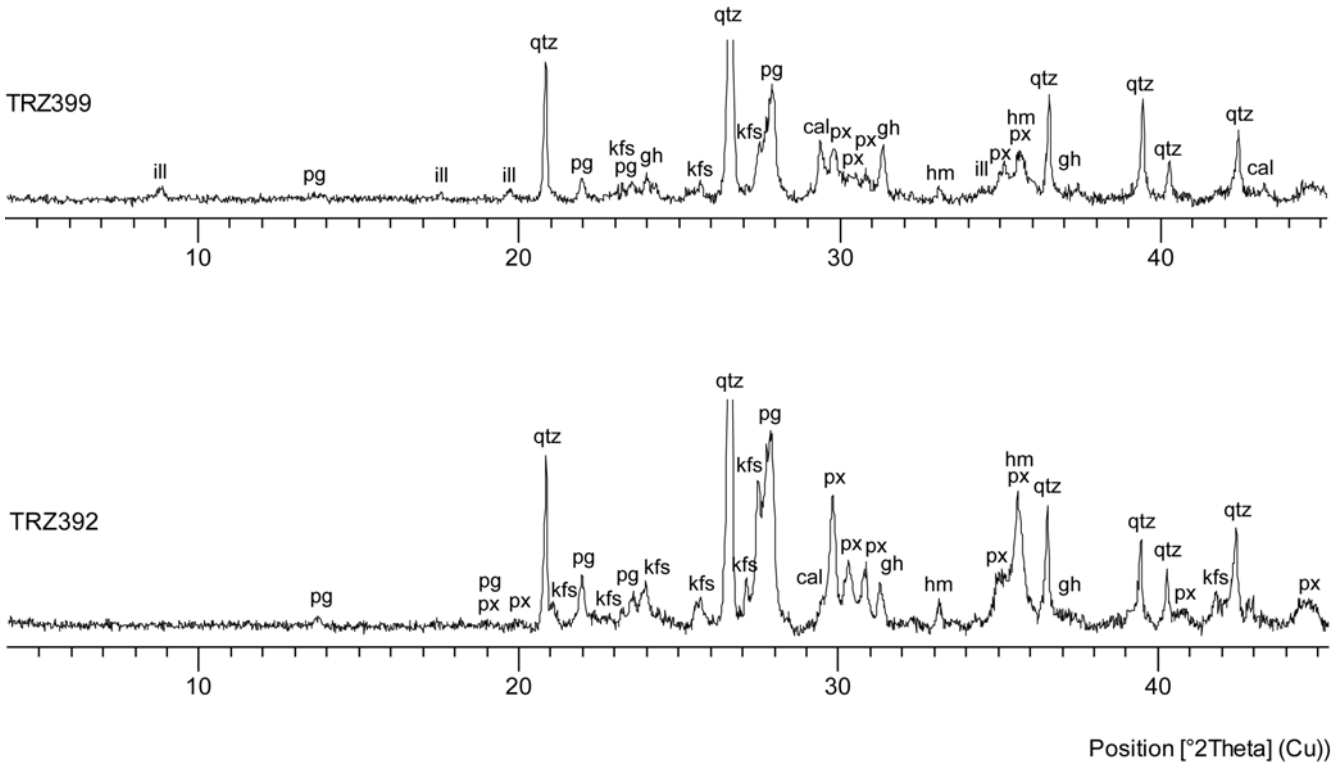

Figure 81: Diffractograms of the individuals TRZ392 and TRZ399 from **TRK-A**; cal: calcite, gh: gehlenite, hm: hematite, ill: illite-muscovite, kfs: k-feldspar, pg: plagioclase, px: pyroxene, qtz: quartz

The low calcareous cooking wares **TRZ397** (**TRK-B1**) and **TRZ398** (**TRK-B2**) are characterised by the simultaneous presence of primary and firing phases, specifically by quartz, k-feldspars, plagioclase hematite and spinel. The total decomposition of illite muscovite and the presence of spinel under advanced state of development leads to an EFT higher than 1000°C (Figure 82a).

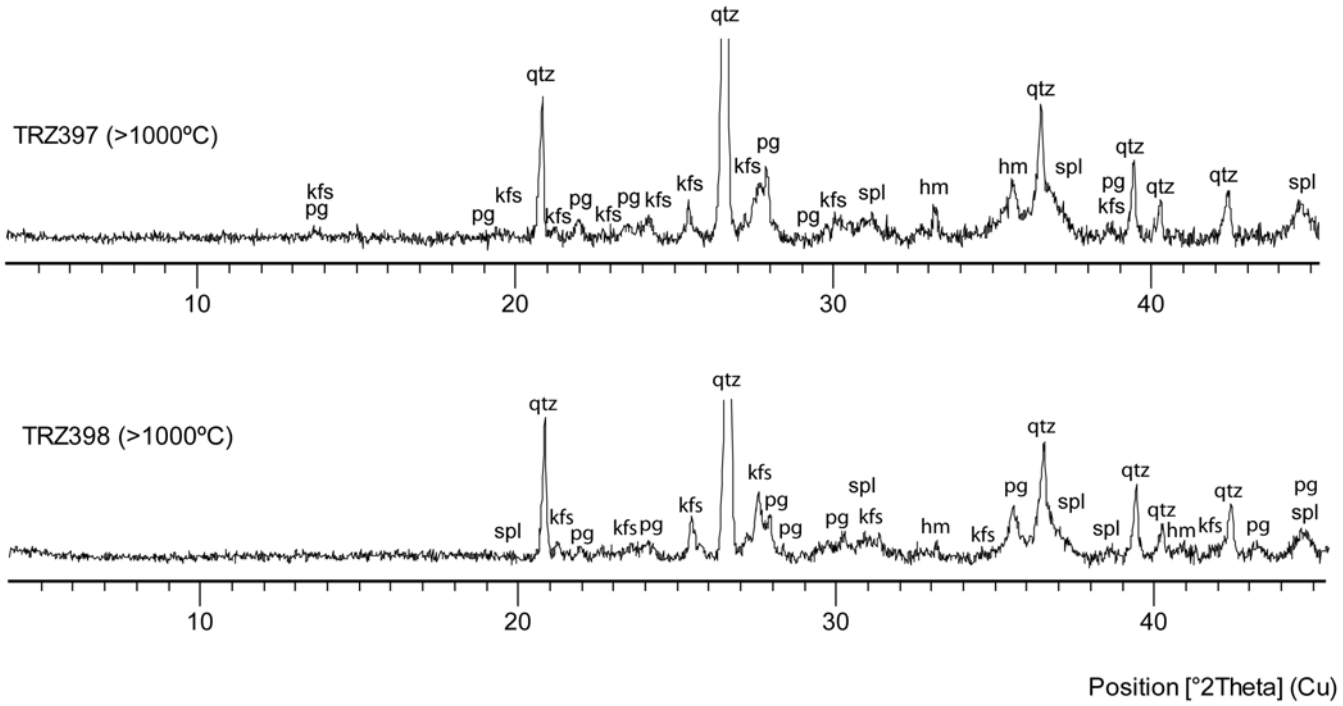

Figure 82: Diffractograms of the individuals TRZ397 and TRZ398 from **TRK-B**; hm: hematite, kfs: k-feldspar, pg: plagioclase, px: pyroxene, qtz: quartz, spl: spinel

8. Islamic Pottery from Termez (*Ancient Military Quarter*). *Integrated results of archaeometrical analysis.*

The archaeological excavations at sector 2 of Ancient Military Quarters (**AC2**) at **Termez** offered some stratigraphical levels related to an Islamic settlement dated to XII century (Martínez, in this volume). The archaeological contexts excavated correspond to a domestic dump, in which ceramics are the most representative findings together with glass objects and glass slags, fauna and metal objects.

From the pottery recovered at **AC2** sector, 22 Islamic shards from eight different stratigraphical units were analysed for the archaeometrical study (TRZ313 to TRZ247: Table 1). Few of these vessels are cooking wares (TRZ320, TRZ323), two are covers or taps (TRZ317 and TRZ319), two are common jars (TRZ318, TRZ321), one is a decorated tap with incised motifs (TRZ330) and one big container (TRZ347). The rest are glazed common wares generally corresponding to plates and bowls (TRZ313, TRZ314, TRZ315, TRZ316, TRZ322, TRZ324, TRZ425, TRZ326, TRZ327, TRZ328, TRZ329, TRZ331, TRZ345 and TRZ346). They are decorated with different motifs made by glazes of different colours (black, blue, green, red and yellow) or calligraphy decoration (TRZ328).

8.1. Chemical composition (XRF analysis)

The first step for the statistical evaluation of the chemical data of 22 islamic shards from **AC2** was to calculate the Compositional Variation Matrix (CVM) upon the subcomposition: Fe_2O_3 as total Fe, Al_2O_3, TiO_2, MgO, CaO, Na_2O, K_2O, SiO_2, Ba, Rb, Th, Nb, Zr, Y, Sr, Ce, Ga, V, Zn, Cu, Ni and Cr, and take a look to total variation and the variability that each element is introducing in the data set.

The CVM calculated for the Islamic ceramics from **AC2** data set can be seen in Table 10b. It has been calculated without considering Mo, Sn, Co, W, MnO P_2O_5 and Pb, for reasons that already have been explained. The CVM gives a clearly high total variation (vt = 3.517), which indicates a very polygenic origin for the data set. The main variability is introduced by Rb ($\tau_{.Rb}$ = 24.12), Cu ($\tau_{.Cu}$ = 22.29) and Ga ($\tau_{.Ga}$ = 11.42) followed of CaO ($\tau_{.CaO}$ = 10.26), Ni ($\tau_{.Ni}$ = 6.881), MgO ($\tau_{.MgO}$ = 6.513), K_2O ($\tau_{.K2O}$ = 6.375), Ce ($\tau_{.Ce}$ = 5.605), Zn ($\tau_{.Zn}$ = 5.505) and Y ($\tau_{.Y}$ = 5.058), from which, however, some of the variability introduced by Na_2O, K_2O, Rb, Th, Sr and Cu as already explained is due to some perturbation processes introduced in the data set. Repeating the CVM calculation without consi-dering these four elements, the vt reduces to 1.437. This value is much lower but still high to consider that Islamic ceramics analysed correspond to a single production. A range of this vt points towards different geochemical origin of the raw materials, without this necessarily meaning that some of them can belong into the same production. In order to assess if **Termez** could be the production area of this Islamic pottery, we included the analytical results obtained on two local clay sediments (G-TRZ-27 and G-TRZ-28) sampled at Ancient Military Quarters sector 2 (**AC2**).

To continue the statistical treatment, the chemical data (subcomposition: Fe_2O_3 as total Fe, Al_2O_3, TiO_2, MgO, CaO, SiO_2, Ba, Nb, Zr, Y, Ce, Ga, V, Zn, Ni and Cr) were transformed into logratios following the considerations of Aitchison (1986) and Buxeda (1999) on compositional data. Fe_2O_3 was used as divisor, as according to the CVM, it was the element less contributing ($\tau_{.Fe2O3}$ = 3.838) to the chemical variability (Buxeda and Kilikoglou, 2003). To visualize the chemical similarity between the 22 vessels, we present the dendrogram of Figure 83 resulting from the cluster analysis performed on the above mentioned subcomposition, using the Square Euclidean distance and the centroid algorithm. Most ceramics are joined together in two main chemical groups (**ACI-1** and **ACI-2**) with except of the glazed wares **TRZ315, TRZ325** and **TRZ323** and the cooking wares **TRZ319** and **TRZ320.** Keeping in mind the very high total variation, we can see now that most variability inside the data set is due to significant chemical differences in composition of these individuals respect to the rest of the shards.

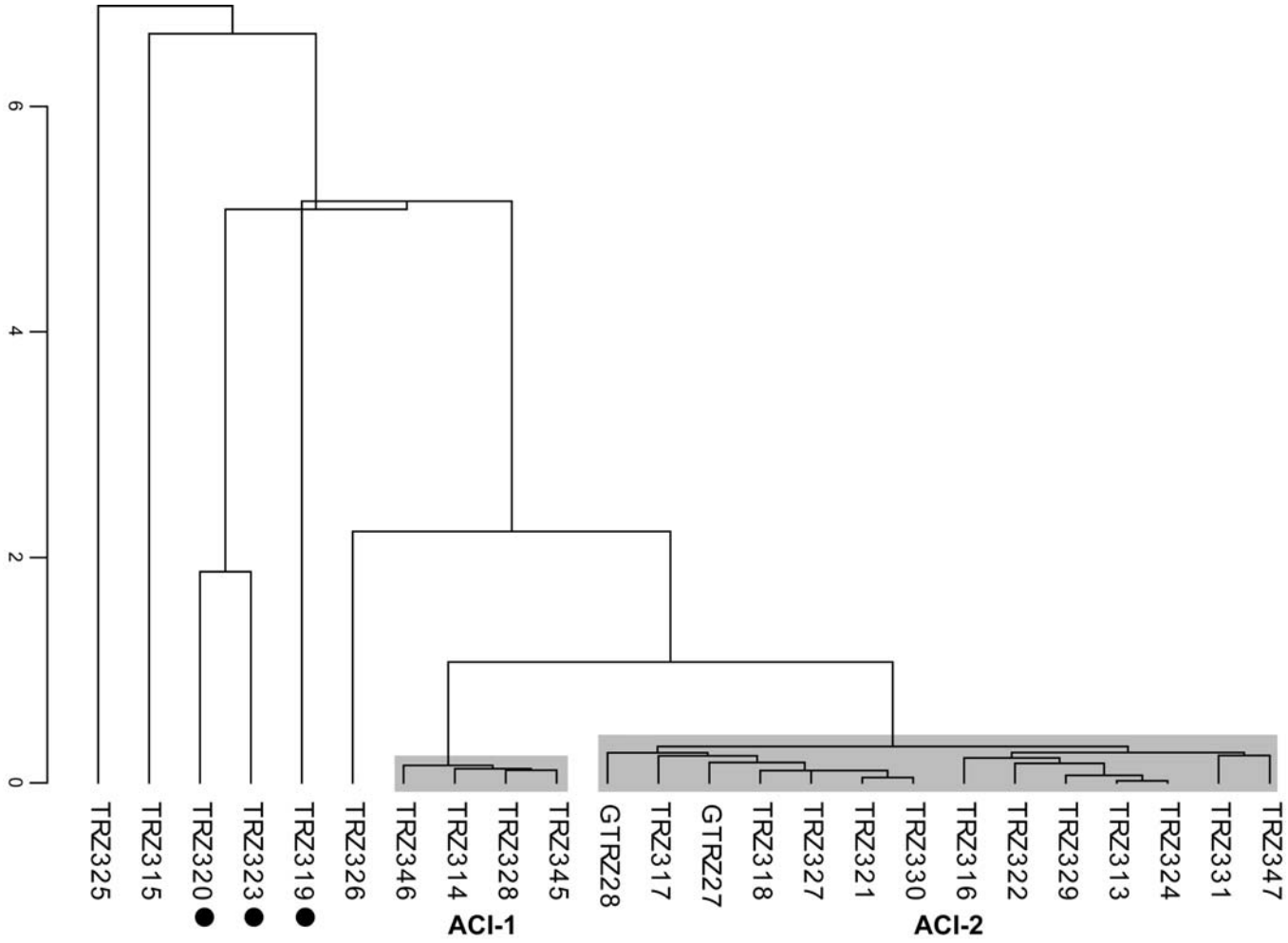

Figure 83: Dendrogram resulted from the cluster analysis performed on the subcomposition Al2O3, TiO2, MgO, CaO, SiO2, Ba, Nb, Zr, Y, Ce, Ga, V, Zn, Ni, Cr and Fe2O3 used as divisor, of 22 Islamic ceramics sampled at sector **AC2** (Termez), using the Square Euclidean distance and the centroid algorithm

The three cooking wares **TRZ319, TRZ320** and **TRZ323** (Figure 84) are low calcareous ceramics whereas the common wares are calcareous. At Table 12, where the chemical composition of these individuals is presented, important chemical differences, not only respect to the rest of the material, but also between them, can be observed. That leads to the conclusion that they are loners and that they are probably representing tree different cooking ware productions (Table 12).

According to this same table, the glazed wares **TRZ315, TRZ325** and **TRZ326** (Figure 83) are clearly very different to the analysed material from sector **AC2**. **TRZ315** is separated from the others due to really higher Fe_2O_3, MgO, CaO, Ni and Cr relative concentrations and lower Al_2O_3, Ba, Zr and Y contents. **TRZ325** and **TRZ326** are not only calcareous but also present significant differences in other chemical elements (Table 12). **TRZ325** that is common ware decorated with a green glaze differs mainly by its very high value in Cu, Ga and Y and the fairly low in Rb. These differences are significant to consider this specific individual of a probable foreign origin. The monochromatic white glazed ware **TRZ326**, on the other hand, presents a very calcareous paste with high Sr content. To these differences must be added the lower Al_2O_3, TiO_2, K_2O, Ce, V and Cr values wich indicates that this individual is clearly an chemical outlier (Table 12). Both represent by themselves different productions. Nevertheless, to be able to see if these productions are representative in the site, the expansion of the chemical study is needed and thin section analysis would be necessary for the identification of their probable origin.

Elements	ACI-1 (n=5)		ACI-2 (n=11)		TRZ315	TRZ319	TRZ320	TRZ323	TRZ325	TRZ326
	m	s	m	s	nc	nc	nc	nc	nc	nc
Fe_2O_3 (%)	6.20	0.25	6.21	0.44	7.46	6.76	4.43	3.39	6.33	4.97
Al_2O_3 (%)	15.78	0.38	15.67	0.88	13.02	18.17	18.69	20.80	16.11	12.82
TiO_2 (%)	0.70	0.02	0.68	0.04	0.71	0.84	0.66	0.90	0.69	0.59
MgO (%)	3.57	0.22	3.44	0.15	7.68	2.20	1.38	0.76	3.83	2.98
CaO (%)	10.57	0.88	11.21	1.93	20.41	1.68	3.52	2.72	10.71	19.94
Na_2O (%)	1.47	0.13	1.55	0.23	1.76	1.90	1.09	0.74	1.44	1.63
K_2O (%)	3.05	0.28	3.08	0.33	0.76	3.35	3.66	3.71	3.31	1.47
SiO_2 (%)	58.48	1.21	57.99	1.32	48.03	64.96	66.39	66.85	57.17	55.44
Ba (ppm)	486	16	550	40	215	375	609	300	397	380
Rb (ppm)	99	14	131	17	64	154	185	175	2	37
Th (ppm)	18	1	18	2	12	18	21	20	12	13
Nb (ppm)	18	1	18	1	18	17	20	21	18	17
Zr (ppm)	175	6	165	6	130	193	207	227	202	193
Y (ppm)	41	3	31	3	22	32	34	34	103	39
Sr (ppm)	381	38	391	76	392	186	227	212	367	466
Ce (ppm)	56	9	60	8	35	68	75	86	37	28
Ga (ppm)	60	11	25	5	21	22	23	24	290	63
V (ppm)	100	4	96	8	101	150	107	110	105	84
Zn (ppm)	112	6	104	12	101	105	51	24	148	93
Cu (ppm)	121	132	53	22	100	36	26	33	2263	94
Ni (ppm)	55	5	51	4	279	40	35	33	92	56

Table 12: The mean chemical composition (m) and the standard deviation (sd) using normalised data of **ACI-1** and **ACI-2** chemical groups and the raw normalised chemical composition (nc) of the ceramics outliers TRZ315, TRZ319, TRZ320, TRZ323, TRZ325 and TRZ326 from Ancient Military Quarters sector 2 (Termez).

The rest of the pottery (TRZ314, TRZ328, TRZ345 and TRZ346) is joined together in group **ACI-1** (Figure 83). Calculating the CVM of **ACI-1** on the above last mentioned subcomposition, vt = 0.0565, that indicates that this specific group represent one single production, that in this case it can be considered one of the PCRU's of the glazed and decorated Islamic common wares of the site. The typology of this group is represented in Figure 86.

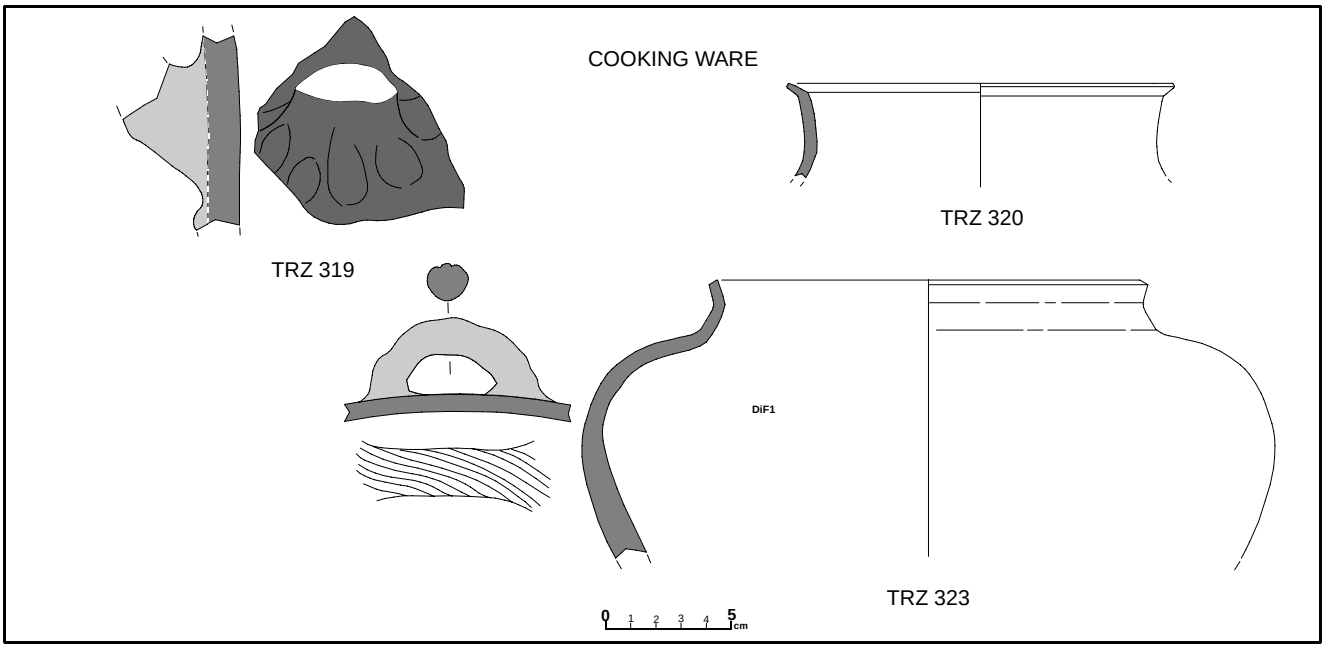

Figure 84: Typology of the outliers cooking wares TRZ319, TRZ320 and TRZ323 from **AC2** (Termez)

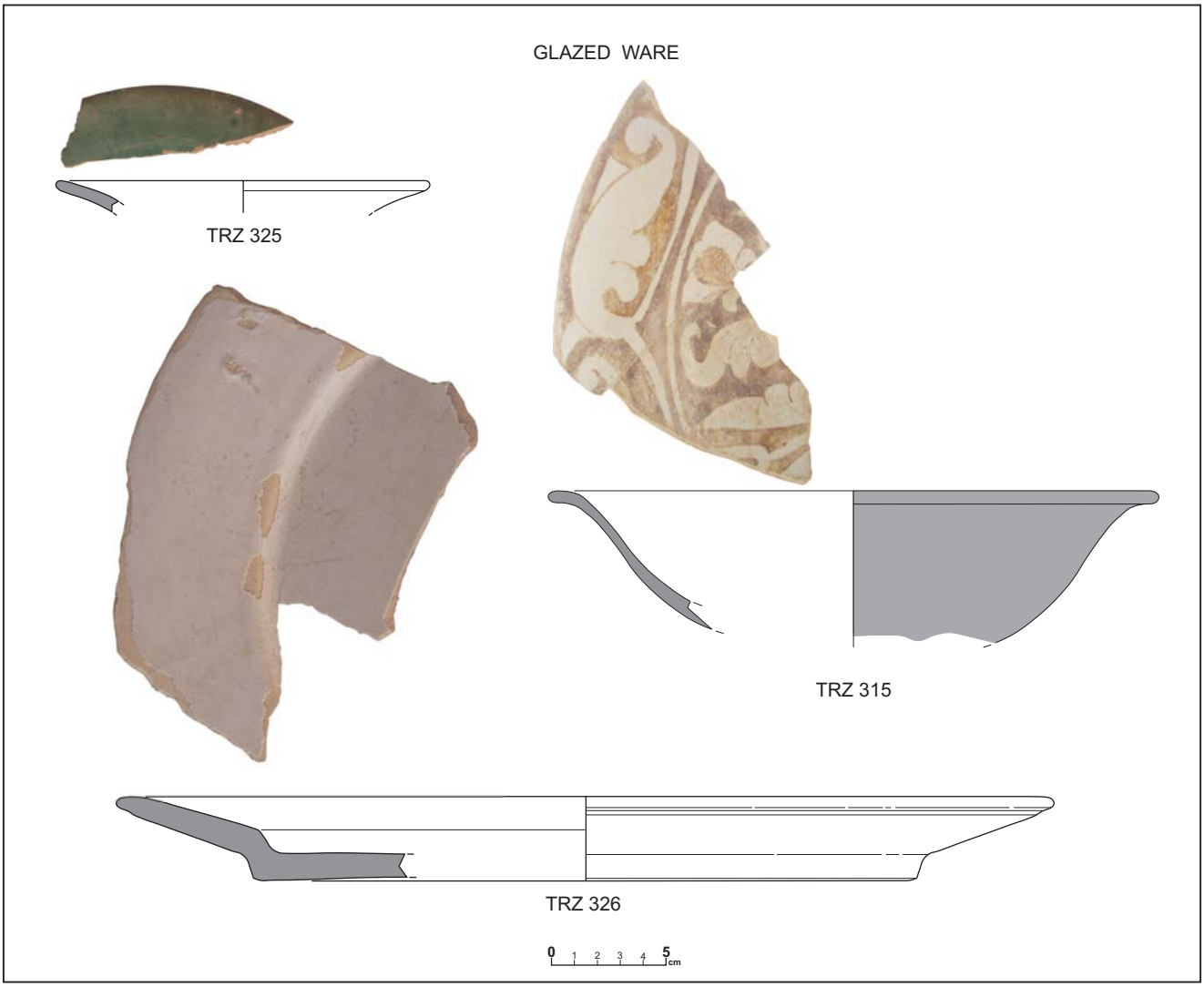

Figure 85: Typology of the outliers glazed wares TRZ315, TRZ325 and TRZ326 from **AC2** (Termez)

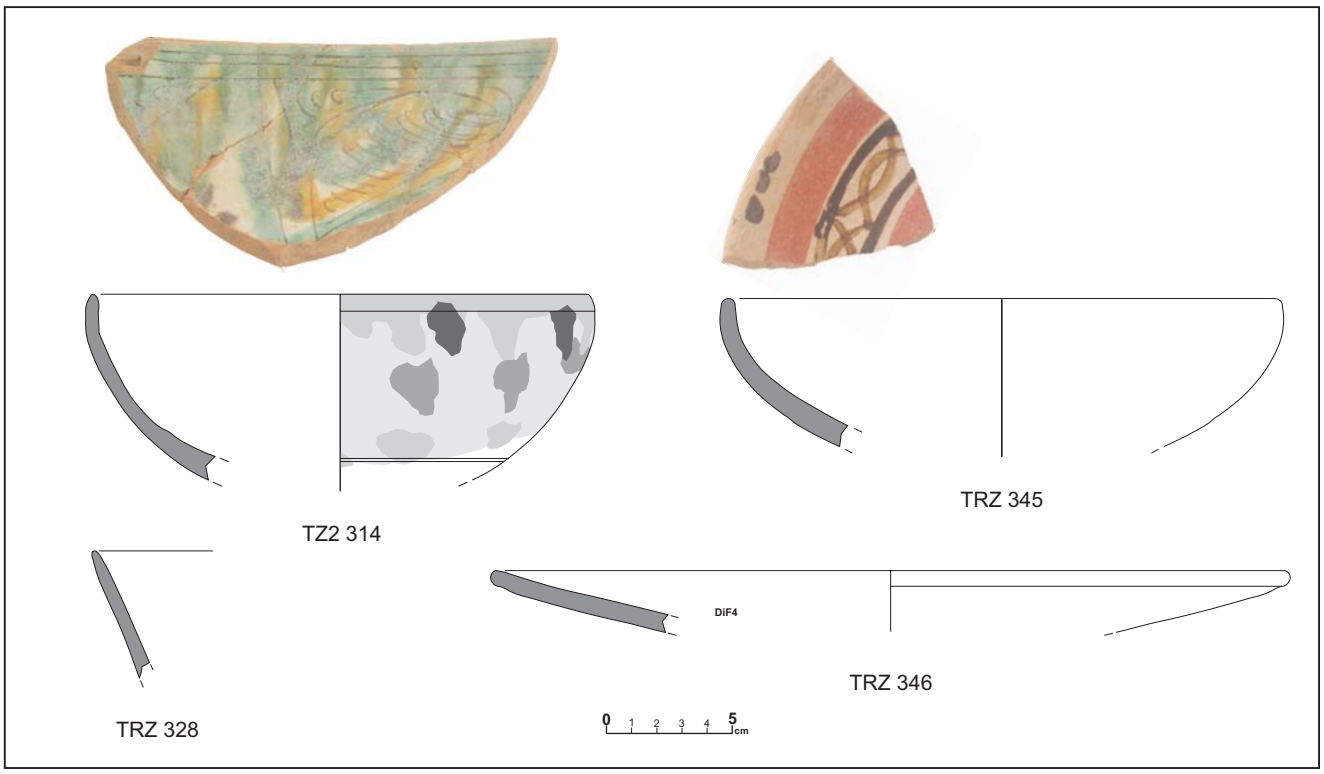

Figure 86: Typology of the **ACI-1** group (TRZ314, TRZ328, TRZ345 and TRZ346)

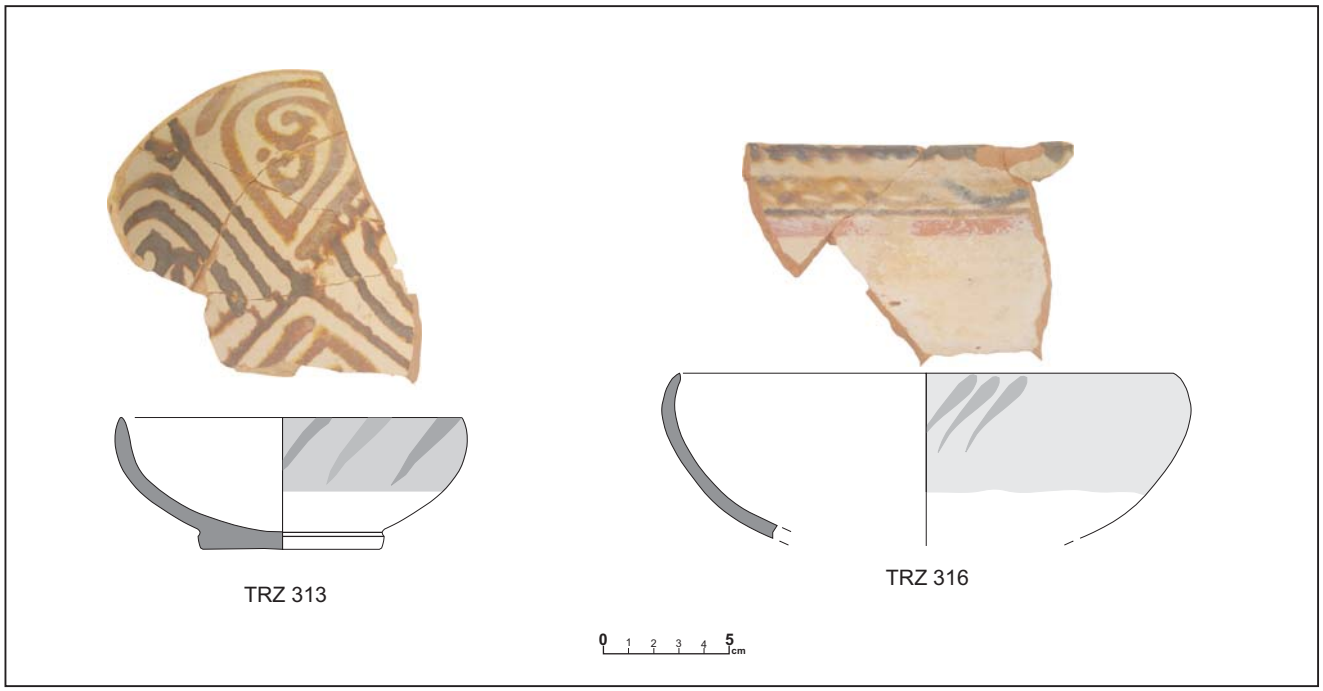

Figure 87: Typology of the **ACI-2** group
(TRZ313, TRZ316, TRZ317, TRZ318, TRZ321, TRZ322, TRZ324, TRZ327, TRZ329, TRZ330, TRZ31, TRZ347)

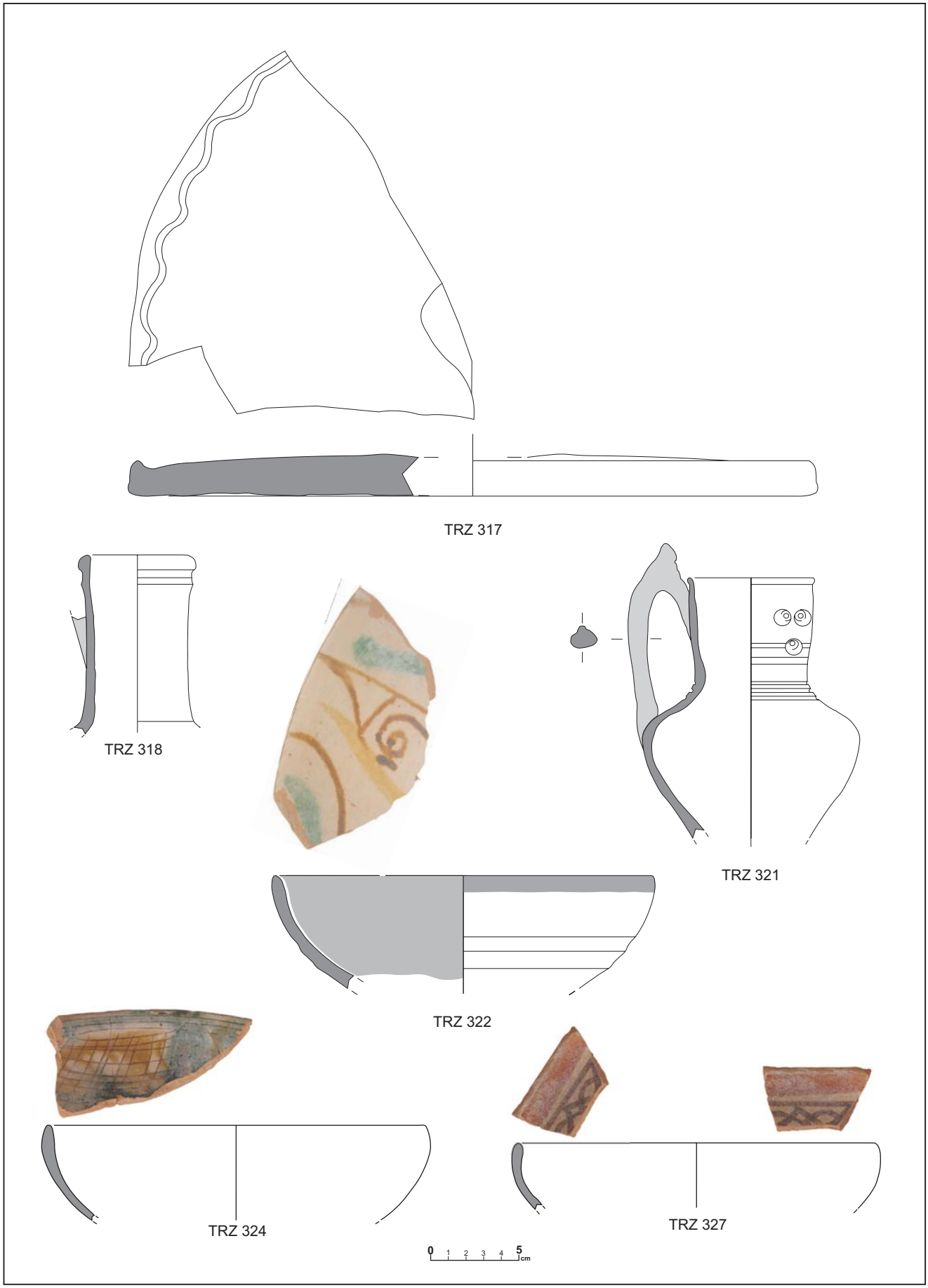

Figure 87: Typology of the **ACI-2** group
(TRZ313, TRZ316, TRZ317, TRZ318, TRZ321, TRZ322, TRZ324, TRZ327, TRZ329, TRZ330, TRZ31, TRZ347)

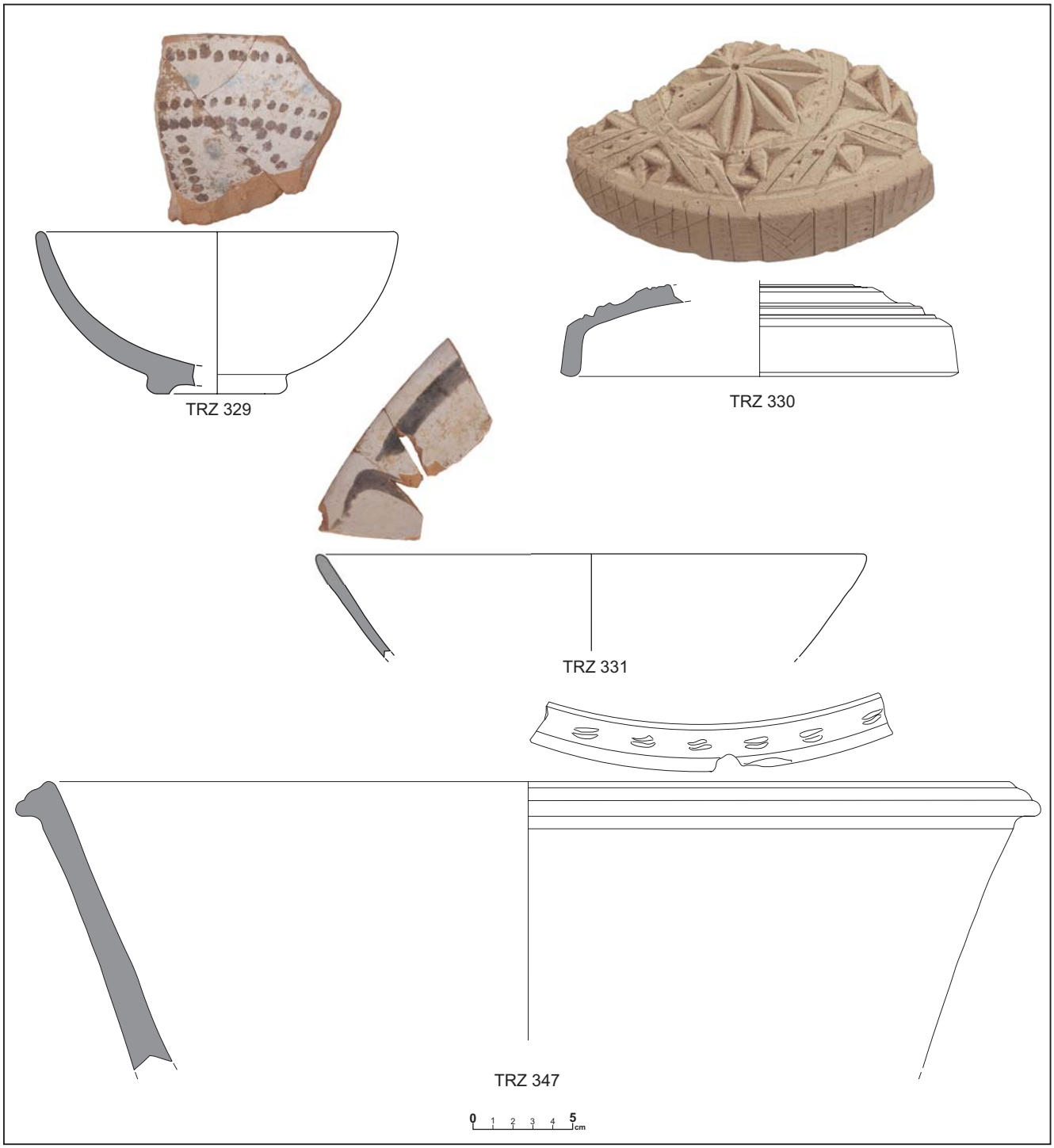

Figure 87: Typology of the **ACI-2** group
(TRZ313, TRZ316, TRZ317, TRZ318, TRZ321, TRZ322, TRZ324, TRZ327, TRZ329, TRZ330, TRZ31, TRZ347)

ACI-2 in Figure 87 contains 12 common wares (TRZ313, TRZ316, TRZ317, TRZ318, TRZ321, TRZ322, TRZ324, TRZ327, TRZ329, TRZ330, TRZ31, TRZ347) and the two analysed clay sediments. The vt obtained for this group calculating the CVM is 0.3072, wich is low enough to consider **ACI-2** chemically monogenetic (Figure 87) and the second PCRU for the Islamic pottery of the site. At Table 12 the main chemical composition and the standard deviation of this group is presented, as well. By comparing the mean composition of both groups, the main variations are given by Ba, Rb, Zr, Y, Ga and Cu. Typologically the pottery classified into **ACI-2** corresponds to glazed bowls and unpainted fine wares (predominantly jars and storage jars). The fact that the two clay samples are belonging to these groups means a similar or common geologic origin for these clays and the pottery classified as this group. As

the clays are local, in fact they were sampled at the same area where the analysed pottery was recovered, a possible local origin for this production is valid. Nevertheless this hypothesis will be attested in the future by petrography.

According to the chemical results, the existence of several ceramic productions for the Islamic Period at **Termez** is possible. Two of these pottery productions have been identified in this work **ACI-1** and **ACI-2**. However, we can not precise yet the specific provenance of these vessels. Althoug some pottery kilns have been recovered in the broader area of Ancient Termez, non ceramics from these kilns have been yet characterized. Because of that, we can not stil relate ceramics from **AC-2** to this pottery workshops.

8.2. Mineralogical composition (XRD analysis)

The low calcareous Islamic cooking wares considered as chemical outliers were fired at two different temperatures according to their diffractograms (Figure 88). In the case of **TRZ320** and **TRZ323**, only primary phases have been identified (quartz, illite-muscovite, k-feldspar, plagioclase and hematite), which indicates a low EFT around 800-850ºC. Nevertheless, the EFT of cooking ware **TRZ319** is higher than 1000ºC because illite-muscovite have totally disappeared at the same time that advanced crystallisation of spinel can be distinguished at the diffractogram as clear firing phase. Finally, the pronounced peaks of hematite indicate that it corresponds to a firing phase in this specific case.

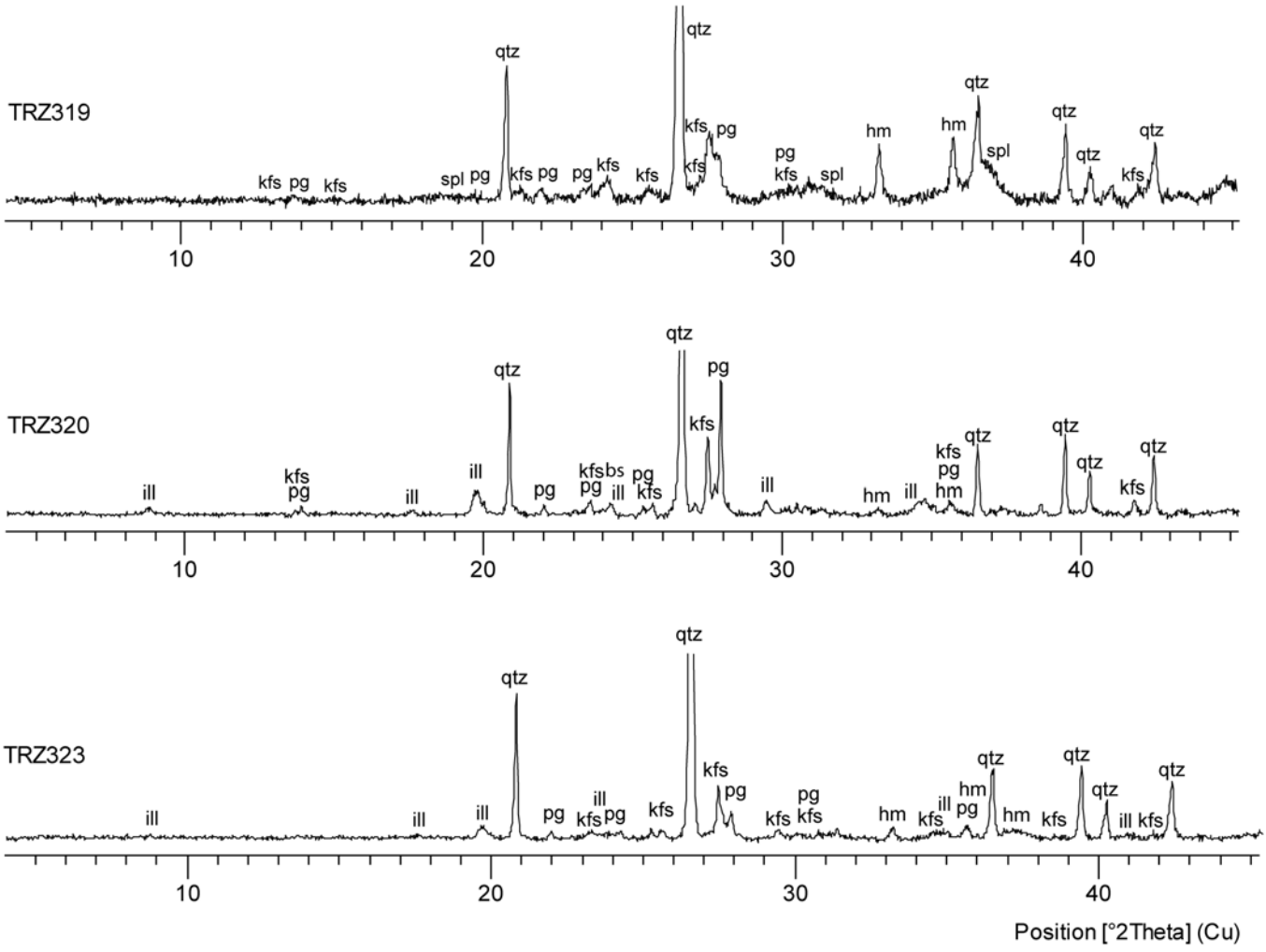

Figure 88: Diffractograms of the Islamic cooking wares TRZ319, TRZ320 and TRZ323 from **AC2**; hm: hematite, ill: illite-muscovite, kfs: k-feldspar, pg: plagioclase, px: pyroxene, qtz: quartz, spl: spinel

Diffractograms of three glazed common wares which appear isolated at dendrogram of Figure 83 (TRZ315, TRZ325 and TRZ326) show several differences with respect the whole set of ceramics analysed in this work from different periods. As deduced by XRF analyses, these mineralogical differences serve to confirm a suspected foreign origin for these glazed Islamic ceramics (Figure 89). The high calcareous **TRZ315** shard was fired at fairly high temperature according to the total decomposition of the illite-muscovites and the develop state of the pyroxenes. Thus, the estimated EFT for this glazed plate is higher than 1000ºC. The monochrome green glazed plate **TRZ325** was also well fired (EFT around 900-950ºC) as it is confirmed by the simultaneous presence of rare primary phases (illite-muscovite) together with well-developed firing phases (pyroxenes). Finally, according to the diffractogram of **TRZ326**, that corresponds to a calcareous monochrome white glazed plate, the total decomposition of illite-muscovite and the advanced crystallisation of firing phases (gehlenite and pyroxene) indicate high firing temperature (approximately 1000ºC).

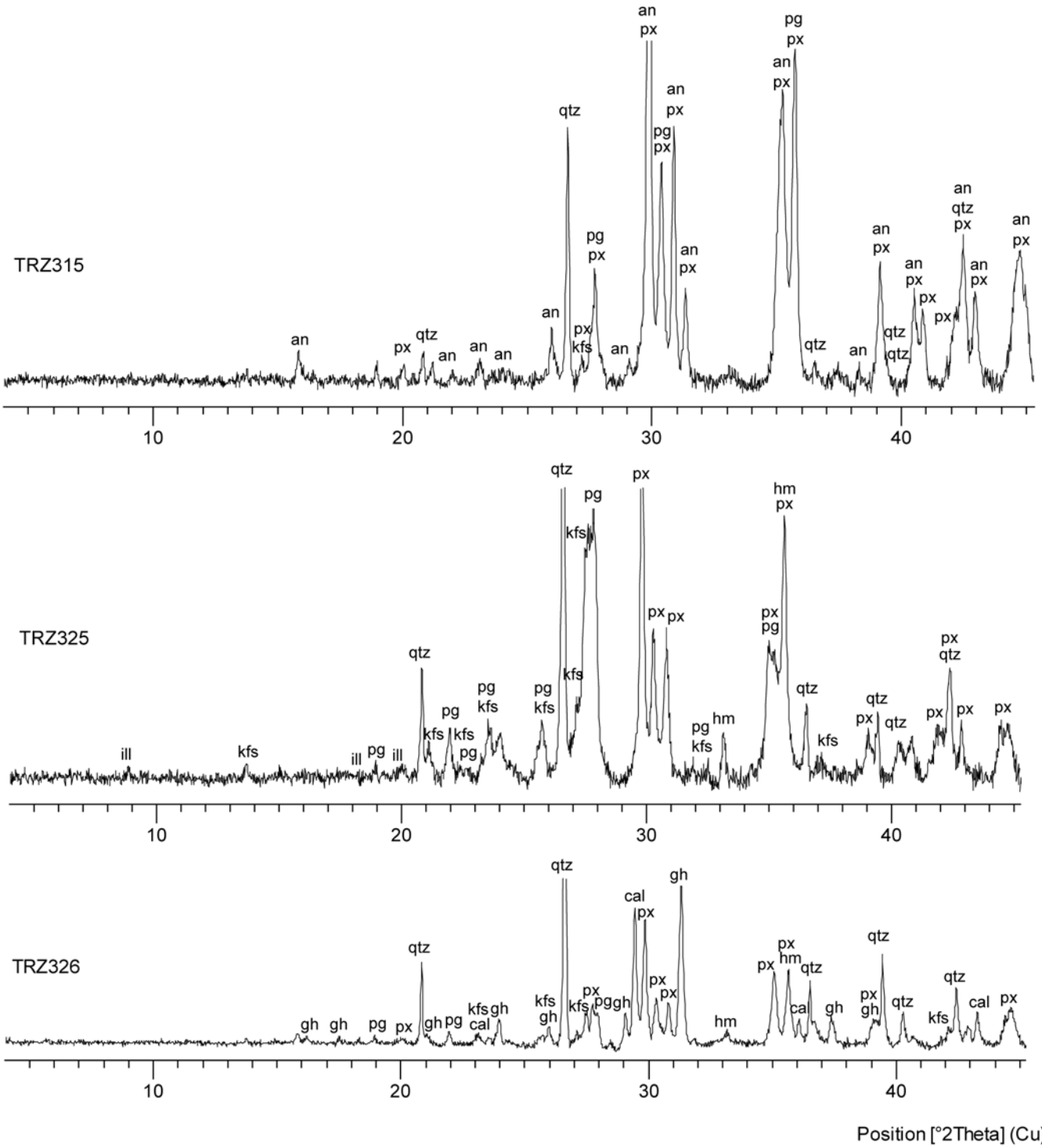

Figure 89: Diffractograms of the Islamic common wares TRZ315, TRZ325 and TRZ326 from **AC2**; an: anorthoclase; cal: calcite, gh: gehlenite, hm: hematite, ill: illite-muscovite, kfs: k-feldspar, pg: plagioclase, px: pyroxene, qtz: quartz

Four glazed common wares from **ACI-1** PCRU (TRZ314, TRZ328, TRZ345 and TRZ346) seem to be well fired with estimated ETC around 900-950ºC (Figure 90), due to the reduced presence primary phases (quartz, illite-muscovite, k-feldspar, plagioclase and possibly hematite) and the clear presence of firing phases (pyroxene and gehlenite) in its XRD spectra.

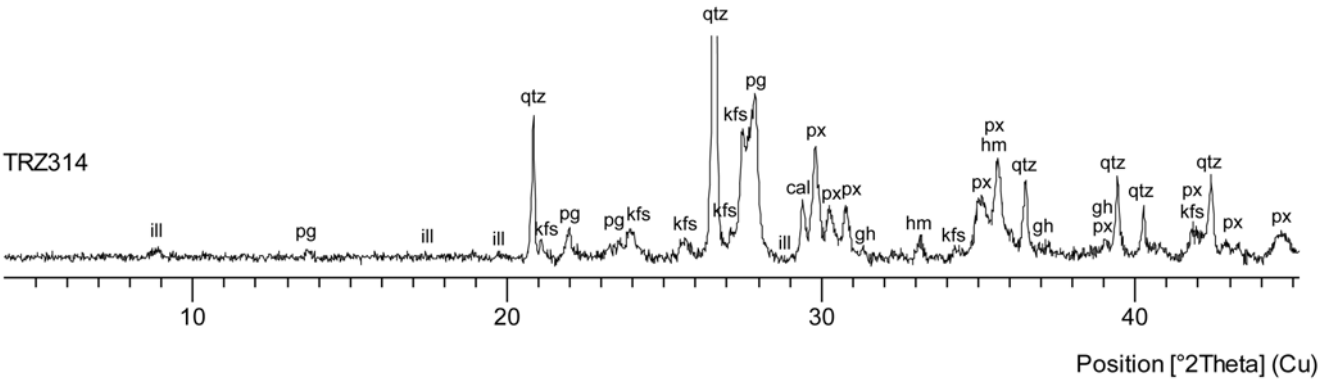

Figure 90: Diffractogram of the Islamic common ware TRZ314 from **ACI-1**; cal: calcite, gh: gehlenite, hm: hematite, ill: illite-muscovite, kfs: k-feldspar, pg: plagioclase, px: pyroxene, qtz: quartz

Finally, twelve glazed common wares from **ACI-2** chemical group can be divided in two different mineralogical categories, associated to two different (EFT's). On the one hand, vessels TRZ313, TRZ316, TRZ322, TRZ324, TRZ327, TRZ329, TRZ331 and TRZ347 show the simultaneous presence of primary phases (quartz, illite-muscovite, calcite, k-feldspar, plagioclase and possibly hematite) and firing phases (pyroxene and gehlenite). The EFT for all these shards must be estimated around 900-950ºC. Though, in the diffractograms of TRZ317, TRZ318, TRZ321 and TRZ330, the total decomposition of illite-muscovite and the advanced decomposition of calcite together with the increment of pyroxenes and gehlenite points to a EFT higher than 1000ºC (Figure 91). In the case of TRZ318, the presence of analcime as secondary phase is also observed.

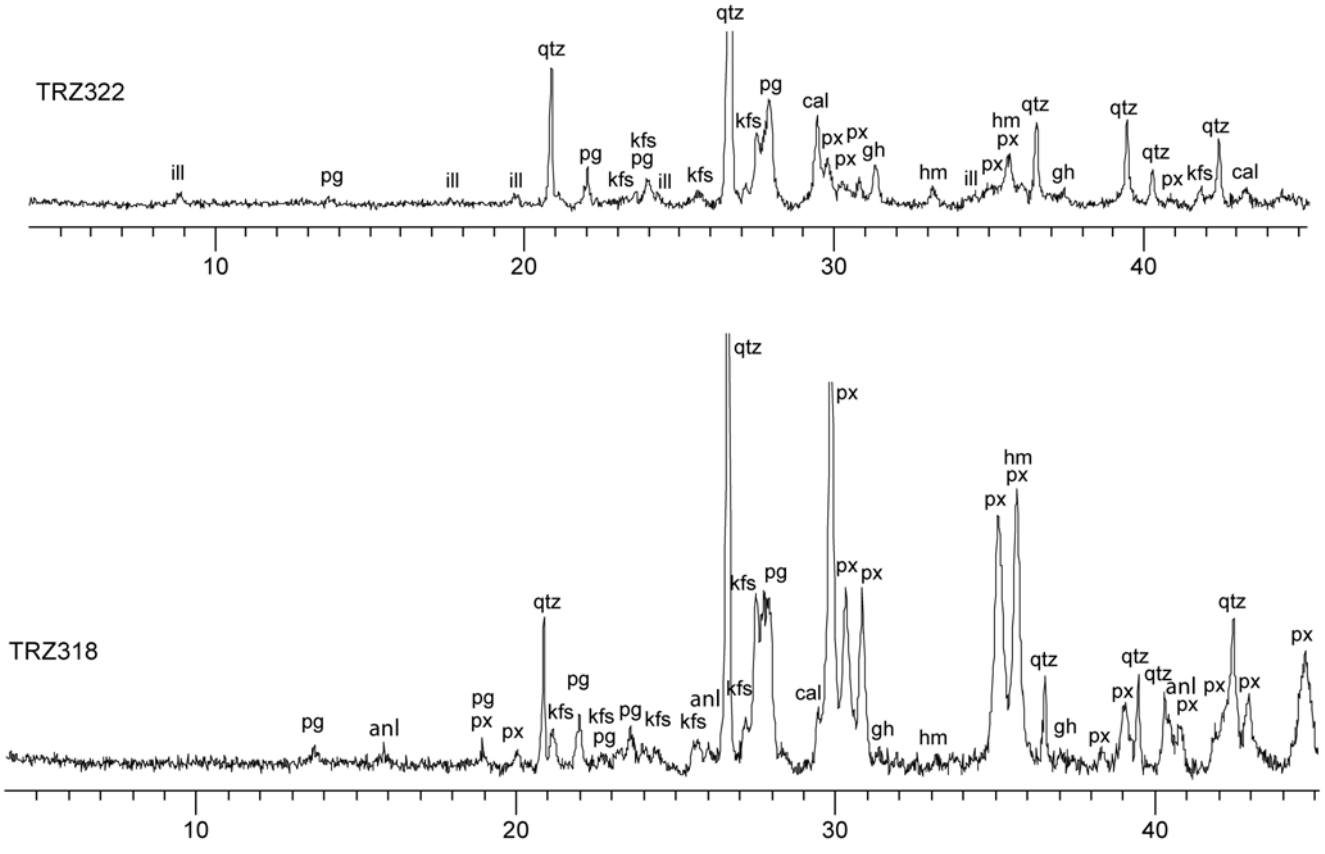

Figure 91: Diffractograms of the Islamic common wares TRZ322 and TRZ318 from **ACI-1**; anl: analcime, cal: calcite, gh: gehlenite, hm: hematite, ill: illite-muscovite, kfs: k-feldspar, pg: plagioclase, px: pyroxene, qtz: quartz

9. Conclusions

Regarding to the pottery dated to the Hellensitic and Fist Kushan Period, the identification of productions that are fairly different from the rest of the analysed material and clearly associated to **Kampyr Tepe,** indicates the unique character of this pottery. Typologically, the pottery classified into these specific groups represents the eldest forms within the analysed shards (**KT-1**, **KT-4** and **KT-6**). Other analysed individuals from **Kampyr Tepe (KT-2 and KT-3)**, however, are associated to groups formed by the individuals recovered at the sector 2 of the Antique Military Quarters (**AC2**), while the pottery sampled at **AC1** (sector 1 Antique Quarters) forms its own chemical group. The archaeometrical differences, though, in this case, seems to correspond to chronological differences. That is because the context analysed from **AC1** is dated to the Fist Kushan period, while all the other groups of **Kampyr Tepe** and the group of **AC2** formed by pottery that, according to all the typological study developed up to now represent Pre-kushan forms (lot of these typologies are identical to the ones recovered at the Graeco-Bactrian Ciutadelle of **Termez**, and have been typologically systemised by Shakir Pidaev (1991). Therefore, all indicates that the archaeometrical configuration of the groups or productions can not be only result other than of randomness, it seems to represent also the historical reality.

As for the Kushan-Sassanian pottery of **Termez,** specifically the one of **Tchinguiz Tepe**, the existence of clearly differentiated production is obvious by the archaeometrical results. On the one hand, there is a main group (Reference Group **TTG**) that clusters together all the common wares with a chronology defined between the end of 1st century and the late 4th century. This group is chemically homogenous and even though it associates typologically diversified pottery, all of them can be attributed to the same historical context. The *in situ* existence of pottery kilns and the fact that the over fired discards are also classified within this group, permits think about one single attribution for this group or RG. The other analysed shards from **Tchinguiz Tepe** forms clearly dedifferentiated small clusters or even singletons with one common characteristic, all of them are cooking wares. Most of these cooking wares can be dated between the 3d and 4th century, although some of them can be latest (e.g. the PCRU: **TTB**).

Regarding to the pottery analysed from **Zar Tepe** that is only a small selection of samples taken from the site, all of which dated to the Kushan-Sassanian period, the archaeometrical study permitted to compare them to the previously described pottery of **Tchinguiz Tepe,** dated at the same period. The results point towards important differences between the two sites. Practically, none of the analysed shards of **Zar Tepe** is associated to any of the groups or chemical outliers identified for **Tchinguiz Tepe**. The results lead to the plausible hypothesis that each one of the sites represent different cultural horizon (the archaeological prove of that is that the typologies defined for the two sites are similar but not identical) within a generally common historical context where the existence of various production sites is evident and the pottery follows different trade routes.

Finally, concerning the medieval pottery, the lack of archaeological and archaeometrical data prevents any firm conclusion on the ceramic production during this period. However, **Tchurobkurgan** is a clear example of the existence of possible local ceramic productions. For the ceramics from the Islamic period, we find the same limitations at the moment. Nevertheless, we infer the existence of local productions of glazed and unglazed common wares and a wide commercial distribution of glazed ceramics from foreign areas.

Bibliography

Aitchison, J., 1986, *The Statistical Analysis of Compositional Data*, Chapman and Hall, London.

Ariño, E., Sala, R., Lafuente, M., Gurt i Esparraguera, J.M., Pidaev, S., Stride, S., 2007, The Ceramic Kilns of Kara Tepe, in J.M. Gurt, S. Pidaev, A.M. Rauret and S. Stride (eds.), *IPAEB: Preliminary Report of the work of the International Pluridisciplinary Archaeological Expedition to Bactria*, vol. 1, pp. 13-44.

Ariño, e., 2009, Archaeological record: Sector RC (*Tchinguiz Tepe*), en Verònica Martínez, S. Pidaev, A.M. Rauret and S. Stride (eds.), *IPAEB 2008, Preliminary Report of the work of the International Pluridisciplinary Archaeological Expedition to Bactria*, vol. 3, pp. 7-109.

Buxeda i Garrigós, J., 1999, Alteration and Contamination of Archaeological Ceramics: The perturbation problem, *Journal of Archaeological Science*, 26, pp. 295-313.

Buxeda i Garrigós, J., Cau Ontiveros, M.A., 1995, Identificación y significado de la calcita secundaria en cerámicas arqueológicas, *Complutum*, 6, pp. 293-309.

Buxeda i Garrigós, J., Kilikoglou, V., Day, P., M., 2001, Chemical and mineralogical alteration of ceramics from Late Bronze age kiln at Kommos, Crete: the effect on the formation of a Reference Group, *Archaeometry,* 43, pp. 349-371.

Buxeda i Garrigós, J., Mommsen, H., Tsolakidou, A., 2002, Alterations of Na, K and Rb concentrations in Mycenaean pottery and a proposed explanation using X-ray diffraction, *Archaeometry*, 44, pp. 187-198.

Buxeda i Garrigós, J., Kilikoglou, V., 2003, Total Variation as a Measure of Variability in Chemical Data Sets, in L. van Zelts (ed.), *Patterns and Process: a Festschrift in honour of Dr. Edward V. Sayre*, Smithsonian Center for Materials Research and Education, Suitland, Maryland, pp. 185-198.

Cau Ontiveros, M.A., Day, P.M., Montana, G., 2002, Secondary calcite in archaeological ceramics: evaluation of alteration and contamination processes by thin section study, in *Modern trends in scientific studies on ancient ceramics*, V. Kilikoglou, A. Hein, Y. Maniatis (eds.), BAR International Series 1011, pp. 9-18, Archaeopress, Oxford.

Gurt Esparraguera, J.M., 2009, Archaeological record: Sector AC, military camp (former barracks), in J.M. Gurt, S. Pidaev, A.M. Rauret and S. Stride (eds.), *IPAEB 2008, Preliminary Report of the work of the International Pluridisciplinary Archaeological Expedition to Bactria*, vol. 3, pp. 187- 217.

Gurt, J.M., Pidaev, S., Rauret, A.M., Stride, S., 2007, *Preliminary Report of the work of the International Pluridisciplinary Archaeological Expedition to Bactria*, IPAEB 2006, vol. 1, Barcelona.

Gurt, J.M., Pidaev, S., Rauret, A.M., Stride, S., 2008, *Preliminary Report of the work of the International Pluridisciplinary Archaeological Expedition to Bactria*, IPAEB 2007, vol. 2, Barcelona.

Gurt, J.M., Pidaev, S., Rauret, A.M., Stride, S., 2009, *Preliminary Report of the work of the International Pluridisciplinary Archaeological Expedition to Bactria*, IPAEB 2008, vol. 3, Barcelona.

Hein, A., Tsolajidou,a., Iliopoulos, I., Monnsen, H., Buxeda i Garrigós, J., Montana G, Kilikoglou, V., 2002, Standardisation of elemental analytical techniques applied to provenance studies of archaeolgoical ceramics an inter laboratory calibration study, *Analyst*, 127, pp. 542-553

Leriche, P., 2007, Bactria, Land of a Thousand Cities, in *After Alexander Central Asia before Islam*, Proceedings of the British Academy, 133, pp. 121-153

Leriche, P., Pidaev, Sh., 2007, Termez in Antiquity, in *After Alexander Central Asia before Islam*, Proceedings of the British Academy, 133, pp. 179-211.

Leriche, P., Pidaev, Sh., 2008, *Termez sur Oxus. Cité-capitale d'Asie Centrale*, ed. Maisonneuve & Larose, París.

MARTÍNEZ, V., 2009, Archaeological record: Sector RF (*Tchinguiz Tepe*), in J.M. Gurt, S. Pidaev, A.M. Rauret and S. Stride (eds.), *IPAEB 2008 Preliminary Report of the work of the International Pluridisciplinary Archaeological Expedition to Bactria*, vol. 3, pp. 111- 186.

MARTÍNEZ, V., TSANTINI, E., GURT, J.M., PIDAEV, S, 2008, Archaeometrical study of the ceramics coming from the archaeological site of Termez in Uzbekistan, in J.M. Gurt, S. Pidaev, A.M. Rauret and S. Stride (eds.), *IPAEB 2007, Preliminary Report of the work of the International Pluridisciplinary Archaeological Expedition to Bactria*, vol. 2, pp. 141-194.

MARTÍNEZ, V., TSANTINI, E., GURT, J.M., PIDAEV, S., 2009, Provenience and Technological study of the ceramics coming from the archaeological sites of Termez, Kampyr Tepe and Zar Tepe in Uzbekistan, in J.M. Gurt, S. Pidaev, A.M. Rauret and S. Stride (eds.), *IPAEB 2008, Preliminary Report of the work of the International Pluridisciplinary Archaeological Expedition to Bactria*, vol. 3, pp. 231-348.

MATHSOFT 1999, *S-PLUS 2000. User's Guide*, Data Analysis Products Division, MathSoft, Seatle, Washington, USA.

PIDAEV, SH. R., 1991, *The pottery of greco-bactrian period from Stary Termez fortified settlement,* pp. 210-224, Moscow.

SÁNCHEZ DEL CORRAL, A., 2009, Geomorphology of Tchinguiz Tepe and the valley of the Surkhan Darya (Uzbekistan), in J.M. Gurt, S. Pidaev, A.M. Rauret and S. Stride (eds.), *IPAEB: Preliminary Report of the work of the International Pluridisciplinary Archaeological Expedition to Bactria*, vol. 3, pp. 359-385.

SCHWEDT, A., MOMMSEN, H., ZACHARIAS, N., BUXEDA I GARRIGÓS, J., 2006, Analcime crystallization and compositional profiles-comparing approaches to detect post-depositional alterations in archaeological pottery, *Archaeometry*, 48, 2, pp. 237-251.

STRIDE, S., 2005, *Géographie archéologique de la province du Surcan Darya* (Ouzbékistan du sud/Bactriane du nord). Tesis Doctoral, Sorbonne, Paris.

TSANTINI, E., MARTÍNEZ, V., GURT I ESPARRAGUERA, J. M., 2007, Results of all the available archaeological and archaeometrical information on the excavation of Kara Tepe, in J.M. Gurt, S. Pidaev, A.M. Rauret and S. Stride (eds.), *IPAEB 2006, Preliminary Report of the work of the International Pluridisciplinary Archaeological Expedition to Bactria*, *v*ol. 1, pp. 67-90.

WHITBREAD, I.K., 2001, Ceramic petrology, clay geochemistry and ceramic production—from technology to the mind of the potter, in *Handbook of archaeological sciences* D. R. Brothwell and A. M. Pollard (eds.), pp. 449–59, John Wiley, Chichester.

WHITBREAD, I.K., JONES, R.E., PAPADOPOULOS, J. K., 1997, The Early Iron Age kiln at Torone, Greece: geological diversity and definition of control groups, in A. Sinclair, E. Slater and J. Gowlett (eds.), *Archaeological sciences 1995: proceedings of a conference on the application of scientific techniques to the study of archaeology*, pp. 88–91, Oxbow Monograph, 64, Oxbow, Oxford.

Index of figures of the analysed ceramics

TRZ051	Figure 43	TRZ166	Figure 43	TRZ225	Figure 19d
TRZ052	Figure 43	TRZ167	Figure 43	TRZ226	Figure 19d
TRZ053	Figure 43	TRZ168	Figure 43	TRZ227	Figure 19d
TRZ054	Figure 43	TRZ169	Figure 43	TRZ228	Figure 19b
TRZ055	Figure 43	TRZ170	Figure 36	TRZ229	Figure 18
TRZ056	Figure 43	TRZ171	Figure 39	TRZ230	Figure 19b
TRZ057	Figure 43	1TRZ72	Figure 38	TRZ231	Figure 19d
TRZ058	Figure 43	TRZ173	Figure 43	TRZ232	Figure 19b
TRZ059	Figure 43	TRZ174	Figure 43	TRZ233	Figure 19c
TRZ060	Figure 43	TRZ175	Figure 43	TRZ234	Figure 19d
TRZ062	Figure 43	TRZ176	Figure 43	TRZ235	Figure 18
TRZ063	Figure 41	TRZ178	Figure 43	TRZ236	Figure 19d
TRZ064	Figure 43	TRZ179	Figure 43	TRZ237	Figure 19f
TRZ065	Figure 43	TRZ180	Figure 43	TRZ238	Figure 19d
TRZ066	Figure 43	TRZ181	Figure 43	TRZ239	Figure 19c
TRZ067	Figure 43	TRZ182	Figure 38	TRZ240	Figure 19d
TRZ068	Figure 43	TRZ183	Figure 43	TRZ241	Figure 19d
TRZ069	Figure 43	TRZ184	Figure 43	TRZ242	Figure 19d
TRZ070	Figure 43	TRZ185	Figure 43	TRZ243	Figure 64C
TRZ071	Figure 43	TRZ186	Figure 43	TRZ244	Figure 64B
TRZ072	Figure 43	TRZ187	Figure 38	TRZ245	Figure 64E
TRZ073	Figure 43	TRZ188	Figure 43	TRZ246	Figure 64D
TRZ074	Figure 43	TRZ189	Figure 37	TRZ247	Figure 64A
TRZ075	Figure 43	TRZ190	Figure 43	TRZ248	Figure 64C
TRZ076	Figure 43	TRZ191	Figure 43	TRZ249	Figure 64C
TRZ077	Figure 41	TRZ192	Figure 43	TRZ250	Figure 64D
TRZ078	Figure 43	TRZ193	Figure 43	TRZ251	Figure 64B
TRZ079	Figure 43	TRZ194	Figure 43	TRZ252	Figure 63
TRZ080	Figure 43	TRZ195	Figure 43	TRZ253	Figure 64A
TRZ081	Figure 43	TRZ196	Figure 43	TRZ254	Figure 64C
TRZ082	Figure 43	TRZ197	Figure 43	TRZ255	Figure 65
TRZ083	Figure 43	TRZ198	Figure 43	TRZ256	Figure 64A
TRZ084	Figure 40	TRZ199	Figure 43	TRZ257	Figure 64A
TRZ085	Figure 43	TRZ200	Figure 43	TRZ258	Figure 64F
TRZ086	Figure 43	TRZ201	Figure 43	TRZ259	Figure 64F
TRZ087	Figure 43	TRZ202	Figure 43	TRZ260	Figure 64F
TRZ088	Figure 42	TRZ203	Figure 19b	TRZ261	Figure 64A
TRZ145	Figure 6b	TRZ204	Figure 19a	TRZ262	Figure 63
TRZ146	Figure 6b	TRZ205	Figure 19d	TRZ263	Figure 64A
TRZ147	Figure 6a	TRZ206	Figure 19c	TRZ264	Figure 64A
TRZ148	Figure 6a	TRZ207	Figure 19d	TRZ265	Figure 66
TRZ149	Figure 6a	TRZ208	Figure 19b	TRZ266	Figure 66
TRZ150	Figure 6a	TRZ209	Figure 19b	TRZ267	Figure 64D
TRZ151	Figure 6b	TRZ210	Figure 19b	TRZ268	Figure 64B
TRZ152	Figure 5	TRZ211	Figure 19b	TRZ269	Figure 64C
TRZ153	Figure 6b	TRZ212	Figure 19b	TRZ270	Figure 64F
TRZ154	Figure 6b	TRZ213	Figure 19b	TRZ271	Figure 63
TRZ155	Figure 6b	TRZ214	Figure 19b	TRZ272	Figure 62
TRZ156	Figure 5	TRZ215	Figure 19b	TRZ273	Figure 65
TRZ157	Figure 43	TRZ216	Figure 19g	TRZ274	Figure 64A
TRZ158	Figure 43	TRZ217	Figure 19d	TRZ275	Figure 62
TRZ159	Figure 43	TRZ218	Figure 19f	TRZ276	Figure 64E
TRZ160	Figure 43	TRZ219	Figure 19f	TRZ277	Figure 65
TRZ161	Figure 37	TRZ220	Figure 19d	TRZ278	Figure 65
TRZ162	Figure 39	TRZ221	Figure 19d	TRZ279	Figure 62
TRZ163	Figure 36	TRZ222	Figure 19b	TRZ280	Figure 64D
TRZ164	Figure 43	TRZ223	Figure 19d	TRZ281	Figure 64D
TRZ165	Figure 43	TRZ224	Figure 19d	TRZ282	Figure 62

TRZ283	Figure 64C
TRZ284	Figure 64F
TRZ285	Figure 66
TRZ286	Figure 65
TRZ287	Figure 64C
TRZ288	Figure 66
TRZ289	Figure 64A
TRZ290	Figure 64C
TRZ291	Figure 43
TRZ292	Figure 43
TRZ293	Figure 36
TRZ294	Figure 36
TRZ295	Figure 36
TRZ296	Figure 43
TRZ297	Figure 43
TRZ298	Figure 43
TRZ299	Figure 43
TRZ300	Figure 43
TRZ301	Figure 43
TRZ302	Figure 43
TRZ303	Figure 43
TRZ304	Figure 43
TRZ305	Figure 40
TRZ306	Figure 43
TRZ307	Figure 43
TRZ309	Figure 36
TRZ310	Figure 43
TRZ311	Figure 42
TRZ312	Figure 43
TRZ313	Figure 87
TRZ314	Figure 86
TRZ315	Figure 85
TRZ316	Figure 87
TRZ317	Figure 87
TRZ318	Figure 87
TRZ319	Figure 84
TRZ320	Figure 84
TRZ321	Figure 87
TRZ322	Figure 87
TRZ323	Figure 84
TRZ324	Figure 87
TRZ325	Figure 85
TRZ326	Figure 85
TRZ327	Figure 87
TRZ328	Figure 86
TRZ329	Figure 87
TRZ330	Figure 87
TRZ331	Figure 87
TRZ332	Figure 7c
TRZ333	Figure 7c
TRZ334	Figure 7c
TRZ335	Figure 7d
TRZ336	Figure 7c
TRZ337	Figure 7c
TRZ338	Figure 7c
TRZ339	Figure 5
TRZ340	Figure 7a
TRZ341	Figure 7c
TRZ342	Figure 7c
TRZ343	Figure 7d
TRZ344	Figure 7c
TRZ345	Figure 86
TRZ346	Figure 86
TRZ347	Figure 87
TRZ349	Figure 7c
TRZ350	Figure 7c
TRZ351	Figure 7c
TRZ352	Figure 7b
TRZ353	Figure 7b
TRZ354	Figure 7d
TRZ355	Figure 7c
TRZ356	Figure 7c
TRZ357	Figure 5
TRZ358	Figure 7c
TRZ359	Figure 7c
TRZ360	Figure 7d
TRZ361	Figure 7c
TRZ362	Figure 7a
TRZ363	Figure 7d
TRZ364	Figure 7c
TRZ365	Figure 19f
TRZ366	Figure 19f
TRZ367	Figure 19b
TRZ368	Figure 19d
TRZ369	Figure 19f
TRZ370	Figure 19a
TRZ371	Figure 19f
TRZ372	Figure 19d
TRZ373	Figure 18
TRZ374	Figure 19g
TRZ375	Figure 19f
TRZ376	Figure 19d
TRZ377	Figure 18
TRZ378	Figure 19e
TRZ379	Figure 19e
TRZ380	Figure 18
TRZ381	Figure 18
TRZ382	Figure 19e
TRZ383	Figure 18
TRZ384	Figure 19c
TRZ385	Figure 18
TRZ386	Figure 18
TRZ387	Figure 19d
TRZ388	Figure 19c
TRZ389	Figure 19c
TRZ391	Figure 78
TRZ392	Figure 78
TRZ393	Figure 78
TRZ394	Figure 78
TRZ395	Figure 78
TRZ396	Figure 78
TRZ397	Figure 79
TRZ398	Figure 79
TRZ399	Figure 78

GRANULOMETRIC ANALYSIS OF THE SURFACE FORMATIONS OF TCHINGUIZ TEPE AND SURROUNDING AREAS

Ana Sánchez del Corral

1.- INTRODUCTION

The purpose of this granulometric study is to characterise and interpret the genesis and behaviour of the sediments, or surface formations (SFs), and the bedrock of the hill of Tchinguiz Tepe. The work involves systematically sampling the previously defined geological stratigraphy and archaeology of the southern and western cross-sections of trial excavation RC, which is optimal for the definition of a representative granulometric sequence based on its position and size. The granulometric characterisation of the surface formations is further supplemented by samples of the stratigraphic levels from the top of trial excavation RC II gathered in a small survey focused on the base of the slope and seasonal wind contributions.

Another set of samples comes from small quarries, which were located in the floodplain of the Surkhan Darya and acted as a source of raw materials for bricks, and from materials prepared in a small local brick-making workshop. The objective of these samples is to characterise the granulometries of the material used in the modern manufacture of bricks and the employed sediments generated by basically fluvial contributions. Lastly, in order to characterise deposits of purely wind-blown materials, the study also examines the granulometry of a typical loess deposit located in the middle valley of the Surkhan Darya.

These external samples enable us to compare and contrast the surface formations that cover Tchinguiz Tepe and give form to the archaeological site (table 1).

Laser diffraction is the method used to determine the particle-size distribution. In particular, we use the Beckman Coulter Particle Size Analyzer LS 13320-1. The method is based on the principle that particles act as dispersion centres when exposed to electromagnetic radiation. The resulting dispersion model can be measured electronically and analysed mathematically to deduce a particle-size distribution.

The descriptive statistical analysis appears in tables 2, 3 and 4. The statistical measurements in use are: **common averages** (mean, median and mode); **dispersion measures** such as standard deviation (S.D.), variance, coefficient of variation (C.V.) and Kurtosis, and **asymmetry measures** such as skewness.

We also consider the effective diameters *d10*, *d50*, *d60* and *d90*, which reflect particle size and correspond to 10, 50, 60 and 90% of the sample weight, respectively. The figures are obtained from the volume statistics gathered in the sample. The graphs show cumulative frequencies for these variables.

One factor of interest in the textural analysis is the **Uniformity Coefficient (C_U)**, which is defined as the grain size that corresponds to 60% (by weight) of a sample of sand (60% of the sediment is finer than a given size), divided by the size at which 10% of the same sample (by weight) passes through a sieve (10% is finer than a given size). A C_U of 1 indicates that all the particles are the same size. When the number rises, the size differentiation also increases. The expression of C_U is:

$$C_U = \frac{d60}{d10}$$

Where:

d60 = particle size corresponding to P = 60% of the granulometric curve (60% of the particles are finer than *d60* and 40% is less fine)

d10 = particle size corresponding to P = 10% of the granulometric curve (10% of the particles are finer than *d10* and 90% is less fine)

The values of $\mathbf{C_U}$ rise as granulometric uniformity falls.

The analysed samples fall into two broad groups:

1. samples from the hill of Tchinguiz Tepe, further clustered into RC South, RC II, RC West and the bedrock, and
2. samples external to Tchinguiz Tepe, from current quarries or raw material sources used in the manufacture of adobe bricks in the floodplain of the Surkhan Darya and from loess deposits in the fluvial domain of the same river.

Code	GSL	SU	Remark
		THINGUIZ TEPE	
S_1	RC-S_1	SU 1	Sand surface level
S_2	RC-S_2	SU 2	Fine, associated with the level of fallen adobe bricks. Sand, charcoal, quicklime = SU 2
S_3	RC-S_3	SU 18	Average-sized to very fine, heterogeneous sand, highly disturbed sandstone fragments, dark gravel, charcoal, white base beneath collapse --> surface sealed
S_4	RC-S_4	SU 19	Lens-shaped sand, large and abundant charcoal, ash, quicklime, pottery
S_5	RC-S_5	SU 21	Sand below S_3, trodden level of use = SU 21
S_6	RC-S_6	SU 5 – SU 19	Sand in pockets, lateral contact with S_3, under S_4
S_38	RC-II_1	NO	Seasonal aeolian mantle
S_36	RC-II_2	SU 2	Sand beneath surface level = SU 2
S_37	RC-II_2 bis	SU 2	Dark facies = SU 2
S_7	RC-W_a	SU 1	Sand surface level = RC a = SU 1
S_8	RC-W_b	SU 1	Sand = RC b, no gravel, fine
S_9	RC-W_c	SU 5?	Sand = RC c, some homogeneous gravel, pottery, transition to lower level stratification in fine sheets
S_10	RC-W_d	SU 5?	Very fine sand = RC d, scarce pottery
S_11	RC-W_e	SU 6?	Sand = RC e, similar to previous level, more compact, pottery and bones, quicklime
S_12	RC_W_f	SU 10	Sand = RC f, fine sand over substrate, pottery, bones and quicklime
S_39	Sondeo Isa	NO	Sand
S_13	Escarpe 1	NO	Sandstone level 1
S_14	Escarpe 2	NO	Sandstone level 2
		SURKHAN DARYA VALLEY (Extraction areas and loess)	
S_29	Muestra 1	NO	Sand. Quarry no. 1 Surkhan Darya
S_30	Muestra 2_A	NO	Sand. Quarry no. 1 Surkhan Darya unconsolidated upper level
S_31	Muestra 2_B	NO	Sand. Quarry no. 1 Surkhan Darya compact sand lower level
S_32	Muestra 3	NO	Sand. Quarry no. 1 Surkhan Darya. Sand from NE cross-section of ditch
S_33	Muestra 4	NO	Sand, raw material in adobe brick-making, “Manchuzar Uchasco”.
S_34	L_1	NO	Loess, over train
S_35	L_2	NO	Loess, over pipes

Table 1.- *List of samples grouped by point of origin and coded according to the key used in the study; the second and third columns from the left refer to: GSL = Geological Stratigraphic Level; SU = Archaeological Stratigraphic Unit*

	RC SOUTH						RC II		
	Sample_1	Sample_2	Sample_3	Sample_4	Sample_5	Sample_6	Sample_38	Sample_36	Sample_37
From (μm)	0,04	0,04	0,04	0,04	0,04	0,04	0,04	0,04	0,04
To (μm)	2000	2000	2000	2000	2000	2000	2000	2000	2000
Volume	100	100	100	100	100	100	100	100	100
Mean:	**231,967**	147,746	**100,975**	140,328	140,312	182,702	161	110	124
Median:	98,6142	84,8112	**56,1726**	99,5441	117,163	**151,089**	147,02	62,94	75,89
Mean/Med ratio:	2,35227	1,74205	1,79758	1,4097	1,19758	1,20924	1,092	1,744	1,639
Mode:	**905,109**	127,646	**45,7513**	245,228	203,494	185,371	185,37	50,22	140,13
S.D.:	**298,513**	163,433	110,808	129,019	112,115	155,284	114,02	119,3	133,93
Variance:	**89110,3**	26710,4	12278,4	16645,9	12569,7	24113,2	12999,7	14231,2	17936,7
C.V.:	128,688	110,618	109,738	91,9412	79,904	84,9931	71,03	108,68	107,67
Skewness:	1,64787	1,75636	1,57454	1,28472	1,0235	1,92779	0,792	1,6	1,699
Kurtosis:	1,50965	2,97523	1,95063	1,35807	0,888991	6,95419	0,328	2,178	2,899
d10:	13,9798	12,5699	7,12411	13,9248	17,8283	25,6031	25,5	7,27	9,55
d50:	98,6142	84,8112	56,1726	99,5441	117,163	151,089	147,02	62,94	75,89
d60	147,1	129,62	82,84	133,56	149,22	184,06	175,41	91,52	109,47
d90:	809,542	395,672	271,376	327,575	295,296	382,015	320,03	290,85	324,98
UC=d60/d10	10,52	10,31	**11,63**	9,59	8,37	7,19	6,88	**12,59**	11,46
d50/d10	7,05	6,75	**7,88**	7,15	6,57	5,90	5,77	8,66	7,95
d90/d50	8,21	4,67	4,83	3,29	2,52	2,53	2,18	4,62	4,28
d90/d10	57,91	31,48	38,09	23,52	16,56	14,92	12,55	40,01	34,03

Table 2.- Statistical measurements from the samples in RC South and RC II

	RC WEST							Sandstone sustratum	
Sample ID:	Sample_7	Sample_8	Sample_9	Sample_10	Sample_11	Sample_12	Sample_39	Sample_13	Sample_14
From	0,04	0,04	0,04	0,04	0,04	0,04	0,04	0,04	0,04
To	2000	2000	2000	2000	2000	2000	2000	2000	2000
Volume	100	100	100	100	100	100	100	100	100
Mean:	136,142	149,311	146,008	**124,477**	136,286	**166,742**	134,000	191,582	167,701
Median:	102,908	120,714	111,485	**88,702**	90,390	**141,744**	78,540	166,690	143,053
Mean/Med.ratio:	1,323	1,237	1,310	1,403	1,508	1,176	1,700	1,149	1,172
Mode:	185,371	185,371	**223,389**	203,494	185,371	**168,863**	50,220	168,863	140,125
S.D.:	119,548	124,241	121,814	**109,117**	130,619	132,221	129,600	139,923	118,316
Variance:	14291,8	15435,8	14838,7	**11906,5**	17061,3	17482,3	16796,6	19578,4	13998,8
C.V.:	87,8116	83,2095	83,4301	87,6605	95,842	79,2967	97,06	73,0354	70,5519
Skewness:	1,06044	1,05336	1,10549	1,13543	1,3327	1,22673	1,4	0,921483	1,50218
Kurtosis:	0,530421	0,69601	0,842906	0,777477	1,36743	1,57434	1,356	0,653107	2,96354
d10:	12,5295	18,899	20,8523	14,8807	13,0059	25,4273	21,43	22,531	41,4161
d50:	102,908	120,714	111,485	88,7023	90,3904	141,744	78,54	166,69	143,053
d60	139,46	159,84	147,22	121,92	132,33	171,68	112,75	199,27	164,82
d90:	316,847	330,54	322,456	286,687	332,233	351,188	338,12	393,836	322,901
C_U=d60/d10	11,13	8,46	7,06	8,19	10,17	**6,75**	**5,26**	8,84	3,98
d50/d10	8,21	6,39	**5,35**	5,96	6,95	5,57	3,66	7,40	3,45
d90/d50	3,08	2,74	2,89	3,23	3,68	2,48	4,31	2,36	2,26
d90/d10	25,29	17,49	15,46	19,27	25,54	13,81	15,78	17,48	7,80

Table 3.- *Statistical measurements from the samples in RC West and the sandstone substrate.*

2.- GRANULOMETRIC ANALYSIS OF TCHINGUIZ TEPE

Trial excavation RC (5 x 15 m) is found inside the fortified wall around Tchinguiz Tepe. The surface in which the trial excavation is dug can be found where the topographical level that starts at the fortification converges with the topographical level of the southern slope of the hill (see IPAEB, 2009). The stratigraphy of the southern cross-section is organised in stacked levels (S_1, S_2, S_3 and S_5) from the fortification toward the interior of the enclosure. These levels come into lateral contact with levels S_4 and S_6 which are wedged between S_2 and S_3. As can be seen in figure 1, the base stratum S_5 supports all the other strata and the level on top (S_1) covers all the others. In general, small discrepancies with the archaeological stratigraphy stem from lateral splitting of strata. For example, stratum S_5 is equivalent to the archaeological stratigraphic unit (SU) 21 (left-hand part of figure 1) and to SU_23 in the right-hand part of the photo (Ariño, IPAEB, 2009 and Ariño & Sánchez del Corral, under publication). In levels S_4 and S_6, additional archaeological levels can be distinguished as well. Despite the difficulties of interpretation, however, the sediment matrix containing the anthropic remains is basically the same.

Samples S_36, S_37 and 38 belong to trial excavation RC II, an extension of RC in the part against the fortification.

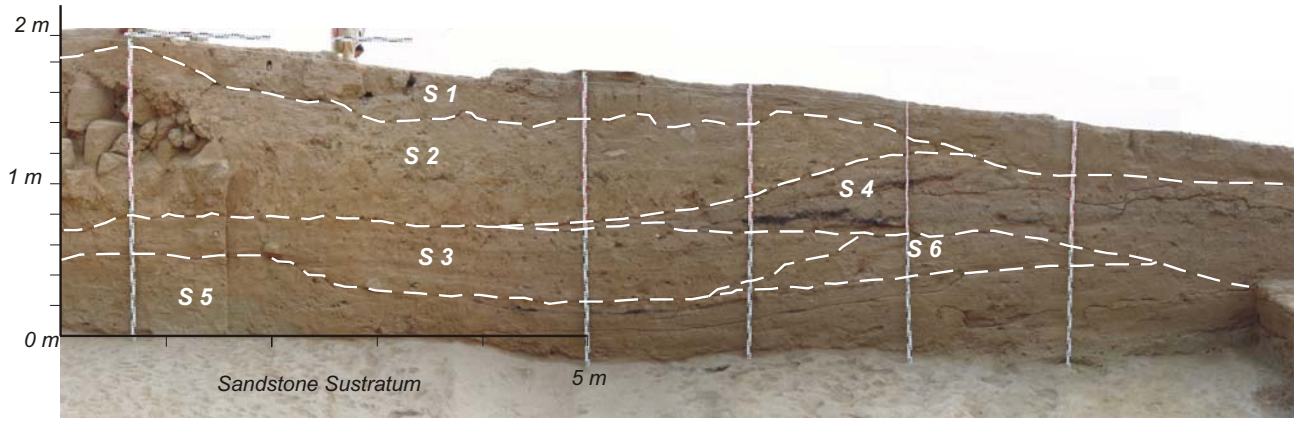

Figure 1.- Location of samples S 1 to S 6 in RC South. The broken white lines show interpreted discontinuities in the stratigraphy.

2.1.-South cross-section of trial excavation RC

The granulometry of the samples analysed in the south cross-section is characterised by frequency distribution curves that are polymodal (S_1, S_2, S_3, S_36 and S_37), bimodal (S_4) and unimodal (S_5 and S_6). Mean, median and mode values are as follows:

the Mean ranges from very fine sand (100.9 µm) to fine sand (231.9 µm)

the Median varies from silt size (62.9) to fine sand (151)

the Mode falls at 50.22 µm (coarse silt) in S_36 and 905.1 in S_1. The latter value reflects a behaviour quite different from the other samples, with a very marked secondary mode in the area of “coarse sand” (figure 2, c, d).

The ratios of maximum to minimum values for these three measures are 2.3, 2.69 and 19.7, respectively.

The dispersion measures point to leptokurtic curves, although the Kurtosis values range from 0.32 (S_38) to 6.95 (S_6). The graph with the cumulative frequencies (figure 2b) shows a cluster of curves of similar shape, with end-points represented by samples S_38 and S_6 on the right (steeper and more likely to have large grain sizes) and sample S_3 on the left, indicating a predominance of finer granulometry.

The asymmetric statistics measurements indicate positive asymmetries in all cases (right-skewed) as can be seen by the Skewness values (table 2) and more directly in the graphs in figure 2. Obviously in all cases, the distribution has a tail extending toward the finest diameters.

The highest granulometric uniformity (C_U) belongs to sample S_38 (C_U = 6.88) and the lowest figure comes from samples S_3 (C_U = 11.63) and S_36 (C_U = 12.59) (table 2).

Notably, the curves for samples S_5 and S_6 are unimodal, while S_4 has two relatively unmarked modes and similar symmetry. These are sediments from the base stratum and the stratigraphic levels that are wedged in the middle zone of the south cross-section of the trial excavation. Their accumulated frequency curves show the steepest slopes overall (figure 3), expressing a greater concentration of sizes, which is also reflected in a Uniformity Coefficient C_U (between 7.19 and 9.59) that is among the lowest in their group, indicating intermediate uniformity of grain size (table 2).

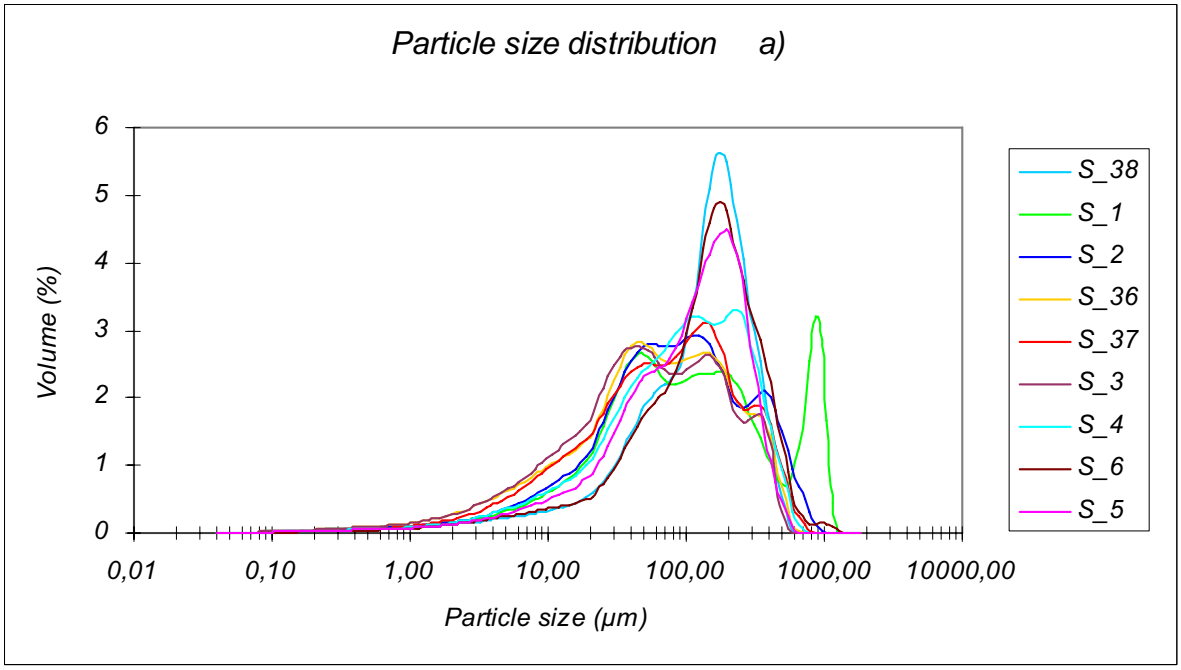

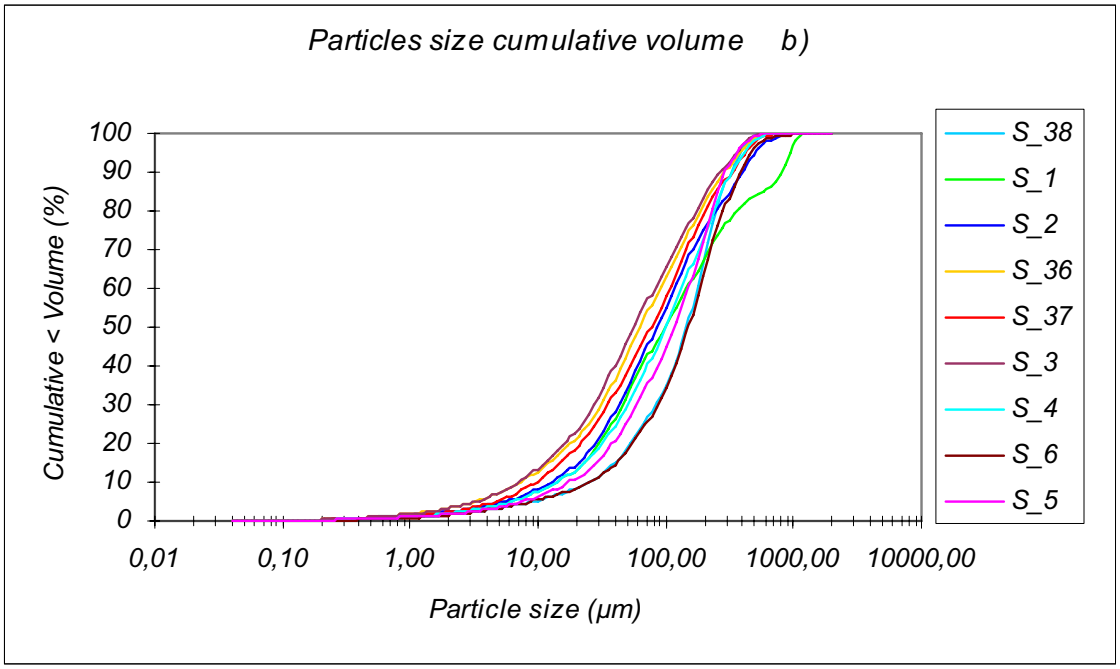

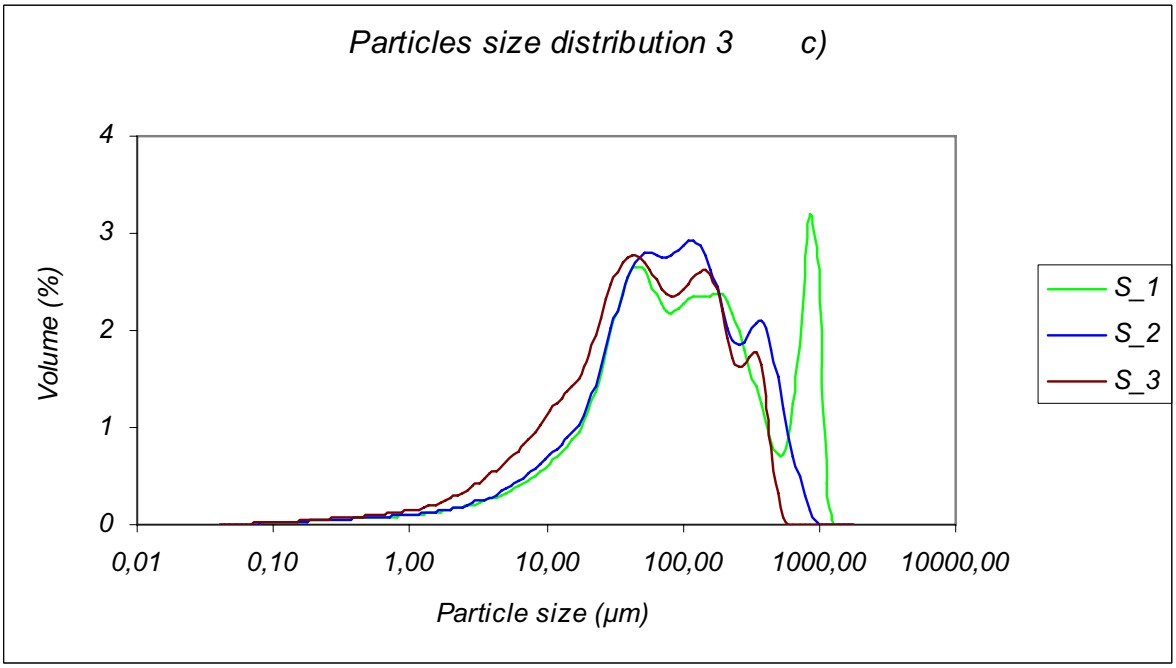

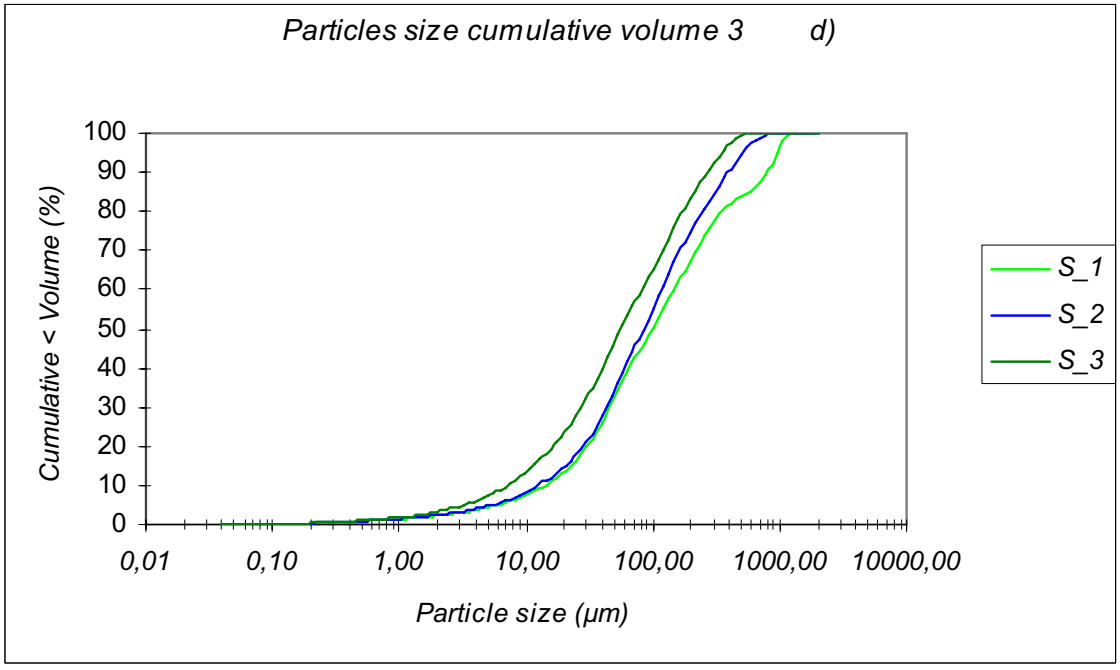

Figure 2. Frequency curves, granulometric and cumulative, for the samples from RC South, along with three samples from RC II (extension of RC), S_38, S_36 and S_37. The curves appear in order from top to base in A) and B). Graphs C) and D) provide detail for samples S_1, S_2 and S_3.

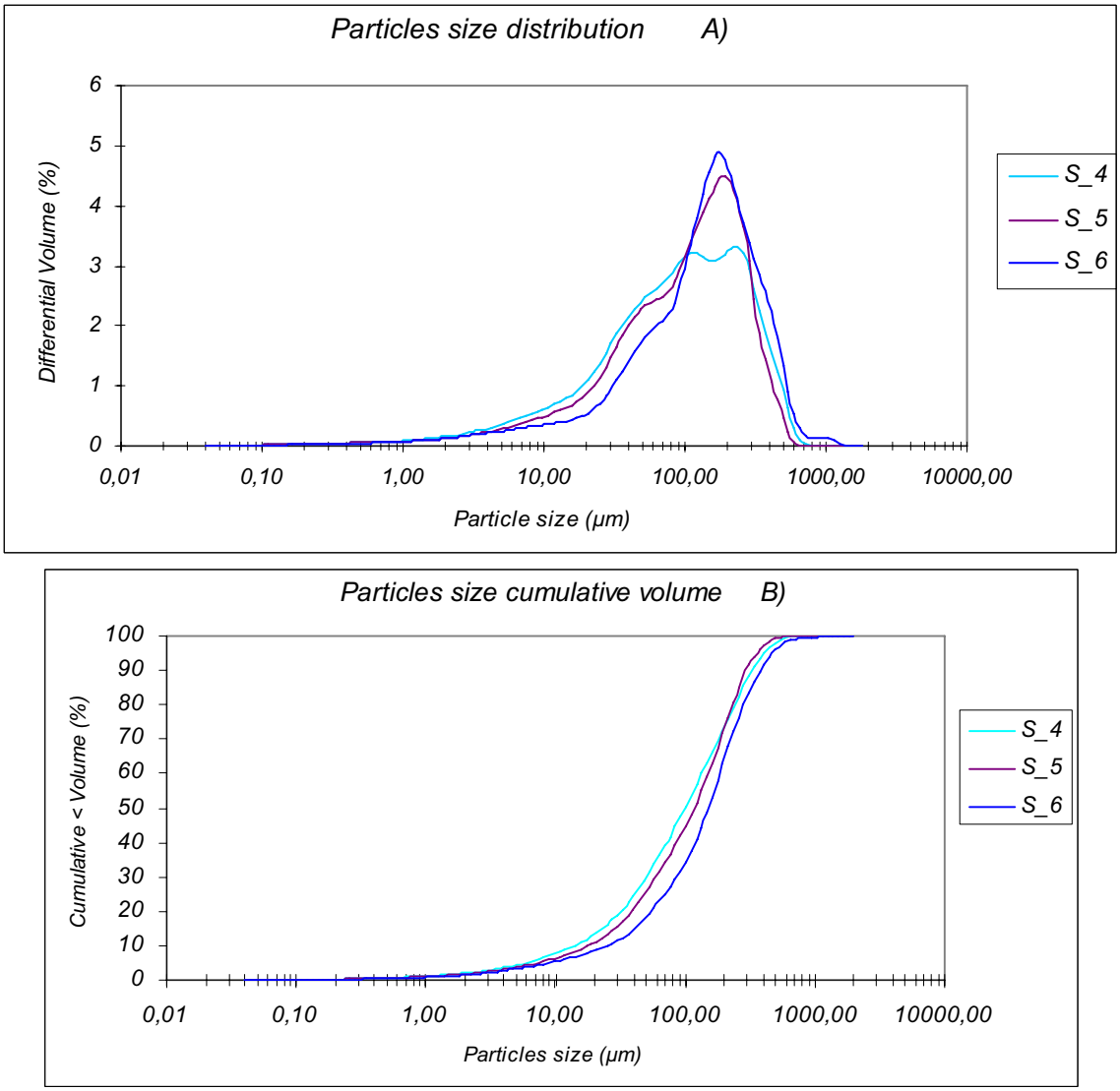

Figure 3. The curves for samples S_4, S_5 and S_6 are similar in shape and slope.

In an examination of the samples by granulometric size (Wentworth size class), six of the nine samples have more silt-sized content than other classes, although the proportion never exceeds 50% in any one sample (figure 4). No trend toward greater or lesser size is observable from top to bottom. Samples S_38 (seasonal aeolian mantle), S_5 and S_6 and, to a lesser extent, S_4 contain a greater predominance of sizes larger than fine and average-sized sand; these are also the most uniform sediments (See Uniformity Coefficients C_U).

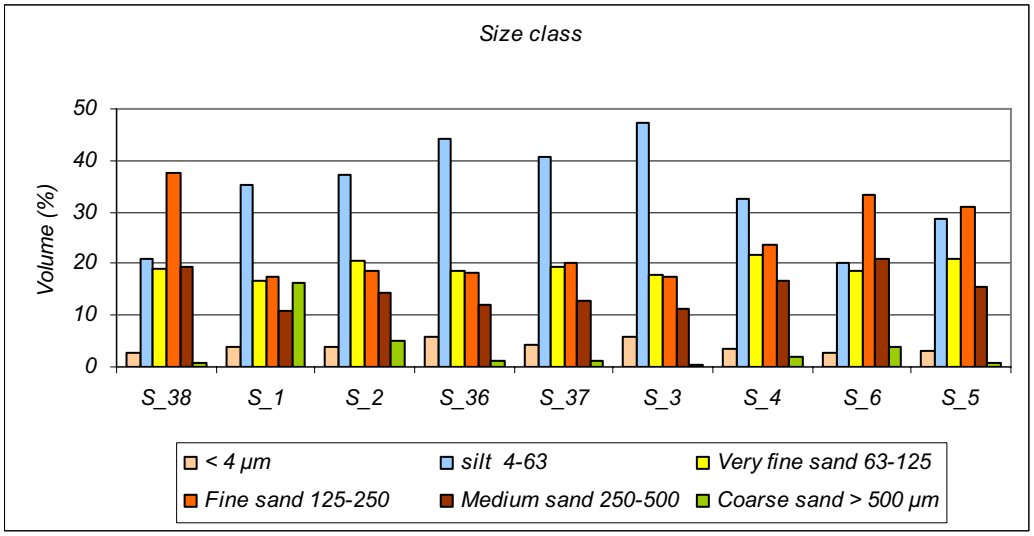

Figure 4. Histogram showing the clusters by Wentworth size class for the RC South samples, in order from top to base.

Thick sand only accounts for a significant proportion in S_1 (top of column), making the statistical values of the calculated measurements somewhat different from the others, as can be observed in table 2.

2.2.- West cross-section of trial excavation RC

The samples from the RC West, S_7 (top of profile) to S_12 (base), are described statistically along with sample S_39, which was taken as part of the survey conducted in the base area of the hill at approximately 20 metres from the western boundary of the trial excavation and at 60 cm of depth (table 1).

The six samples taken from RC West are very homogeneous. They present no great variations in the distribution of frequencies, which show a tendency toward being bimodal. The tendency is much stronger in S_11, while S_9 and S_12 tend to present a single mode (figures 5, C and 6, A). Mean, median and mode have the following characteristics:

Mean, median and mode are not highly separated (ratio of maximum to minimum values = 1.3; 1.6 and 1.3), except on the south side (ratio = 2.3, 2.69 and 19.7, respectively) where the influence of the granulometric sizes from the archaeological ruins is greater.

Mean, median and mode reveal a grain size in the “fine sand” class (between 149 and 250 µm). Exceptions are found in the median values corresponding to the “very fine sand” class in sample S_39 (78.5 µm) and S_10 (88.7 µm).

The samples with the finest grain size are S_10 (mean 124.5; median = 88.7) and S_12 (mode = 168.8) and the ones with the thickest are S_12 (mean = 166.7, median = 141.7) and S_9 (mode = 223.4) (table 3 and figure 5).

Sample S_39 presents the lowest values of all the samples, with “fine sand” for the mean “very fine sand” for the median” and “coarse silt” for the mode, giving a frequency curve with a marked mode in the area and two less marked secondary figures (table 3 and figure 6, A, B).

Logically, these characteristics find expression in the measures of asymmetry and dispersion, which are all Leptokurtic with Kurtosis values for the set that are less separated than in RC South. All the samples have positive asymmetries (right-skewed).

Sample S_12 (base of series lying on the sandstone substrate) features a striking mode and high uniformity (Uniformity Coefficient C_U = 6.75) (figures 5 and 6). Sample S_39 has the lowest C_U (C_U = 5.29) and the entire western cross-section of trial excavation RC is more uniform in behaviour than the southern cross-section (figures 6, A and B).

The clustering by granulometric class (Wentworth size class) in figure 6 (Size Class RC West) offers a quite balanced distribution by class, with a slightly higher fraction of silt and no appreciable rising or falling trend in grain size from top to base.

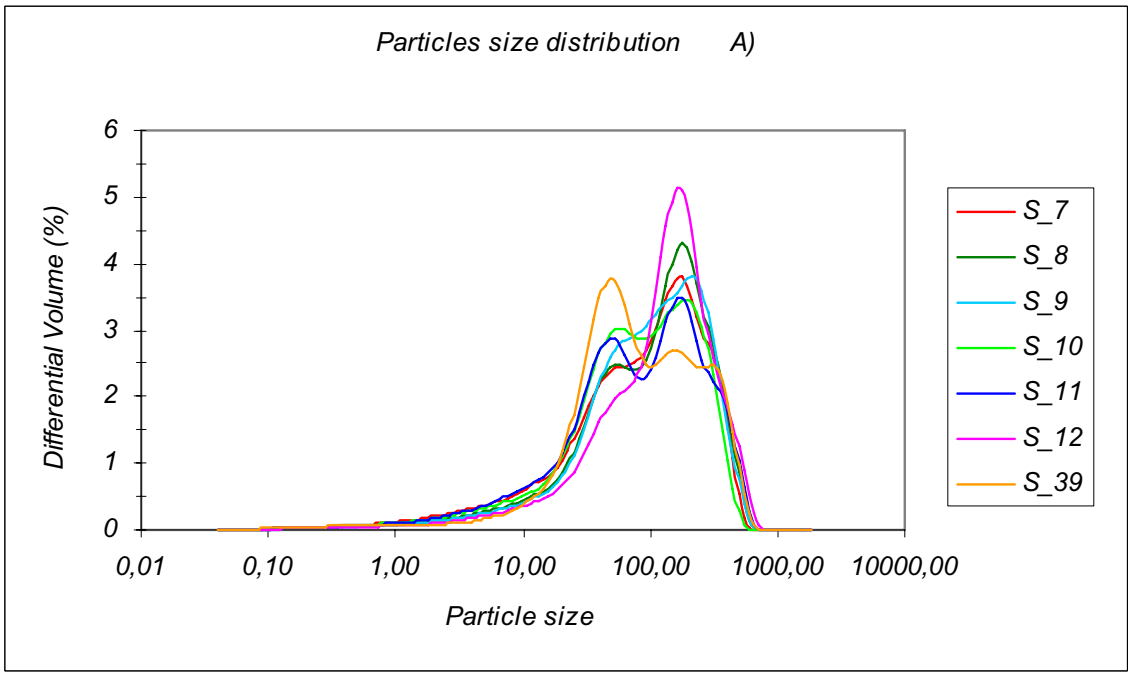
Particles size distribution A)
Differential Volume (%)
6
5
4
3
2
1
0
0,01
0,10
1,00
10,00
100,00
1000,00
10000,00
Particle size
S_7
S_8
S_9
S_10
S_11
S_12
S_39

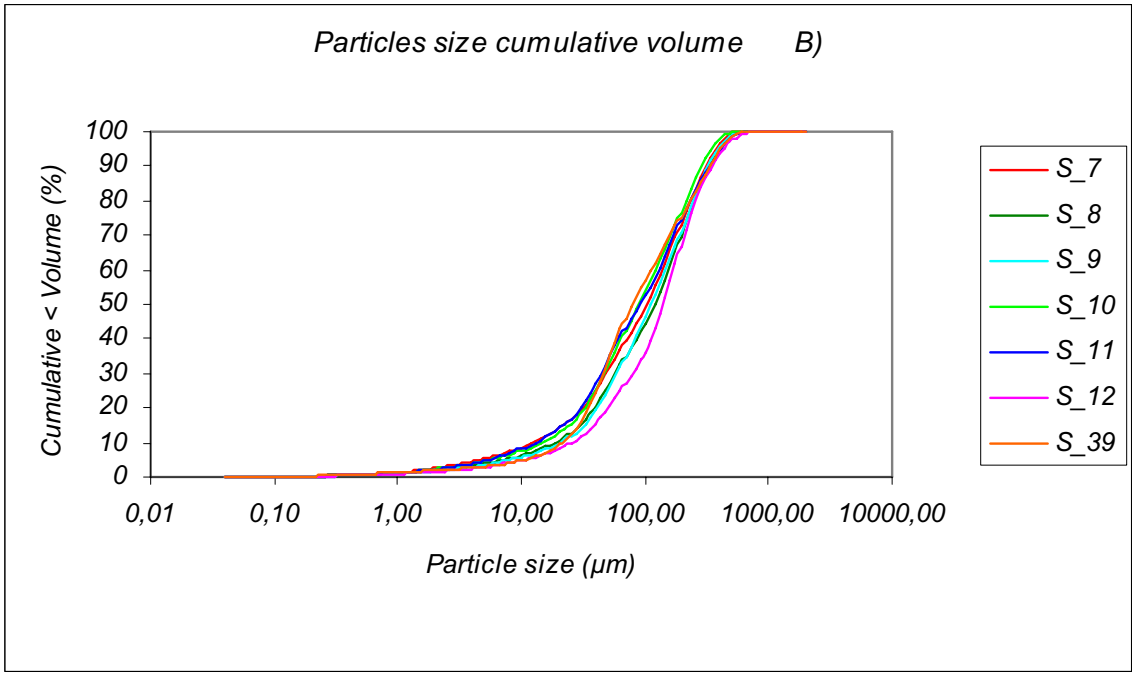
Particles size cumulative volume B)
Cumulative < Volume (%)
100
90
80
70
60
50
40
30
20
10
0
0,01
0,10
1,00
10,00
100,00
1000,00
10000,00
Particle size (µm)
S_7
S_8
S_9
S_10
S_11
S_12
S_39

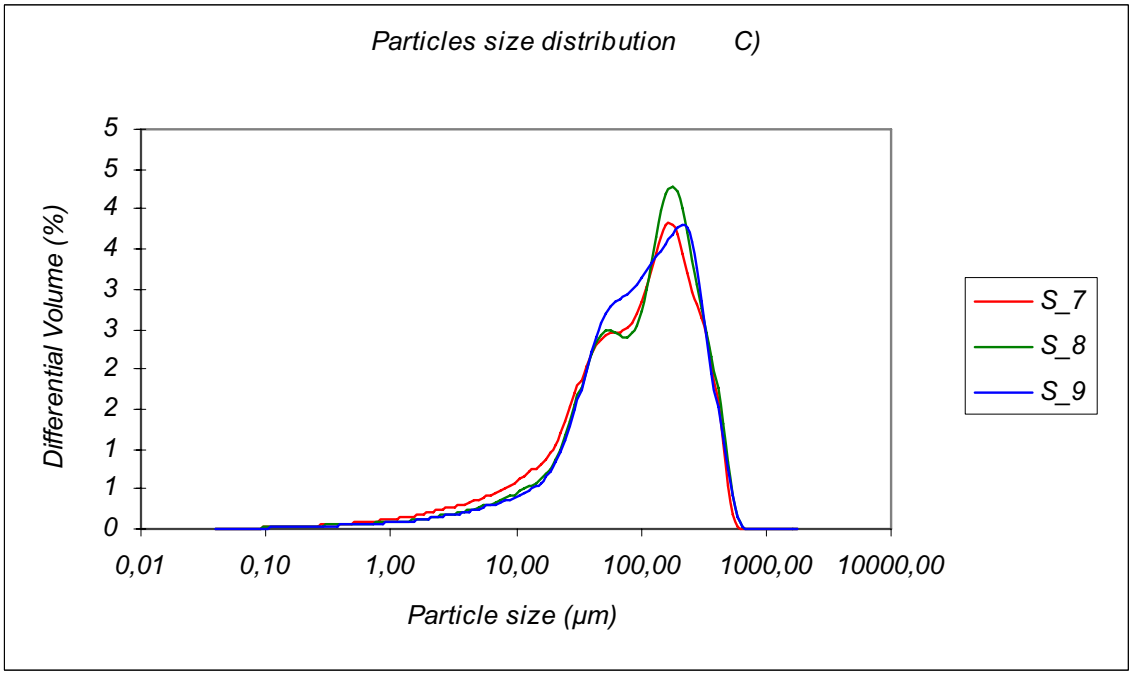

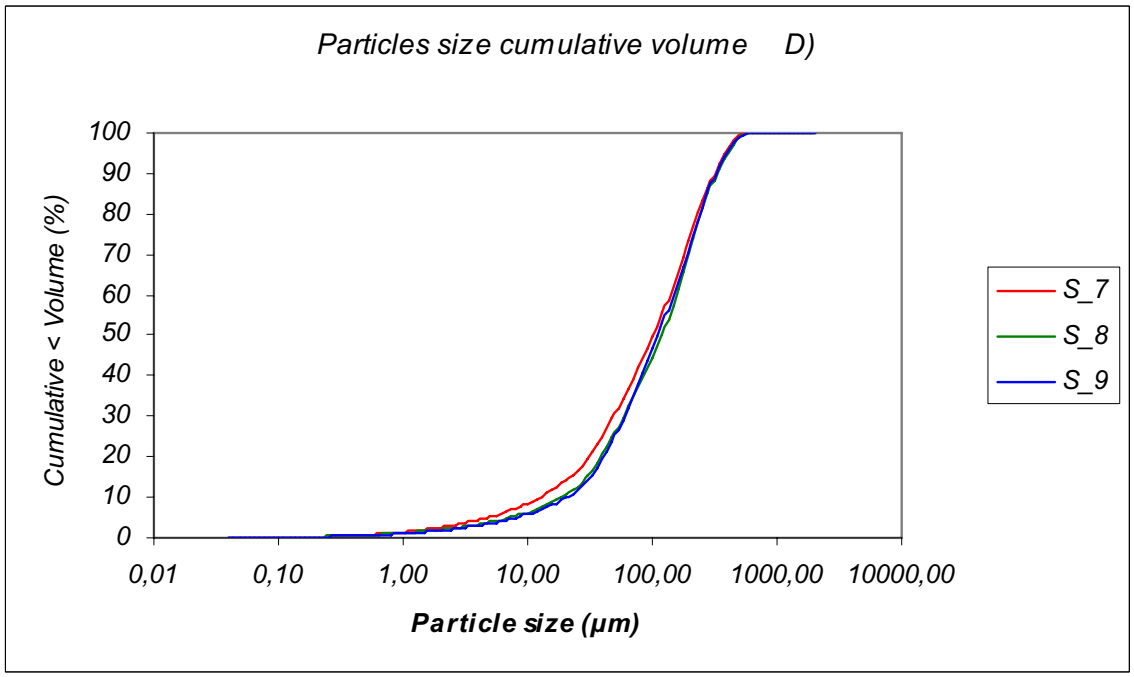

Figure 5. Distribution curves of granulometric frequencies and cumulative frequencies for the samples from trial excavation RC West and sample S_39 of the survey conducted 20 metres from RC at 80 cm from surface A) and B). Graphs C) and D) show the behaviour of the first three levels.

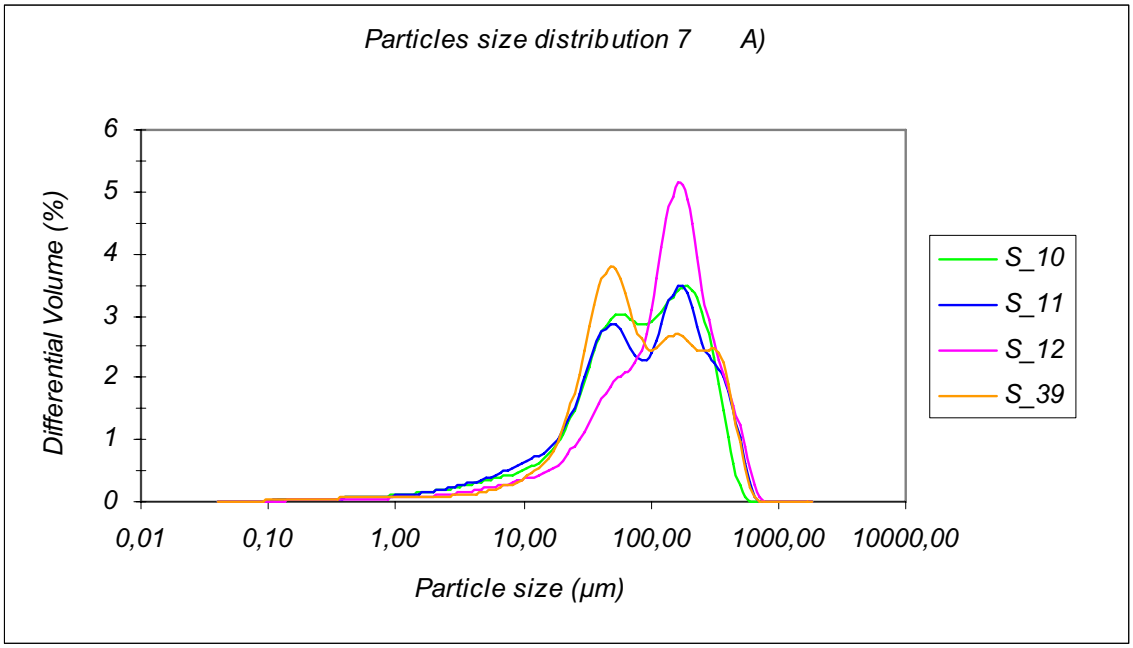

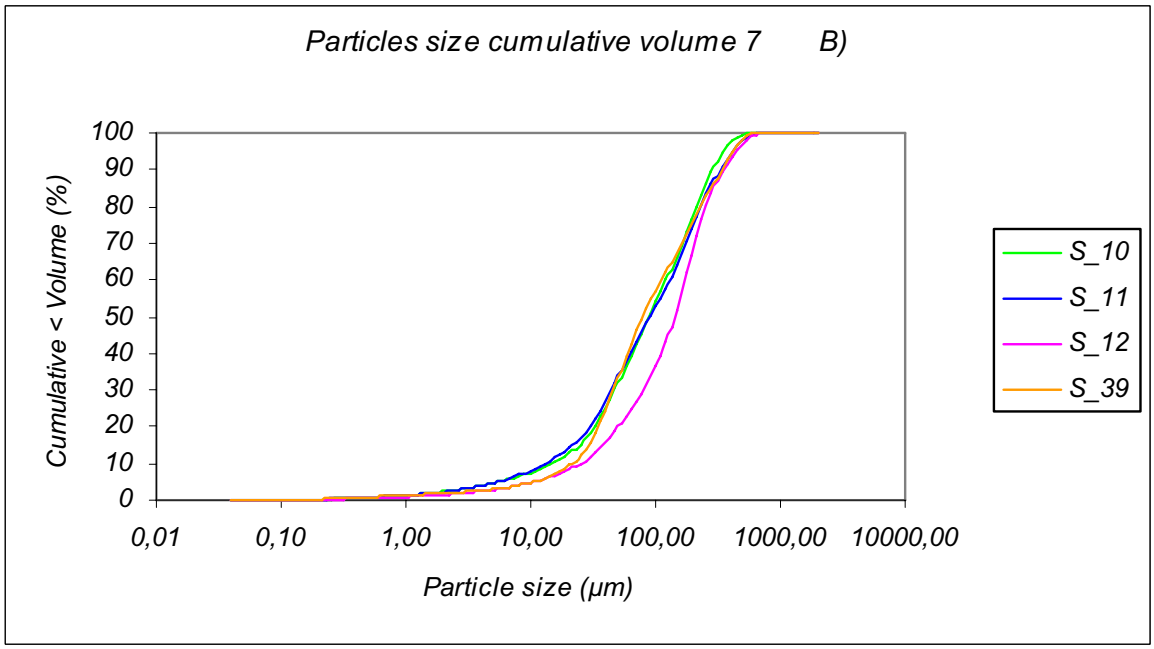

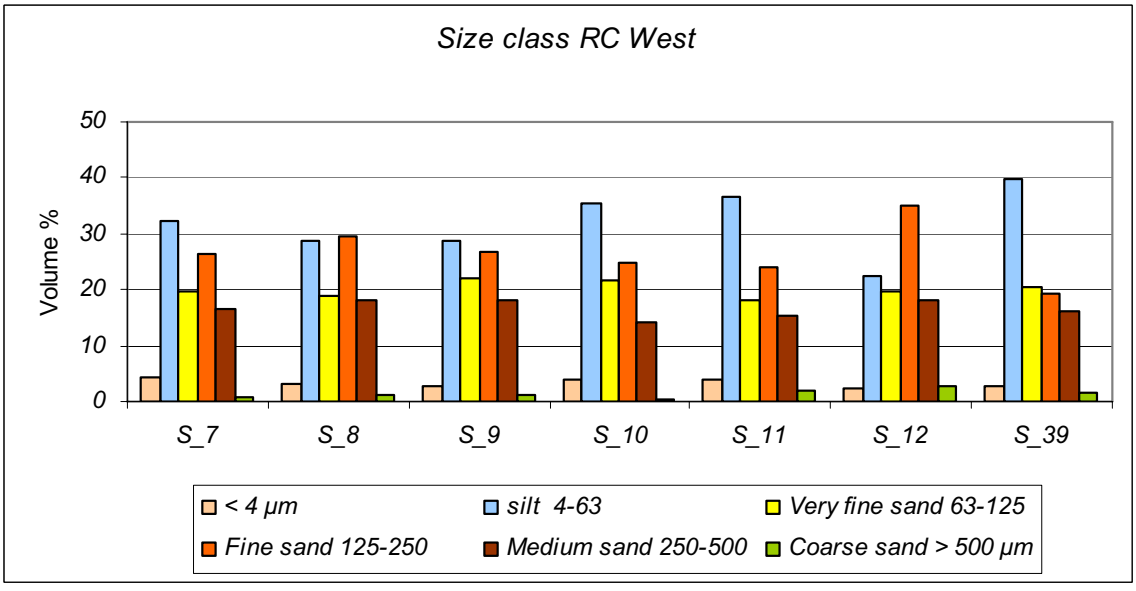

Figure 6. *Detailed view of curves from the lowest levels of RC West (A and B), with clustering by Wentworth size class.*

2.3. Sandstone substrate

Samples S_13 and S_14 belong to the sandstone substrate that constitutes the base of the structures of the hill. The samples were taken in a highly evolved weathering column. Rock crumbles on contact but maintains its structure in situ.

Sample S_13 corresponds to the highest part of the column and sample S_14 corresponds to the level immediately below. Both samples have very similar curves, with significant asymmetry (right-skewed). The presence of two granulometric groups with practically no transitional terms is reflected in the frequency distribution curve by means of a marked inflection and, in the cumulative frequency curve, with two segments that have sharply different slopes (figure 7).

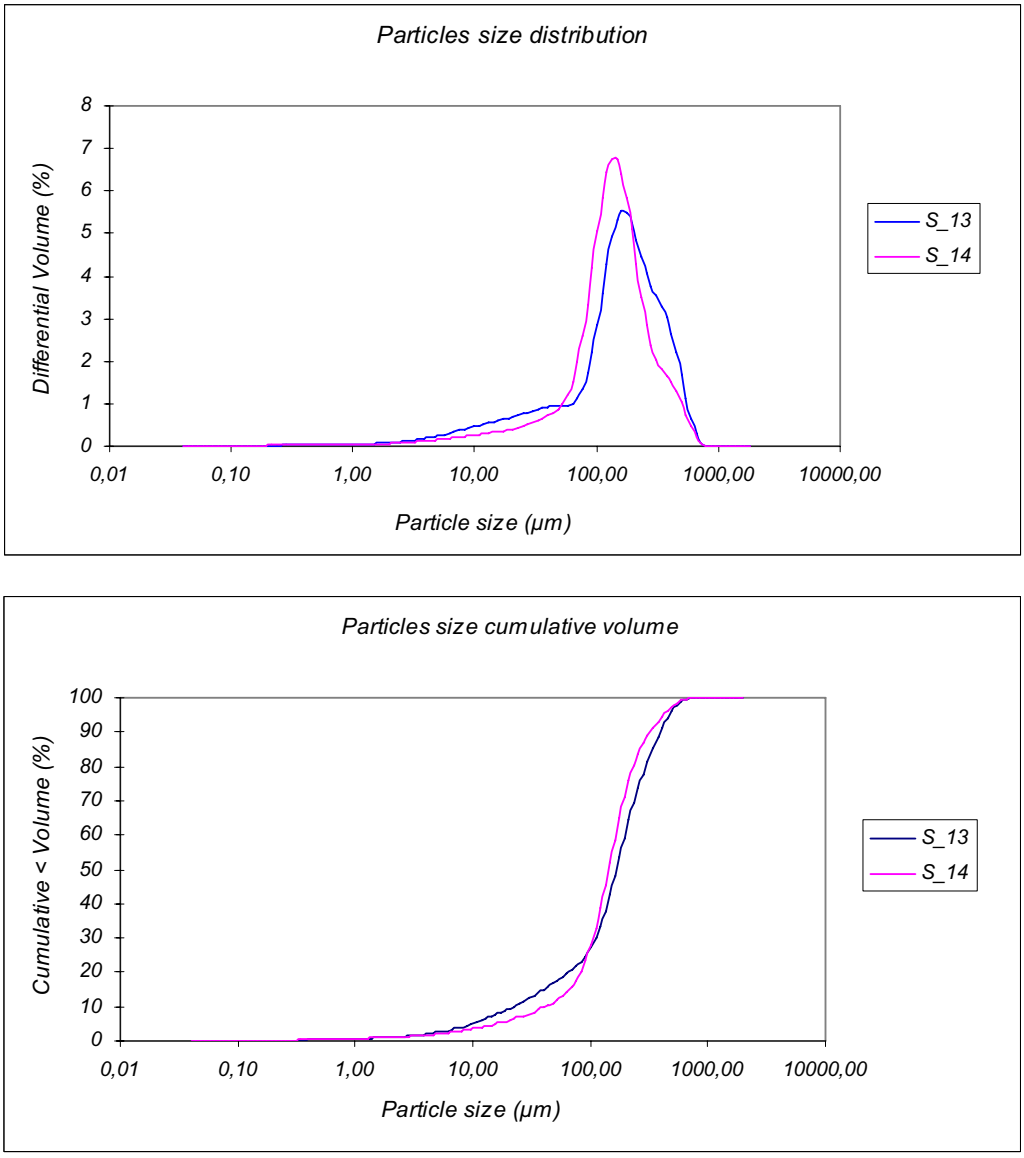

Figure 7. Distribution curve of frequencies and cumulative frequencies of samples S_13 and S_14 belonging to the sandstone substrate beneath the surface formations at Tchinguiz Tepe.

In both samples, the mean, median and mode correspond to the size “fine sand”, which is the size that stands out in the clustering by class. In addition, the samples are quite uniform, particularly S_14, which has a very low C_U indicating a good granulometric uniformity that tends toward the size “fine sand” (table 3).

The vertical variations in grain size in this type of substrate are highly influenced by post-sedimentary processes such as edaphic processes, biological activity, etc. The presence of palaeosoils introduces granulometric variations that are alien to the intrinsic nature of the rock, but pertinent to the characterisation of the sample.

2.4. Quarries and loess deposits

The samples analysed statistically below correspond to raw material used in the manufacture of bricks (S_29 to S_32) and to the material prepared in a local brick-making workshop. The quarries are located in the floodplain of the Surkhan Daryha, in an area prone to flooding. Therefore, they contain fine fluvial deposits.

Samples S_29 to S_32 present a bimodal behaviour indicating the presence of two highly defined populations: 1) “coarse silt”, which represents the greatest amount in the sample, and 2) “medium sand”, which defines the secondary mode. Sample S_33 is unimodal, i.e. it has a greater concentration of sizes.

Table 4 shows the values of statistical indicators in which notable differences can be observed with respect to the sediment samples from Tchinguiz Tepe, namely that they are much finer and greater in uniformity. Details include:

- The lowest mean, median and mode values arise in sample S_33 (brick manufacturing) corresponding to “coarse silt” (mean = 42.00, median, 31.86, mode = 37.97). The highest values occur in sample S_32 (quarry) and concern “very fine sand” and “fine sand”. The frequency distribution curve shows a shift to the right (toward finer grain sizes) for the S_32 curve and the S_33 curve has a single mode with a slight asymmetry toward to the side of finer grain sizes (figure 8, A, B).

Of all the samples, the loess samples (S_34 and S_35) are by far the most symmetrical, the best-selected and the most uniform in terms of silt grain size. They represent the prototype for very fine, very well-calibrated wind deposits.

	QUARRY (EXTRACTION AREAS)					*LOESS*	
	Sample_29	*Sample_30*	*Sample_31*	*Sample_32*	*Sample_33*	*Sample_34*	*Sample_35*
From	*0,04*	*0,04*	*0,04*	*0,04*	*0,04*	*0,04*	*0,04*
To	*2000*	*2000*	*2000*	*2000*	*2000*	*2000*	*2000*
Volume	*100*	*100*	*100*	*100*	*100*	*100*	*100*
Mean:	72	76	57	**124**	**42**	36	37
Median:	39,3	47,99	44,33	**91,56**	**31,86**	33	32,5
Mean/Med. ratio:	1,843	1,581	1,284	1,353	1,305	1,102	1,142
Mode:	37,97	45,75	55,13	**127,65**	**37,97**	37,97	37,97
S.D.:	100,6	86,43	63,29	118,15	36,35	22,76	26,16
Variance:	10119,3	7470,9	4005,7	13959	1321,5	518,2	684,4
C.V.:	138,9	113,95	111,21	95,36	87,41	62,59	70,5
Skewness:	2,793	2,534	4,291	1,669	1,245	0,931	1,17
Kurtosis:	7,545	7,478	25,03	2,701	1,218	1,087	1,635
d10:	9,87	9,13	7,85	15,45	4,46	10,07	7,83
d50:	39,3	47,99	44,33	91,56	31,86	33	32,5
d60:	47,93	60,61	54,11	117,31	40,19	38,21	38,11
d90:	155,39	168,76	107,04	293,45	95,83	67,04	72,15
UC=d60/d10	4,86	6,64	6,89	7,59	9,01	3,79	4,87
d50/d10	3,98	5,26	5,65	5,93	7,14	3,28	4,15
d90/d50	3,95	3,52	2,41	3,21	3,01	2,03	2,22
d90/d10	15,74	18,48	13,64	18,99	21,49	6,66	9,21

Table 4. Statistical measurements of the samples from RC South and the sandstone substrate.

Figure 8 C shows the loess curve along with the curve for S_33 (brick-making), which reflects a predominantly silt grain size and a single mode. The S_33 curve is quite different from the loess deposits and this difference is apparent in its lesser uniformity and its granulometric distribution, which includes thicker sizes. As a result, the S_33 curve extends beyond the loess curves to the right and to the left, owing to the fact that the transport agent, water, is less selective than wind.

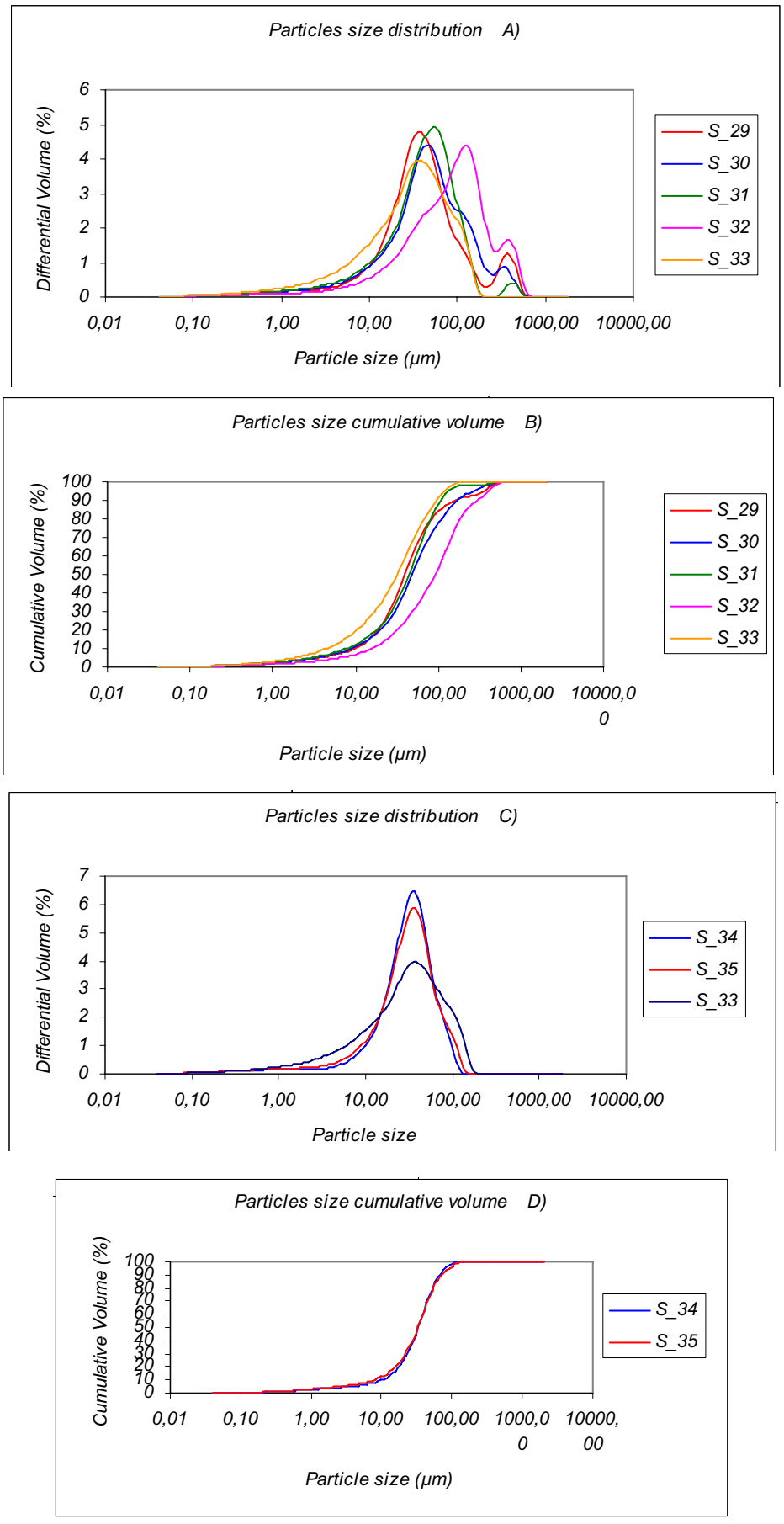

Figure 8. Distribution curves of frequencies and cumulative frequencies of the samples from the brick-making site (S_29 to S_33) and the loess deposits (S_34 and S_35): in C), the curve for S_33 (brick-making site) is included to show the striking difference involved.

The histogram of grain sizes (figure 9) clearly shows that the most plentiful class is silt. It also shows that the variety of sizes in the loess samples is the most limited of all the samples analysed in the study, with a clear predominance of silt.

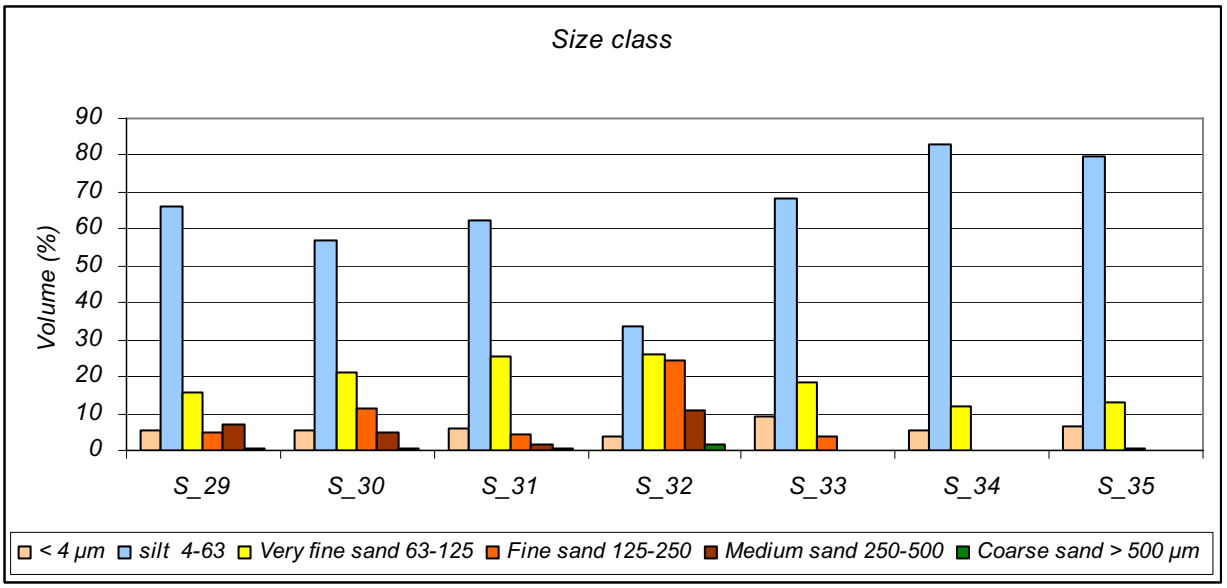

Figure 9. Wentworth size classes for the samples from the brick-making workshop (S_29 to S_33) and loess deposits (S_34 and S_35)

3.- INTERPRETATION AND CONCLUSIONS

After the statistical analysis of the samples and the pertinent clustering and comparisons were completed, the following summary and interpretation were prepared with the geomorphological context of the sample in mind.

The samples from the surface levels S_1 (RC South) and S_7 (RC West) present greater variation in grain size with very high uniformity coefficient (C_U) values (10.5 and 11.13), which are only exceeded by the sample S_3 linked to the level underlying the fortification wall. The mean value for **S_1** is the highest in the set (231.9 µm, fine sand) (tables 2 and 3). The striking mode around the thicker grain sizes is also peculiar to this sample and can be interpreted as a sediment of diverse origins, from the finest fractions of wind-blown origin to the thickest fractions from the slope run-off of Tchinguiz Tepe.

S_1 and **S_7** are comparable to **S_38** which is of purely wind-blown origin without the slope contributions evident in the earlier cases. It is a highly selected sediment as indicated by the dispersion measurements and the value of C_U = 6.88, one of the lowest in the analysed set (figure 10, A and B).

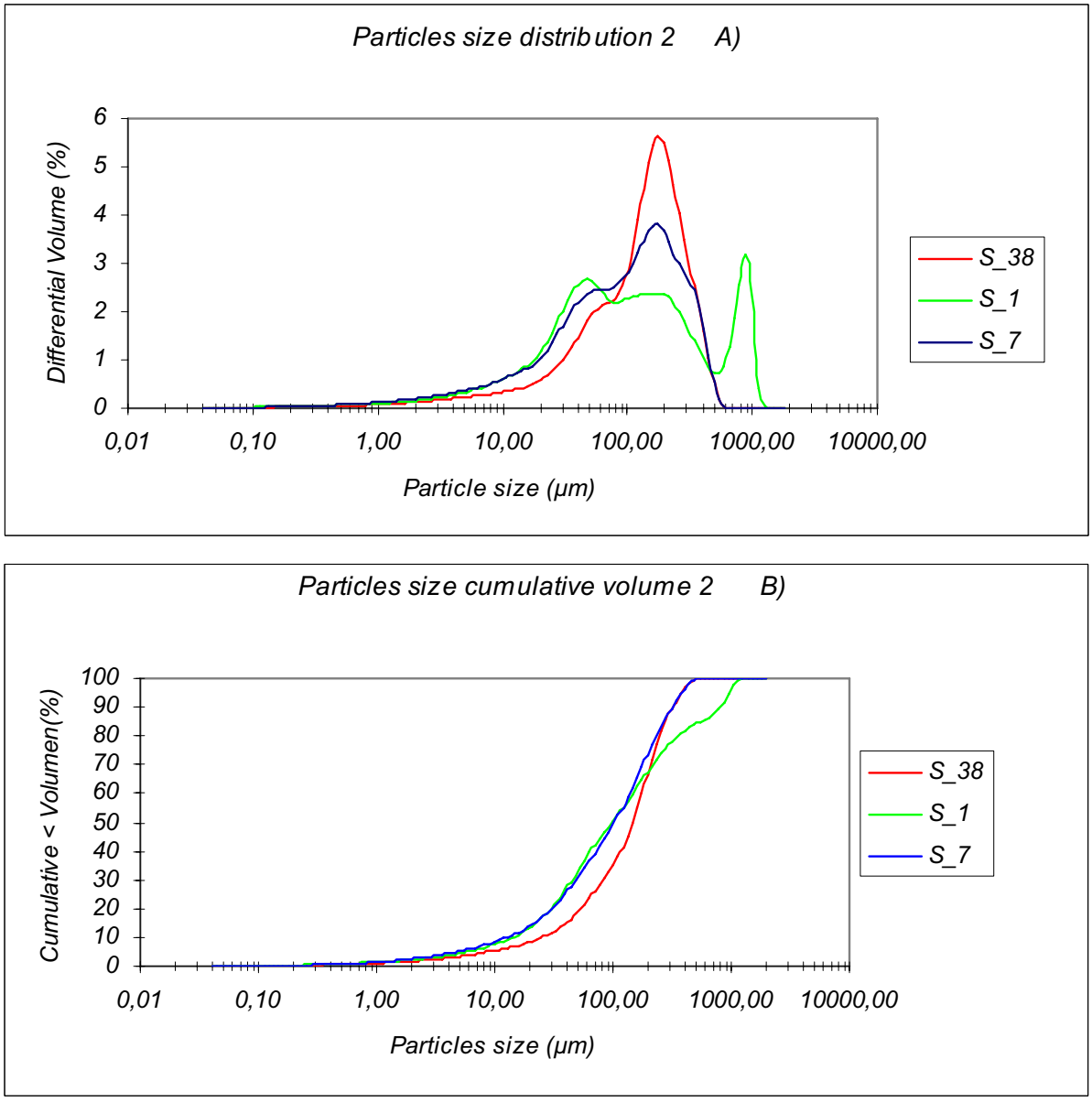

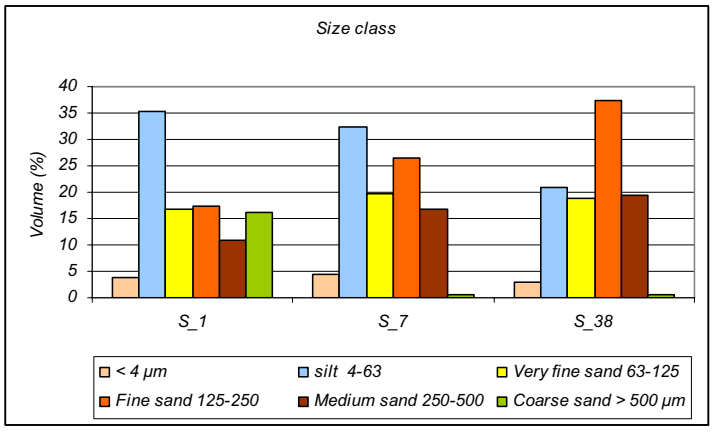

Figure 10. Distribution curves of granulometric frequencies (A) and cumulative frequencies (B) and a histogram of Wentworth size classes for the samples corresponding to the top of the column in RC.

Las muestras corresponden segundo nivel estratigráfico en RC Sur y RC II son S_2, S_36 y S_37 (figura 11). La **S_2** de RC Sur está definida por el derrumbe de la muralla; la **S_36** pertenece a RC II y la **S_37** a este mismo nivel en una zona localmente muy oscura. Presentan diferencias poco significativas. Sin embargo la muestra **S_8** -mismo nivel en RC Oeste- contiene un mayor volumen de la fracción arena fina. En este sentido, los valores de Media, Mediana y Moda son más elevados en S_8 y la Moda se acusa en torno al tamaño 185 µm (tabla 2 y figura 11). Los valores de C_U son muy elevados en S_36 (C_U = 12,59, el más elevado de todo el conjunto analizado) y en S_37 (C_U = 11,46) lo que indica poca uniformidad granulométrica. Como muestras de contraste se añaden en los gráficos las curvas de las muestras **S_38** (manto eólico estacional) y **S_39** (sondeo) Figura 11).

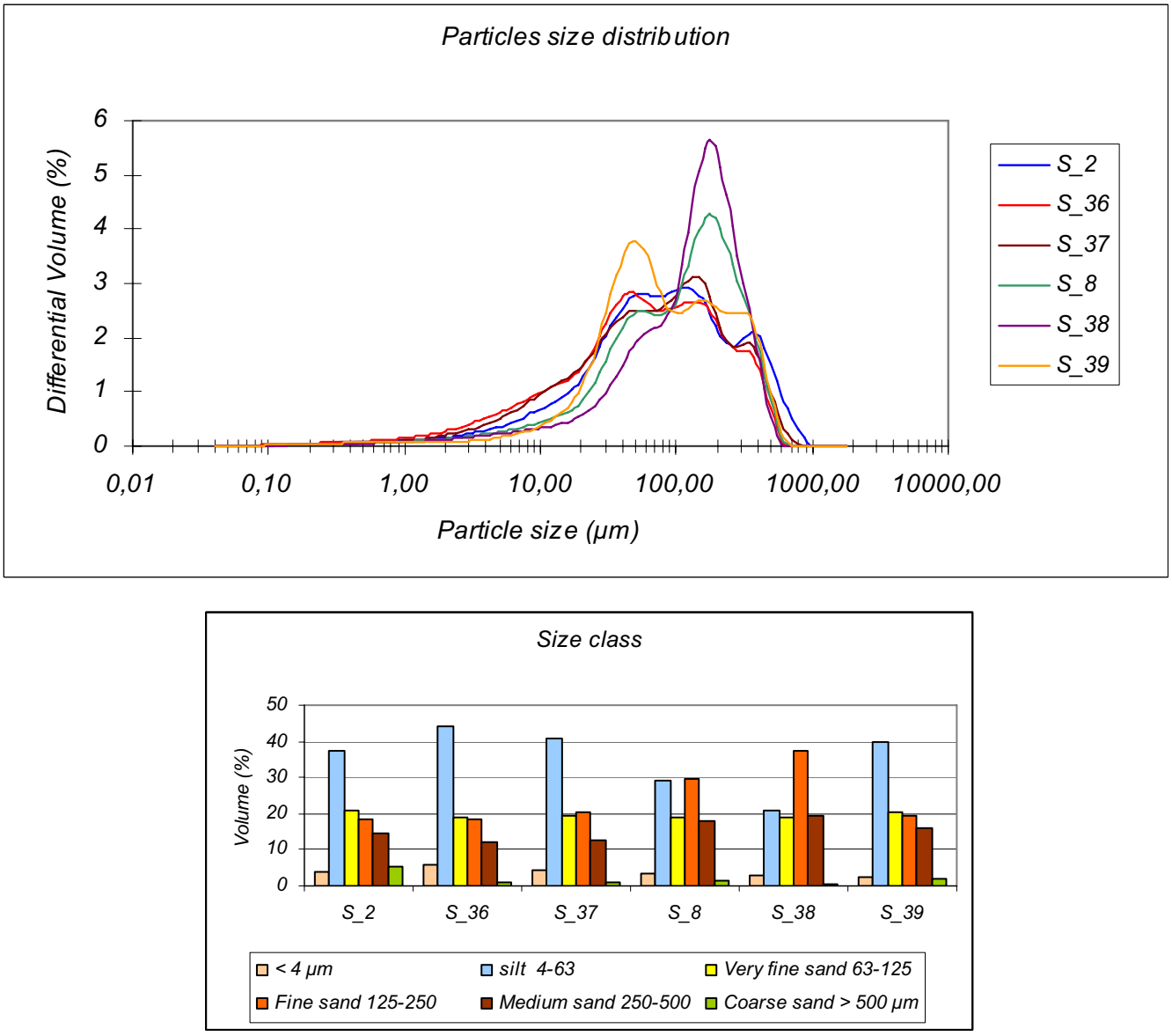

Figure 11.- Granulometric curves from the samples corresponding to the second stratigraphic level (SU 2) in RC South (S_2), RC II (S_36 and S_37) and RC West (S_8), all showing a similar behaviour that varies only in S_8 where the quantity of fine sand is higher.

The principle difference in the curves is the wide-ranging distribution of grain sizes across all samples, except in S_38 which stands out with a well-defined mode and a higher concentration. Although sample S_38 has a wide distribution, it has a mode that is more notable in the finer sizers. The behaviour is interpreted in relation to the degree of selection exercised by the transport agents.

Ordering the granulometric characteristics of all the RC samples from top to base, we can determine that the greatest variability in the statistical indices occurs in RC South, which has the stratigraphic levels with the highest and lowest means, medians and modes. To add nuance to this assessment, the Uniformity Coefficient C_U reveals that the most uniform sample is S_39, followed by S_12. As can be seen in table 5, the samples from RC West are in the lower half with the exception of S_7. In other words, they have greater granulometric uniformity than most of the samples from RC South.

SEQUENCE C_U=d60/d10			
Sample	GSL	SU	C_U
S_36	2	SU 2	12,59
S_3	3	SU 18	11,63
S_37	2	SU 2	11,46
S_7	1	SU 1	11,13
S_1	1	SU 1	10,52
S_2	3	SU 2	10,31
S_11	5	SU 6?	10,17
S_4	7	SU 19	9,59
S_8	2	SU 1	8,46
S_5	9	SU 21	8,37
S_10	4	SU 5	8,19
S_6	8	SU 5 - EU 19	7,19
S_9	3	SU 5?	7,06
S_38	1	NO DATA	6,88
S_12	6	SU 10	6,75
S_39	Sondeo	NO DATA	5,26

RC West	*RC Sur & RC II*

Table 5.- Samples in order from lower to higher granulometric uniformity (decreasing value of the Uniformity Coefficient, C_U). GSL = Geological Stratigraphic Level, SU = Archaeological Stratigraphic Unit.

In summary, the following interpretations and conclusions can be made:

- With respect to the samples from Tchinguiz Tepe, the distribution of grain sizes is better in RC West than in RC South and the mean, median and mode values show less separation in RC West. This could be related to the distance from the fortification wall and the more direct influence of human contribution, which exert an influence on granulometric variability. In general, they appear to be finer, more uniform sediments and could be related to infill material for construction (and other) purposes. They may possibly be selected intentionally, because one characteristic of sediments with good uniformity is that they compact better.

- In the highest levels closest to the surface, some samples are seen to have a wide, asymmetric granulometric distribution ranging from very poorly selected sediments to highly selected samples with very fine sediments. Based on their position, these levels are the most recent ones, covering the ruins and remains of settlement in the archaeological zone. Although they incorporate archaeological components, the levels are sediments typically arising from natural agents.

- From the above observations, one possible interpretation is that the sediment is finer when there are slope contributions incorporating sand dragged from highly weathered sandstone outcroppings, along with sometimes thicker materials from the destruction of buildings and/or sections of fortification. The wind contributions come from the dunes of the Afghan zone. The wind is highly selective; at a given speed, it transports a specific granulometric range. As the wind gusts at varying intensities, wind contributions extend across more than one granulometric

class. Wind deposition is controlled by the barrier effect caused by the hill. While the hill is not a permanent sand accumulation zone, a certain amount of wind-blown sand is “trapped” along the slope and has been slightly compacted by humidity, incorporating slope contributions and the ruins of buildings.

- The establishment of a pattern in the stratigraphy or the sediment is hampered by the vertical and lateral variations in grain size, which show no special tendency. However, it is possible to confirm a highly differentiated granulometric behaviour among the surface formations at Tchinguiz Tepe, the weathered sandstone substrate and the samples taken from the exterior of the hill, which are summarised in the histogram of grain-size classes for all the samples analysed (figure 12).

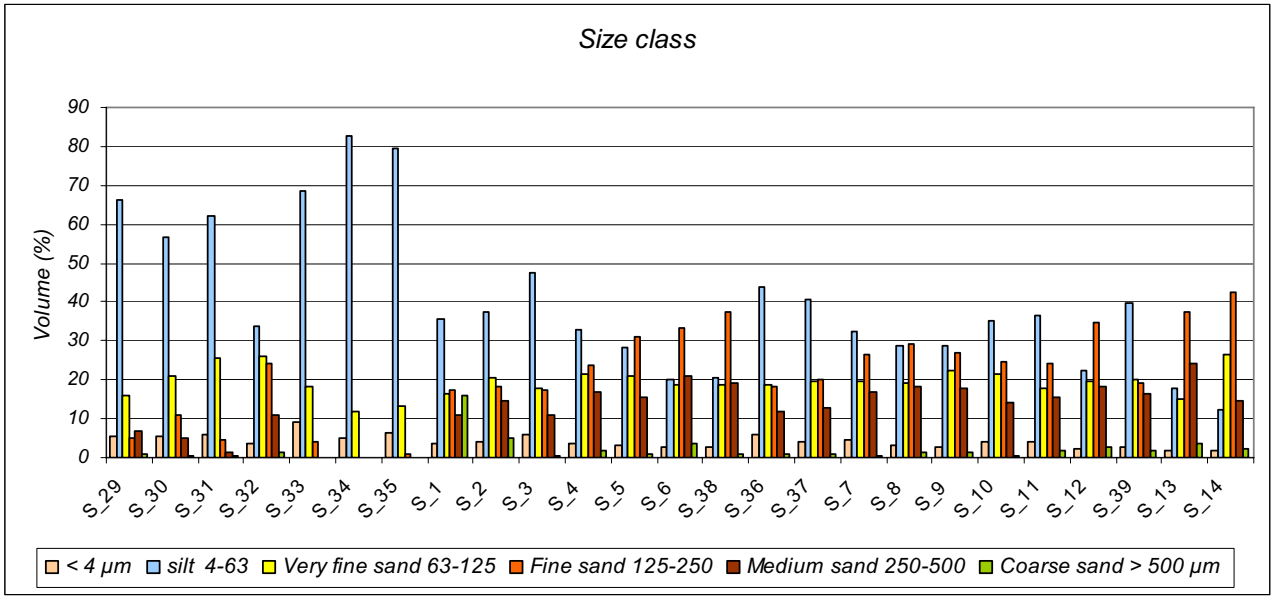

Figure 12.- Histogram of grain-size classes (Wentworth size classes) for all the samples analysed in the study: S_29 to S_34 for the quarries and brick-making sites, S34 and S_35 for the loess deposits, between S_1 and S_39 in the RC zone and S_13 and S_14 with respect to the sandstone substrate.

The histogram shows the quantity of sediment in each grain-size class for each sample. On the left are the samples from the floodplain of the Surkhan Darya and the loess sediments, with the highest proportion of silt. They are followed by the samples from the surface formations of Tchinguiz Tepe, which have a greater variability of grain size and a greater distribution by classes (less selection), and lastly the samples reflecting the distributed sandstone, with a lower amount of finer sizes and similar symmetry.